

Induced Seismicity in Groningen

Assessment of Hazard, Building Damage and Risk

November 2017

By Jan van Elk and Dirk Doornhof

© EP201710209727 Dit rapport is een weerslag van een voortdurend studie- en dataverzamelingsprogramma en bevat de stand der kennis van november 2017. Het copyright van dit rapport ligt bij de Nederlandse Aardolie Maatschappij B.V. Het copyright van de onderliggende studies berust bij de respectievelijke auteurs. Dit rapport of delen daaruit mogen alleen met een nadrukkelijke status-en bronvermelding worden overgenomen of gepubliceerd.

Contents

Summary	7
1 Pre-ambble.....	9
Background to this report.....	9
Reader’s Guide	12
Feedback	14
2 Introduction	15
History of induced earthquakes in Groningen.....	15
Impact on Community	18
3 Research into Induced Seismicity in Groningen.....	22
Objectives of the Studies and Data Acquisition Plan.....	22
Scope of the Studies and Data Acquisition Plan	22
Hazard and Risk assessment for induced Seismicity in Groningen.....	23
Development of the Hazard and Risk Assessments for Groningen	24
Assurance of the Hazard and Risk Assessment for Groningen	26
Summary	34
4 Data Acquisition	37
Improving the sub-surface model.....	38
Subsidence and Compaction.....	39
Monitoring Seismicity	41
5 From Production to Hazard.....	50
Introduction	50
Groningen gasfield.....	50
Groningen reservoir model.....	58
Forecast.....	74
Compaction and Subsidence.....	77
Seismological Model	82
References	91
Ground Motion Prediction.....	93
6 Hazard Assessment	110
Hazard Metric	110
Hazard Map for Peak Ground Acceleration	111
Probabilistic Hazard Assessment.....	113

References.....	125
7 From Hazard to Building Damage and Risk	126
Exposure Database.....	126
Development and Calibration of Seismic Building Response	132
Development of fragility functions	151
Further Plans	152
References.....	155
Consequence Modelling.....	156
References.....	158
8 Building Damage Forecasting.....	160
Introduction	160
Classification of Building Damage; Building Damage States.....	161
Methodology for assessing Building Damage Forecasting	163
Forecast of DS 1 based on Observed Damage from Historical Earthquakes	168
Forecast based on Machine Learning Analysis	177
Forecast of DS 2 and DS3 based on Analytical Modelling and Experimental Tests.....	180
9 Risk and Personal Safety Assessment	183
Risk Metrics.....	183
Probabilistic Risk Assessment	185
Appendix A Research to gain a Fundamental Understanding of Earthquakes in the Groningen field	196
Introduction	196
Fault Interpretation & Modelling.....	196
Evaluation of production scenarios	199
2D Dynamic rupture simulation.....	200
3D Dynamic rupture simulation.....	202
Characterization of fault surface roughness.....	205
Geophysical data acquisition & Interpretation.....	206
Analysis and Interpretation research efforts.....	207
Experimental and related results.....	213
Further steps.....	218
References	218
Appendix B – List of Abbreviations	220
Appendix C – Complete Bibliography of Technical and Scientific Reports and Papers	224

a) Technical and Scientific Reports “Onderzoekrapporten”	224
b) Papers in Peer-reviewed Journals.....	233
Appendix D – Experts.....	237
Appendix E – Universities and Knowledge Institutes.....	242
Appendix F – Raw Data Sharing with Universities and Knowledge Institutes	243

Summary

The current report, “Induced Seismicity in Groningen – Assessment of Hazard, Building Damage and Risk” has been prepared in response to articles 3.2, 7 and 8 of the instemmingsbesluit Winningsplan Groningen 2016. It contains an update of the probabilistic assessment of seismic hazard, building damage and fatality risk, a description of the technical study work supporting this update, which covers the full cause-to-effect chain from gas production from the reservoir to building damage and risk.

Important new features included in this assessment are:

- The model of the reservoir is further improved by history matching of the model with pressure data (including pressure data obtained at the flowing tubinghead), subsidence data and water ingress data from well logging as well as with gravity measurements acquired in 2015.
- An improved seismological model was introduced, including geomechanical complexity and heterogeneity based on extreme threshold failure theory and aftershock modelling.
- Further enhancements to the Ground Motion Prediction Model include the simulation of finite ruptures for larger earthquakes and scenario-dependence of the site amplification factors.
- The GEM building taxonomy has been used for the exposure database, which contains details of the buildings in the Groningen area. This will facilitate future updating of the database with new building inspection data. Inspection results for the central area (within the “0.2 g contour”) have been incorporated in the database.
- Fragility curves are based and calibrated on many additional tests in the laboratory of structural systems and full-scale buildings. Additional focus of the laboratory testing has been on collapse conditions and testing of cast-in-place reinforced concrete and pre-fabricated concrete buildings.

The current assessment of hazard includes forecasts for several metrics of ground acceleration and velocity. The interest in velocity-based hazard metrics was driven by the focus on building damage and the requirement to compare with the building damage guidelines of the SBR (Stichting Bouw Research). The largest mean PGA over the Groningen area, with a return period of 475 years, is less than 0.21 g, for the period 2018 to 2023. This is slightly lower than in previous assessments.

After more empirically driven assessments, this is the first probabilistic assessment of DS1, DS2 and DS3 building damage in the Groningen area. Forecasts have been prepared for damage states DS1, DS2 and DS3 as described in the EMS-98 report. Using the analysis of building damage data by TNO described in the TNO-kalibratiestudie, a forecast for DS1 damage was prepared. This estimate for DS1 damage indicates that in the coming 5-year period some 2,500 (range 1,000 to 6,000) buildings could incur aesthetic (non-structural) damage. Additionally, a machine learning approach was applied to the damage claims database compiled by NAM and CVW since 2012. This study suggests that forecasted damage claim rates possibly could be as high as 35,000 claims over the 5-year period. Although, the relationship between damage claim and building damage is complex, this suggests a higher damage rate than assessed using the TNO kalibratiestudie is a possibility.

Additionally, the *maatschappelijk risico* for building damage is presented as F/N curves prepared for the Groningen area and 7 selected communities. Based on the TNO kalibratie-methodology, this shows that for the Groningen area there is a 10% chance within the 5-year period of an event causing DS1 damage to 6,000 buildings. Using fragility curves derived from the laboratory experimental results, *maatschappelijk risico* for building damage was also assessed for DS2 and DS3 damage. This shows a less than 1% chance of DS2 damage over the 5-year period. However, if DS2 damage does occur, it is in that case expected to affect multiple buildings during a single earthquake.

Also, the probabilistic assessment of Local Personal Risk (LPR) was updated in this report. In previous risk assessments, the Inside Local Personal Risk (ILPR) resulting from structural collapse of buildings was considered. The

risk of falling objects was dealt with separately. In the current risk assessment, the risk in and around the buildings, due to structural collapse (for up to 3 different collapse states), collapse of gables and chimneys were all included in a single assessment of Local Personal Risk (LPR).

The probabilistic assessment of risk shows that there are no buildings where the mean local personal risk exceeds the Meijdam norm of 10^{-4} per year. The number of buildings where the Meijdam norm of mean LPR equal to 10^{-5} per year is exceeded amounts to some 2,800 buildings. This number is larger than previous estimates, but a direct comparison is difficult because in this assessment partial collapse of gables, chimneys and other smaller building elements are considered, affecting both people inside and outside the building. These modelling results are not yet systematically adjusted for corrective and mitigating measures already taken, especially on the falling objects mentioned. The probabilistic assessment of the number of buildings that do not meet the norm, does not directly translate into the scope of the structural upgrading program. This scope will consist of a larger number of buildings.

1 Pre-amble

Background to this report

On the 1st of April 2016, NAM submitted the Groningen Winningsplan 2016 (Ref. 1) to the Minister of Economic Affairs and SodM. This Winningsplan was accompanied with a Technical Addendum providing further background to the technical assessments used in the Winningsplan. The Mining Law requires that winningsplannen are approved by the Minister of Economic Affairs. The approval was granted in the Instemmingsbesluit Winningsplan Groningenveld, issued on the 30th of September 2016 (Ref. 2).

In response to the instemmingsbesluit, NAM will submit three documents to the Minister of Economic Affairs and SodM:

1. An assessment of hazard, building damage and risk (this document) and
2. A study of optimisation of the distribution of production over the field with the aim to reduce seismicity.
3. An overview of the main risks for industrial installations, infra-structure and levees.

For the assessment of building damage and risk, two articles of the Instemmingsbesluit have prompted NAM to prepare additional assessments, as follows:

Article 7 concerns with damage to buildings, and requires that NAM shall:

1. Provide a methodology to forecast damage by 1st February, 2017;
2. Provide the actual forecast of building damage by 1st November, 2017.

Article 8 concerns with risk, and requires that NAM shall:

4. Provide an overview of the main risks related to buildings by 1st November 2017.

An assessment of hazard, building damage and risk

In particular, article 7 states a forecast needs to be prepared for building damage using the damage states as described in EMS-98 document (Ref. 3). On the 1st February 2017, NAM issued the report “Methodology Prognosis of Building Damage and Study and Data Acquisition Plan for Building Damage” (Ref. 4). This document contains a description of the methodology for forecasting building damage including a further extension to the Study and Data Acquisition Plan with laboratory experiments and complementary studies into building damage. The building damage assessment is an extension of the existing probabilistic hazard and risk assessment methodology beyond the regular reach of such a probabilistic seismic risk assessment.

Artikel 7

1. De Nederlandse Aardolie Maatschappij B.V. dient uiterlijk op 1 februari 2017 een rapport in bij de Minister van Economische Zaken waarin een methodiek is opgenomen voor het berekenen van de mate van schade – als gevolg van geïnduceerde bevingen - voor de schadegrenstoestanden DS1, DS2 en DS3 uit het EMS-98, European Seismological Commission, 1998.
2. De Nederlandse Aardolie Maatschappij dient uiterlijk 1 november 2017 een rapport in bij de Minister van Economische Zaken, waarin de methodiek, als bedoeld onder het eerste lid, is uitgewerkt voor het productieniveau uit artikel 2, eerste lid. Tevens wordt in het rapport een raming opgenomen van de factor MR(S), zijnde het schadedeel van de definitie van maatschappelijk risico.

Figure 1.1 Text of article 7 in the Instemmingsbesluit Winningsplan Groningenveld (Ref. 1).

The current report fulfils the requirements of Article 7 by presenting the full hazard and building damage assessment, following the methodology of Ref. 4.

Article 8 concerns fatality risk. It states NAM needs to prepare an overview of the main risk related to buildings. The risk assessment presented in this document provides this overview.

Artikel 8

De Nederlandse Aardolie Maatschappij B.V. dient uiterlijk op 1 november 2017 een rapport in bij de Minister van Economische Zaken waarin een overzicht is opgenomen van voornaamste risico's gerelateerd aan gebouwen, industriële installaties, infrastructuur en waterkeringen. Tevens dient in het rapport een berekening te worden opgenomen van het maatschappelijk risico voor het gehele Groningenveld en voor alle dorpen en steden binnen het invloedsgebied van de gaswinning uit het Groningenveld.

Figure 1.2 Text of article 8 in the Instemmingsbesluit Winningsplan Groningenveld (Ref. 1).

The overview for the risks associated with industry, infra-structure and dikes/levees is provided in a separate report: "An overview of the main risks for industrial installations, infra-structure and levees".

Study of optimisation of the distribution of production over the field with the aim to reduce seismicity.

Article 3.2 of the Instemmingsbesluit requires NAM to investigate whether an alternative distribution of the production over the clusters could result in a lower seismic hazard and risk.

Artikel 3

2. De Nederlandse Aardolie Maatschappij B.V. onderzoekt of een alternatieve verdeling van de productie over alle regio's tot een lagere seismische dreiging of

seismisch risico leidt en brengt daarover uiterlijk 1 november 2017, ten genoegen van de inspecteur-generaal der mijnen, een rapport uit aan de Minister van Economische Zaken. Hiertoe dient de Nederlandse Aardolie Maatschappij B.V. uiterlijk op 1 februari 2017 een plan van aanpak in bij de inspecteur-generaal der mijnen. Uiterlijk op 1 september 2017 dient de Nederlandse Aardolie Maatschappij B.V. ter beoordeling van de inspecteur der mijnen een concept-rapportage in. Een eventuele alternatieve productieverdeling wordt niet ingevoerd voordat deze ten genoegen van de inspecteur-generaal der mijnen is.

Figure 1.3 Text of article 3.2 in the original Instemmingsbesluit Winningsplan Groningenveld (Ref. 2).

This instruction was reconfirmed in the Wijzigingsbesluit Winningsplan Groningenveld (Ref. 5), issued by the Minister on the 23rd of May 2017. The dates for the draft and final submission were changed to 1st October and 1st December respectively.

Artikel 2

Het tweede en derde lid van artikel 3 komen te luiden:

2. De Nederlandse Aardolie Maatschappij B.V. onderzoekt of een alternatieve verdeling van de productie over alle regio's tot een lagere seismische dreiging of seismisch risico leidt en brengt daarover uiterlijk op 1 december 2017 ten genoegen van de inspecteur-generaal der mijnen, een rapport uit aan de Minister van Economische Zaken. Daarbij wordt tevens in detail voor alle clusters onderzocht of clusteroperaties verder geoptimaliseerd kunnen worden ten einde (ook regionale) fluctuaties zo veel mogelijk te beperken. De Nederlandse Aardolie Maatschappij B.V. brengt uiterlijk op 1 februari 2017 een plan van aanpak in bij de inspecteur-generaal der mijnen. Uiterlijk op 1 oktober 2017 dient de Nederlandse Aardolie Maatschappij B.V. ter beoordeling van de inspecteur-generaal der mijnen een concept-rapportage in. Een eventuele alternatieve productieverdeling wordt niet ingevoerd voordat deze ten genoegen van de inspecteur-generaal der mijnen is.

Figure 1.4 Text of article 2 in the Wijzigingsbesluit Winningsplan Groningenveld (Ref. 5).

The current report will provide supporting information for the investigation of the alternative production distribution as reported in the draft report of 1st October 2017. This report will describe the scientific research supporting the assessment of hazard and risk and will present the base case. Optimisation of the distribution of gas production from the areas of the field to reduce seismicity will be reported in a separate document. This is more practical in view of the different submission dates of these deliverables mentioned in the Instemmingsbesluit and Wijzigingsbesluit.

The current report therefore fulfils the requirements for an assessment of building damage (article 7 of Instemmingsbesluit - Winningsplan 2016) and building related risk (article 8 of Instemmingsbesluit - Winningsplan 2016) and supports the requirement for an optimisation of production over the clusters with the objective to reduce seismicity (article 3 of instemmingsbesluit - Winningsplan 2016 and article 2 of Wijzigingsbesluit - Winningsplan 2016).

Reader's Guide

This report

This report reflects the status of research into induced seismicity as of the 1st of November 2017. An update is presented of the previous Hazard and Risk Assessment (April 2016), extending it with a building damage assessment. The full scope of the hazard and risk assessment methodology will be presented with emphasis on recent enhancements and improvements in the calibration of the models with newly acquired data. The methodology to additionally cover building damage, will be presented as an extension to the hazard and risk assessment. The assessment of building damage required an extension of the knowledge of the response a population of buildings to an earthquake. For the risk assessment, fragility curves for damage states DS4 and DS5 are required covering all buildings typologies of the Groningen field area. Essentially, for the forecasting of building damage, the hazard and risk assessment is now extended to cover fragility curves for all damage states, including the ‘non-life threatening’ but impactful¹ damage states DS1 to DS3.

The results presented in this report are supported by data acquired in the Groningen field area. The data presented should be read or interpreted with due caution, taking into account the remaining scientific uncertainties and further calibration and refinement of models. The “Meet- en Regelprotocol” (Measurement and Control Protocol) ensures the continuous data acquisition and monitoring needed for Hazard and Risk Management (Ref. 6).

The structure of the report follows the causal chain from gas production to hazard (Chapter 5) and from hazard to building damage and risk (Chapter 7).



Figure 1.1 Structure of the Studies and Data Acquisition Program from Cause (gas production) to Effects (impact on personal Safety and Building Damage).

This report starts with an introduction of the history of earthquakes in Groningen (Chapter 2). Chapter 3 introduces the methodology for the hazard and risk assessment and the study and data acquisition plan into induced seismicity in Groningen. The structure of the entire program contains a number of checks and balances to ensure the results are based on objective research. These checks and balances include transparency with a freely accessible web-site where all study reports are published, a multi-layered assurance process involving respected scientists from all over the world and publication of studies in reputable peer-reviewed journals. More details are presented in the appendices.

Chapter 4 describes the data acquisition projects that have been carried out or are in progress. The collected seismic data form the foundation of the study program led by NAM. The raw data have been made available to interested independent researchers.

In chapter 5, the technical foundation for the assessment of the seismic hazard, resulting from the production of gas from the reservoir, is presented. The impact of gas production on reservoir pressure, water table rise in the reservoir and the rock compaction is discussed. A summary of the modelling of compaction (subsidence), seismicity and resulting ground accelerations is provided. Emphasis is put on the latest data gathering, on calibration of the models, and on the new insights derived from this data.

¹ In the Winningsplan these ‘lower’ Damage States are tagged as societal impacts, to be addressed but formally not a part of the risk.

Chapter 6 introduces the earthquake hazard metrics chosen for the hazard assessment and presents forecasts for these metrics in hazard maps. Additional hazard metrics, based on ground velocity instead of on ground acceleration, are introduced for the benefit of the assessment of building damage.

Results from the building damage studies are presented in chapter 8. The probabilistic hazard and risk assessment is an update of earlier hazard and risk assessments, based on additional data acquired and on insights from recent studies. The probabilistic assessment of building damage, for damage states DS1 to DS3, is completely new and presented in this report for the first time.

Chapter 9 provides insight into the risk, based on the hazard presented earlier in chapter 6. This chapter presents a number of significant earthquake risk metrics in risk maps. It describes how the risk assessment influences the program for structural upgrading and how this program serves to mitigate future risk and to increase safety of people in the area.

This report will not discuss the optimisation of the distribution of the production over the different areas of the field, as that will be the subject of a separate document.

More Information

NAM Led Research Program

In the main text, references will be given to detailed technical reports, where more in-depth descriptions of underlying studies and results of the data acquisition have been documented. The NAM reports can be downloaded from the “onderzoeksrapporten”-page at the NAM website www.nam.nl. A chronological list of all reports, allowing download of each of the reports, can be directly accessed through this link:

<https://www.nam.nl/feiten-en-cijfers/onderzoeksrapporten>

Each of the reports is prefaced by a short introduction explaining the place of the research in the larger framework of the study and data acquisition program, the vintage of the research and the assurance provided by external experts. A new browse functionality has been added to the web-site, allowing the user to quickly locate all the reports for a specific area of interest.

More information by research by EUcentre

The reports on the building tests can also be accessed through the web-site of Eucentre. The following link brings you to the NAM-Project page of the Eucentre web-site: <http://www.eucentre.it/project-nam/>.

Apart from reports, this page also contains movies of shake-table tests and a form to request the results of the experiments.

Research by Other Organizations

More information by research by KNMI

KNMI is the Dutch authority on seismicity, both tectonic earthquakes (in the south of The Netherlands) and induced seismicity. The reports prepared by KNMI can be found on their web-site www.knmi.nl and accessed via the link below.

<https://www.knmi.nl/kennis-en-datacentrum/zoekresultaten?q= groningen>

More information by research by TNO; NLOG

Reports prepared by TNO on induced seismicity, including studies undertaken by TNO and reviews by TNO of studies undertaken by NAM, can be found at www.nlog.nl, a website maintained by TNO.

More information by research by CBS

The CBS (Centraal Bureau voor de Statistiek) performed several statistical analyses on the Groningen production and seismicity data at the request of SodM. Reports on this can be found at www.cbs.nl. The following link accesses an overview page, with further links to all reports: <https://www.cbs.nl/nl-nl/dossier/bodembewegingen-groningen>. The latest report by CBS can be accessed via this link:

<https://www.cbs.nl/nl-nl/achtergrond/2017/16/reservoirdruk-daling-en-aantallen-aardbevingen>

Feedback

If you have questions or suggestions, please do not hesitate to contact NAM.

That can be done via

Phone: +31 (0) 592 368222

or

E-mail: nam-communicatie@shell.com

References

1. Winningsplan Groningen – 2016, NAM, April 2016
2. Instemmingsbesluit Winningsplan Groningenveld, Ministerie van Economische Zaken, Directoraat-generaal Energie, Telecom & Mededinging, Directie Energie en Omgeving, 30 September 2016
3. European Seismological Commission (G. Grünthal), European Macroseismic Scale 1998, EMS-98, 1998
4. Methodology Prognosis of Building Damage and Study and Data Acquisition Plan for Building Damage, NAM, Jan van Elk, Jeroen Uilenreef & Dirk Doornhof, February 2017
5. Wijziging Instemmingsbesluit Winningsplan Groningenveld, Ministerie van Economische Zaken, Directoraat-generaal Energie, Telecom & Mededinging, Directie Energie en Omgeving, 23 May 2017
6. Meet- en Regelprotocol Groningen veld, NAM, June 2017

2 Introduction

History of induced earthquakes in Groningen

Since 1986, relatively small magnitude earthquakes have been recorded near producing gas fields in the provinces of Groningen, Drenthe and Noord-Holland as well as in northern Germany. The first recorded earthquake in 1986 was located near Assen with a magnitude of $M_L = 2.8$. These earthquakes were attributed to gas production by Dr. Meent van der Sluis (Ref. 1). Initially, this was not supported by NAM, but it led to a number of studies (Ref. 2 to 7). A multidisciplinary study on the subject of induced seismicity was initiated by the Ministry of Economic Affairs in the early 1990's, and was guided by an Advisory Committee (Begeleidingscommissie Onderzoek Aardbevingen, BOA) (Ref. 8 to 10). NAM was also represented in this study. It was concluded that the observed earthquakes were indeed of non-tectonic origin and induced by reservoir depletion (*i.e.* gas production). This multidisciplinary study was published in 1993 (Ref. 10) and concluded:

“Given the results of the research into the relationship between gas production and earthquakes, the committee concludes that under certain circumstances earthquakes are a consequence of gas production.”²

Furthermore, the committee concluded:

“From a statistical point of view, the maximum expected magnitude of earthquakes in the Northern Netherlands is calculated to be $M_L = 3.3$ on Richter's scale. The likelihood of such a quake is negligible.

Geomechanical modelling also estimates the maximum expected earthquake. The value of 2.9 on Richter's scale is, despite the totally different approach, in line with the result of seismology.

The results of multidisciplinary research indicate that, as a result of the maximum expected earthquake, even in the least adverse case, there is only a slight chance of slight damage to structures in a restricted area around the epicentre.”

Following up on the conclusions, it was agreed between NAM and the Royal Dutch Meteorological Institute (KNMI) to install a shallow borehole seismometer network in the Groningen area. The network was designed to detect earthquakes, pinpoint their locations and quantify their magnitudes, and has been operational since 1995. Additional accelerometers were installed in areas with highest earthquake frequency.

Following the publication of the BOA report in 1993, several studies into induced seismicity were carried out. This was primarily done by research institutes KNMI, Deltares, TU Delft, RGD and TNO, often sponsored by oil and gas producing companies operating in The Netherlands and under the umbrella of the Werkgroep Aardbevingen and later the Technisch Platform Aardbevingen TPA (Ref. 9 and 11 to 43). The focus of many of these studies was on the

² Report was written in Dutch. Original text is:

“Gezien de resultaten van het onderzoek naar de relatie tussen gaswinning en aardbevingen komt de commissie tot de slotsom dat onder bepaalde omstandigheden aardbevingen het gevolg zijn van gaswinning.” Verder concludeerde de commissie:

“Statistisch gezien is de maximaal te verwachten magnitude van aardbevingen in Noord-Nederland berekend op $M_L = 3,3$ op de schaal van Richter. De kans dat een dergelijke beving optreedt, is verwaarloosbaar klein.

Uit de geomechanische modellering is ook een schatting gemaakt voor de maximaal te verwachten aardbeving. De waarde van 2,9 op de schaal van Richter is ondanks de totaal andere aanpak in goede overeenstemming met het resultaat uit de seismologie.

De uitkomsten van het multidisciplinaire onderzoek geven aan, dat als gevolg van de maximaal te verwachten aardbeving, zelfs in het ongunstigste geval, slechts een kleine kans bestaat op lichte schade aan bouwwerken in een beperkt gebied rond het epicentrum.

[.....]

Gezien de resultaten van het onderzoek naar de relatie tussen gaswinning en aardbevingen komt de commissie tot de slotsom dat onder bepaalde omstandigheden aardbevingen het gevolg zijn van gaswinning. Het aantal aardbevingen en de sterkte ervan zijn in Noord-Nederland niet van dusdanige aard dat dit aanleiding hoeft te zijn tot enige verontrusting.”

determination of the maximum possible magnitude of the induced earthquakes in the North Netherlands and the impact of earthquakes on buildings.

The seismic monitoring network showed a gradual increase in seismic activity with time, during the following 20 years. Especially after 2003, the seismicity did increase. Initially, this increase was considered to be a statistical variation within the uncertainty range of the measurements and NAM did not take sufficient heed to this development. The earthquake near Westeremden in 2006, with a magnitude $M_L = 3.5$, was still below the expected maximum (3,9 at that time), but should in hindsight have triggered more alertness and curiosity and a more critical (re)assessment of the induced earthquakes.

Additional studies were initiated, such as the detailed mapping of all faults in the reservoir, the “Kalibratie-studie” by TNO (Ref. 37) and the assessment of building damage by Deltares (Ref. 38). The main focus was on surveying damage and understanding the damage pattern, not on reassessing the geomechanical and seismological paradigm. The Dutch Safety Board (Onderzoeksraad voor Veiligheid, OVV) concluded in 2015 (Ref. 45):

“.....The parties involved in gas extraction for a long time felt no urgency to do research to reduce the uncertainties surrounding the gas extraction from the Groningen field. Until the warning from the regulator in 2013, knowledge development about the potential impact of gas extraction was performed fragmentarily. No integral and independent scientific research was carried out into the deep subsurface in Groningen and the effective mechanisms taking place at depth. Moreover, the parties did not have an open attitude towards critical voices questioning the correctness of assumptions. Those involved should, in the opinion of the council, have realized at an early stage that a large-scale and long-term intervention, such as the exploitation of the Groningen field, might carry unknown risks. Uncertainty and the reduction thereof should have been at the basis of all their actions.”³

A renewed focus on the issue of seismicity induced by gas production in Groningen started in 2012. This was triggered by three factors. First, the earthquake near Huizinge (16th August 2012) with a magnitude $M_w=3.6$ was felt as more intense and with a longer duration than previous earthquakes in that area. Compared with previous earthquakes, significantly more building damage was reported as a result of this earthquake. Secondly, a general realization had started to materialize that over the past few years seismicity in the Groningen area had increased beyond statistical variation. Third, and most important, studies by SodM (Ref. 44), KNMI and NAM concluded that the uncertainty associated with the earthquake hazard in the Groningen field was larger than previously thought. It was realized for the first time that the induced earthquakes could pose a potential safety risk.

After the Huizinge event, NAM started to prepare a detailed seismic hazard and risk assessment. To that end, NAM set up an extensive accelerated research program. This research program has produced many important new or revised insights in the subject of induced seismicity and seismic risk.

Studies into induced seismicity in Groningen by SodM, KNMI and TNO continued after 2012, with results published in reports and incorporated in the hazard and risk assessments. Recently, in response to the report in February 2015

³ The report by the OVV was written in Dutch. The Dutch text is: “.....de bij de gaswinning betrokken partijen lange tijd geen urgentie voelden om onderzoek te doen dat de onzekerheden kon reduceren waarmee de gaswinning uit het Groningen veld omgeven was. Kennisontwikkeling over de mogelijke gevolgen van de gaswinning vond tot de waarschuwing van de toezichthouder in 2013 fragmentarisch plaats. Er was tot 2013 geen sprake van een integraal en onafhankelijk wetenschappelijk onderzoeksprogramma om de diepe ondergrond in Groningen en de daar werkzame mechanismen in kaart te brengen. Daarnaast hadden de betrokken partijen geen open houding tegenover kritische tegengeluiden die de juistheid van aannames ter discussie stelden. Betrokkenen hadden zich, naar het oordeel van de raad, al in een vroeg stadium moeten realiseren dat een grootschalige en meerjarige ingreep, zoals the exploitatie van het Groningen veld, onbekende risico's met zich mee zou brengen. Onzekerheid en de reductie ervan hadden het uitgangspunt moeten zijn van hun handelen.”

by the OVV, SodM and MEA have initiated the KEM research program, while a research program under the auspices of the NWO will commence early 2018. This last program is in part funded by a contribution from NAM.

At several times, production restrictions have been imposed by the MEA on the advice of SodM. In June 2017, the Measurement and Control Protocol (Meet- en Regelprotocol) was approved by SodM. Since then, the protocol is in effect and special reports have been prepared by NAM and shared with SodM. Figure 2.1 shows these have been effective in reducing seismicity induced by the production of gas.

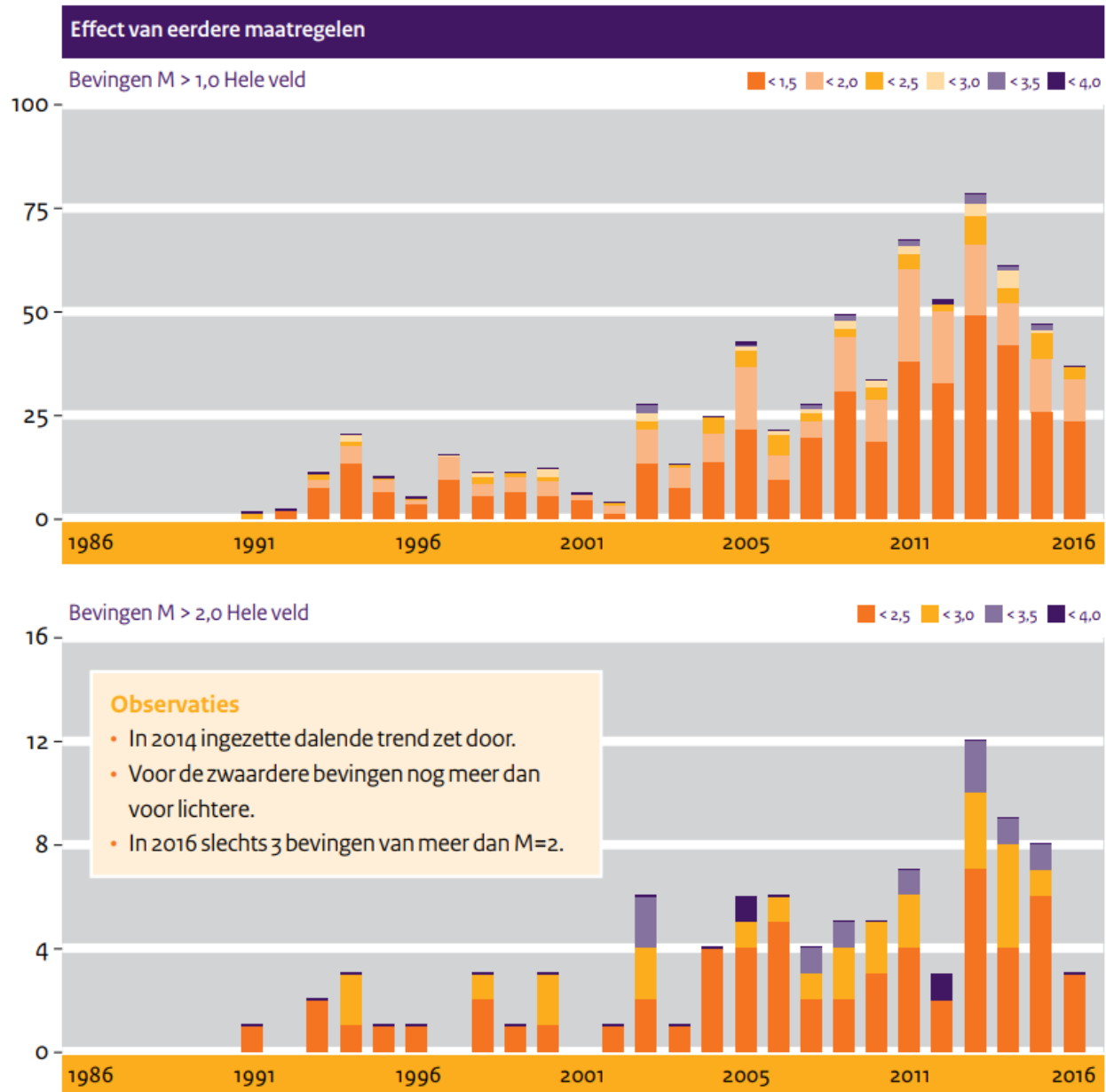


Figure 2.1 The number of earthquakes with magnitude $M_L \geq 1$ (above) and $M_L \geq 2$ (below). The figure was taken from the annual report of SodM (Ref. 47). Observations: The decreasing trend in seismicity from 2014 onwards has persisted in 2016 for both heavier and lighter earthquakes. In 2016 there were only three earthquakes larger than $M_L \geq 2$.

(source: SodM)

Impact on Community

The earthquakes have left a deep imprint on the local population. This is documented for example, in a book by Mike Tomale called “Bevingen” (Ref. 48), which describes the community response to the earthquakes and in particular to the Huizinge earthquake. The people living in the Groningen field area have been confronted with the negative social effects of induced earthquakes.

This current report is nevertheless primarily a technical report addressing hazard, personal risk and building damage, resulting from the induced earthquakes in Groningen. Relevant data pertinent to the specific Groningen situation data was initially scarce or non-existent. Due to this paucity of data, the first attempt to derive a hazard and risk assessment necessarily had to be largely based on analogies with tectonic earthquakes. This yielded a conservative scientific assessment of hazard and risk (often coupled with images of tectonic events), which caused unrest in society.

With the increasing amount of data becoming available from acquisition campaigns in Groningen, each study update or new hazard and risk assessment could be even more based on data and models tailored specifically for induced seismicity in the Groningen field. As a result, the reliability of hazard and risk assessment has significantly increased with time as well. Unfortunately, the feelings of insecurity have not subsided in many parts of the community.

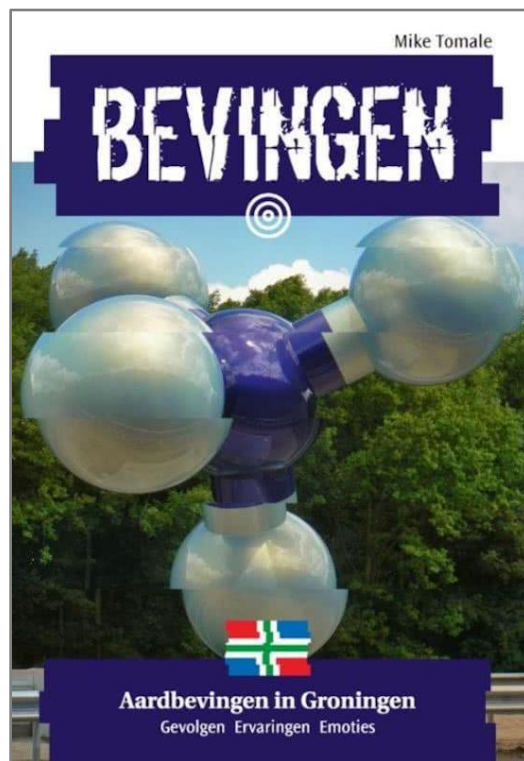


Figure 2.2 Cover of the book “Bevingen – aardbevingen in Groningen; Gevolgen – Ervaringen – Emoties” by Mike Tomale. (Photo: Jenny de Groot).

Research into the social effect of the earthquakes has been carried out by social scientists of the RUG (Ref. 49 and 50) and by Groningsperspectief commissioned by the NCG⁴ (Ref. 51 to 53). A review of these liveability studies was carried out (Ref. 54) with the aim to recommend methodological improvements. NAM did not - in line with the

⁴ The Nationaal Coördinator Groningen (NCG) is a partnership between twelve municipalities in the earthquake area, the province Groningen and the National Government. Hans Alders leads the partnership.

envisaged role seen by e.g. the OVV and committee Meijdam - actively initiate an own studies program into the social impact of earthquakes, but follows the developments by annual social impact inventories based on the available independent research (Ref. 55 and 56). The TU Delft/OTB has done social research on the impacts on the quality of life of the inhabitants. Additionally, the effects on the housing market have been studied by numerous institutes (CBS, TU Delft, VU Amsterdam) and the economic impacts are being studied, both negative (housing values) and positive (creating new employment due to building activities).

A review of some of these liveability studies was carried out by experts from Leiden and Utrecht University (Ref. 53) with the aim to recommend methodological improvements. NAM did not actively initiate a studies program into the social impact of earthquakes, but has annually prepared social impact inventory based on the available research done independently from NAM (Ref. 54 and 55).

The key challenge is to further define, develop and execute the action plans to reduce and mitigate the impact of production-induced seismicity. Responsible parties include NAM, the ministry of Economic Affairs, State Supervision of Mines (SodM) and the National Coordinator Groningen, in close cooperation with other stakeholders. To this end, the instruments currently in place for assessing and mitigating these effects – as set down in mining regulations, risk policies and, for example, building codes – are being extended and tailored to the Groningen situation.

References

1. Aardbevingen in Noord-Nederland, over bodemtrillingen en bodemdaling, Dr. Meent van der Sluis, Stubeg, March 1988
2. A Study on the possibility of generation and/or reactivation of faults by depletion of gas in the Groningen gas field (The Netherlands), Shell (KSEPL), Rapport RKER.86.120., 1986
3. Studieresultaten betreffende ongelijkmatige zakkingen in verband met aardgaswinning in de provincie Groningen – Deelstudie I: Mogelijkheid van breukbeweging door gas productie uit het Groningen gasveld, Deelstudie II: Mogelijkheid van schade aan de bebouwing door wijzigingen in het peil van polder en boezemwater, Commissie Bodemdaling door Aardgas winning, March 1987
4. Bodemdaling in de praktijk – het Groningen Gasveld. In: Bodemdaling in Nederland, Symposium verslag, faculteit der Mijnbouwkunde en Petroleumwinning, Technische Universiteit Delft, 1990
5. Subsidence at the Groningen Gas Field – An evaluation of the subsidence program directed by NAM, M.N. Toksöz and J.B. Walsh, MIT, January 1990
6. Rapportage vertrouwenscommissie van de provincie Groningen, inzake prognose bodemdaling door aardgaswinning Groningen 1990 van de NAM en de “second opinion” van het Massachusetts Institute of Technology (MIT) te Boston U.S.A., April 1990
7. Seismische registraties in Nederland tegen de achtergrond van de aardbevingen van Assen, Hooghalen en Purmerend, Symposium verslag, faculteit der Mijnbouwkunde en Petroleumwinning, Technische Universiteit Delft, 1990
8. Voortgangsrapportage Multi-Disciplinair Onderzoek, Begeleidingscommissie Onderzoek Aardbevingen, November 1992
9. Geomechanische analyse lichte aardshokken in het Eleveld reservoir – Bijdrage T.U. delft aan het multidisciplinair onderzoek naar de relatie tussen gaswinning en lichte aardbevingen, Faculteit Mijnbouwkunde en Petroleumwinning T.U. Delft, J.P.A. Roest and W. Kuilman, September 1993
10. Eindrapport multidisciplinair onderzoek naar de relatie tussen gaswinning en aardbevingen in Noord-Nederland, Begeleidingscommissie Onderzoek Aardbevingen, November 1993
11. Schade aan bouwwerken door trillingen, Meet- en beoordelingsrichtlijn, Richtlijn 1, Stichting Bouw Research, P.C. van Staalduinen, 1993: ISBN 90-5367-079-3

12. Seismische analyse van aardbevingen in Noord-Nederland, Wetenschappelijk rapport WR-94-1, KNMI, H. Haak and T. De Crook, 1994
13. Seismische analyse van de aardbeving bij Alkmaar op 21 September 1994, KNMI, 1994
14. Analyse van het seismisch risico in Noord-Nederland, Technisch rapport TR-168, KNMI, T. De Crook, B. Dost and H.W. Haak, 1995
15. Seismische analyse van de aardbevingen bij Middelstum op 30 juli 1994, Annen op 16 augustus 1994 en Annen op 31 januari 1995, Technisch rapport TR-186, KNMI, December 1995
16. Gaswinning en Aardschokken, Informatiefolder, Min EZ, provincies Groningen en Drenthe, KNMI en NAM, 1995
17. A Seismic zoning map conforming to Eurocode 8, a practical earthquake parameter for The Netherlands, T. de Crook, *Geologie en Mijnbouw*, 75:11-18, 1996
18. Rapport Diepe Ondergrond en Bodemdaling – Denken in vier dimensies, Technische Commissie Bodemdaling, January 1996
19. Seismische Risico in Noord-Nederland, KNMI, TR-205, T. De Crook, H.W. Haak and B. Dost, February 1998
20. Seismische analyses van de aardbevingen bij Roswinkel in de periode 1992-1998, KNMI, B. Dost en H.W. Haak, 1998
21. Attenuation in the northern part of the Netherlands; implications for ML determination, KNMI, B. Dost en H.W. Haak, 1998
22. De relatie tussen schade aan gebouwen en lichte, ondiepe aardbevingen in Nederland: inventarisatie, TNO-Bouw, 97-Con-R1523-1, P.C. van Staalduinen, C.P.W. Geurts en H.S. Buitenkamp, 1998
23. Evaluatie van Liquefactie door kleine ondiepe aardbevingen in Noord-Nederland, CO-383750/12- versie 02, Grondmechanica Delft, G.A.M. Kruse, November 1998
24. Aardbevingen in Noord-Nederland in 1998 – met overzicht over de periode 1986 – 1998, KNMI-Publicatie 189, 1999
25. Subsidence, tremors and society, H.J. Gussinklo, H.W. Haak, R.C.H. Quadvlieg and P.M.F.M. Schutjens, *Geologie en Mijnbouw / Netherlands Journal of Geosciences* 80, May 2000
26. Seismische analyse van de aardbevingen bij Alkmaar op 9 en 10 september en Bergen op Zee op 10 oktober 2001, H.W. Haak, B. Dost and F.H. Goutbeek, TR-239, KNMI, October 2001
27. Invloed aardbevingen op overstromingsrisico's, Rijkswaterstaat, Dienst Weg- en Waterbouwkunde, H.J. Verheij, F. Diermanse, T. van Eck, G. de Lange, J. Lindenberg, H.J. Simmelink en H.J.T. Weerts, December 2002
28. Seismische hazard van geïnduceerde aardbevingen – rapportage fase 1, B.B.T. Wassing, D. Maljers, R.S. Westerhoff, J.H.A.Bosch and H.J.T.Weerts, TNO-rapport NITG 03-185-C, November 2003
29. Modelling of stress development and fault slip in and around a producing gas reservoir, F.M.M. Mulder, proefschrift, TU Delft, 2003
30. Seismische hazard van geïnduceerde aardbevingen – rapportage fase 2, B.B.T. Wassing, D. Maljers, J.H.A.Bosch, H.J.T.Weerts, A. Koopman, A. Dullemond and W. Roos, TNO-rapport NITG 03-186-C, January 2004
31. Seismic hazard due to small shallow induced earthquakes, T. van Eck, F. Goutbeek, H. Haak, en B. Dost, KNMI, Scientific report; WR 2004-01, 2004.
32. Deterministische hazard analyse voor geïnduceerde seismiciteit, R. M. H. E. van Eijs, F. M. M. Mulders, M. Nepveu, TNO-rapport NITG 04-171-C, 2004
33. Seismisch hazard van geïnduceerde aardbevingen - Integratie van deelstudies, B.B.T. Wassing, T. van Eck, R.M.H.E. van Eijs, TNO rapport NITG 04-244-B, KNMI publicatie 208, ISBN 90-369-2263-1, December 2004
34. Seismic Hazard due to small-magnitude, shallow-source induced earthquakes in The Netherlands, T. van Eck, F. Goutbeek, H. Haak and B. Dost, *Engineering Geology* 87 (2006) 105-121, 2006

35. Correlation between hydrocarbon reservoir properties and induced seismicity in the Netherlands, R. M. H. E. Van Eijs, F.M.M. Mulders, M. Nepveu, C. Kenter, and B. C. Scheffers, *Engineering Geology*, 84, 99-111. 2006.
36. Geïnduceerde aardtrillingen in of nabij het Groningen gasveld, TNO Bouw en Ondergrond – Adviesgroep EZ, October 2009
37. Kalibratiestudie schade door aardbevingen, W. Roos, P.H. Waarts and B.B.T. Wassing, TNO rapport, TNO-034-DTM-2009-04435, November 2009
38. Gebouwschade Loppersum, G. de Lange, N.G.C. van Oostrom, S. Dortland, H. Borstje and S.A.J. de Rlichemont, 1202097-000BGS-0003, TNO/Deltares, February 2011
39. Methodiek voor onderzoek naar oorzaken van gebouwschade – versie 2, H. Borstje and S.A.J. Rlichemont, Deltares/TNO rapport TNO-060-DTM-2011-02980
40. Maximale schade door geïndiceerde aardbevingen – inventarisatie van studies met toepassing op Bergermeer, W. Kantten-Roos, B. Dost, A.C.W.M. Vrouwenvelder and T. Van Eck, 2011
41. Monitoring induced seismicity in the North of the Netherlands: status 2010, B. Dost, T. Goutbeek, T. van Eck, and D. Kraaijpoel, KNMI, KNMI Scientific Report WR 2012-03, July 2012
42. Deterministische hazard analyse voor geïnduceerde seismiciteit in Nederland, K. van Thienen-Visser, M. Nepveu and J. Hettelaar, TNO, TNO-rapport 2012 R10198, June 2012
43. Seismische hazard van geïnduceerde aardbevingen – Integratie van deelstudies, B.B.T. Wassing and B. Dost, December 2012
44. Re-assessment of the probability of higher magnitude earthquakes in the Groningen gas field, Staatstoezicht op de Mijnen, 16th January 2013
45. Aardbevingsrisico's in Groningen, Onderzoek naar de rol van veiligheid van burgers in de besluitvorming over de gaswinning (1959 – 2014), Onderzoeksraad voor de Veiligheid, February 2015
46. Aardbevingsrisico's in Groningen, Stand van zaken opvolging aardbevingen, Onderzoeksraad voor de Veiligheid, March 2017
47. Jaarverslag 2016, Staatstoezicht op de Mijnen, August 2017
48. Bevingen, aardbevingen in Groningen, Gevolgen – Ervaringen – Emoties, Mike Tomale, 2014.
49. Energy security and human security in a Dutch gasquake context: a case of localized performative politics, Kester, J., *Energy Research & Social Science*, 24 (2017) 12–20.
50. Perceived risks, emotions, and policy preferences, Perlaviciute, G., Steg, E., Hoekstra, E., Vrieling, L., *Energy Research & Social Science*, DOI: 10.1016/j.erss.2017.04.012
51. Veiligheidsbeleving, gezondheid en toekomstperspectief van Groningers – Wetenschappelijk Rapport #1, Groningen Perspectief, Prof. T. Postmes, Dr. K. Stroebe, Drs. J. Richardson, Drs. B. LeKander, Dr. F. Oldersma, 15th July 2016
52. Veiligheidsbeleving, gezondheid en toekomstperspectief van Groningers – Wetenschappelijk Rapport #2, Groningen Perspectief, Prof. T. Postmes, Dr. K. Stroebe, Drs. J. Richardson, Drs. B. LeKander, Dr. F. Oldersma, Dr. J. Broer, Dr. F. Greven, 7th February 2017
53. Veiligheidsbeleving, gezondheid en toekomstperspectief van Groningers – Wetenschappelijk Rapport #3, Groningen Perspectief, Prof. T. Postmes, Dr. K. Stroebe, Drs. J. Richardson, Drs. B. LeKander, Dr. F. Oldersma, Dr. J. Broer, Dr. F. Greven, 3rd July 2017
54. Het meten van de gevolgen van aardbevingen op de leefbaarheid in Groningen – een methodologische review naar leefbaarheidsonderzoeken, Peter Lugtig, Emma ter Mors and Jelke Bethlehem, 7 July 2017
55. Maatschappelijke Effecten Inventarisatie van aardbevingen in Noordoost-Groningen - Inventarisatie, Royal Haskoning DHV for NAM, 11th February 2016
56. Maatschappelijke Effecten Inventarisatie van aardbevingen in Noordoost-Groningen 2016, Tweede Inventarisatie, 2016, Royal Haskoning DHV for NAM, 1 March 2017

3 Research into Induced Seismicity in Groningen

The “Study and Data Acquisition Plan” describes the objectives and interdependencies of all studies in the research program into induced seismicity led by NAM. The first edition of the plan was shared with SodM and the Ministry of Economic Affairs in November 2012 and made public in January 2013 (Ref. 1). Since then the plan has been updated regularly (Ref. 2). The last update was issued April 2016, together with Winningsplan 2016 (Ref. 3). An update of progress and schedule was issued December 2016 (Ref. 4).

The plan is coordinated by NAM, and executed in close collaboration with a large group of independent universities, knowledge institutes and academics worldwide. In this chapter, the scope, objectives and structure of the “Study and Data Acquisition Plan” will be presented, with emphasis on the assurance processes in place to safeguard the objectivity of the study results.

Objectives of the Studies and Data Acquisition Plan

The main objectives of the Study and Data Acquisition Plan are to:

1. Understand the impact of the earthquake hazard on buildings and other structures and the subsequent impact on safety of the community;
2. Perform a fully integrated Hazard and Risk Assessment for the Groningen region, with all uncertainties fully and consistently recognised and quantified;
3. Identify, evaluate and develop mitigation options to reduce safety risk:
 - Production measures, i.e. changes in the production from the field
 - An optimised Structural Safety Upgrading program:
 - Identify buildings and/or building elements that pose a safety risk
 - Establish optimal structural upgrading methodologies
 - Measures for industry and infrastructure.

Other important objectives are to:

4. Discuss the merits of alternative scientific views, and initiate additional studies and/or data acquisition to promote consensus amongst the knowledge institutes;
5. Monitor compaction, subsidence and seismicity;
6. Continuously improve our understanding of the physical mechanisms leading to induced seismicity and the resulting hazard;
7. Reduce the uncertainty in the hazard and risk assessment.

To achieve these objectives, NAM mobilized the support of universities, knowledge institutes and laboratories and sought the assistance and advice from external experts for each relevant expertise area. The main institutes involved in the research are listed in Appendix E, while the most prominent experts and their roles are listed in Appendix D. It is important that the results of the studies are shared with the scientific community and the inhabitants of Groningen, and safety risks are presented in a transparent manner, in order to minimize the gap between the risk assessment and perceived risks as much as possible.

Scope of the Studies and Data Acquisition Plan

The research areas included in the Study and Data Acquisition Plan are:

- Changing reservoir pressure (depletion) in response to gas production
- Reservoir compaction in response to pressure depletion
- Generation of seismicity at faults (earthquakes) due to reservoir compaction / stress changes

- Movement of the ground surface, due to earthquakes
- Response of buildings to the movement of the ground (i.e. building damage)
- Negative impact on safety of people residing in or near buildings, caused by severe damage or collapse of these buildings.

By investigating these areas, an integrated view emerged of the possible consequences of gas production from the Groningen field. The impact is expressed in risk metrics such as local individual risk, but also potential building damage. This type of information is of critical importance to be able to take decisions on future gas production and to take measures to mitigate the associated risks for people and buildings in the Groningen region.

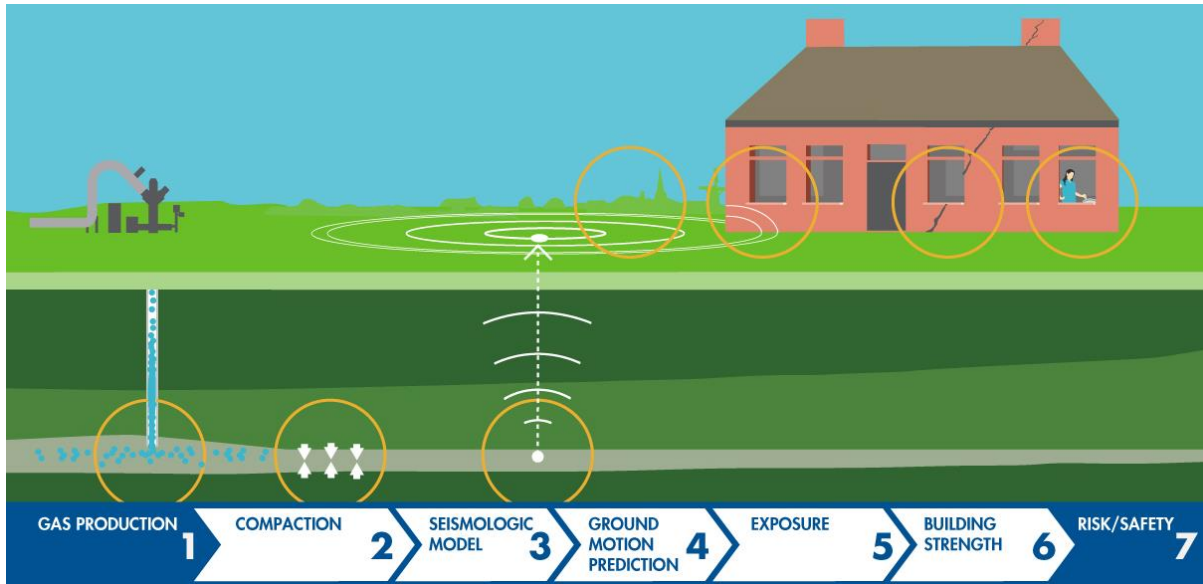


Figure 3.1 Causal chain from gas production to safety of people in or near a building. The personal risk assessed by experts can be very different from the risk perceived by the community.

Figure 3.1 shows the causal chain of processes starting with gas production and ultimately leading to the consequences in terms of risk. The first part (steps 1 to 4) requires detailed knowledge of the deep geology of the gas reservoir. The second part (steps 5 and 6) requires knowledge of the buildings and presence of people in the Groningen area. Areas of required knowledge and expertise range from geology to civil engineering. The final part (step 7) on risk and safety is described in the following.

Hazard and Risk assessment for induced Seismicity in Groningen

Risk Assessment Methodology

In a letter to the Minister of EZ dated 13th January 2014, SodM advised that NAM should prepare a fully probabilistic seismic risk analysis⁵ as soon as possible. Such a hazard and risk assessment was first published in November 2015, following a period of intensive data acquisition and study. This was the first risk assessment that was fully based on data acquired in Groningen.

⁵ Brief aan de Minister of EZ betreffende “aanbieding advies “wijziging Winningsplan 2013” en “meet- en monitoringsplan” van 13 januari 2013, sectie 3.4.6 Conclusies Bodembeweging: “NAM dient op zo kort mogelijke termijn een volledig probabilistische seismisch risicoanalyse uit te voeren.”.

The model used to assess hazard and risk resulting from induced seismicity in Groningen is based on the Probabilistic Seismic Hazard and Risk Assessment (PSHA) methodology introduced by Cornell in 1968 (Ref. 5), which has since then become the internationally recognised standard method for seismic risk assessments. This probabilistic risk assessment method fits well with the methods used to determine other risks, such as those resulting from floods, plane crashes around airports and industrial accidents. The implementation of the model is based on the Monte Carlo technique.

The PSHA methodology has been further developed since its inception in the 1960's (Ref. 6 to 9), and forms the basis of seismic risk assessments developed in the USA under the auspices of regulators like the NRC and USGS. Also, the HAZUS risk assessment method and tools of FEMA are based on a similar probabilistic method for seismic risk assessment. The method allows the assessed seismic risk to be compared to safety norms set by society. For induced seismicity in The Netherlands, the norms were developed by the "Committee Meijdam" (Ref. 10) and set by the Minister of Economic Affairs (MEA).

The methodology used for the assessment of hazard and risk (PSHA) for induced seismicity in Groningen and the implementation (Monte Carlo) are based on standardised accepted and established processes, with adaptations and innovation in view of the local situation as needed. Central to the probabilistic assessment of hazard and risk – in general and especially in current (new) safety policies in the Netherlands – is the identification, quantification and the consistent treatment of all uncertainties throughout the calculation chain of the Monte Carlo procedure. The data acquisition activities forming part of the study and data acquisition plan are therefore critical for the quantification of the uncertainties and for the reduction of the epistemic uncertainty.

Development of the Hazard and Risk Assessments for Groningen

Since 2012 several updates of the hazard and risk assessment for the induce earthquakes in Groningen have been prepared. The updates by NAM were in general prepared in response to requests from SodM and MEA and included in technical notes and supporting documentation for Winningsplan 2013 and Winningsplan 2016.

Hazard and Risk Assessments by NAM

The table below present an overview of the Hazard and Risk Assessments that have been issued by NAM since 2012:

Title	Scope of the Study	Date Issued
Winningsplan 2013 (Technical Addendum to the Winningsplan Groningen 2013; Subsidence, Induced Earthquakes and Seismic Hazard Analysis in the Groningen Field)	Fully probabilistic hazard assessment and scenario based risk assessment. (The hazard assessment was primarily based on the analogy with tectonic earthquakes in southern Europe)	29 th November 2013
Hazard Assessment for the Eemskanaal area of the Groningen field	Fully probabilistic hazard assessment for south-western area of the Groningen field.	1 st November 2014
Hazard and Risk Assessment for Induced Seismicity Groningen, Study 1 Hazard Assessment	Fully probabilistic hazard assessment based on Groningen measurements of ground motion.	1 st May 2015 (Version 1)
Hazard and Risk Assessment for Induced Seismicity Groningen, Study 2 Risk Assessment	Fully probabilistic risk assessment; not calibrated with building experiments.	1 st May 2015
Hazard and Risk Assessment for Induced Seismicity in Groningen - Interim Update November 2015	Fully probabilistic hazard and risk assessment. (Hazard assessment incorporated site-response based on local soil conditions. Risk assessment is calibrated with building	7 th November 2015 (Version 2)

	experiments and shake-table test for a terraced (URM) house.	
Hazard and Risk Assessment for Induced Seismicity in Groningen – Winningsplan 2016	Fully probabilistic hazard and risk assessment. (The hazard and Risk Assessment was shared in a Technical Addendum to the Winningsplan 2016.)	1 st April 2016

Hazard Assessments by KNMI

Independent hazard assessments for induced earthquakes in Groningen have been prepared by KNMI, which is the knowledge centre on seismicity in The Netherlands. In the scientific area of Ground Motion Prediction, KNMI has made use of some of the data acquired by NAM and has thoroughly reviewed and assured some of NAM's study results. They have prepared the following hazard assessments:

Title	Date Issued
Report on the expected PGV and PGA values for induced earthquakes in the Groningen area	December 2013
Probabilistic Seismic Hazard Analysis Induced Earthquakes Groningen	April 2014
Probabilistic Seismic Hazard Analysis for Induced Earthquakes in Groningen; Update 2015.	October 2015 (Version 1)
Probabilistic Seismic Hazard Analysis for Induced Earthquakes in Groningen; Update 2016.	June 2016
Probabilistic Seismic Hazard Analysis for Induced Earthquakes in Groningen; Update 2017.	June 2017

The ground accelerations of the KNMI hazard maps are in general similar to the calculations made by the NAM. The latest hazard map of the KNMI is compared to the map published by NAM. The NAM calculation is based a different method and another model for the occurrence of earthquakes. Despite these differences, the outcomes are within a margin of approximately 10% equal to each other. That difference is small (0.01-0.02g) for these calculations.

The seismic model that the NAM uses is partly based on production scenarios - the volumes of gas extracted from the reservoir - while the KNMI relies solely on the historically observed seismicity. The results of the calculations of the KNMI therefore provide an independent verification of the NAM hazard calculations.

Assurance of the Hazard and Risk Assessment for Groningen

NAM clearly has a vested economic interest in the outcome of the research program into induced seismicity in Groningen. A strong sense of suspicion or distrust regarding the study results is therefore to be expected, and is considered reasonable and even essential. NAM could in principle have tried to deliberately steer the research into certain directions. Furthermore, biases of the researchers could have influenced the results.

NAM has taken extensive transparency and assurance measures to ensure the quality of the research, to avoid biases that impact the conclusions and to safe-guard the integrity of the research and the objectivity of the outcomes:

- The research is as much as possible based on data acquired in the Groningen area. In chapter 4, an overview of the data acquisition projects of the NAM-led in the “Study and Data Acquisition Plan” is given.
- The acquired raw seismic earthquake data has been made available to independent researchers. Appendix F lists the academics that have requested and received raw (unprocessed) data acquired in Groningen. The distribution and sharing of the seismic earthquake data will in future be available through the EPOS (European Plate Observation System) without any involvement of NAM.
- All research is carried out by reputable experts and leading research institutes. A list of the institutes taking part in the research is provided in Appendix E. The experts are listed in Appendix D.1. The researchers strictly adhere to the “The Netherlands Code of Conduct for Academic Practices” issued by the VSNU (Ref. 14). This also requires that all researchers are open and transparent about their funding and sources of data and acknowledge NAM’s contribution to the research.
- Studies are reviewed using a multi-layer assurance process involving the top scientists in each research field. This assurance process is described later in this chapter. The members of the assurance teams are listed in Appendix D.2.
- Study results are presented and discussed with the regulator (SodM) and their advisors.
- Results of the studies and reviews are shared in the public domain and available for download from a dedicated web-page. The reports are presented in a chronological listing and a browse functionality is available which directs to the reports on a topic of interest. All reports are listed in Appendix C. More than 100 reports have been issued into the public domain. Many of these address a very specific research question and are written by and for specialist experts on the subject.
- Research results are shared with the scientific community through conference papers, while novel research is published in reputable peer-reviewed papers. Appendix C.2.2 lists the most important conference papers submitted to date. The published peer-reviewed papers and an overview of reputable journals are provided in Appendix C.2.1.
- Several institutes carry out independent hazard and risk assessments. For instance, the hazard mapping by KNMI is independent from and complementary to NAM’s hazard and risk assessment. Also within TNO hazard and risk assessments are carried out in parallel. These independent assessments in general give results that are close to those achieved by NAM.

- Stimulate independent research. This is primarily a role (as per advice of e.g. the OVV) for the government and difficult for NAM to achieve, especially because any involvement of NAM might taint the perception of the independence of the research, leading to suggestion the research might not be objective. NAM has maintained deliberate separation from some study initiatives in order to ensure clear independence. However, NAM has made a “no-strings-attached” donation of 15 mln Euro to NWO for research into induced seismicity (Ref. 16).

Transparency

Relevant data on seismicity in Groningen are available on the web-site www.nam.nl and the “feiten en cijfers” webpage. This includes:

- Pressure data;
- Gas production volumes;
- Subsidence data;
- Earthquake locations both in (interactive) map view and in depth;
- Damage notifications and progress of the repair process.

Both basic raw data and finalized study reports are published in the public domain on www.nam.nl. The reports can be downloaded from:

<http://feitenencijfers.nam.nl/onderzoeksrapporten/>

Raw Seismic Data

To stimulate further research by other independent parties, the raw unprocessed subsidence and seismic data collected by NAM is made available on request to academic and non-academic researchers for analysis and study. These are often very large data sets which are too big to be downloaded from a website. Exchange of a hard disk is often the most practical approach to share this data. Appendix F lists all significant data exchanges with external independent researchers. This data is shared “no-strings-attached”. These researchers are under no obligation to share progress or results with NAM.

KNMI Data Portal

Another important source for data on induced seismicity in Groningen is www.knmi.nl, which contains acceleration data and geophone data for larger seismic events.

Analyse	Datum en tijd (UTC)	Plaats	Magnitude	Diepte (km)	Type aardbeving	Details
Reviewed	2016-01-26 22:22:33	Harkstede	1.5	3.0	Geïnduceerd	Detail page
Reviewed	2016-01-20 03:57:08	Woltersum	0.6	3.0	Geïnduceerd	Detail page
Reviewed	2016-01-19 13:19:07	't Zandt	0.6	3.0	Geïnduceerd	Detail page
Reviewed	2016-01-17 11:57:33	Siddeburen	1.5	3.0	Geïnduceerd	Detail page
Reviewed	2016-01-14 14:03:58	Sandkrug	2.9	3.0	Geïnduceerd	Detail page
Reviewed	2016-01-13 06:41:42	Siddeburen	1.3	3.0	Geïnduceerd	Detail page
Reviewed	2016-01-11 05:31:35	Froombosch	0.6	3.0	Geïnduceerd	Detail page
Reviewed	2016-01-07 05:25:55	Zuidbroek	1.6	3.0	Geïnduceerd	Detail page
Reviewed	2016-01-02 00:04:28	Sint-Annen	0.5	3.0	Geïnduceerd	Detail page
Reviewed	2015-12-25 04:19:36	Ten Post	1.3	3.0	Geïnduceerd	Detail page
Reviewed	2015-12-22 06:00:13	Bergheim	2.4	1.0	Geïnduceerd	Detail page
Reviewed	2015-12-15 07:43:55	Noordwolde (Gr.)	1.7	3.0	Geïnduceerd	Detail page
Reviewed	2015-12-15 00:01:50	Delfzijl	1.6	3.0	Geïnduceerd	Detail page
Reviewed	2015-12-14 02:47:45	Emmen	1.4	3.0	Geïnduceerd	Detail page
Reviewed	2015-12-13 15:18:13	Kantens	0.4	3.0	Geïnduceerd	Detail page

Figure 3.2 Example of data available on the website of the KNMI.

KNMI offers three services that provide direct access to seismological data from the KNMI operated geophone and accelerometer network:

1. Seismological and acoustic data portal; an interface with event information and raw data from the seismological station,
2. Rapid Raw Strong Motion Data portal for The Netherlands. A specialist interface for scientists and engineers to raw acceleration data and derived peak ground accelerations (PGA),
3. FDSN (International Federation of Digital Seismograph Networks) web services for direct access to continuous raw waveform data from the past 12 months. Earlier data can be downloaded around the time of specific earthquakes, or obtained for other time intervals by request to KNMI.

Figure 3.3 Seismological and acoustic data portal; an interface with event information and raw data from the seismological station.

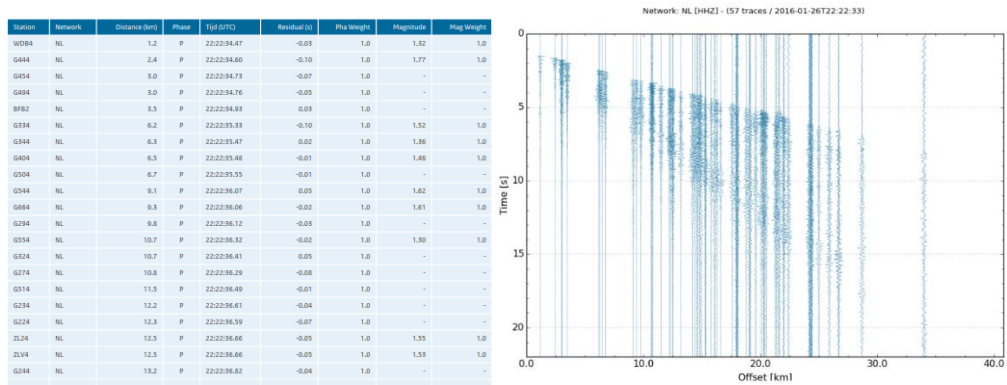


Figure 3.4 Example of data available on the website of the KNMI for the Harkstede earthquake of magnitude 1.5 on 26 January 2016.

Latest earthquakes last 12 months

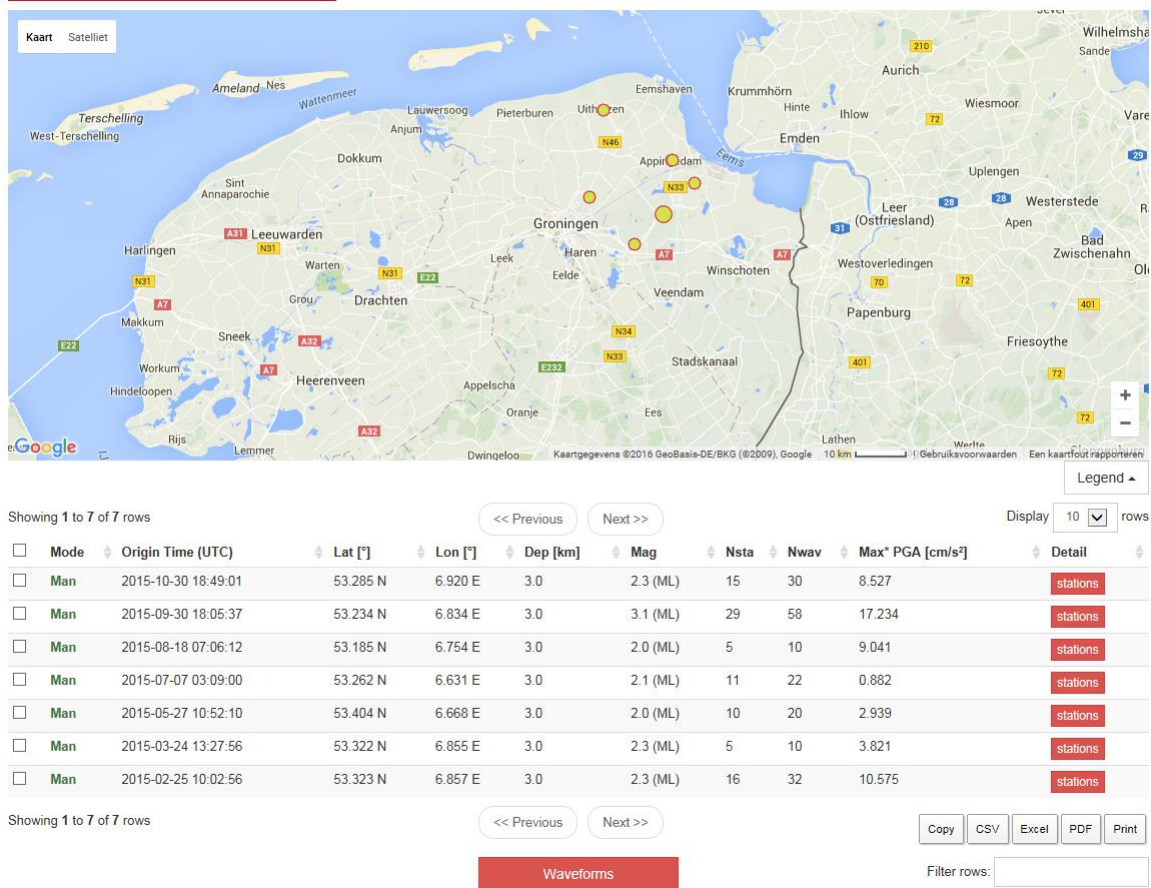


Figure 3.5 Example of data available on the website of the KNMI.

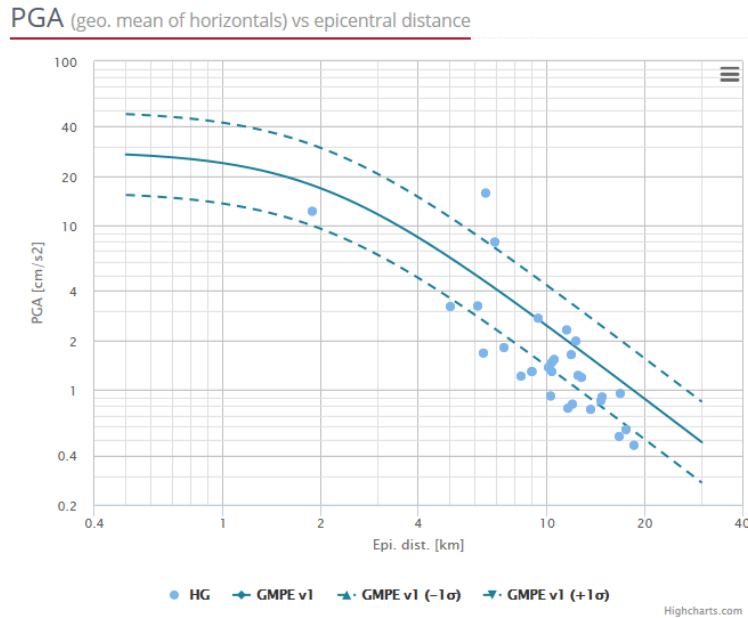


Figure 3.6 Example of data available on the website of the KNMI.

Study Reports

The technical reports describing the study results in support of the hazard and risk assessment have been published on www.nam.nl on the page “onderzoeksrapporten”. This allows scrutiny by experts from other stakeholders, including NGO’s.

A full list of all the reports that can be downloaded from this web-page is included in Appendix C. More than 100 technical reports can be downloaded. The reports can be accessed through a chronological list of all reports or through a browse functionality.

Peer-reviewed and Conference papers

Much of the novel research done on induced seismicity in Groningen as part of the research program led by NAM, is documented in detailed reports available at the NAM website and published in peer-reviewed journals. Publication in peer-reviewed journal provides additional assurance that the research is original and scientifically sound. These papers are published in reputable scientific journals with editorial boards consisting of highly respected independent experts recognised in their field. To promote independence of the reviewers working on behalf of the journal, their identity is kept anonymous. The peer review process is employed by the journal to determine an academic paper’s suitability for publication and maintain standards of quality. The review of these papers by peer scientists and academics provides additional credibility. A list of all peer-reviewed papers published in the public domain is included in Appendix C.2.2.

The peer review process can take several months, to in some cases more than a year. However, while papers are being peer-reviewed reports describing the work in detail are already shared at www.nam.nl. To share the study results as soon as possible, often the work is also presented at scientific conferences, poster sessions and workshops. The most important conference papers are listed in Appendix C.2.3.

Assurance Winningsplan 2016

Hazard and risk assessment is critically important to ensure that public safety is within agreed norms set by the Meijdam Committee (Ref. 10). It is therefore essential that the regulator, decision makers and the local community

have confidence in the assessment of hazard and risk. This requires oversight. With proper oversight, stakeholders can be confident that the data and the derived models are technically sound and that any remaining uncertainty has been adequately captured.

Therefore, each research study carried out by or on behalf of NAM is subjected to both internal review and various types of external and fully independent reviews and verification. In this process, six layers of assurance were implemented:

1. Internal NAM-assurance;
2. Independent assurance requested by NAM;
3. Independent assurance, requested by Ministry of Economic Affairs;
4. Independent assurance by regulator SodM ;
5. Independent assurance, requested by regulator SodM;
6. Independent critics;
7. Transparency.

1. Internal NAM-assurance

Internal technical assurance is carried out by internal experts from NAM and its shareholders (Shell and ExxonMobil) in those areas where in-house knowledge is available, primarily geology, geophysics, geomechanics and petroleum engineering. The results are incorporated in the studies and study reports.

2. Independent assurance requested by NAM

Independent review covering the complete work scope is carried out by independent external experts; that is, experts who are not affiliated with NAM in any way. The internal assurance of research on geology, geophysics and petroleum engineering, is followed by external assurance carried out by the consultancy company SGS Horizon. SGS is the world's leading inspection, verification, testing and certification company active around the world in many industries. For more information on SGS visit the site <http://www.sgs.co.uk/>. Their conclusions will be shared at the *onderzoeksrapporten* page of the nam-site.

Dedicated assurance teams have been assigned to different scientific areas. Appendix D lists the assurance teams and the members of the assurance teams. These dedicated assurance teams have been informed by extensive technical documentation and in workshops. Their recommendations have been incorporated in the technical reports (section further work) and in this document. The seismological models supporting the hazard and risk assessment, which are highly mathematical in nature, have been reviewed by Prof. Ian Main (of Edinburgh University). Prof. Main has prepared review letters, which have been shared. The studies on building fragility have additionally been reviewed by Ron O. Hamburger of the consultancy Gumpertz & Heger.

3. Independent assurance, requested by Ministry of Economic Affairs

For both Winningsplan 2013 and Winningsplan 2016, the Minister of Economic Affairs has installed dedicated assurance committees to provide an additional layer of independent scientific assurance for the studies supporting hazard and risk assessments for these Winningsplans. The Minister of Economic Affairs has set up the Technische Begeleidingscommissie Ondergrond (TBO) and the Technische Begeleidingscommissie Bovengrond (TBB) for Winningsplan 2013 and the Groningen Scientific Advisory Committee (SAC) for Winningsplan 2016.

These committees monitored and reviewed the investigations executed out by NAM or its contractors as part of the development of the Hazard and Risk Assessments and ensure the quality, completeness and impartialness of these investigations. The members of SAC were as follows:

- Drs Lucia van Geuns, TNO and KNGMG; chair
- Professor Rune Holt, NTNU & SINTEF; Rock Mechanics
- Dr Stefan Baisch, QCON; Induced Seismicity
- Dr Hein Haak, Algemene Bestuursdienst; Risk management
- Professor Jan Dirk Jansen, TU Delft; Subsurface Modelling and
- Dr Iunio Iervolino, University of Naples Federico II; Structural Engineering

Independent observers:

- Dr Jaap Breunese, TNO-AGE
- Dr Bernard Dost, KNMI
- Dr Hans de Waal, SodM

These assurance committees stimulated the sharing of information between all parties to ensure that available knowledge and information is used to develop broadly shared views where possible. To enhance the efficiency of the process, SodM, TNO and KNMI attended workshops as observers. The SAC monitored and reviews the (intermediate) results of the study and data acquisition program. The SAC also has the right to propose adjustments to the investigations. The SAC reports its findings and suggested adjustments to the Ministry of Economic Affairs.

The Committee is supported by Expert Groups. Depending on subject and required expertise, Expert group members have been appointed to discuss detailed definition, execution and technical progress of the various investigations. Additional members and observers of the expert groups are:

- Brecht Wassing, TNO
- Raphael Steenbergen, TNO and NEN-NPR
- Karin van Thienen-Visser, TNO-AGE
- Hans Roest, SodM
- Annemarie Muntendam-Bos, SodM
- Ilse de Vent, SodM

Since its establishment by the Minister of Economic Affairs, the Scientific Advisory Committee has organized three 2-day workshops, with NAM and 9 expert meetings. The SAC reported their review of the Hazard and Risk Assessment report of November 2015 together with findings and recommendations to the Ministry of Economic Affairs on the 1st December 2015. This SAC report can be downloaded using the following link:

<https://www.rijksoverheid.nl/rijksoverheid/rapporten/progress-note-groningen-scientific-advisory-committee/progress-note-groningen-scientific-advisory-committee.pdf>.

In its report, the SAC notes: *“The SAC members are impressed by the quality of the work performed within the project, which is of high scientific level. NAM/Shell/contractor staff involved are genuinely aiming for a best possible hazard and risk quantification within the constraints of time and data available. The researchers involved are open-minded and willing to communicate and discuss the results of their work.”* The SAC also offers a large number of valuable recommendations requiring further studies. These have been used to prepare the current *“Continued Study and Data Acquisition Plan Induced Seismicity in Groningen for Post-Winningsplan 2016”*.

4. Independent assurance by regulator Staatstoezicht op de Mijnen (SodM)

The mission of SodM is *“Staan voor veiligheid en gezondheid van burgers en werknemers, bescherming van het milieu en zorg voor onze natuurlijke hulpbronnen. Dat is de missie voor het toezicht dat SodM houdt op de delfstoffenwinning in Nederland.”* (sodm.nl). As part of this role the studies of the NAM research program are reviewed by the supervisory body SodM and their advisors TNO-AGE and KNMI. Experts of these organisations are primarily informed by experts conducting these studies through the SAC workshops and expert meetings. Additional

data is also shared. For instance NAM has shared the static and dynamic model of the Groningen gas reservoir with TNO-AGE.

SodM has requested at times additional studies from TNO-AGE, KNMI and CBS to verify the studies conducted as part of the NAM research program. The reports prepared by TNO-AGE can be downloaded from www.nlog.nl (a website maintained by TNO) or <https://www.sodm.nl>.

5. Independent assurance requested by regulator (SodM)

SodM has engaged international experts to provide technical advice and review the NAM report “Hazard and Risk Assessment – Interim Update November 2015). These were technical experts from the Swiss Seismological Survey (SED, Schweizerischer Erdbebendienst) and the U.S. Geological Survey (USGS).

Knowledge Program Impact of Mining (KEM Kennisprogramma Effecten Mijnbouw)

Recently, an expert panel, Knowledge Program Impact of Mining, has been installed to advise SodM and MEA on the development of knowledge of the impact of mining activities. The panel of experts will report annually on the progress of knowledge development, the independence of research and the possible effects of mining and thus plays a crucial role in the development of the knowledge program. The panel consists of independent experts Stefan Wiemer, Junio Iervolino, Frank Baaijens (chairman), Robert Zimmerman and Ipo Ritsema (secretary).

6. Independent critics

Several independent observers have made critical comments on the hazard and risk assessment in the media or through blogs on the internet. An effort has been made to collect these comments, to address these and to incorporate valuable suggestion in this plan. Recommendations to improve the study plan by Prof. Manuel Sintubin of the Catholic University in Leuven (Belgium) in his blog:

<https://earthlymattersblog.wordpress.com/category/earthquakes/induced-seismicity/>

deserve special mention here. Also technical recommendations by other critics like Drs. Peter van der Gaag and Ir. Adriaan Houtenbos have been addressed where possible.

Proposal for future assurance

NAM proposes to continue to work with the current framework of 7 layers of assurance, but to strengthen the entire assurance system by subjecting all future studies to a rigorous assurance based on application of the SSHAC (Senior Scientific Hazard Analysis Committee) Level 3 process. This is the ‘gold standard’ for oversight. This would cover all scientific studies into induced seismicity in Groningen.

The SSHAC process for multiple-expert assessment of hazards was developed by the US Nuclear Regulatory Commission (USNRC), US Department of Energy (DOE) and Electric Power Research Institute (EPRI). These institutions saw themselves confronted with two widely diverging seismic hazard studies for nuclear power plant sites in central and eastern United States. There were also very large divergences among the individual experts within each study. The SSHAC concluded that the problem resided not in technical details of the studies but in the lack of clear procedural guidelines for how to conduct such studies.

The original SSHAC guidelines were issued in 1997 as USNRC publication NUREG/CR-6372, in which procedures were laid out for conducting multiple-expert hazard assessments with clearly defined roles and responsibilities for all participants and with the common goal of capturing the full range of epistemic uncertainty. Four study levels were proposed with the complexity and effort increasing from Level 1 to Level 4 together with a corresponding increase in the likelihood of achieving regulatory assurance.

The SSHAC Level 4 process was applied to the assessments of seismic and volcanic hazards at the Yucca Mountain radioactive waste repository in Nevada and in the PEGASOS project for seismic hazard assessment at nuclear power

plant sites in Switzerland. A review after 15 years of experience in applying the SSHAC guidelines was documented in the following report “Implementation of the SSHAC Guidelines for Level 3 and 4 PSHAs—Experience Gained from Actual Applications, by Thomas C. Hanks, Norm A. Abrahamson, David M. Boore, Kevin J. Coppersmith, and Nichole E. Knepprath (U.S. Geological Survey Open-File Report 2009-1093)”, which can be downloaded using the following link to the website of the USGS:

<http://pubs.usgs.gov/of/2009/1093/of2009-1093.pdf>

A key conclusion from the review was that the Level 4 process has proved to be somewhat cumbersome and that detailed implementation guidelines were needed for Level 3 studies. This led to the issue of practical implementation guidelines by USNRC in 2012, which are available through this link:

<http://www.nrc.gov/reading-rm/doc-collections/nuregs/staff/sr2117/>

In these new guidelines, USNRC makes no distinction between Level 3 and 4 studies in terms of regulatory assurance and views both processes as equally valid approaches. The SSHAC Level 3 process has been successfully applied to many seismic hazard assessments for critical infrastructure, including:

- Seismic source characterization for PSHA at all nuclear sites in central and eastern United States, CEUS-SSC (completed 2012)
- Probabilistic seismic hazard analysis (PSHA) for hydroelectric dams in British Columbia, Canada (completed 2013)
- PSHA for the DOE Hanford site in Washington State, USA (completed 2014)
- PSHA studies for the Diablo Canyon (California) and Columbia Generating Station (Washington) nuclear power plants in response to USNRC 50.54(f) Fukushima response plan (completed 2014)
- PSHA for the Thyspunt nuclear site in South Africa (completed 2013)
- PSHA for all nuclear power plant sites in Spain (2016-2019)

In addition to providing regulatory assurance, the SSHAC process accommodates the assurance needs of both scientific and academic experts (a key feature of the process is broad participation from members of the relevant communities), local communities and decision-makers. The clearly structured process of a SSHAC Level 3 study, subject to continuous independent peer review of both technical details and procedural adherence, is transparent, open to observation, extensively documented and widely viewed as the gold standard for multi-expert assessment of hazard (and perfectly amenable to extension to risk assessment as well). The process should, together with other stakeholders (e.g., NCG) be adapted to local circumstance and demands while respecting the basis requirements for compliance with the specifications of a SSHAC Level 3 study.

Summary

The studies performed as part of the NAM-led “Studies and Data Acquisition Plan” are funded by NAM. The Code of Conduct for Academic Practices (Ref. 14) does not prohibit funding by industry, but demands transparency of the funding. This we also require of academics working with us. In the acknowledgement of papers describing the studies, NAM’s role as provider of funds and/or data is always clearly stated.

Assurance and transparency processes have been put in place to guarantee objectivity of the study results. The book “Merchants of Doubt” (Ref. 15), which is in general very critical of industry funded research, concludes in the final summary that:

“So it comes to this: we must trust our scientific experts on matters of science, because there is no alternative. And because scientists are not (in most cases) licensed, we need to pay attention to who the experts actually are – by asking questions about their credentials, their past and current research, the

venues in which they are subjecting their claims to scrutiny and the sources of financial support they are receiving.”

We are convinced that “Studies and Data Acquisition Plan” is executed to the highest standards of scientific research and that the outcomes are objective.

References

1. Study and Data Acquisition Plan for Induced Seismicity in Groningen - Planning Report, Nederlandse Aardolie Maatschappij BV, Jan van Elk and Dirk Doornhof, November 2012,
2. Study and Data Acquisition Plan Induced Seismicity in Groningen for the update of the Winningsplan 2016, Nederlandse Aardolie Maatschappij BV, Jan van Elk and Dirk Doornhof, December 2014, submitted in March 2015
3. Study and Data Acquisition Plan Induced Seismicity in Groningen for the update post Winningsplan 2016, Nederlandse Aardolie Maatschappij BV, Jan van Elk and Dirk Doornhof, April 2016
4. Schedule for Study and Data Acquisition Plan Induced Seismicity in Groningen for the update post Winningsplan 2016, Nederlandse Aardolie Maatschappij BV, Jan van Elk and Dirk Doornhof, December 2016
5. Cornell C.A. (1968). Engineering Seismic Risk Analysis. "Bulletin of the Seismological Society of America", 58(5):1583-1606.
6. Scawthorn, C., 2007. A brief history of seismic risk assessment, in Risk Assessment, Modelling and Decision Support: Strategic Directions, A. Bostrom, S.P. French and S.J. Gottlieb (Editors), Springer-Verlag, Heidelberg New York, Tokyo.
7. Scawthorn, C., 2008. History of seismic risk analysis, Proceedings of the 14th World Conference on Earthquake Engineering, Beijing, China, Paper no. 10-0036.
8. Calvi, G. M., Pinho, R., Magenes, G., Bommer, J.J., Restrepo-Vèlez, L.F., and Crowley, H., 2006. The development of seismic vulnerability assessment methodologies for variable geographical scales over the past 30 years, ISET Journal of Earthquake Engineering Technology 43(3), 75-104.
9. Bommer, J. J., H. Crowley, and R. Pinho, A risk-mitigation approach to the management of induced seismicity, Journal of Seismology, Vol: 19, Pages: 623-646, ISSN: 1383-4649, February 2015.
10. Commissie-Meijdam, Eindadvies Handelingsperspectief voor Groningen Adviescommissie 'Omgaan met risico's van geïnduceerde aardbevingen', 14 december 2015
11. Probabilistic Seismic Hazard Analysis for Induced Earthquakes in Groningen, Update 2015, Koninklijk Nederlands Meteorologisch Instituut, B Dost, J Spetzler, June 2015
12. Probabilistic Seismic Hazard Analysis for Induced Earthquakes in Groningen, Update June 2016, Koninklijk Nederlands Meteorologisch Instituut, B Dost, J Spetzler, June 2016
13. Probabilistic Seismic Hazard Analysis for Induced Earthquakes in Groningen, Update June 2017, Koninklijk Nederlands Meteorologisch Instituut, B Dost, J Spetzler, June 2017
14. The Netherlands Code of Conduct for Academic Practices, VSNU, 2004
15. Merchants of Doubt – How a handful of scientists Obscured the Truth on Issues from Tobacco Smoke to Global Warming, Naomi Oreskes and Erik M. Conway, Bloomsbury Press, 2010
16. Overeenkomst ten behoeve van de uitvoering van onafhankelijk wetenschappelijk onderzoek – DeepNL, NWO and NAM, 2 October 2017

4 Data Acquisition

The observed seismicity in the Groningen area is scientifically exceptional in three important aspects. First, it is induced by the withdrawal of gas. Most of the seismicity taking place on earth is due to tectonic processes and most seismicity related to oil and gas activity is the results of injection of water or other fluids (Ref. 1). Second, the subsurface of the Groningen area consists of thick layers of poorly consolidated deposits, overlying a chalk sequence and a high-velocity salt-dominated sequence. The earthquakes originate in the sandstone reservoir below the salt. And third, the buildings in the Groningen area have been designed and constructed without consideration for the horizontal loads these buildings will experience during an earthquake. This means that the ground acceleration levels at which damage and certain structural consequences take place, tend to be lower in Groningen than in typical tectonically active regions.

These specific conditions in the Groningen area require that the hazard and risk assessment should best be based on local data specific for Groningen. This chapter describes data acquisition projects set out to obtain such data. Some of the data is routinely measured as part of the standard reservoir management process. But the focus will be on an extensive program of data acquisition projects carried out in the framework of the study and data acquisition program for induced seismicity. It will also be explained where these Groningen data are used as input for multiple studies in the NAM-led research program and studies of independent academics.

The main activities initiated to improve monitoring of compaction, subsidence and seismic activity in the field are briefly listed below, and will be described in more detail in the rest of this chapter:

1. **Gravimetric survey.** Acquisition over the full field area and surrounding aquifers.
2. **Extensive wireline logging and pressure measurements.** Acquisition in newly drilled wells near Borgsweer, Zeerijp (two wells) and Bedum, including acquisition of shear and pressure wave velocity data over the full length of three of these well.
3. **Coring.** Coring of a large section of the gas- and water-bearing part of the Rotliegend and Carboniferous formations in Zeerijp-3A, followed by an extensive petrophysical, geomechanical and petrographic analysis program.
4. **10 GPS stations.** Installed at NAM locations throughout the Groningen field to continuously monitor both the vertical and the horizontal component of subsidence. Some 23 additional state-of-the-art GPS stations with InSAR reflectors are planned to be operational early 2018.
5. **Real-time compaction monitoring fibre optic cable.** Installation of a real-time compaction monitoring device (fibre-optic cable) in the Zeerijp-3A well, measuring temperature and compaction along the well trajectory. The same device will also be used for monitoring of micro-seismic events, when the next generation of seismic interrogation units becomes available.
6. **69 geophone wells with accelerometers at surface and 10 accelerometer stations.** Extension of the (existing) passive seismic monitoring network, to improve the resolution over the whole Groningen field. Four broadband geophone stations will be drilled in 2017 and are expected to be online early 2018. This network is operated by KNMI.
7. **Three temporary and two dedicated vertical geophone arrays.** Installation of a geophone array over the reservoir section in deep wells located in the Loppersum area, to improve the determination of earthquake hypocenters:
 - a. Temporary geophone arrays were placed at and around the reservoir interval (at 3 km depth) in two deep observation wells in the Loppersum area (Zeerijp-1 and Stedum-1) and near Harkstede (Harkstede-2A).
 - b. The temporary geophone arrays in the Loppersum area were replaced in 2015 by permanent seismic monitoring arrays in two newly drilled wells (Zeerijp-2 and Zeerijp-3A).

8. **Detailed map of the composition of the shallow subsurface.** This map was primarily compiled from CPT data followed by an extensive soil property measurement campaign.
9. **Measurements with a flexible geophone network.** These are primarily measurements of the properties of the shallow subsurface (less than 800 m deep), but the results can also be used to address questions related to building response and vibrations caused by other sources than earthquakes.
10. **Installation of more than 300 accelerometers in the foundations of buildings.** A network of sensors to assess the vibrations experienced by the buildings at the time of an earthquake. The network is operated by TNO.
11. **Tiltmeters.** Tiltmeters have been placed in a farmhouse as a pilot to investigate the added value of tiltmeters.

The data acquired through the above activities form the basis of the current hazard and risk assessment and the research described in this study and data acquisition plan. All acquired seismic data are publicly available for additional analysis and are widely shared with academia around the world. A list of universities and knowledge institutes with whom this data has been shared is provided in Appendix E.

Improving the sub-surface model

Additional data acquisition activities include the continuous recording of wellhead pressures and produced gas volumes at the production clusters. Reservoir pressure and gas-water movement is regularly measured in dedicated observation wells. These field data are part of the routine Groningen reservoir surveillance and management program, but play an equally important role in the assessment of hazard and risk. They will be referred to in the remainder of this chapter where relevant.

The results of the wide variety of data acquisition activities are implemented in a three main themes within the study and data acquisition program. These are 1) improving the subsurface model, 2) subsidence and compaction, and 3) monitoring seismicity.

Gravimetric survey

A new gravity survey gathering data from 92 locations over the Groningen field was acquired in September 2015. The gravity survey was carried out by Quad Geometrics in consultation with TU Delft (Ref. 2). At each location, three measurements were taken. Previous gravity surveys in the Groningen field were carried out in 1978, 1984, 1988 and 1996. The 2015 gravity survey in combination with the reprocessing of historical gravity data resulted in measurable and interpretable gravity changes at a number of stations at in the Groningen field.

After correction for tides and local ground water levels, the small changes over time in the local gravity (time-lapse) could be used to evaluate water influx into the depleting gas reservoir. This provides a means for further constraining the reservoir model, by using the time-lapse gravimetric data as a history matching parameter. Measured gravity changes are consistent with GWC measurements and support more water influx than currently modelled in the North-East of the field, less water influx in the Stedum area, and depletion in the gas-bearing part of the Carboniferous. There is a fair amount of uncertainty related to the modelling limitations and gravity data itself. The survey will be repeated in the 2021-2023 time frame.

Wireline logging and pressure measurements in new wells

Two new seismic monitoring wells have been drilled in the Loppersum area and one new water injection well on the Borgsweer location. This provided an opportunity to acquire additional wireline log data in these wells (Ref. 3):

- Density over the full length of the well for calibration of the velocity model and determination of vertical stress,

- Sonic velocity of both shear and compressional waves over the full length of the well. Shear and compressional data have been taken at 360-degree phase to determine main stress directions and stress anisotropy,
- Formation evaluation logs such as resistivity,
- Image logging over the reservoir section for stress field direction,
- MDT pressure measurement.

The option of obtaining a formation water sample in the Zeerijp-3A well was discarded so as not to compromise its primary seismic observation objective.

Core

Approximately 200 m of core was taken from well ZRP-3A, covering the largest part of the penetrated Rotliegend and Carboniferous intervals. Samples of this core are now used for compaction and other geomechanical experiments at the University of Utrecht, the Shell laboratory in Rijswijk and the ExxonMobil laboratory in Houston. Experiments on fault (re-)activation are performed at the University of Utrecht (Ref. 4).

The core material is also used to characterize the textural and mineralogical composition of the reservoir rocks. These petrographic parameters are likely to affect or partially control reservoir properties and geomechanical behaviour at the micro scale. Furthermore, a formation water sample was successfully extracted from the core by centrifuging.

Subsidence and Compaction

Subsidence in the Groningen area is monitored by various surveying techniques. These are spirit levelling, PS-InSAR (Satellite Radar Interferometry), and GPS (as part of GNSS: Global Navigation Satellite System). In situ compaction at reservoir level is measured in observation wells by gamma ray markers and fibre-optic methods.

Spirit Levelling

This technique has been used for the Groningen field area since 1964, with a recent repeat interval of five years. Surveys are based on the specifications defined by RWS-DID (Ref. 5).

The method makes use of certified, self-registering, optical levelling instruments and barcode level staffs. Measurements are registered fully automatically in a registration and validation system defined by RWS-DID.

PS-InSAR

Since 2010, vertical deformation is also measured with PS-InSAR remote sensing technology, in conjunction with a number of spirit levelling trajectories at the surface, for validation.

Deformation is estimated from phase differences between the acquisitions of the persistent scatterers (Hanssen, 2001). The spatial resolution depends on the presence of natural reflectors, such as buildings. To obtain a precision comparable to levelling, potential sources of noise (such as atmospheric disturbance and orbital inaccuracies) need to be identified and corrected for. This requires a time series of satellite images (>20-25 images) and a dense distribution of scatterers. The rate at which deformation takes place is estimated, from InSAR observations, to be 0.5-2 mm/year (see Ketelaar, 2009).

The big advantages of the InSAR technique are its high temporal resolution (> 10x per year) and the dense spatial resolution. No survey crew is required in the field, as with spirit levelling, hence no disturbance of the area and no security risks. Moreover, the accuracy of PS-InSAR is comparable to levelling.

Global Positioning System Stations

Global Positioning System (GPS) stations have been placed at 10 Groningen field facilities: Eemskanaal, Froombosch, 't Zandt, Overschild, Tjuchem, Tankenpark Delfzijl, Zuiderveen, Stedum, Usquert and Zeerijp. One GPS station was already placed in 2013 on the Ten Post location. The new stations are recording since March 2014. GPS stations are continuously monitoring the horizontal and vertical components of movement of the ground surface. They are best placed on an existing building. Locations Stedum, Usquert and Zeerijp, did not have buildings, so had concrete constructions placed to anchor the GPS stations. Data is transferred from the GPS locations by 3G/4G modems.

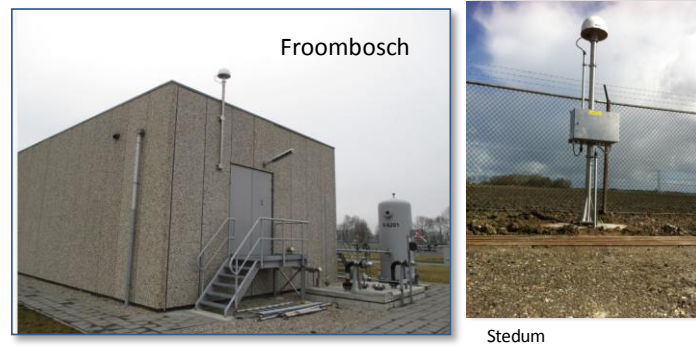


Figure 4.1 Example of a GPS station attached to buildings in the Groningen field (left) and of a GPS station anchored on a tripod construction in the Groningen field.

A series of newly developed GPS stations will be placed in the Groningen area in early 2018. These will also be equipped with a marker for levelling surveys and a reflector for the InSAR satellite positioning system. This will allow measurement of subsidence at the same location using the spirit levelling, InSAR and GPS techniques, in combination with the measurement of horizontal displacements.

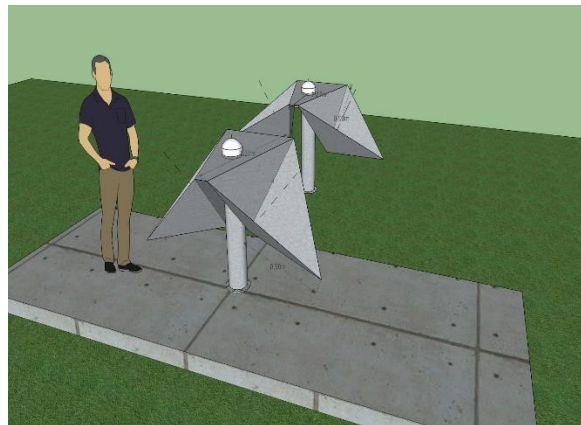


Figure 4.2 Design of the new integrated InSar reflector and GPS station.

Compaction in Observation Wells using Gamma-ray Markers

Since the nineteen sixties, gamma ray markers have been placed in several wells across the Groningen field to measure compaction. The markers are placed at regular depth intervals over the reservoir section (Ref. 6). Monitoring the change in the distance between markers over time gives insight into the in-situ compaction in the reservoir. The markers were originally installed in 11 wells across the Groningen field. Six of these are still accessible for surveying, but only three wells are logged regularly. The marker interval data have been recorded over several decades, and have always been reported as average reservoir strains.

A new technique for measuring in situ compaction has been implemented in the recently drilled well Zeerijp-3A. Here, a fibre-optic cable has been installed to measure compaction (strain) and temperature.

Compaction in Observation Well Zeerijp-3 using Fibre Optics

In well Zeerijp-3 a fibre-optic cable was run outside the casing and cemented in place with the casing. The cable allows various measurements along the well path:

1. DTS : Distributed Temperature Sensing,
2. DSS : Distributed Strain Sensing,
3. DAS : Distributed Acoustic Sensing.

A light signal is sent from surface through the glass fibre optic cable and back scattered waves are received back. Changes in the reflected intensity are caused by changes in the optical path length and are very sensitive to both strain and temperature variations of the fibre. The Real-Time Compaction Imager (RTCI) applies advanced fibre-sensing technology to monitor well integrity in real time without well intervention. At a later stage, the fibre-optic cable can also be used for acoustic sensing, but this application is still under development.

Monitoring Seismicity

The seismic monitoring facilities in the Groningen area have been extended significantly as part of the study and data acquisition plan. The primary objective is to increase the geomechanical understanding of the earthquake hazard. This requires high resolution mapping of seismicity and lowering of the earthquake detection threshold. The improved determination of the locations of earthquake hypocentres allows better tie-in with the fault model of the Groningen Field.

Extension of the KNMI passive Seismic Geophone Network

A seismic monitoring network has provided field-wide coverage over the Groningen area since 1995. The original configuration allowed for the detection and location of all events with a magnitude larger or equal to 1.5 ($M \geq 1.5$ events). This North Netherlands network consisted of 8 borehole stations, and was extended in 2010 with 6 additional stations and 18 accelerometers. The network is operated by KNMI. It recorded a catalogue of 233 $M \geq 1.5$ events between January 1995 and December 2015. KNMI reports horizontal location with uncertainties of about 0.5 km and the events are assumed to occur at a depth of 3km with an uncertainty range of 1 km.

The extension of this monitoring network commenced in 2013. This extended network has two key advantages over the original one: improved sensitivity and improved accuracy.

- Improved sensitivity: a more reliable detection and location of $M < 1.5$ events within the field allows more robust statistical analysis of the relationship between the number of earthquakes and gas production.
- Higher accuracy: reduced uncertainty in earthquake locations helps reveal their relationship with mapped faults. Together with the earthquake depth distribution relative to the reservoir this will improve the understanding of the causal mechanism of these earthquakes.

To deliver the earthquake data necessary to realize these objectives, the performance criteria for the monitoring network were set as follows:

- Reduce the magnitude of completeness⁶ from $M=1.5$ to $M=0.5$.

⁶ Magnitude of completeness is the smallest magnitude earthquake that can be identified and located irrespective of the location in the field at all times. Earthquakes with smaller magnitude might not be detected above the background noise.

- Locate all detected events with a standard horizontal error of less than 200 m and a standard vertical error of less than 500 m (this criterion might not be met everywhere in the field because of the locally complex geological configuration).

The extension of the passive seismic monitoring network included the installation of additional seismometers in 69 new boreholes on a 6x6km grid. Each monitoring borehole is drilled to a depth of 200 m and equipped with a 3 component geophone at 50, 100, 150 and 200 meters depth and one accelerometer at surface.

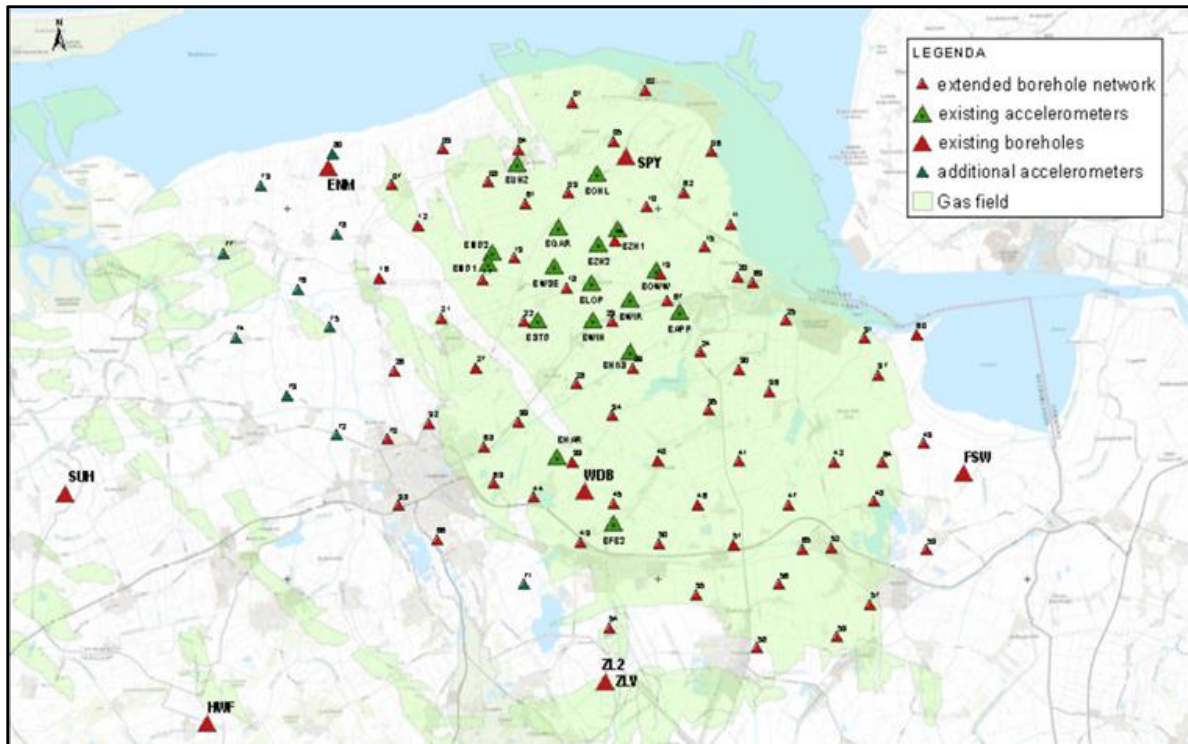


Figure 4.3 Extension of the shallow borehole geophone network with 69 stations and 10 accelerometers.

The 69 locations have been chosen in collaboration with KNMI. Local restrictions related to the impact of noise emanating from for instance railroad, pipeline or traffic have been considered, together with proximity to electricity and data cables and landownership. These practical restrictions have caused the grid to be slightly irregular. Densification of the grid has taken place in some areas to locally optimize the lateral or vertical event location accuracy, which is affected by the varying thickness of the Zechstein salt. Studies are in progress to refine the monitoring grid in more of these locations. Several additional stations (some 10) only equipped with an accelerometer have been placed mainly west of the field.

The operations to drill the additional shallow geophone boreholes commenced in May 2014 and finished in October 2014. Since then, the geophone stations gradually came on-line. The project was managed by engineering company Antea. Upon completion of the network the ownership was handed over to KNMI, who operates and maintains the network. The data is directly streamed to their offices in De Bilt.

Another four boreholes will be equipped with strong motion sensors (low frequency geophones) in order to record the signals for the largest potential events and enable ongoing recalibration/updating of the ground motion attenuation relations associated with high range potential earthquakes. The technical design of these four stations was done in close collaboration with KNMI and drilling of the last three wells is expected to be completed in 2017.

Subsurface vertical seismic arrays

Downhole seismic geophone arrays allow for monitoring at substantially reduced noise conditions thereby improving the magnitude detection threshold and the precision of the hypocentre determination. The vertical location of earthquakes is fixed by KNMI at a depth of 3 km, the average depth of the gas reservoir. Implementation of subsurface seismic arrays therefore provides the much needed increase in the accuracy in the vertical location of the detected events, albeit with a spatial detection threshold of approximately 5km. Thus far, the locations results indicate that all events do indeed occur within the reservoir interval, supporting the KNMI location solutions.

The study and data acquisition plan included the drilling of two dedicated wells for installing permanent seismic arrays at depth. Because drilling such wells requires significant preparation time, it was decided to firstly install temporary arrays in existing observation wells in the Loppersum area to accelerate the data acquisition process.

It should be noted that the deployment of down-hole sensors has shown to be challenging due to the harsh operating conditions, with elevated pressure and temperature in a complex completion fluid chemistry. Proper engineering of the downhole recording instruments as well as the wellbore itself is therefore essential.

Temporary vertical seismic arrays

Temporary seismic arrays were installed in wells Stedum-1 and Zeerijp-1. Both wells were drilled more than 35 years ago, and were not initially designed as seismic observation wells. The downhole seismic arrays were installed without performing a workover, whilst a more permanent seismic monitoring option in dedicated wells was developed (see next section). Advantage of this solution was deployment at short notice. However, the disadvantage is that the vertical coverage was limited to the reservoir section only (below the tubing already installed in the well).

Based on the experience gained in Bergermeer (gas storage facility operated by Taqa), a system was designed and installed in October 2013. Two arrays were installed with 8 and 11 stations respectively, and with 30m station spacing. The installation required killing of the well to avoid gas inflow, followed by the installation of additional pressure control equipment, and communication and data collection equipment. The objective was to have the equipment operational until the permanent monitoring wells were in place. Continuous monitoring started immediately after installation; and data was made available via a GSM connection to KNMI and Magnitude-BakerHughes for further analysis.

The temporary geophone string installed in the Stedum observation well started to record data in November and in the Zeerijp well in December 2013. Both the Stedum-1 and the Zeerijp-1 geophone strings suffered from regular failures caused by the hostile operating environment. Despite these failures, valuable data on earthquakes in the Loppersum Area has been collected to date.

With the new seismic monitoring wells fully operational, data acquisition from the Stedum-1 and Zeerijp-1 wells has been phased out. Both observation wells will return to their original duties; monitoring compaction, reservoir pressure and water influx into the reservoir. The Stedum well has gamma ray markers and is one of three wells monitored regularly for compaction at reservoir level (see section on Compaction), while the Zeerijp-1 well is an important well for monitoring the aquifer influx from the Oldorp aquifer (pressure and TDT).

From 6th October 2016 until 6th January 2017, a third temporary downhole-array seismic monitoring campaign was completed at HRS-2A, close to the city of Groningen. The overall level of seismicity detected by this downhole array was low. A total of 191 minor earthquakes was detected, with a magnitude in the range from -2.0 to 1.4

The Harkstede array was able to detect events long distances away from the Groningen area (M=5.8 in Italy, M=4.5 in Poland, and M=3.8 in the Southern North Sea). This demonstrated the sensitivity of the downhole array, but also the seismic quiescence of the Harkstede area. Of the 55 internal earthquakes in the reservoir near the geophones, 3 events were also detected and located by the KNMI surface arrays, magnitude ranging from 0.2 to 1.4 (Ref. 9).



Figure 4.4 Temporal coverage of the seismic observations wells in Stedum, Zeerijp and Harkstede.

Permanent vertical seismic arrays

Two permanent subsurface arrays have been installed in the Loppersum area in wells ZRP-2 and ZRP-3A. These wells have been drilled as part of the data acquisition efforts of the earthquake study plan. They have sensors covering the lower Zechstein, the Rotliegend reservoir and the top of the Carboniferous. This results in a wider aperture for the monitoring setup compared to the temporary arrays, and improved interpretation options. The downhole array is designed for a target event magnitude range of $M=-2.5$ to $M=+1$ within a distance of 10 km from the borehole.

From an operational standpoint, using a geophone array in existing observation wells is complicated and requires special safety precautions. Replacing geophone strings in new wells is inherently safer as these wells are not perforated.

To date, the geophones in the two permanent wells have not been performing up to specs. Although data have successfully been gathered for many weeks, the geophones experience repeated failure. This lack of tool performance has triggered the initiation of a substantial joint effort between Avalon Inc. and NAM-Shell to pinpoint the root cause of the geophone failures with the ultimate goal to redesign the tool such that it can withstand the harsh reservoir environment for prolonged periods of time (a notional 12-month target has been proposed). Currently identified way forward, designed in close cooperation with the geophone vendors, is to change out the completion brine (KCI) for a different, less reactive composition (water). This was implemented in October 2017.

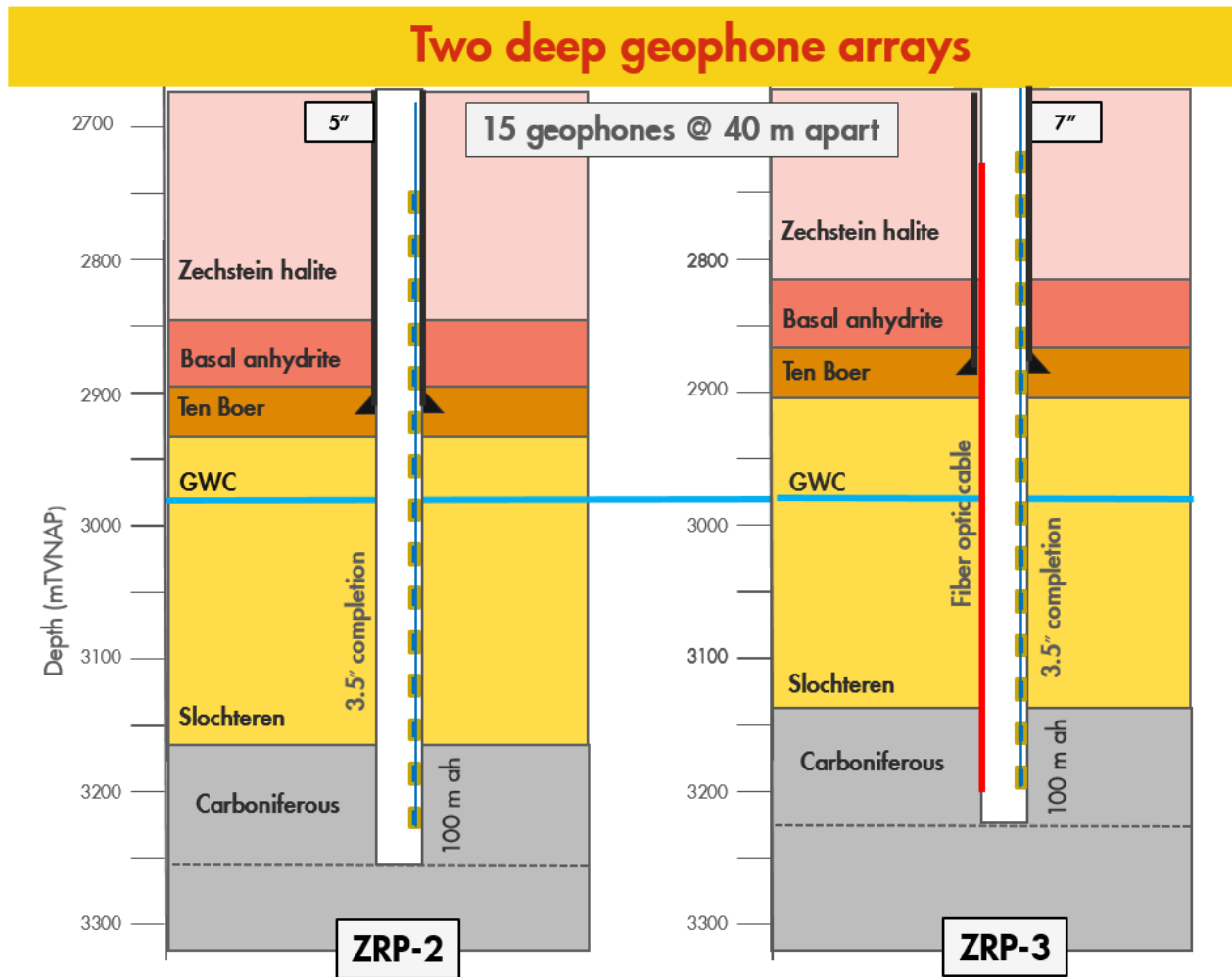


Figure 4.5 Downhole geophone setup in the two dedicated deep boreholes at Zeerijp.

Flexible Geophone Network

The shallow and deep borehole geophone network described above was extended in 2016 by a flexible surface geophone network developed by Rossingh Geophysics BV from Gasselte. The network currently consists of 400 nodes with 3 recording channels each, allowing the use of 400 3-component geophones or 1200 single ones. Each node consists of a separate battery pack, a data logger and a geophone. These nodes can be installed independently of each other allowing maximal flexibility, e.g. at variable distances from each other, in- and outside buildings, at different projects in parallel and for short and long (one year+) projects. There is a variety of data acquisition projects identified for the network. Most of these are in support of the development of the seismological model and the ground motion prediction methodology (Ref. 10).

Until October 2017, the network has been deployed over eight areas of 7 by 7 km each by using all 400 nodes in a grid of 350 meters spacing. The main objective is the assessment of the shear-wave (V_s) velocity in the shallow subsurface down to 800 m depth ($V_{s,800}$). Processing of the data from the first area by Sisprobe and Seismotech companies has now been completed.

Building Sensors

The deployed accelerometers consist of a tri-axial vibration sensor and a central unit supplied by GeoSig. The central unit is for signal conditioning (sensor conditioning, filtering) and transfer of the data to the TNO remote data centre.



Figure 4.7 Vibration monitoring system – recorder (left) and sensor (right)

Vibration is sampled continuously at 250Hz and stored in an internal buffer. When vibration exceeds a certain threshold level (set at velocity of 1 mm/s in accordance to the SBR guidelines)⁷ the Data Centre is notified by sending the time of triggering. At that time logging of the event starts with a pre-trigger duration of 10 seconds. After collecting data for 20 seconds (at 250 Hz) the time traces (one per channel) are instantaneously sent to the data centre (Fig. 4.9). In addition to the communication of measurements during the events, the vibration measurement system also sends a regular 'heartbeat' containing the peak vibration velocity and acceleration over the last minute. Examples of the heartbeat signal and a recording of a seismic events are shown in figure 4.8.

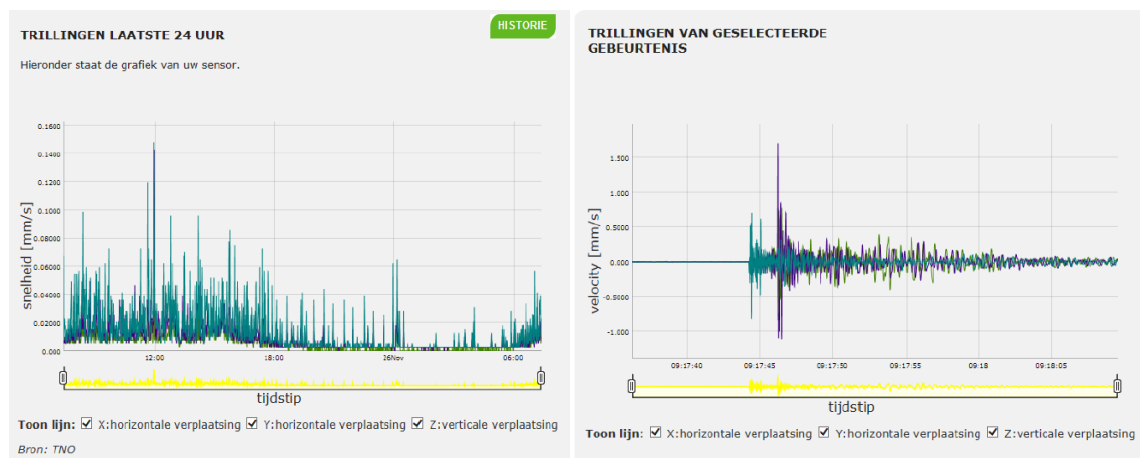


Figure 4.8 Example of a graph with results of heartbeat measurement (left) and of a graph with results of an event (right).

⁷ The trigger level of 1 mm/s is in the order of the strictest limits of the SBR directive for vibration damage. Other vibration sources like traffic may cause such, or higher, levels. These levels tend not to occur often but when they do, they may be relevant.

Building Inspections

Regular building damage inspections are carried out to improve the understanding of how sensitive buildings in the Groningen field area are for damage caused by earthquake vibrations. An initial inspection of damage on the outside of the building (e.g. cracks in exterior walls) is carried out as part of the sensor installation. During this initial inspection, all building characteristics that may become relevant for damage analysis at a later stage are logged. A repeat inspection is carried out after each significant earthquake to establish the additional damage caused by the earthquake.

The observed damage is then classified in a damage category that is, in turn, related to the vibration. By plotting the measurements of all the buildings in the monitoring network against the vibration velocity, relationships can be established between the two.

Data Transmission and Communication

The total accelerometer network consists of the building sensors and the TNO Vibration Data Centre, which collects and handles the measured data. Data is securely transferred from the building to this Vibration Data Centre using the internet connection of the building itself. The data is analysed and sent through to NAM, where it is published on the website www.nam.nl. There are limitations to the level of detail at which the vibration data can be shared publicly, for reasons of privacy of the house owners.

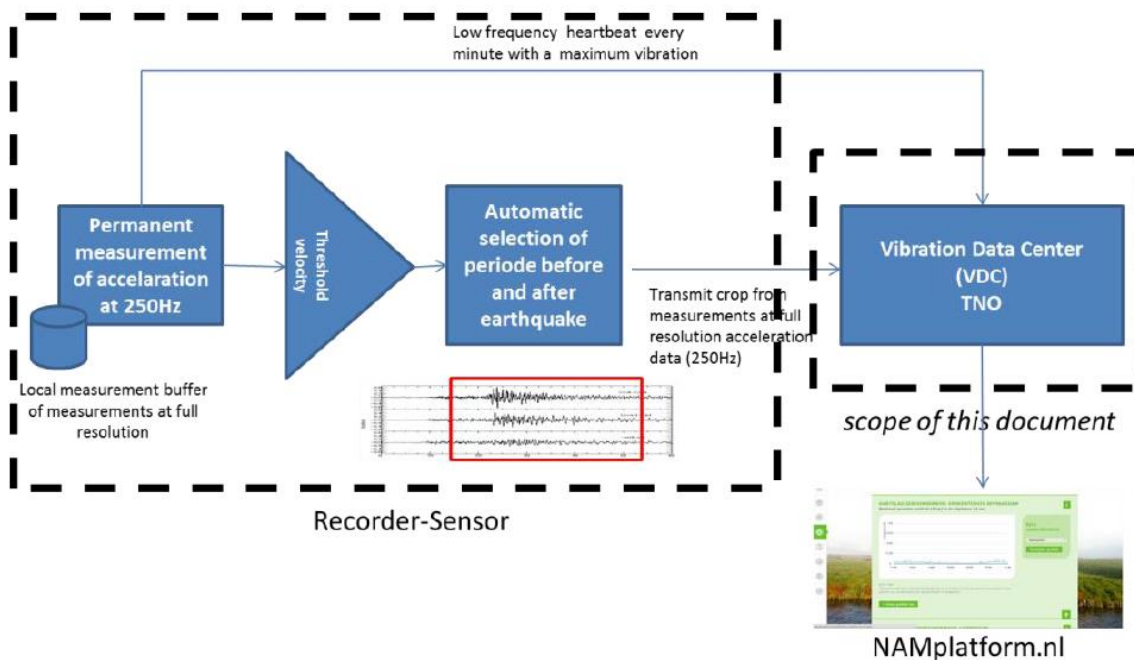


Figure 4.9 Data transfer from vibration monitoring system to Vibration Data Center (VDC)

References

1. Human induced Earthquakes, Gillian Foulger, Miles Wilson, Jon Gluyas and Richard Davies, Durham University and Newcastle University, July 2016.
2. Gravity monitoring of the Groningen gas field 2015, Quad Geometrics, Ola Eiken, April, 2016.
3. Petrographic study of well Zeerijp-3A (ZRP-3A) Final Report, Panterra Consultants, November 2016.
4. Hunfeld, L. B., Niemeijer, A, R, and Spiers, C. J., (2017), Frictional properties of simulated fault gouges from the seismogenic Groningen gas field under in-situ P-T-chemical conditions, Journal of Geophysical Research, 2017
5. RWS-DID, 'Productspecificaties Beheer NAP, Secundaire waterpassingen t.b.v. de bijhouding van het NAP, versie 1.1 van januari 2008'.
6. In-situ compaction measurements using gamma ray markers, Pepijn Kole, NAM, June 2015
7. Voortgangsrapportage Diepe Geofoons, Nederlandse Aardolie Maatschappij BV, September 2014.
8. A re-estimate of the earthquake hypo-centre locations in the Groningen Gas Field, Matt Pickering, March 2015.
9. Harkstede 2A microseismic monitoring summary, Jelena Tomic, NAM, February 2017
10. Wat gebeurt er met het Flexibele Gefoon Netwerk?, Stand van zake 1 maart 2017, Nederlandse Aardolie Maatschappij BV, February 2017, Jan van Elk & Dirk Doornhof
11. TNO Monitoringsnetwerk gebouwentrillingen – Analyse aardbevingen 2014 tot 2015, ir. H. Borsje, ir. J.P. Pruiksmā and ir. S.A.J. de Richemont TNO 2016 R11323/A, December 2016

5 From Production to Hazard

Introduction

The causal chain from gas production to building damage and personal risk was introduced in section 3.1. The current chapter further elaborates on the first steps of the causal chain starting with the production of gas from the reservoir to the movement of the ground. In the next chapter (section 6) the hazard will be addressed. The second section of the causal chain from ground movement to building damage and personal risk will be described in chapter 7. This is followed by chapters on building damage and personal safety.

Groningen gasfield

The Groningen field was discovered in 1959 by a well drilled near Slochteren (SLO-1). A general sense of urgency was felt by the Dutch Government in the development and marketing of the Groningen gas, as it was believed that there was only a limited window of opportunity for the utilization of this resource. It was generally thought that nuclear energy would replace fossil fuel within the near future (Ref. 1).

The Groningen field was initially developed by several production clusters in the southern part of the field. At the time, the full extent of the field was not known and it was thought that the entire field could be produced through these southern clusters. However, additional appraisal drilling in the Northern part of the field proved that the Groningen gas volumes were larger than previously assumed. Only by then it was realized the Groningen field was one of the largest onshore gas fields in the world (Ref. 2 and 3). Furthermore, pressure measurements indicated that the Northern part was declining in pressure with a significant delay (Figure 5.1), hence additional production clusters in the North were required. Production from the field commenced in 1963. In the early seventies, the rapid development of the field continued with several production clusters added in the Northern part of the field. Not only a total 29 gas production and processing locations (clusters and custody transfer stations or “overslagen”) were built by NAM, but Gasunie realized a gastransport network including thousands of kilometres pipeline to supply the whole Netherlands with gas from the Groningen field. Because the Groningen field produces gas with a different quality (as indicated by the heating value or Wobbe index of the gas) a separate pipeline network had to be built to deliver the gas to a dedicated gas market (Ref. 4).

Currently, the gas is produced through 20 processing locations (clusters) and 2 satellite production sites, each cluster consists of multiple wells (typically 8 to 12), gas treatment facilities and compressors. The production from the field causes the reservoir pressure to decline in a same manner as seen in most other gas fields (Fig. 5.1).

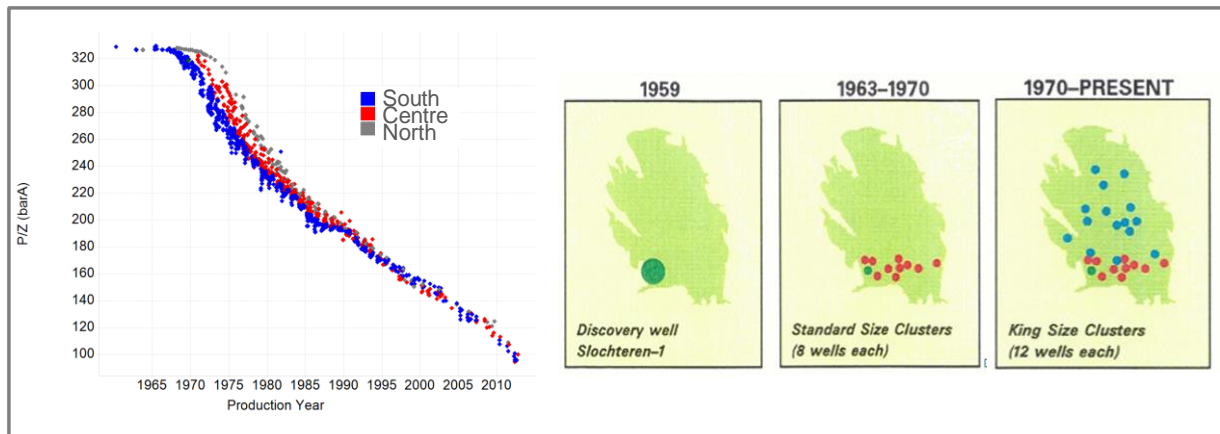


Figure 5.1 Phased development of Groningen field and historical pressures. This pressure data is available on Feiten en Cijfers at www.nam.nl.

Changed role of the Groningen field

After the first oil crisis in 1973 (Ref. 5), the Dutch government realized that nuclear energy would not replace fossil fuels within a foreseeable time frame and the rapid depletion of the Groningen field was not considered desirable any longer (Ref. 6 to 8). Therefore, the Small Fields Policy was introduced, which intended to stimulate the exploration and development of smaller gas reservoirs onshore and offshore in The Netherlands and thus conserving the Groningen gas as a strategic energy reserve.

The development of small fields resulted in a decrease of Groningen yearly gas production, with small fields providing base load (constant) production to the market and Groningen to cover for peak market demand (in cold periods). Resulting in a new role for the Groningen field the so called Swing producer role. The impact of the Small Fields Policy is illustrated in Figure 5.2.

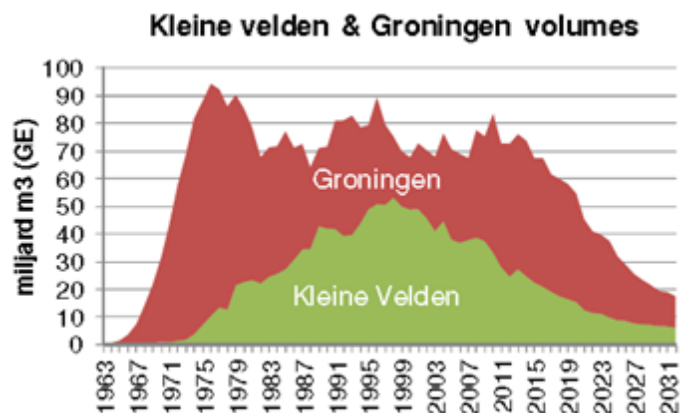


Figure 5.2 Annual contribution to gas production by the Groningen field and small gas fields ("kleine velden")

Groningen Field and Underground Gas Storage development

From the mid-1980's until 2014 a production philosophy was followed with an objective to minimize pressure differences in the field by balancing production from the various clusters in the Groningen field. This philosophy follows the principles of prudent operatorship and was first formalized in the Groningen Winningsplan 2003. In practice, this meant that the clusters in the North of the field, where the cluster density is lower and therefore in-

place volumes per cluster are larger, were produced throughout the year with the highest priority whilst clusters in the South of the field were when required (e.g. during winter), or at lowest priority.

This production policy depends on the relatively good connectivity between the different areas of the field. An exception to this is the relatively small South-Western part of the field where the reservoir pressure decline is lower than in the main area of the Groningen field.

Towards the end of the 1980's the Groningen field produced at full capacity. In the early 1990's field capacity decline was such that compression at production clusters would be required to have sufficient production capacity available in winter. By installing compression the wells are produced against reduced wellhead pressures. By then market predictions indicated that during the summer months the gas production from the small fields would exceed market demand, even with Groningen producing at minimum flow. In order to increase production capacity in winter and to be able to maintain Groningen production in summer, it was decided to develop Under Ground Storages (UGS). This is illustrated in Figure 5.3.

In the mid-1990's UGS's were developed by NAM (in Norg and Grijpskerk) and one by Amoco (later BP and currently TAQA) in Alkmaar. These UGS's are considered part of the Groningen system and are effectively managed as an extension of the Groningen main field (Ref. 9).

In 1998 the GLT project was initiated in which compression was installed on 20 production clusters (first cluster Tjuchem (1998) and last cluster Slochteren (2009)), two clusters were changed into satellites (Sappemeer connected to Tusschenklappen and Froombosch connected to Slochteren). The remaining production clusters (Midwolda, Nieuw-Scheemda, Noordbroek and Uiterburen) were suspended.

Over the years the contribution of the small gas fields and the production capacity of the Groningen field further declined leading to a more frequent utilisation of the UGS's to accommodate the fluctuating seasonal market demand. This led to the initiation of the UGS Norg expansion project, with the objective to increase working volume and production capacity. The UGS Norg expansion project was completed in 2013.

Further decline of reservoir pressure leads to additional compression requirement, or 2nd stage, in order to maintain production capacity. To prove the selected 2nd stage concept a first cluster (Schaapbulten) was reconfigured in 2013.

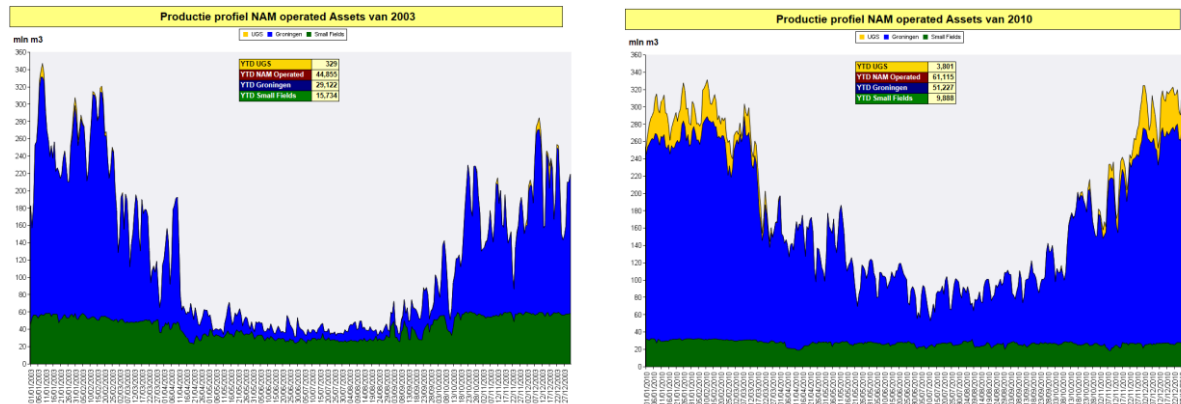


Figure 5.3 Intra-year production of NAM, 2003 versus 2010. (Small gas fields in green, Groningen main field in blue and the UGSs in yellow)

Groningen field production caps

To influence the successfulness of the Small Fields Policy a production cap for the Groningen field was imposed by the minister in 2006. The first cap limited production from the Groningen field to 425 Bcm over a ten-year period

(2006-2015) with an average yearly volume of 42.5 Bcm. In 2010 a second cap of 425 Bcm was imposed covering the years 2011 till 2020.

In an attempt to lower induced seismicity in the Groningen field, the Minister of Economic Affairs has imposed additional restrictions on the yearly production volumes from the Groningen field, described in the Instemmingsbesluit Groningen Winningsplan 2013 of January 2014 (Ref. 10), Wijzigingsbesluit of January 2015 (Ref. 11), Instemmingsbesluit Groningen Winningsplan 2016 (Ref. 12) and Wijzigingsbesluit of May 2017 (Ref. 13). Not only the annual volume but also regional distribution (regions East, Southwest, Eemskanaal, Loppersum) over the field was introduced in an attempt to reduce seismicity. Utilization of the five production clusters around Loppersum (Leermens, Overschild, de Paauwen, ten Post and 't Zandt) was restricted to a minimum.

A ministerial decision further limits production from Groningen field to 21.6 Bcm as from 1st October 2017. Based on an analysis by GTS contribution of 21.6 Bcm from Groningen field should be sufficient to cover market demand in an average-temperature year. To cover for colder years, an additional volume from Groningen is allowed based on the "Graaddagen" - formula proposed by GTS, described in article 2 of the Wijzigingsbesluit May 2017.

Operationalization of this formula is difficult due to the large statistical spread of number of graaddagen per year and the fact that the number of graaddagen is only known at the end of a gasyear, whereas demand for additional volume is typically in winter.

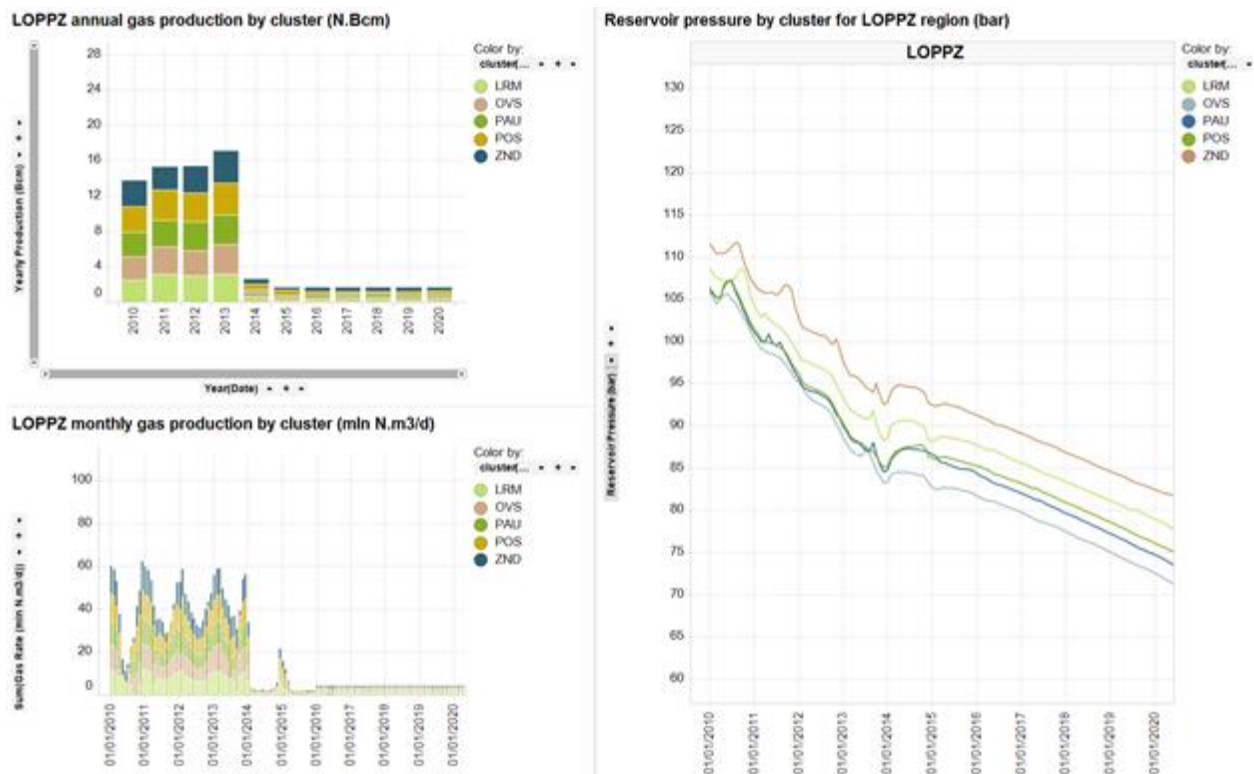


Figure 5.4 Historical production and forecast of gas production from the regions of the Groningen field.

Groningen Field – Production clusters and Production Regions



Groningen Field – Hydrocarbon Column Map (Slochteren Fm)

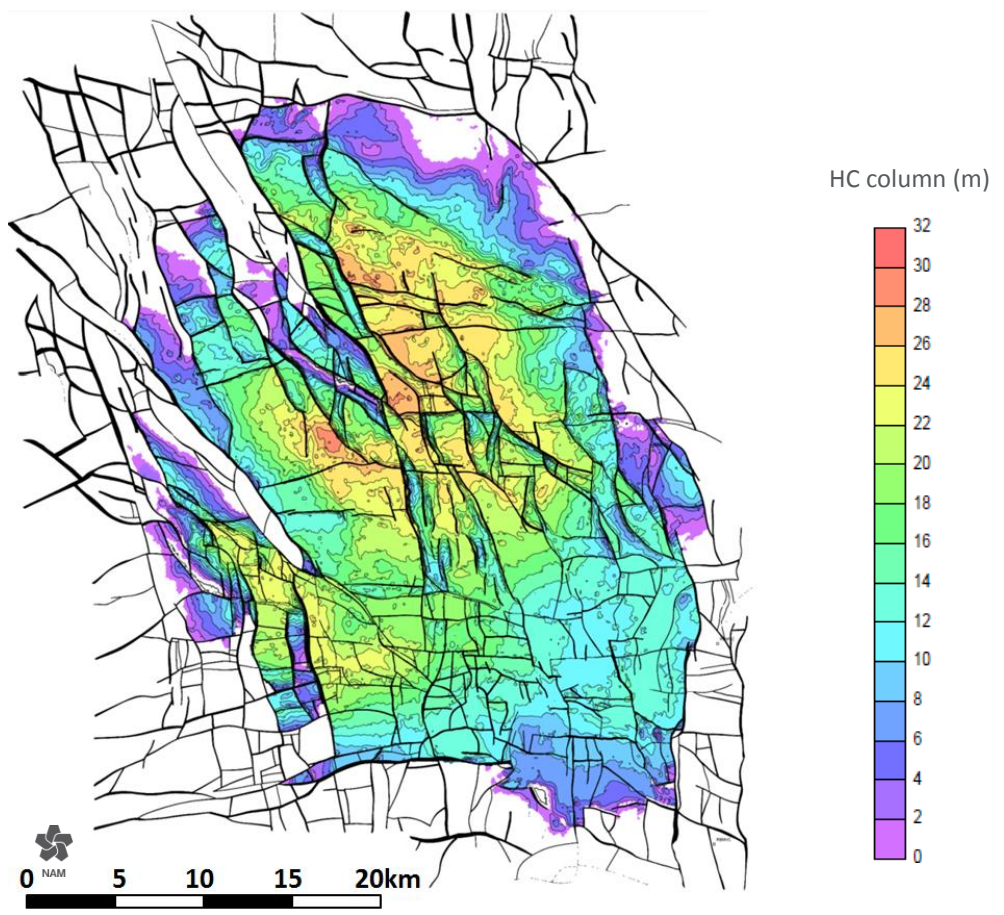


Figure 5.5 Production regions for the Groningen field, and Hydrocarbon column map. The constrained LOPPZ clusters are located in the most prolific area of the field (highest column thickness and lowest cluster density). The production cap imposed on the LOPPZ clusters caused an effective reduction of the Groningen field capacity by some 25%.

Groningen field production system

At the 20 production clusters, produced gas is compressed and processed. The clusters are connected via a pipeline network, the Groningen ring, via which gas is supplied to the national gas grid through seven custody transfer stations (a.k.a. “Overslagen”) (Fig. 5.6). Water and condensate is separated from the gas at the production clusters and transported via separate pipeline (Waco) to the Delfzijl tankenpark. At the custody transfer stations the gas is metered and delivered to the Gasunie Transport Services (GTS) pipeline system. Distribution of the gas over the custody transfer stations is controlled by GTS by manipulating pressure in the transportgrid. This distribution is mainly impacted by the geographical location of clusters and Overslagen. GTS is responsible for redistribution of the gas in the national grid to supply the market.

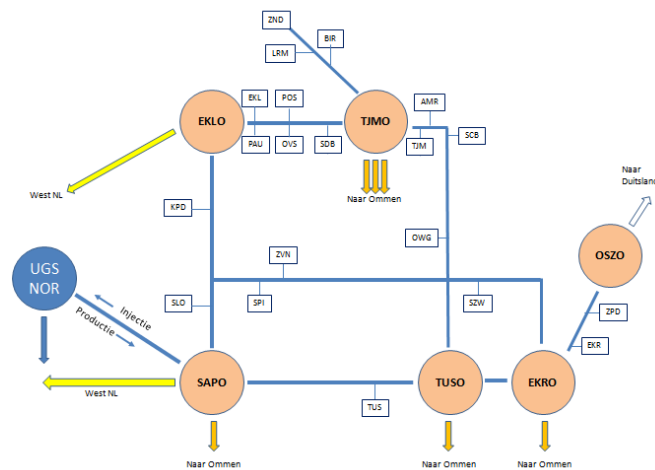


Figure 5.6 Schematic overview of the Groningen production system

The Underground Gas Storage (UGS) Norg is an integral part of the Groningen production system. The UGS is used to supply Groningen quality gas in periods of high capacity demand (winter) and is refilled during periods of low market demand (summer), resulting in a flattened production profile of the Groningen field. In 2015, the UGS capacity expansion project was completed and a dedicated pipeline (NorGroN) between the Groningen Ring and the UGS was taken into operation. One of the advantages of this dedicated pipeline is the possibility to increase the compressor suction pressure on UGS Norg resulting in a more efficient gas injection.



Figure 5.7 Areal overview of the Eemskanaal Cluster

Operational constraints

The system is operated within a set of contractual and technical constraints impacting the flexibility of the system, for instance related to distribution and gas quality constraints. Some of the constraints are listed below.

1. Operational constraints
 - Scheduled production stops, an extensive maintenance and inspection program is being executed in order to keep up the high reliability of the system. During maintenance periods production stops are required leading to lower available capacity. Historically periods in which maintenance, inspection, testing, and other activities are executed, are scheduled in summer.
 - Unscheduled production stops, unforeseen system failure can lead to (partially) shutdown of production clusters. Statistical analysis of historical data give insight in the number (and geographical position) of the clusters that should be available to guarantee production capacity with certain degree of certainty.
2. Minimum flow requirements. Both the Overslagen and the production clusters cannot be operated below a certain minimum flow. Production start from shut-in clusters requires time, whereas during start-up gas quality and capacity cannot be guaranteed. Restart of shut-in Overslagen requires close collaboration with GTS because of possible pressure differences up -and downstream the Overslag. Production clusters with back-up functionality cannot be shut-in but are kept at their minimum flow (Ref. 14).
3. Distribution constraints
 - UGS injection requirements. To achieve an efficient injection into the UGS Norg compressor suction pressure is kept as high as feasible. The dedicated NorGroN pipeline (between Overslag Sappemeer and UGS Norg) facilitates the possibility to manipulate the compressor suction pressure on UGS Norg, but specific set-up in the Groningen production system, impacting the operational flexibility in terms of distribution.

- Distribution over the Groningen ring. Distribution of the gas over the Groningen ring depends on inflow (production from clusters in the ring) and outflow (production in the GTS transport network via custody transfer stations). The outflow per custody transfer station is controlled by GTS and depends on market demand. An in-balance of inflow and outflow can result in excessive process (pressure) conditions leading to production failures.
- 4. Meet- & Regelprotocol (MRP). Observed seismicity might result in adjustments in the areal distribution of the gas production or reductions in production, and might lead to in balance of inflow and outflow conditions.
- 5. Gas quality. The gas needs to be delivered at the custody transfer stations within a very tight gas quality specification band. Gas produced from the Eemskanaal cluster has a different composition and a calorific content above the higher limit of the quality specification. This gas is currently brought to the required specifications by blending with gas from other clusters.
- 6. Other factors. Other factors and constraints impacting available capacity and/or system flexibility include ambient temperature, GTS system pressure and local demand and unforeseen unavailability of clusters.

Groningen reservoir model

Introduction

This section discusses the models built for characterizing the Groningen gas reservoir. The models comprise both the gas-bearing rock interval (or reservoir) and its immediately adjacent and underlying water bearing equivalents (the aquifers). The static model describes the structural framework, i.e. the top and base surfaces, natural faults and internal layering, and the reservoir properties such as porosity and permeability. This part of the reservoir model has been built in the software package Petrel (by the company Schlumberger). The dynamic model describes the flow of gas and water through the reservoir formations, due to the withdrawal of gas (and small volumes of water) and injection of water through wells. The dynamic model was built on top of the static model using the reservoir simulator MoReS (a Shell company software).

Construction of the current model of the Groningen reservoir model commenced in 2009 with the first release of the model ready early 2012. This version of the model is referred to as the Groningen Field Review model 2012 (GFR2012 in short). This model was reviewed and assured by SGS Horizon (Ref. 15) and used in Winningsplan 2013 (Ref. 16).

Since 2012, the reservoir model has been improved continuously with regular updates. The recommendations from the assurance review and comments by other external reviewers have been addressed in these updates. A very significant update was completed in 2015, to support the hazard and risk assessment for Winningsplan 2016 (Ref. 17). This update of the reservoir model has also been reviewed and assured by SGS Horizon (Ref. 18). Based on insights from the 2015 modelling exercise, a list of recommendations to further improve the Groningen dynamic model was issued as part of the study and data acquisition plan. These recommend changes were incorporated in the 2017 dynamic model update (Ref. 23).

The model updates have been carried out for a number of reasons:

- The availability of new data acquired since the last model update,
- Changing requirements for the model with increased focus on parameters controlling compaction, subsidence and seismicity,
- Opportunity to use and incorporate new developments in modelling software,
- Suggestions from model reviews by internal and external reviewers (incl. TNO-AGE and SodM).

Emphasis of these updates has been on collecting more data and additional data types and improving the calibration of the reservoir model with these data. This process of calibration of the model is often referred to as history matching of the reservoir model.

The main aim of the reservoir model of the Groningen field is to predict the flow of the gas and water through the reservoir and the areal and temporal pressure response of the reservoir to the extraction of gas from the reservoir. It is this pressure response that drives the reservoir compaction, which in turn is an essential driver for the seismicity. The model therefore covers the area of the gas reservoir and the adjacent aquifers, where a pressure drop could result. The model therefore covers a large area outside the gas bearing reservoir, especially towards the west. As a result, also some smaller gas fields in the Groningen concession, not in direct contact with the Groningen field, fall in the area of interest of the Groningen reservoir model. These fields are: (1) Annerveen-Veendam, (2) Bedum, (3) Bedum South, (4) Midlaren, (5) Rodewolt, (6) Usquert, (7) Zuidwending East (8) Feerwerd, (9) Warffum (10) Rodewolt and (11) Kiel-Windeweer.

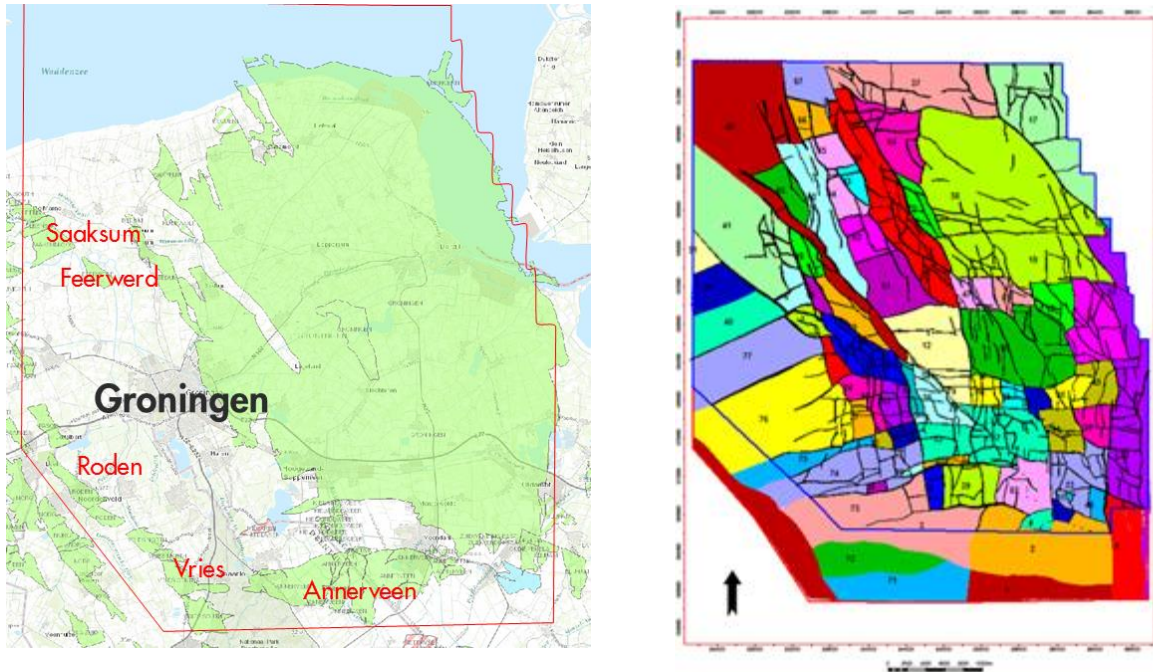


Figure 5.8 Topographic map (left) showing the extent of the static reservoir models and the segment map (right), indicating the segments of the Groningen reservoir model, with the contours of the dynamic model in blue.

New data acquired to improve the reservoir model

The following geoscience data have become available during the last years:

- 3D seismic data for the entire northern Netherlands have been reprocessed following the latest developments in processing algorithms. This has resulted in a clearer image of the formation interfaces and faults. The 3D data for the Groningen field has been reprocessed and reimaged using experimental algorithms.
- New wireline log data from wells Borgsweer-5, Zeerijp-2 and Zeerijp-3, which have all been logged extensively. A standard logging suite has been acquired in the Bedum-5 well just outside the Groningen field but inside the model area (Fig. 5.9).
- V_{clay} and porosity logs from all wells included in the model have been quality-controlled, which has resulted in removal or adjustment of outlier values for formation properties.
- A new set of permeability logs has been prepared, by applying different porosity-permeability relationships for the gas zone and the water zone. This has resulted in slightly lower permeabilities for the water zone and (very) slightly higher permeabilities for the gas-saturated parts of the field. Formation water extracted from this core is used to calibrate the properties of the reservoir water.
- Time-lapse gravity data. An extensive gravity survey has been acquired in 2015 (see chapter 4).
- Measurements on the core taken in well Zeerijp-3 of the gas relative permeability to water,
- In the Uithuizermeeden well, located in the north of the field, a PNX log has been acquired over the aquifer section. Aim is to accurately establish the gas saturation below the FWL.
- Tubing-head (surface) pressures measured at high frequency were filtered to a set of pressures recorded during cluster shut-ins, these closed-in tubing head pressures were converted to bottom-hole (reservoir) pressures using a conversion that was calibrated to match to actual down-hole measurement.
- Reservoir compaction is measured regularly at 3 wells by comparing the distance between markers that were installed at different depths these wells. The change in depth is a direct measurement of compaction in the reservoir. As a QC step the modelled compaction is compared to these measurements.

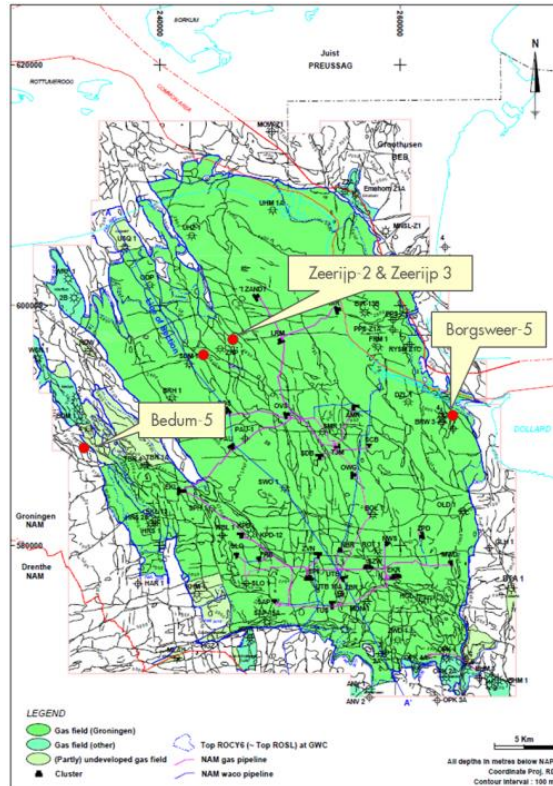


Figure 5.9 General map of the Groningen Field indicating the wells drilled since 2012.

Static model

Reservoir models are in general primarily based on 3D seismic data, geological concepts and observations at wells drilled through the reservoir. The seismic data and geological concepts are used to steer the interpolation between the wells. As a result, the static model is best calibrated in the areas near the wells and between the wells. Areas towards the periphery of the field, where fewer wells have been drilled, and of the aquifers are in general less well calibrated. The properties of the reservoir rock in these areas have therefore in general greater uncertainty. Data acquisition and further history matching of the reservoir model have focused especially on these areas.

The basic input for the structural framework of the Groningen reservoir models comprises a Top_Rotliegend depth attribute map and a fault model, both interpreted from seismic. The Top_Rotliegend surface is tied to the Top_Rotliegend depths that have been found in more than 400 well penetrations in the model area. More than 1,100 faults have been interpreted from seismic at Top_Rotliegend level (Fig. 5.10).

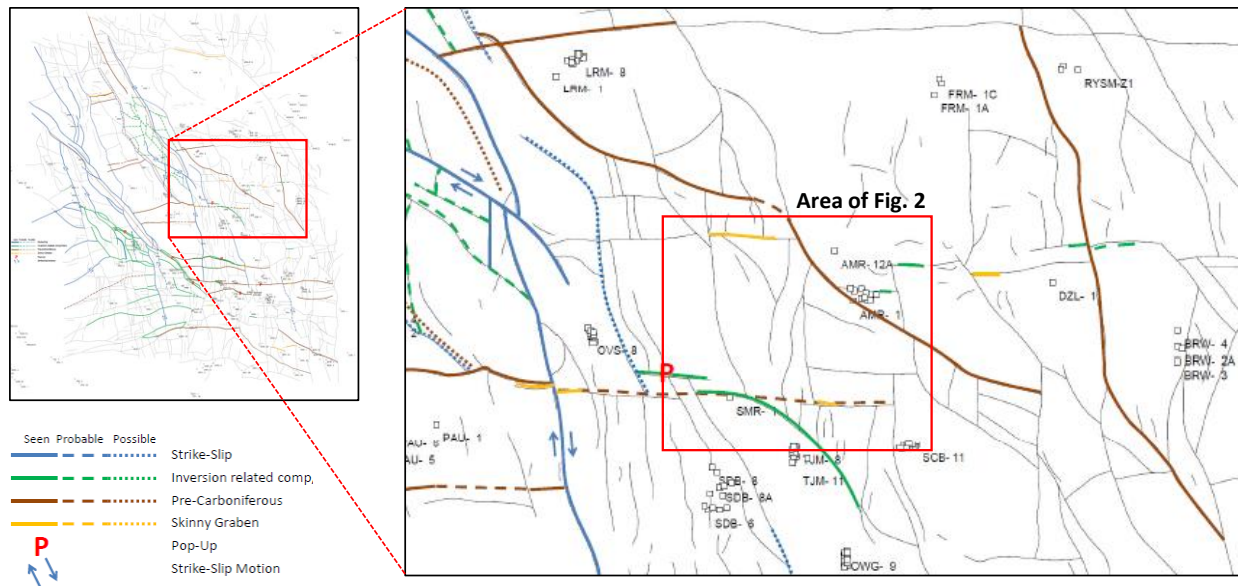


Figure 5.10 The Top_Rotliegend surface based on seismic interpretation and tied to 400 well penetrations in the model area. The 1,100 faults interpreted from seismic at Top_Rotliegend level are shown together with an interpretation of the kinematic nature of part of the faults.

The top surface and fault data were combined to construct a 3D grid. A grid cell size of 100 x 100 m was chosen as a compromise between the level of geological detail and the required processing time for subsequent modelling steps. For similar reasons, the number of faults included in the grid was reduced to around 700. These were connected, extended or combined to make up a structural model consisting of 70 segments (Fig. 5.11). The 400 mapped faults excluded from the gridding exercise all had very limited lateral extent and throw, and are positioned inside the segments. As such, they are not affecting the flow properties of the reservoir.

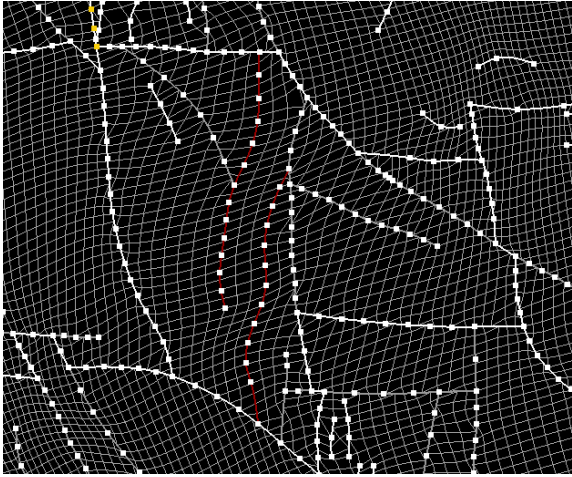


Figure 5.11 Example of a section of the static model grid. The faults in the reservoir are indicated.

The Rotliegend in Groningen has been subdivided in 12 zones, based on picks from wireline logs and core, and supported by the Top_Rotliegend interpreted on seismic. The zones are further subdivided into a total of 175 reservoir layers. There are 5 thicker reservoir zones, separated by 4 thin heterolithic zones. The upper part of the section is subdivided in three clay to silt-rich zones (Fig. 5.12). This zonation largely follows the stratigraphic subdivision into Lower Slochteren Sandstone, Ameland Claystone, Upper Slochteren Sandstone and Ten Boer

Claystone (Fig. 5.13). The basal onlap architecture is observed in the lowermost zones which do not extend to the south of the model area. The full 3D grid consists of approximately 6 million cells.

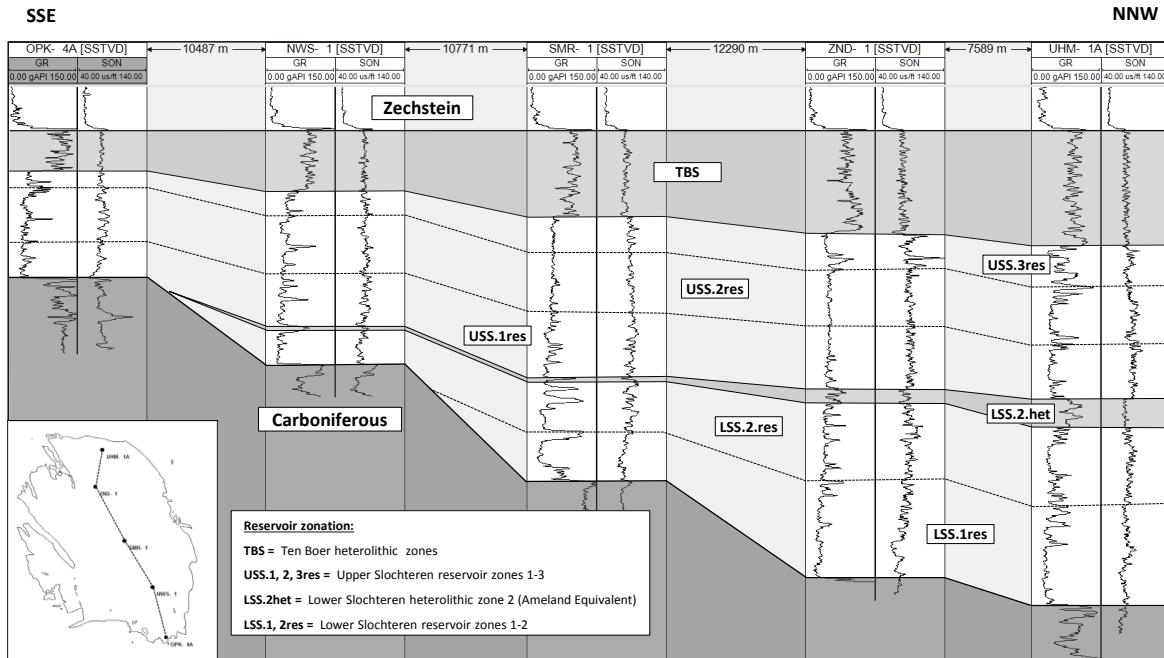


Figure 5.12 Cross-section through the Groningen Reservoir from South (left) to North (right) with zonation of the Groningen field

The last step in the construction of the static model is to assign reservoir properties to the model grid cells. The general method is based on geostatistical techniques. For a given reservoir property, wireline logs are upscaled to derive mean values for each model cell that is crossed by the well trajectories. The total distribution of all upscaled values is analyzed to identify vertical and lateral trends and to derive vertical and horizontal variograms. The modelling algorithm then creates values for each grid cell by (1) honouring the upscaled log values for grid cells crossed by wells, and (2) simulate values for the interwell areas by sampling from the distribution of upscaled log data and honouring the variogram characteristics (Fig. 5.14). Additional constraining of the simulations can be done with trend maps derived from other data sources, such as seismic attributes, facies models and so on. A full account of the methodologies, data and trends applied can be found in reference 19.

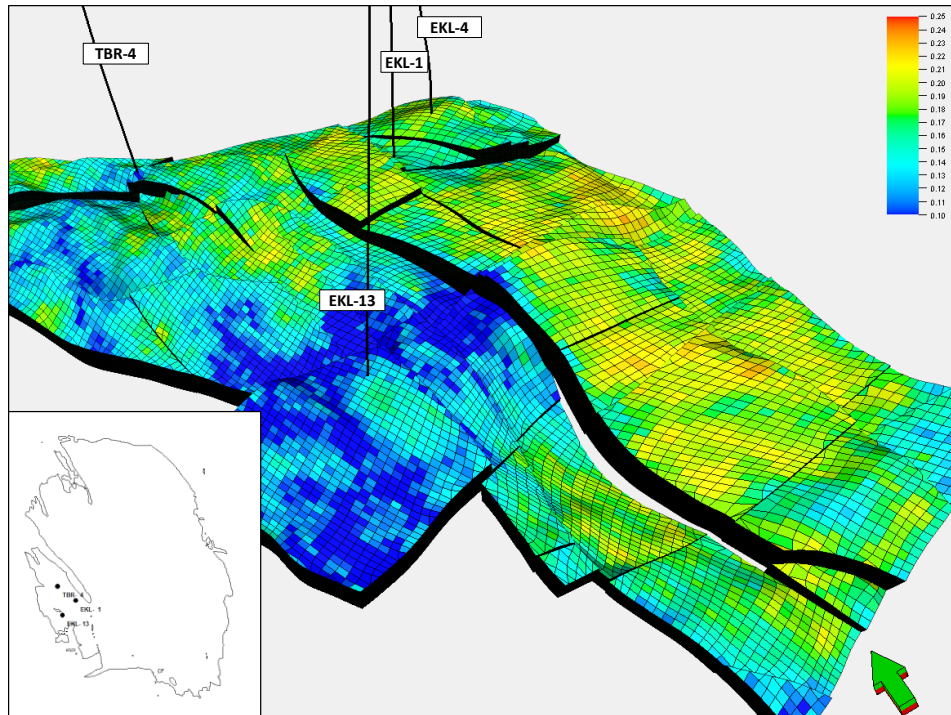


Figure 5.13 Perspective view of the porosity distribution in the Eemskanaal area in the southwestern periphery of the Groningen field.

Once the model cells have been assigned a set of reservoir properties (clay percentage, porosity, water saturation, permeability), it can be calculated how much gas is contained in the entire accumulation, and how that volume is divided laterally and between individual reservoir zones.

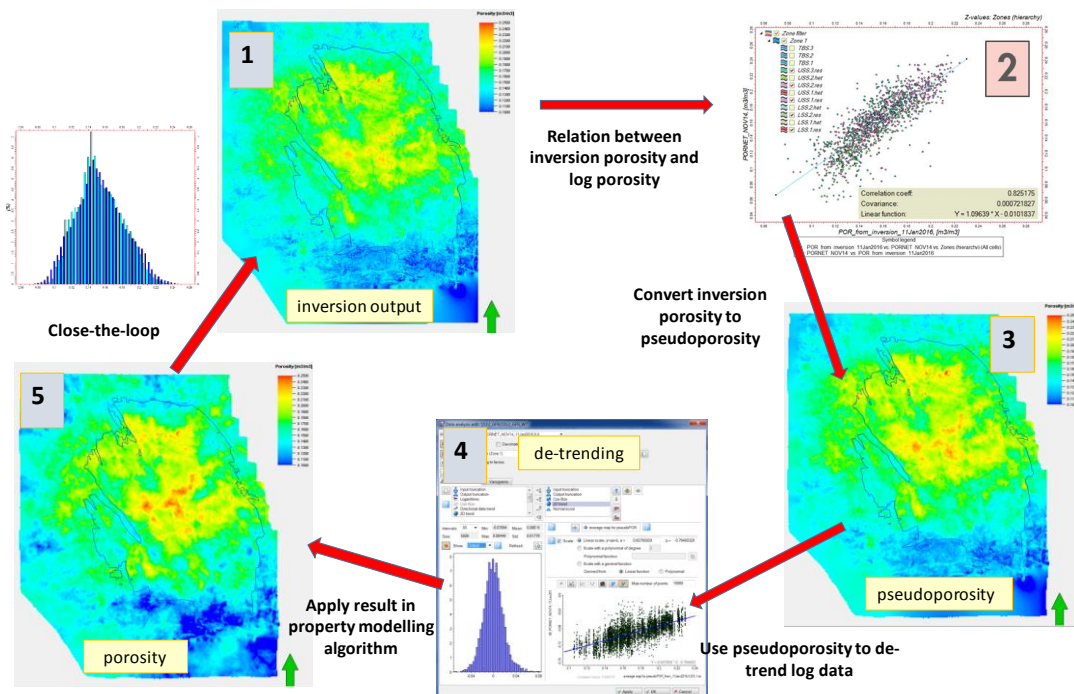


Figure 5.14 Process workflow for construction of the static model; assigning reservoir properties to the model grid cells based on geostatistical techniques.

Dynamic model

Dynamic Compartments and Initialization

The initial pressure in Groningen at the free water level (FWL) is assumed to follow the hydrostatic gradient. However, there is not a single contact level across the Groningen field even though all parts are in pressure communication. The set of FWLs are determined from a combination of open-hole logs, RFT and SPTG measurements, and define the set of dynamic compartments. The exact delineation between compartments follows faults and structures. There is also a temperature variation across the field, with a variation from about 80 to 120° C with higher temperatures in the north (Ref. 15), resulting in different gas properties. All these variations are, as much as possible, taken into account during the hydrostatic initialization.

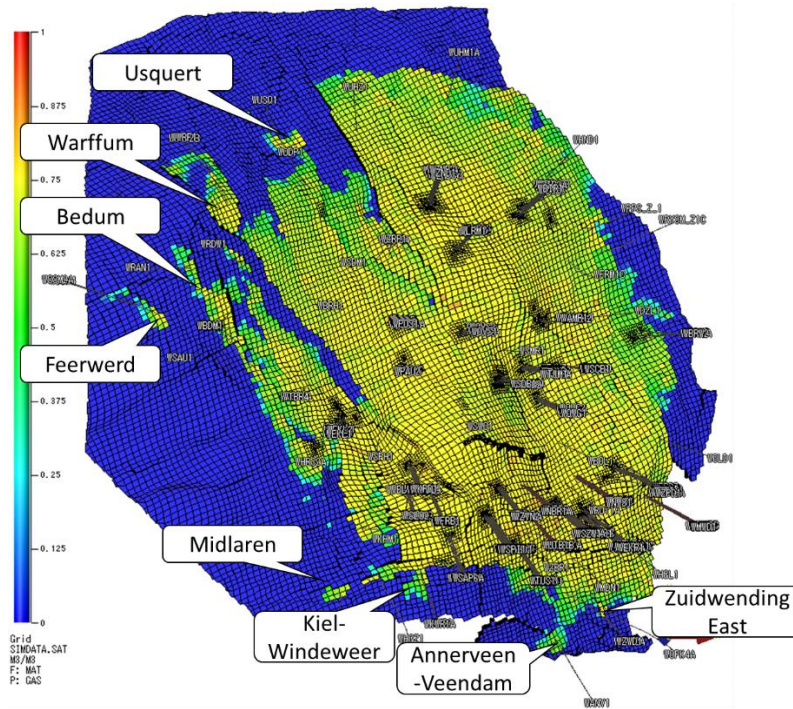


Figure 5.15 The distribution of the gas in the dynamic reservoir model in warmer colours. The smaller fields contained in the model are indicated.

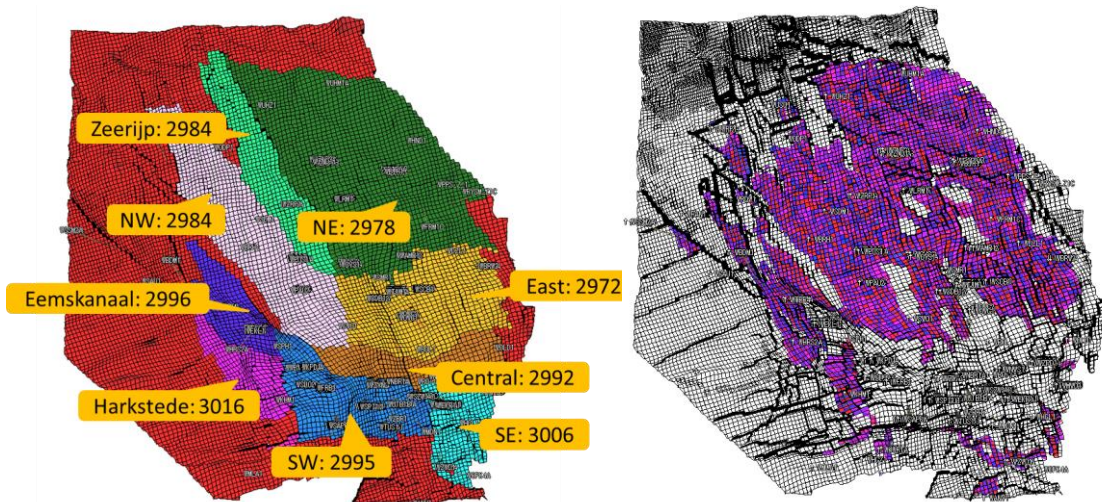


Figure 5.16 Groningen field compartments with different FWL in TVNAP (left). GWC in the model (right)

The additional smaller fields located within the confines of the reservoir model (Fig. 5.15) each have an individual single FWL. Figure 17 (left) shows the dynamic compartments with corresponding FWL's. The area of the model that has an initial GWC within the Slochteren formation is also shown in figure 5.16 (right). In the south, the contact is located in the underlying Carboniferous.

Geological fault throws and sand face juxtaposition as well as the origin of the faults define the sealing capability of the faults, and consequently the flow-paths for the fluid. In Figure 5.17 two east-west cross sections are shown. The major faults separating the north-east (where the ZND cluster is located) from Zeerijp and the north-west (where the ZRP wells are found) are clearly visible (top). Similarly, there are faults separating the north-west from the east (bottom).

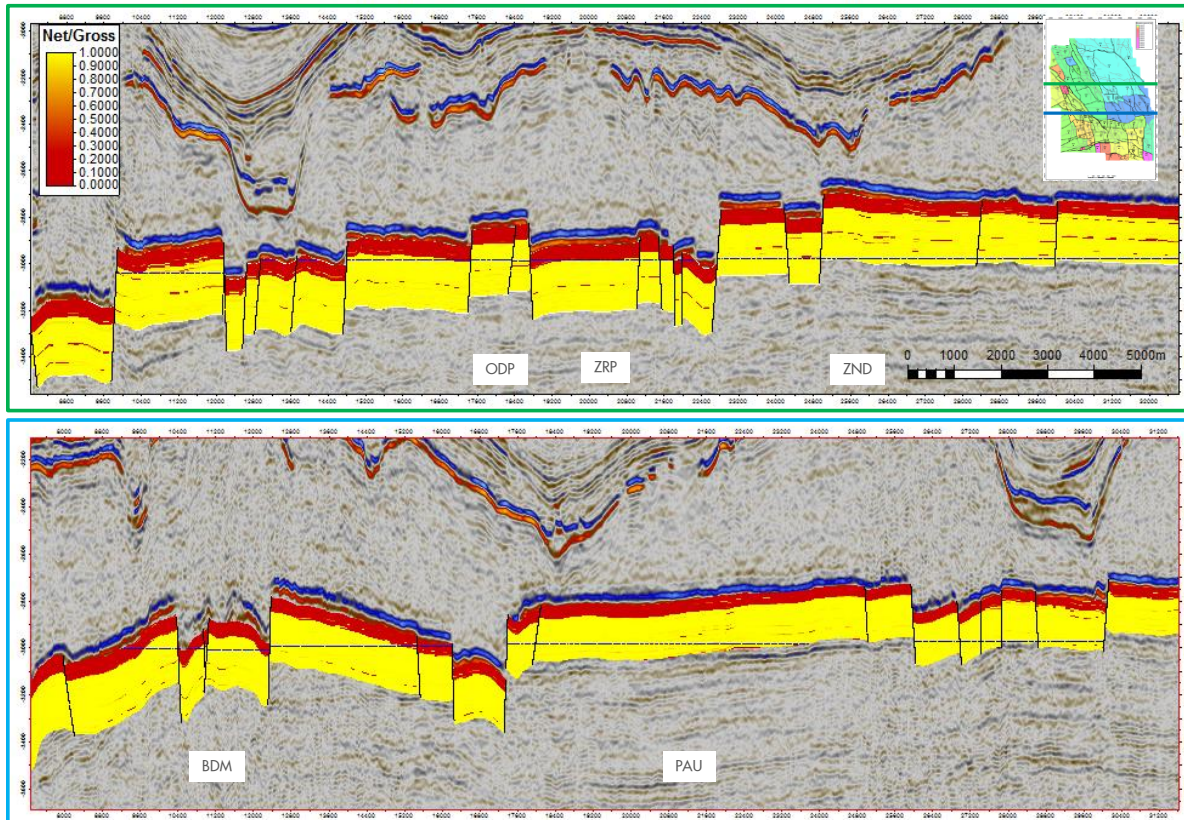


Figure 5.17 Faults with significant throw control the dynamic behaviour of the field

While the main inputs to the history matching process are pressure, PNL data (indicating a rise in the water table) and subsidence data, the model was also checked to ensure that the hydrostatic initialization remains stable in time. It is clear that all parts of the Groningen field are in pressure communication, although many of the faults act as baffles between the different initialization regions.

History matching the reservoir model

Available Data

In the history matching process the gas production and water injection is imposed on the model and the response of the model to the gas production observed and compared with actual measurements. The difference between modelled and observed data, the mismatch, is minimized. Initially, the model was primarily history matched based on the pressure data obtained during drilling of the wells (obtained with the RFT tool) and in the dedicated observation wells (SPTG surveys). Pressure data were collected during the drilling operations of 41 wells. A record of several pressures at different depths in the wells were obtained.

These pressure data in these dedicated observation and production wells (SPTG surveys) were obtained by lowering pressure gauges into the well and measuring the reservoir pressure at reservoir level. This is a relatively accurate and very extensive data set (Fig. 5.18), but has only been collected at the observation well locations. In total 1,800 pressure measurements have been collected via wireline, with a typical measurement error of some ± 0.4 bar. The temporal and areal distribution of this data set leads to a better constrained model in the southern production area of the field and a less well constrained model towards the north and periphery of the field and the adjacent aquifers (where fewer or no wells are located).

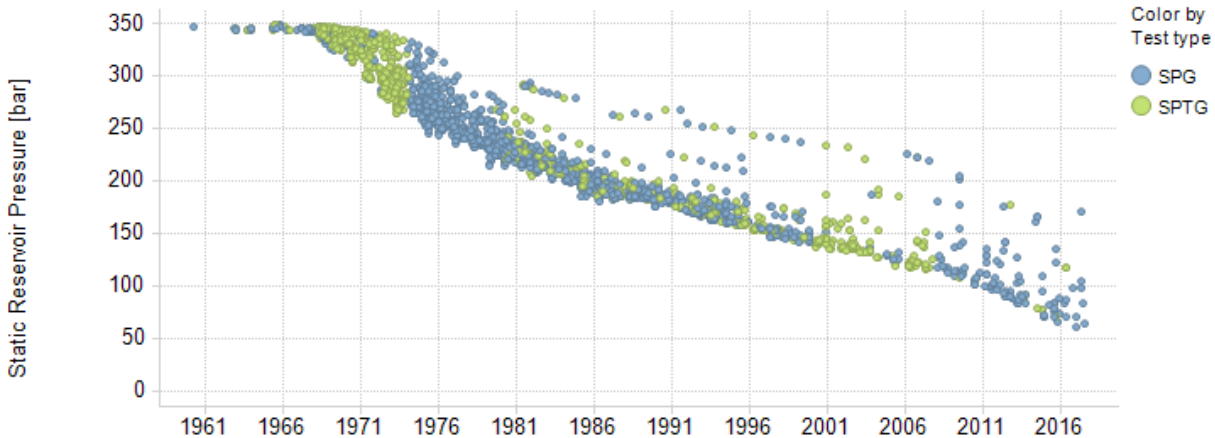


Figure 5.18 Down-hole pressure measurements in the Groningen field over time converted to datum depth (2875m TVD NAP) in the gas phase, from Static Pressure Gradient surveys

To better constrain the model especially during the last years of production and in the areas away from the observation well locations, we have during the last years collected new data and used more of the available data. Main aim of these activities was to enhance the model in areas that have less data available due to the relative sparsity of wells, namely the peripheral areas and the aquifer areas. Especially new or existing data that could aid in this was very valuable. Activities to constrain the model better using the additional data are:

1. To extend the reservoir pressure data set a methodology was developed to estimate reservoir pressure from the pressures measured at the wellhead at surface during production stops when the well pressure stabilises (the closed-in tubing-head pressure CITHP) (Ref. 21). Especially during the last decades, the tubing-head pressures have been recorded continuously by the Groningen DCS system, at all production wells. This data can therefore be used to extend the pressure data temporally (the frequency of SPTG surveys was reduced during the last decade).
2. In some of the wells located near the periphery of the gas field, a rise of the water table is observed. This is measured by lowering specialised tools (PNL) in to observation wells and comparing the tool responses over depth between measurements, which are often separated by several years. Some 223 measurement runs have been obtained in 29 different wells in the Groningen field. The model has been calibrated using 253 measurements in 35 wells including the smaller fields in the model area.
3. By extending the reservoir model functionality to also simulate subsidence, it becomes possible to history match the model also to the subsidence data. Subsidence data is available from 1963 onwards, covering the full on-shore extent of the field since 1972, and it is also available over the periphery of the field and the aquifers. This is a very rich dataset consisting of optical levelling, GPS and InSAR satellite data (see previous and next chapter). Including this into the history matching process therefore allows an improvement of the model especially over these areas. A simplified subsidence model (proxy model) was implemented in the reservoir model to make this possible.

4. To better calibrate the model in the periphery and understand the water ingression into the reservoir and the depletion of gas from the reservoir a gravity survey was collected in 2015. This is the fourth gravity survey in the history of the field and it is more extensive than previous surveys. Changes in the gravity signal are compared to modelled gravity signal changes. Differences between measured and modelled gravity changes are currently used qualitatively in the history matching, but not yet as an integral part of the overall work process.

Process

The Groningen model has been history matched several times. Each time the model was constrained using more data, while the process was also improved. This process consists of several steps outlined below:

1. Quantification of the mismatch. To quantify the mismatch between model output and the dynamic data (SPTG, RFT, PNL, CITHP and subsidence data), a root mean squared error (RMSE) is calculated for each data type. PNL and subsidence mismatches are not weighted differently. Pressure mismatches are weighted based on reliability, which has been quantified 1 (poor) to 10 (good) depending on the tools used and the measurement protocol applied. Over the field life of Groningen, pressure gauges have improved in accuracy and the measurement protocols were improved, allowing longer stabilisation periods prior to taking pressure measurements. A field-average RMSE and local RMSEs per well, cluster, and region are calculated.
2. Some areas are further investigated using the adjoint approach. The adjoint approach uses the model and the mismatch of the modelled and measured pressure to calculate where change in porosity and permeability is required to minimise this mismatch (the derivative of the objective function with respect to grid block porosity or permeability). These changes are used to see where improvements can be made to the set of variable parameters.
3. Choose the most important model parameters. Based on our experience in history matching this model, the important parameters are those that most impact the model performance and are most likely to be able to reduce the model mismatch. In total 96 parameters are used, each with a symmetric range around a base value. Some of these have a global impact others are used to improve the model performance locally in one area.
4. Experimental Design. It will not be practically possible to test the model response for each of the combination of values for these 96 selected model parameters. Therefore, an Experimental Design technique is used to generate 1,000 different models that can give the best insight into the impact of the different combinations of model parameters on the resulting mismatch. Basically, for each realisation the parameters are sampled within their range, resulting in a set of 1,000 different models that cover as good as possible the complete parameter space.
5. Model selection based on the global match. From the set of 1,000 different models, a selection is made of the models with a low field average mismatch to subsidence, pressure, and water influx. A graphical method was used to find an optimal solution. The three separate mismatches are plotted in 3D with RMSE values increasing away from the origin (Figure 5.19). The models closest to the origin are in theory the ones with the best match to the three constraining data sets.

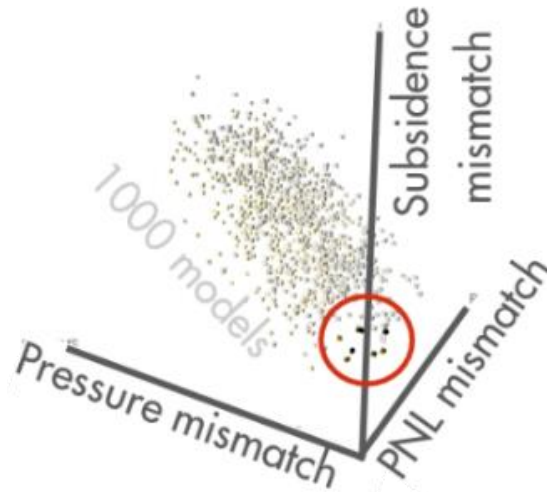


Figure 5.19 Assisted History Matching workflow from the space filling exercise towards the manual tuning.

6. Local model improvements. Analysis of local RSME functions was used to improve the model further. Figure 5.20 shows, as an example, the improvement of the pressure match near the Kolham well. This well is located in a compartment of the field, separated from the main field area by a number of faults. The transmissibility of these faults could, using this procedure, be optimised to achieved an improved match also in this area.

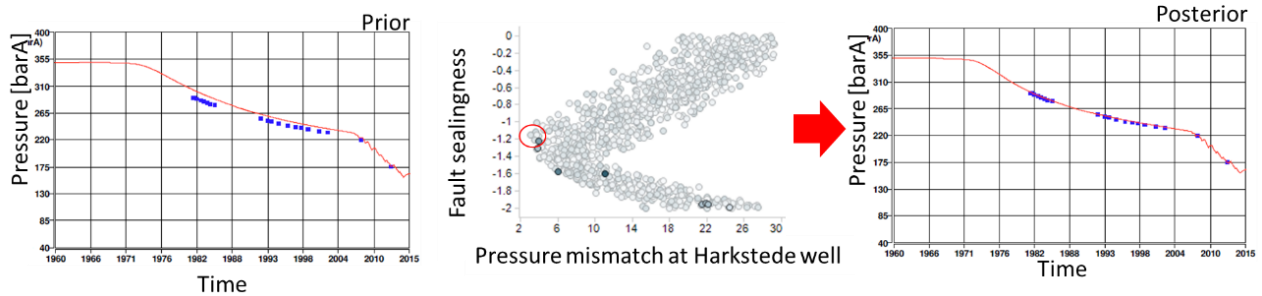


Figure 5.20 Local history match improvements using the ensemble of 1,000 models. [left], a prior model selected in [middle] the correlation between a certain variable fault-group transmissibility and the [right] pressure match of a local well, highlighted are all models selected in [right] applying the best match sealing factor.

Another example of a local refinement of the model is the subsidence in the north of the field near Warffum. Figure 5.21 shows how by adjusting the fault transmissibility of a fault an improvement in the subsidence prediction of the model was achieved. This example demonstrates how the subsidence data can successfully be used to improve the model in area where few or no wells are located and therefore pressure data is scarce.

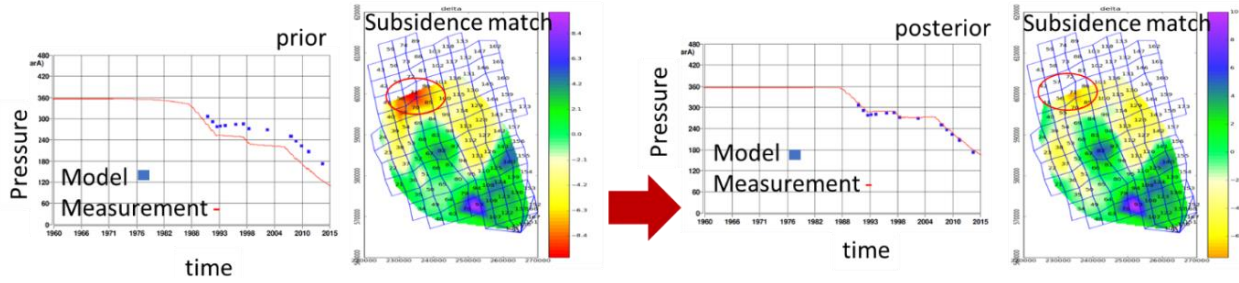


Figure 5.21 Pressure match and subsidence match in the north-western part of the model. Two models are shown, where the only difference is the sealing behaviour of a fault separating the Warffum-2b well from the aquifer. Improving the pressure match improves the subsidence match at this location.

7. Improve set of important model parameters. Detailed analysis of the local history match results sometimes required the set of model parameters to be reconsidered. For instance, many of the model parameters concern the description of the sealing capacity of individual faults. The analysis might show that a fault recognised in the seismic data, but initially not identified as important and therefore not included in to the set of 96 parameters, impacts the local reservoir pressure distribution significantly. The properties of this fault would in such a case need to be added.
8. Repeat 2 to 7 until a satisfactory match with minimised global and local RMSE is achieved.
9. Pressure output from the dynamic models is used in the higher fidelity geomechanical model to forecast subsidence. Measured subsidence and the pressure output from the dynamic model is inverted to compressibility using the high fidelity geomechanical model. This compressibility has an areal trend that is not captured by the linear porosity/compressibility relationship that is initially used in the dynamic model. This compressibility grid is therefore imported into the dynamic model. Since compressibility is a relatively modest energy source in the reservoir the global pressure match is not significantly impacted by this step.

Using the above procedure of 9 steps a reservoir model was constructed, with an average pressure mismatch of ± 2.3 bar to SPTG data, ± 1.4 bar to CITHP data, and no significant trends in the remaining pressure mismatch (Fig. 5.22).

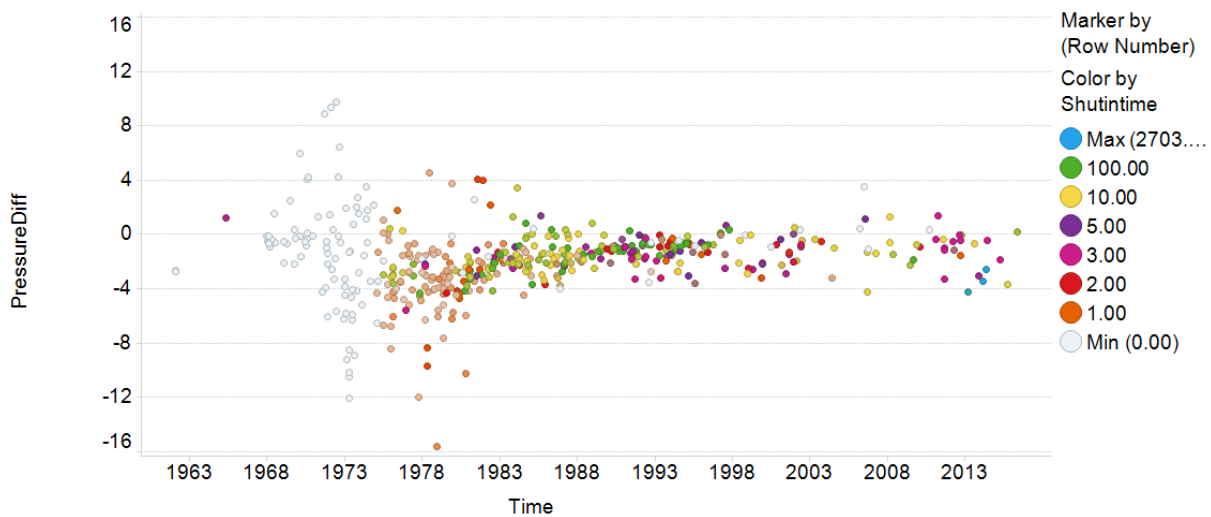


Figure 5.22 Pressure mismatch as a function of time for all SPG data points, the colour indicates the shut-in time in days prior to the survey

Improvements currently in progress

Time-lapse Gravity

Time-lapse gravity measurements can detect mass changes in the field that are caused by mass density changes related to gas extraction (production) and water ingress from the aquifers. Four gravity surveys were acquired over the Groningen field in the past. The first acquisition was in 1978, then in 1984, 1988 and last in 1996. The number of observation points varied between these gravity surveys from 21 (1978) to 26 (1996). Most of these observation points were located at NAM production sites. In 2015, another gravity survey was done, covering a total of 98 stations (Fig. 5.23). However, during the installation of compression on the production sites many of the original observation points have been removed. It was therefore at the time of acquisition not clear where the time-lapse method to interpret the data could be used. Data was acquired at 77 new locations and at 21 locations as near as possible to the original survey locations (4D time-lapse points).

The new survey was of excellent data quality. Quad Geometrics (the survey contractor) re-processed and thoroughly evaluated the historical gravity data, including drift fitting, scale factor re-estimation, and improved tidal corrections (Ref. 23). Other mass changes during the time-lapse period have to be analyzed. The time-lapse gravity signal could be resulting from groundwater variations, salt mining, and gas production from neighbouring gas fields. However, these mass changes were found not to be important compared to the gas production, due to the length of the time elapsed in between the surveys. As a result, a time lapse analysis of the gravity data was feasible.

Preliminary conclusions from the analysis of the time-lapse gravity data are:

- The mass reduction modelling in the North of the field seems too low when compared to the gravity surveys. This indicates the aquifer influx into the North of the field might be currently under-estimated by the model.
- In the South of the field, the modelled mass reduction seems too small. This could indicate gas depletion in the underlying Carboniferous formations.

In further updates of the model the gravity data will be used to further constrain the model in the history matching process.

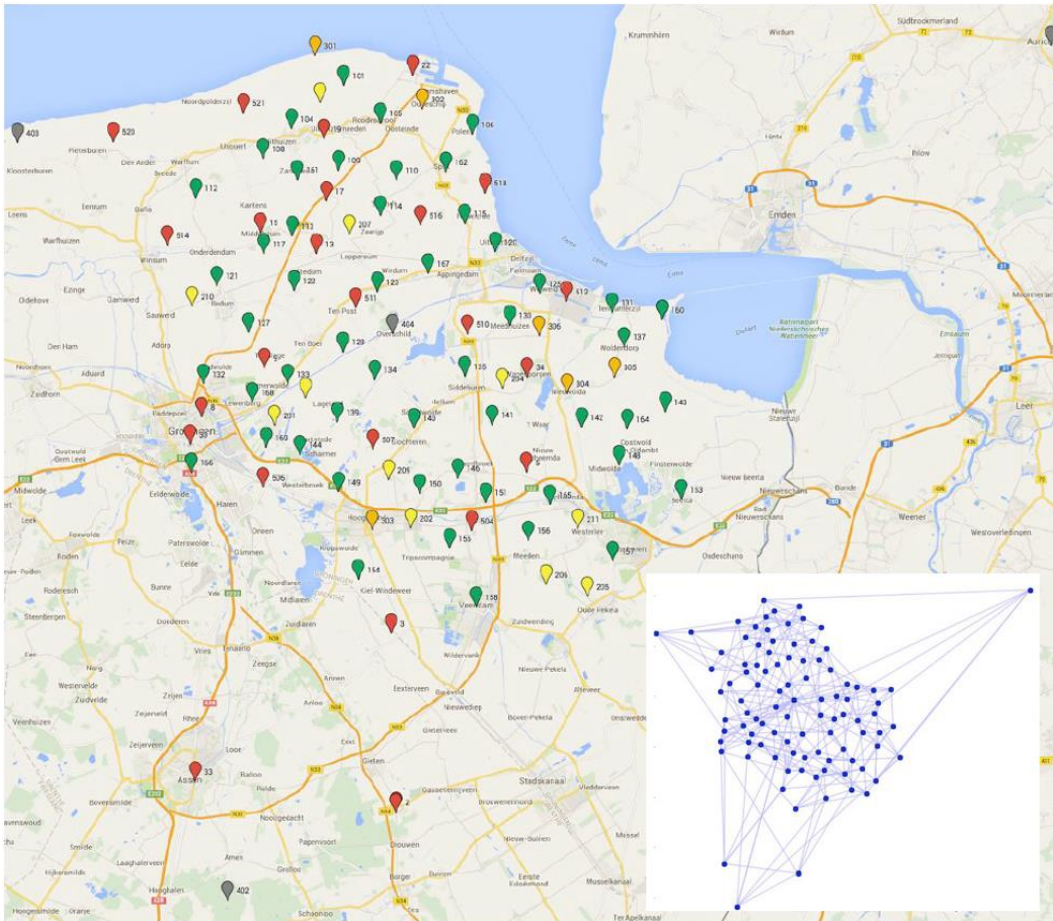


Figure 5.23 The locations of the 2015 gravity survey. The repeat stations are indicated red

Immobile gas saturation in the aquifer

Seismic data, logging data obtained in wells, pressure response measured by RFT in later wells subsidence data and observed water rise in wells (measured by PNL logs) all indicated there is likely immobile gas at low saturations present below the FWL. This has potentially played a role in pressure response of the reservoir and the aquifer, as this gas is much more compressible than water and can when the reservoir pressure is lowered become mobile.

To further investigate this additional data was obtained:

- The newly developed PNX tool of Schlumberger was ran in the Uithuizen-1 well (UHZ-1) in April 2017, confirming the presence of gas.
- Measurements were done on the core acquired in Zeerijp-3 to better understand the water mobility at these gas saturations.

Further studies are required to come to a conclusion on the distribution of the gas below the FWL and the impact on the behaviour of the reservoir. Currently, a survey with the PNX tool is planned in Zeerijp-3. Here we have a core and good mineralogy data for the formation. The combination of core knowledge on the mineral composition of the reservoir and the response of the tool will be very important for the interpretation of the data obtained with this tool.

Improvements in subsequent updates of the Reservoir Model

Since the Hazard Assessment of Winningsplan 2013, the Reservoir Model has been improved with each subsequent update of the hazard and risk assessment. Table 5.1 provides an overview of the improvements of the models since Winningsplan 2013.

The table below gives an overview of the added features over the development phases of the Reservoir Model:

Feature	Hazard Assessment Winningsplan 2013	Hazard and Risk Assessment November 2015 / WP2016	Hazard and Risk Assessment November 2017
Model	GFR 2012+Update 2013	V2 / V3	V4/V5
History Match	Pressure, PNL	Pressure, PNL, and subsidence data	Down-hole Pressure, Converted Closed-in THP, PNL, Subsidence
Prime Purpose	Capacity Planning, Reserves Estimation and Support of Earthquake Studies	November 2015 HRA / WP2016	Jun 2017 Hazard update / Production Optimization stud / Nov 2017 HRA
Model improvements with respect to previous version	Improved fault mapping	Extended grid to include surrounding aquifers and small fields (previously limited to field with analytical aquifers)	Updated top structure map (from 2016 seismic reprocessing of combined Groningen-Friesland-Drenthe surveys)
	Finer grid (with respect to previous model GFR2003)	Included subsidence data + modelling to constrain the history match outside of well control	Porosity model from seismic inversion
	included much larger data set of interpreted petrophysical logs	Further refined fault mapping	Included CITHP-to-CIBHP data in history matching (100,000 additional reservoir pressure points).
	Model all cluster wells (rather than single super well per cluster as was done in 2003)	Revised set of saturation functions, capillary pressure correlation and improved relative permeability model	Closed-loop rock compressibility modelling
	Well deliverability (PQ) matching with AFBC factors derived with WellMon	Revised fluid (PVT) properties, implicitly model condensed water	Local Grid Refinement around production clusters
	Lateral temperature variations included for initialization and PVT model	Well deliverability (PQ) matching using SAS Wikker automated (RT) data filters	Daily timesteps from 2011 onwards
		Refined lift curves (per well)	Added gravity modelling capability and evaluated model against gravity survey data
			Evaluated scenarios for impact of gas-in-aquifer
		Generalized lift curves (for groups of similar wells)	

Table 5.1 Key features of the six phases of Groningen Seismological Model development

Forecast

Over the last 5 years, since Winningsplan 2013, production caps have been applied to the production from the Groningen field aiming to reduce seismicity. Table 5.2 gives an overview of the different decisions impacting the production from the Groningen field.

Date	Description	2015	2016	2017	onwards	comments
29/11/2013	Winningsplan 2013	42.5	42.5	42.5	42.5	Gaswet applies (425 Bcm over a 10y period)
17/01/2014	Kamerbrief	42.5	40			Regional cap on LOPPZ clusters of 3.0 N.Bcm/y
Jan-15	Besluit	39.4	39.4			Regional caps (in N.Bcm per year): LOPPZ: 3.0 EKL: 2.0 SouthWest: 9.9 East: 24.5
14/04/2015	Raad van State	39.4	39.4			Maintain regional caps as per previous.
15/04/2015	Kamerbrief					Only produce LOPPZ for security of supply.
29/06/2015	Besluit	30	33			33Bcm cap in gas year 2015/2016 ¹
07/10/2015	Kamerbrief	30 ²	31 ²			31Bcm cap in gas year 2015/2016 ¹
18/11/2015	Raad van State		27 ²			Besluit Jan-15 and Jun-15 annihilated. Until new Besluit: 27Bcm in gas year 2015/2016 ¹
18/12/2015	Kamerbrief		27 ²			27Bcm cap in gas year 2015/2016 ¹ Subsequent production pending approval WP16
24/05/2016	Ontwerp- instemmingsbesluit		27 ²	24 ²	24 ²	24Bcm cap as per 1/10/2016 ¹ (up to 6 Bcm additional in case of cold winter).
30/9/2016	Instemmingsbesluit					Avoid seasonal swings in production rate.
24/05/2017	Wijziging Instemmingsbesluit			21.6 ²	21.6 ²	21.6Bcm cap as per 1/10/2017 ¹ (up to 5.4 Bcm additional in case of cold winter). Avoid seasonal swings in production rate.

1) Maintain regional caps as per previous.

2) Gas Year (1-Oct to 30-Sep)

Table 5.2 Overview of the development of the production restrictions applied to the production from the Groningen field.

Based on Instemmingsbesluit of 30th September 2016 and Wijzigingsbesluit of 24th May 2017, the current production in an average temperature year is set at 21.6 Bcm/year. However, under special circumstances the production from the field might have to be increased. Two circumstances can potentially lead to production above this annual production level:

1. Groningen gas is mainly used for heating of houses and office buildings. The demand for Groningen gas therefore depends on the weather; ambient temperature and wind. In a year with lower than average ambient temperatures, the gas demand is expected to be higher. As a result, an incremental production volume is specified in article 2 of the Instemmingsbesluit, based on a degree-day formula described in appendix A of the Instemmingsbesluit to a maximum additional volume of 5.4 bcm.
2. In article 2, lid 3 of the Instemmingsbesluit, a number of potential upsets in the gas production and distribution system are listed that could potentially lead to the requirement for a higher gas production from the Groningen field. This potential increment in production can be used at the request of Gas Transport Services BV to a maximum of 1.5 bcm per year.

Both these increments might take average production from the Groningen field above the production level set for an average temperature year of 21.6 Bcm/year. Based on statistical analyse of historical temperature observations and Groningen-gas demand assumptions it is estimated that the average production level from the Groningen field lies between 23 and 24 Bcm/year. In this report, the hazard, building damage and risk assessment was therefore

done based on an average annual production level of 24 Bcm/year. This is a prudent choice ensuring the risk assessment covers these eventualities and is more conservative than a 21.6 Bcm/year scenario.

Optimisation

Optimisation of the distribution of the production over the field to minimise seismicity and risk is in progress. This will be reported separately.

References

1. Hollands Welvaren, De geschiedenis van een Nederlands Bodemschat, Aad Correljé, Tros/Teleac/NOT.
2. Symposium on the Groningen gas field, Verhandeling van het Koninklijk Nederlands Geologische Mijnbouwkundig Genootschap, 15th and 16th March 1968
3. The analysis of the surface subsidence resulting from gas production in the Groningen area, Verhandeling van het Koninklijk Nederlands Geologische Mijnbouwkundig Genootschap, deel 28, The Netherlands, 1973
4. The Texan and the Dutch Gas – Kicking of the European Energy Revolution, Douglas Steward and Elaine Madsen, Trafford Publishing, 2005 vertaald als: Gaswinst – over de Nederlandse Gasbel en het begin van de Europese Energierevolutie, Elaine Madsen and Douglas Steward, NWADAM, 2007
5. The Netherlands and the Oil Crisis – Duca Hellema, Cees Wiebes and Toby Witte, Amsterdam University Press
6. Natural Gas in The Netherlands, Aad Correljé, Coby van der Linde, Theo Westerwoudt, Oranje-Nassau Groep B.V., 2003
7. Groningen-Gasveld Vijftig Jaar, Kloppend hart van de Nederlandse gasvoorziening, Joep Schenk, 2009
8. Onzichtbaar Goud, De betekenis van 50 jaar aardgas voor Nederland, Gasterra, 2009
9. Seasonal Flexibility in the Northwest European Gas Market An Outlook for 2015 and 2020, Clingendael Energy Paper, April 2011
10. Instemmingsbesluit Groningen Winningsplan 2013 of January 2014
11. Wijzigingsbesluit of January 2014
12. Instemmingsbesluit Groningen Winningsplan 2016
13. Wijzigingsbesluit of May 2017
14. Production stand-by of the Loppersum clusters for Security of Supply (waakvlam), NAM, June 2017
15. Technical Addendum to the Winningsplan Groningen 2013; Subsidence, Induced Earthquakes and Seismic Hazard Analysis in the Groningen Field, Nederlandse Aardolie Maatschappij BV (Jan van Elk and Dirk Doornhof, eds), November 2013.
16. Winningsplan Groningen 2013, Nederlandse Aardolie Maatschappij BV, 29th November 2013.
17. Winningsplan Groningen 2016, Nederlandse Aardolie Maatschappij BV, 1st April 2016.
18. Technical Addendum to the Winningsplan Groningen 2016 - Production, Subsidence, Induced Earthquakes and Seismic Hazard and Risk Assessment in the Groningen Field, PART I – Summary and Production, Nederlandse Aardolie Maatschappij BV (Jan van Elk and Dirk Doornhof, eds), 1st April 2016.
19. Independent Review of Groningen Subsurface Modelling Update for Winningsplan 2016, SGS Horizon, July 2016.
20. Groningen Field Review 2015 Subsurface Dynamic Modelling Report, Ulan Burkitov, Henk Van Oeveren, Per Valvatne, NAM, May 2016.
21. Monitoring Reservoir Pressure in the Groningen gasfield, Leendert Geurtsen, en Quint de Zeeuw, NAM, April 2017
22. Groningen Dynamic Model Updates 2017, Henk van Oeveren, Per Valvatne and Leendert Geurtsen, NAM, September 2017
23. Gravity monitoring of the Groningen gas field 2015, Quad Geometrics, Ola Eiken, April, 2016.

24. Bierman, S.M., et al (2015), Regularised direct inversion to compaction in the Groningen reservoir using measurements from optical leveling campaigns, Shell SR.15.11194
25. Bierman, S.M., et al (2017), Bayesian models for reservoir compaction estimation, applied to the Groningen gas field, Shell SR.17.01246

Compaction and Subsidence

Reservoir compaction was estimated by regularized direct inversion using surface displacement measurements from optical levelling surveys, as described in Bierman et al. (2015), at a coarse reservoir grid resolution with blocks of 2500m x 2500m (Figure 5.24). The statistical modelling approach was cast as a Markov Random Field (MRF) model and implemented in a Bayesian framework for uncertainty estimation in Bierman et al. (2017). There were notable differences in assumptions and implementation of the models described in these reports, most notably differences in the assumed structure of the penalty matrices and the variance-covariance of model residuals. Also, there were differences in the way parameters were estimated; non-negative least squares and cross-validation in Bierman et al. (2015) versus no non-negativity constraint and Bayesian statistical methods in Bierman et al. (2017). Despite these differences, both methods yield very similar compaction estimates in most of the Groningen field (see Appendix B in Bierman et al. 2017). The estimates of reservoir compaction are relative in time and space and can be used to understand relative spatio-temporal variation in reservoir compaction and rock compressibilities.

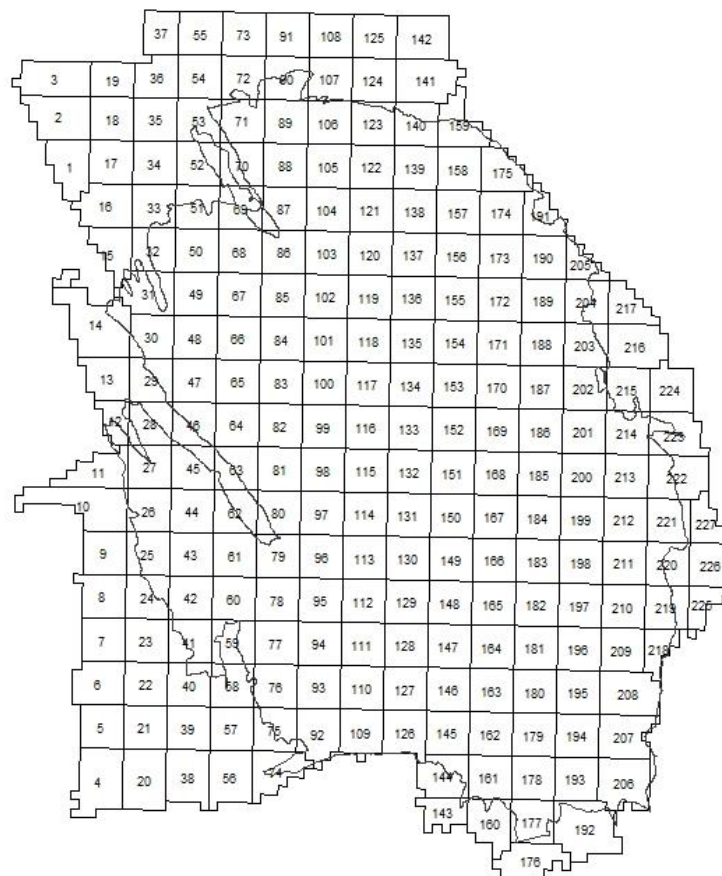


Figure 5.24. Map of the reservoir grid with (“large”) 2500m x 2500m blocks that was used for direct inversion to reservoir compaction using Markov Random Field models (see Bierman et al. 2015, 2017). The reservoir grid was constructed from a fine regular lattice of 500m x 500m (“small”) blocks. Most of the 2500m x 2500m blocks therefore contain 25 of these smaller blocks. At the edges of the grid, some of the large blocks are irregular in shape and may contain more than or less than 25 small blocks (see Bierman et al. 2015).

The MRF models can be thought of as “*non-parametric*”, because in these models reservoir compaction is not parametrically related to any other variable, particularly pressure depletion. In contrast, models based on estimated compressibilities (see for example chapter 5 in Bierman et al. 2017) can be described as “*parametric*”, because they rely on parametric relationships between pressure depletion estimates and compaction. A further characteristic of the MRF models is that the lateral resolution at which estimates of reservoir compaction can be obtained is limited to at least the burial depth of the reservoir, which is about 3 kilometres. For example, in an out-of-sample cross-validation study in Bierman et al. (2017; Appendix H), the ability of the MRF models to predict future surface displacement measurements was optimal at reservoir grid resolutions between 4000m x 4000m and 10000m x 10000m. Compaction estimates may in principle be derived at higher reservoir grid resolutions using the parametric models based on estimated compressibilities if additional information is available, like reservoir porosity-informed priors on compressibilities (Winningsplan Groningen 2016 and Bierman et al. 2017 chapter 5). The uncertainties surrounding spatially resolved estimates of porosity and the uncertainties surrounding the relationship between compressibility and porosity may be such that porosity-informed priors are not useful in deriving more accurate compaction estimates. Perhaps for these reasons, it was found that even at coarse reservoir grid resolutions of 4000m x 4000m or above, the predictive performance of the MRF models is as good as or even better than models based on estimates of compressibilities (Bierman et al. 2015 and Bierman et al. 2017).

The non-parametric nature and the relatively coarse resolution of compaction estimates of the MRF model poses challenges in the forecasting of future compaction using scenarios for future gas production. For forecasting purposes, a parametric model was used, in which compaction estimates are related to pressure depletion estimates on a block-by-block basis in the reservoir (at a resolution of 2500m x 2500m). An estimate of the compressibility thickness of each block is obtained by linear regression of compaction estimates on pressure depletion estimates (linear regression model without intercept; equation 4.11 in Bierman et al. 2015). The slope of the regression models is taken as the estimate of compressibility thickness at a 2500m x 2500m reservoir grid resolution. An illustration of the forecasting model for reservoir blocks 171 – 186 is given in Figure 5.25. In contrast, estimates of pressure depletion are obtained by reservoir models which typically operate at a high spatial resolution in comparison with the MRF models. The pressure estimates therefore should be smoothed before use in the forecasting model. This is justified because it should not be possible to forecast compaction at a higher spatial resolution than the actual compaction estimates on which the forecasting model is based. Because the forecasting model is calibrated (“history-matched”) to compaction estimates obtained through direct inversion from geodetic data, it is relatively robust to transformations or changes in estimates of historical pressures in the reservoir.

The workflow for forecasting reservoir compaction is as follows:

1. Obtain compaction estimates at a 2500m x 2500m reservoir grid resolution, using the methodology as described in Bierman et al. 2015.
2. The pressure estimates from the reservoir model are delivered on an irregular fine grid. These estimates are interpolated onto a regular grid (lattice) with 500m x 500m grid cells.
3. The pressure estimates at the 500m x 500m grids are smoothed using a symmetrical bivariate Gaussian smoothing kernel with a standard deviation of 5000m.
4. For each 2500m x 2500m block and for each epoch as used in the MRF model, the averages of the smoothed pressures of all 500m x 500m grid cells that fall inside these blocks are used to estimate the compressibility thickness using linear regression through the origin (equation 4.31 in Bierman et al. 2017 or, equivalently, equation 4.11 in Bierman et al. 2015).

5. The estimates of compressibilities (at 2500m x 2500m grid resolution) are subsequently multiplied with forecasts of smoothed pressure depletion at a 500m x 500m resolution, to get forecasts of compaction at a 500m x 500m grid resolution.

The forecasting procedure can also be applied without smoothing of reservoir pressures on the 500m x 500 m grid in step 2. Alternatively, it is possible to apply the forecasting model by averaging pressures in the coarser 2500m x 2500m blocks in step 5.

We note that uncertainties in historical compaction estimates (through direct inversion) and forecasts are particularly large in regions of the Groningen field with no or little surface displacement data directly on top of the field; particularly beneath the sea-bed and at the edges of the field. At the western edge of the field, the data are clipped to minimize the influence of surface displacements caused by compaction in neighbouring gas fields. At the eastern edge of the gas field, there is relatively little data to constrain the compaction estimates due to the presence of lateral aquifers and because no optical levelling data is available in Germany. Furthermore, at the edges of the reservoir grid, the smoothness constraints are less effective (see e.g. figures B.6 and C.4. in Bierman et al. 2017). Also, the spatial extent of the grid may not be optimal at the edges, which may further induce errors. Pressure estimates are more uncertain at the edges of the field and in the northern part below the sea-bed (figure C.5 in Bierman et al. 2017). However, in the interior of the field where by and large almost all seismicity to date is observed, estimates of compaction and compressibilities are most robust and reliable.

Compaction forecasts based on reservoir pressures for the 24 Bcm production scenario described in the previous chapter are illustrated in Figure 5.26. In this Figure, some of the grid cells on the western and northern edges of the field have been masked out due to the relatively large uncertainties associated with these estimates.

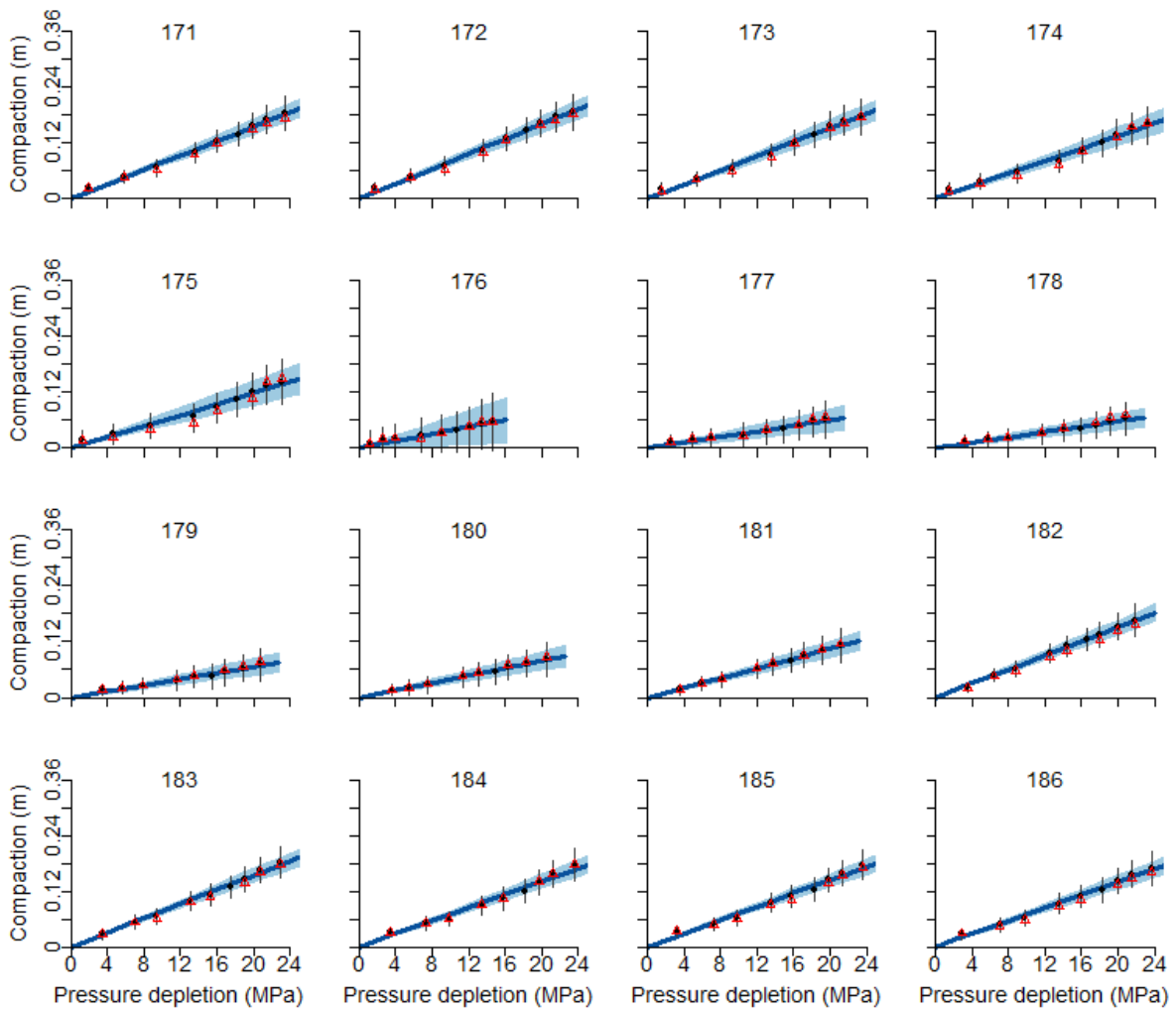


Figure 5.25. Illustration of the model for forecasting reservoir compaction for blocks 171 – 186 in the reservoir (see Figure 1 for the spatial location of these blocks within the reservoir). Straight blue line: best estimate for forecasting (light blue area: 95% confidence interval). Black filled dots and vertical segments: mean and 95% confidence interval of compaction estimates obtained by the MRF model as described in Bierman et al. 2017. Red triangles: compaction estimates from the MRF model as described in Bierman et al. 2015. Results for other blocks are given in Appendix B in Bierman et al. 2017.

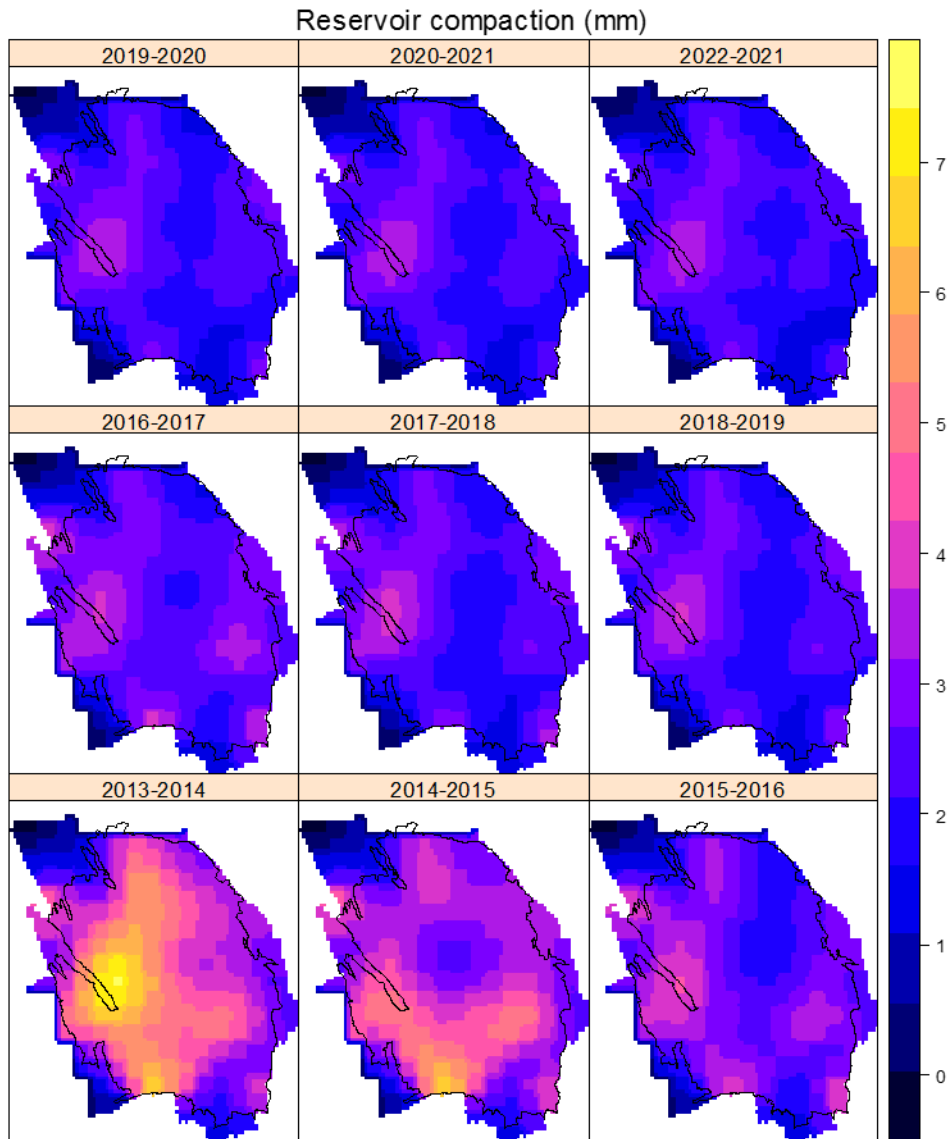


Figure 5.26 Maps with compaction forecasts for 1-year epochs between 2013 and 2022. The forecasts are based on the 24 Bcm scenario.

Seismological Model

Introduction

The seismological model aims to forecast earthquakes induced by gas production. In the Probabilistic Hazard and Risk Assessment (PHRA) workflow, the seismological model simulates possible earthquake catalogues, detailing event locations, occurrence times and magnitudes, by randomly sampling their joint probability distributions according to a model of the underlying geomechanical process and a given production plan. An important feature of seismicity in Groningen is that it is induced by gas production and therefore non-stationary.

When analysing the KNMI catalogue of earthquakes and comparing the location and origin times of earthquakes with the progression of Coulomb stress⁸ increases within the reservoir due to compaction, there is a strong bias in the origin time and location of $M_L \geq 1.5$ events towards larger induced stress states. Figure 5.27 shows that 80% of these events occurred at a time and place when incremental Coulomb stress is at least 0.25 MPa. The location of the first observed $M_L \geq 1.5$ events up to 2000 is within the region of greatest incremental stress. Over the following 15 years, the areal footprint of earthquake locations spreads mostly toward the south-east and approximately tracks an incremental Coulomb stress contours as they extend away from the centre of the field.

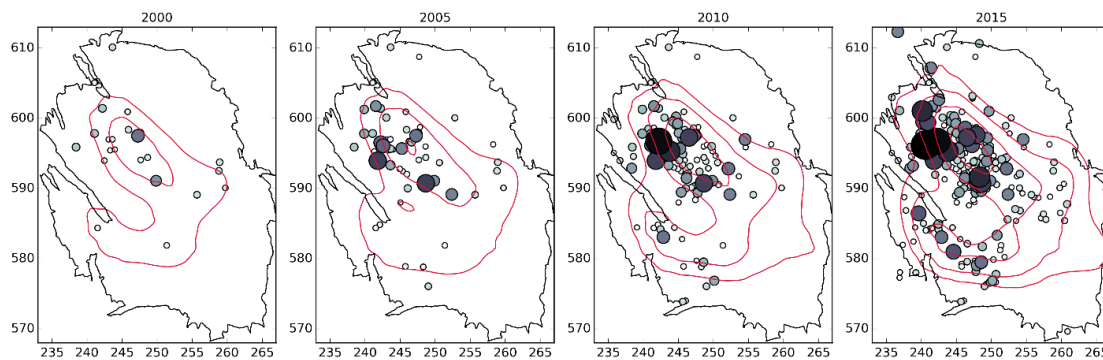


Figure 5.27 The areal extent of $M_L \geq 1.5$ earthquake locations through time remains for the most part (80%) within the 0.25 MPa incremental Coulomb stress contour induced by reservoir compaction according to the linear poro-elastic reservoir deformation model. Red lines denote the 0.25, 0.3, 0.35, and 0.4 MPa incremental Coulomb stress contours.

The time series of $M_L \geq 1.5$ events magnitudes, labelled according to the incremental Coulomb reservoir stress at the time and location of each event (Figure 5.28), suggests there is no single threshold in incremental stress above which induced seismicity occurs but rather a much more continuous and stochastic process where the likelihood of an event occurring increases according to the local incremental stress state.

⁸ Coulomb stress refers to normal stress and shear stress. Mohr–Coulomb theory is a mathematical model (see yield surface) describing the response of brittle materials such as concrete, or rubble piles, to shear stress as well as normal stress. Most of the classical engineering materials somehow follow this rule in at least a portion of their shear failure envelope. Generally, the theory applies to materials for which the compressive strength far exceeds the tensile strength (like rock and concrete).

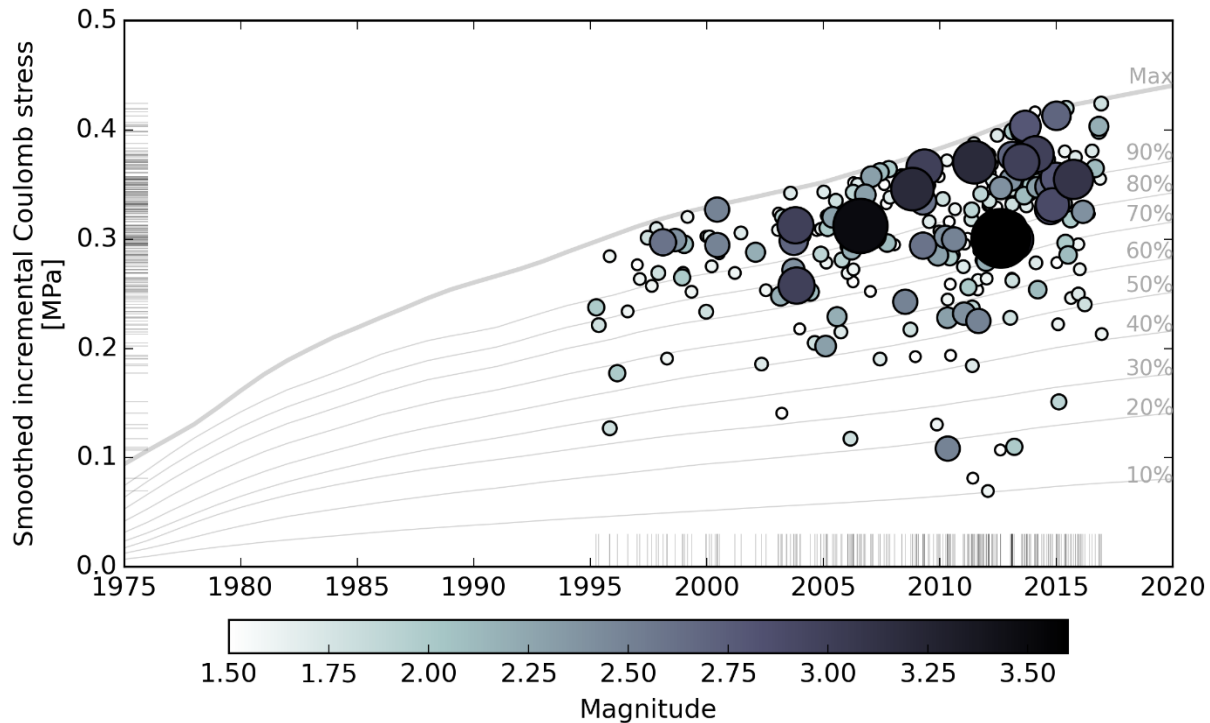


Figure 5.28 Time series of $ML \geq 1.5$ earthquake magnitudes since 1995 versus induced Coulomb stress changes within the reservoir at the origin time and location of each event. Grey lines denote percentiles of reservoir stress states through time. The number and magnitude of induced earthquake are typically larger for larger reservoir stress states.

Coulomb stress changes are computed according to a thin-sheet, poro-elastic geomechanical model calibrated to the resolvable reservoir and fault geometries and the observed history of reservoir pressure depletion and compaction inferred from surface geodesy. These Coulomb stress changes are largest where both local reservoir compaction *and* pre-existing fault offsets are largest. The observation of a strong correlation between compaction-induced stress changes and seismicity provides the basis for forecasting future seismicity based on future production scenarios. Seismicity forecasts are based on an ensemble of model realizations obtained using Bayesian inference.

Seismological Models

In Probabilistic Hazard and Risk Assessment (PSHA) for naturally occurring tectonic earthquakes, the seismological model usually comprises an identified seismically active region with assumed parameter values specifying the expected level of seismic activity. In the Groningen case, reservoir strains and pore pressure depletion cause by gas production from the reservoir have been identified as the geomechanical drivers inducing the seismicity. Seismological models for induced seismicity in Groningen have been built based on the spatially and temporally varying pattern of gas production. Such models will, driven by the production of gas, predict a non-stationary seismicity.

For the 2013 Winningsplan submission (Ref. 1 and 2), the seismological model used in the PSHA calculations was based on earlier work by Kostrov and McGarr, which links the total seismic moment of a catalogue of events to the subsurface strains causing them. A strain partitioning factor was introduced to account for the observed division of strain into seismogenic and aseismic components. This strain-partitioning model forecasted the total seismic moment released as earthquakes, based on the built-up strain energy due to gas production. This model showed

that only a small fraction of the available compaction strain energy is released as earthquakes and that this fraction increases with increasing compaction.

As an alternative to forecasting seismic moment, a model was built forecasting the event rate above a certain magnitude, based on shear strain (Ref. 3 and 4). Models of both types (Strain Based Models and Activity Rate Models) are seen in the literature and the choice between them is ultimately an empirical question: which type of models best fits the observed data? In the Groningen case, we see a better fit for the activity rate model.

Moreover, event rate based models can be naturally extended to incorporate after-shocks. This is particularly useful as it has been shown that spatial and temporal clustering of events needs to be accounted for in the Groningen earthquake catalogue. For these primary reasons, an Activity Rate model incorporating an Epidemic Type Aftershock Sequence (ETAS) model has been developed as the second-generation seismological model.

The performance of this Activity Rate model was further improved by also accounting for the influence of pre-existing fault offsets (fault throw). A simple geometric argument can be used to show that the induced strain on a pre-existing vertical fault in a compacting reservoir is proportional to the product of fault offset and reservoir compaction. Generalising this simplified geometry, using the mechanics of an elastic thin-sheet, it can be shown that replacing compaction in the initial version of the Activity Rate model with a shear strain-thickness attribute accounts for maximum shear strain induced by reservoir compaction in the presence of pre-existing faults that partially offset the reservoir. The exponential relationship between induced shear strains and seismicity was empirically motivated and lacked an explicit link to a physical mechanism.

As well as accounting for the variation of seismicity with the reservoir compaction, the seismological model must also account for the observed statistics of earthquakes magnitudes, in particular the relative abundance of large and small magnitude events described by the Gutenberg-Richter b-value. Consideration of the Groningen catalogue as a whole gives a b-value very close to the value of 1.0, generally found for earthquake populations elsewhere. If, however, the catalogue is subdivided into smaller subsets according to the strain-thickness attribute, then potentially significant systematic variations of the b-value with strain-thickness become apparent with b tending to smaller values at larger values of strain thickness. The fully developed Activity Rate model with aftershocks was the basis for the hazard assessment in Winningsplan 2016.

Subsequently, the thin-sheet reservoir strain model has been generalized to include poro-elastic stresses and extended to include an explicit statistical-physics model for fault failures according to a theory of extreme threshold failures within a mechanically heterogeneous and disordered fault population. This provides an explicit physical mechanism for the emergence of an exponential-like trend in induced seismicity rates relative to the incremental Coulomb stress induced within the reservoir by compaction and depletion. This extreme threshold failure activity rate model with ETAS aftershocks provides improve forecast performance relative to all previous seismological models.

Maximum Magnitude

Originally, the maximum magnitude M_{\max} for the probabilistic seismic hazard analysis (PSHA) conducted for seismicity the Groningen gas field was set at M 6.5, a value obtained from the seismic moment corresponding to the strain energy associated with the entire field compaction at the end of production life being released in a single seismic event. Disaggregation of early hazard and risk estimates showed that the main magnitude contributions were far below this limit and, therefore, that this M_{\max} estimate exerted practically no influence on the hazard results.

However, subsequent hazard and risk assessments for longer response periods, and the consideration of liquefaction prompted consideration of incorporating the epistemic uncertainty in M_{\max} , rather than relying on a single conservative estimate. In view of these considerations, it was decided to charge a panel of qualified experts with

the task of making the assessment of M_{\max} values to be used in the probabilistic seismic-hazard and risk models for Groningen. The objective was to follow the general principles of the Senior Seismic Hazard Analysis Committee (SSHAC) process, which were formulated precisely to facilitate objective multiple-expert hazard assessments in a manner that would most effectively identify and incorporate all epistemic uncertainties. The objective of the SSHAC process has been formulated as capturing the centre, the body, and the range (CBR) of technically defensible interpretations (TDIs) of available data, methods, and models, often referred to as the CBR of TDI.

Kevin Coppersmith was appointed to lead the TI team, based on his extensive experience in geological hazard assessments following the SSHAC process—having been a member of the original SSHAC— and, in particular, of addressing the estimation of M_{\max} (e.g., Johnston et al., 1994). Coppersmith then assembled a panel of internationally recognized experts who collectively brought together a great deal of expertise, both in the estimation of maximum magnitudes for seismic-hazard analysis, and the characterization of induced and triggered earthquakes. A three-day workshop was held in Amsterdam. Here resource experts, who had been asked to study the seismicity in Groningen, presented their study results to the panel.

The report prepared by the expert panel, together with all presentations of the workshop, have been published on the NAM website (Ref. 6). Several of the resource experts have published their studies for the workshop in peer-reviewed journals (Ref. 7 to 8). Figure 5.29 also shows a cumulative density function of the probabilities constructed by assigning the probability mass in each discrete magnitude bin uniformly over the 0.5 magnitude unit bin width centred on the magnitudes shown in the histogram.

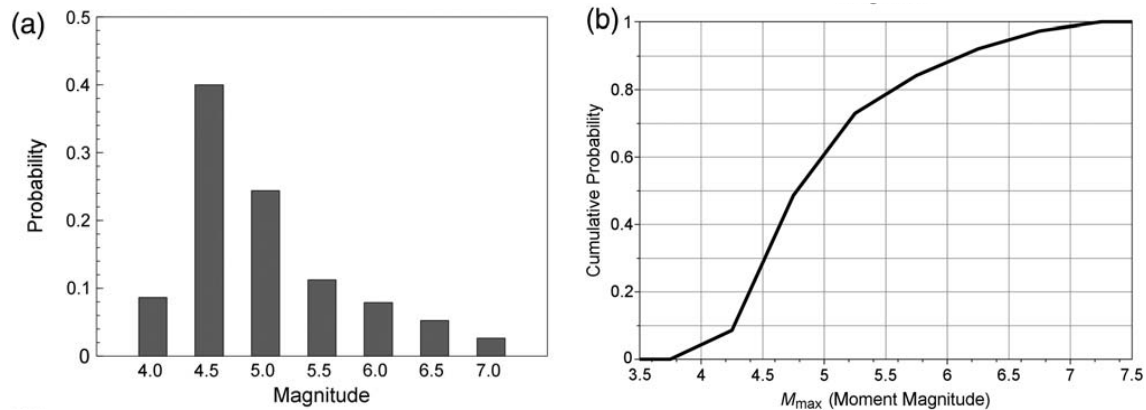


Figure 5.29 (a) Discrete and (b) continuous probability distributions represented by the M_{\max} logic tree.

Model based on extreme threshold failure

As a next step in the development of the seismological model for Groningen, a series of seismological models was developed based on increasing geomechanical complexity and heterogeneity. This approach aimed especially at gaining a better understanding of the empirically observed increasing trend in the cumulative number of earthquakes with reservoir compaction. The geomechanical models are based on an elastic thin-sheet approximation of the reservoir. As the reservoir is some 200-m thick and extends some 30 km laterally, this is a valid approach. In each subsequent model more complexity and heterogeneity is added (Fig. 5.30).

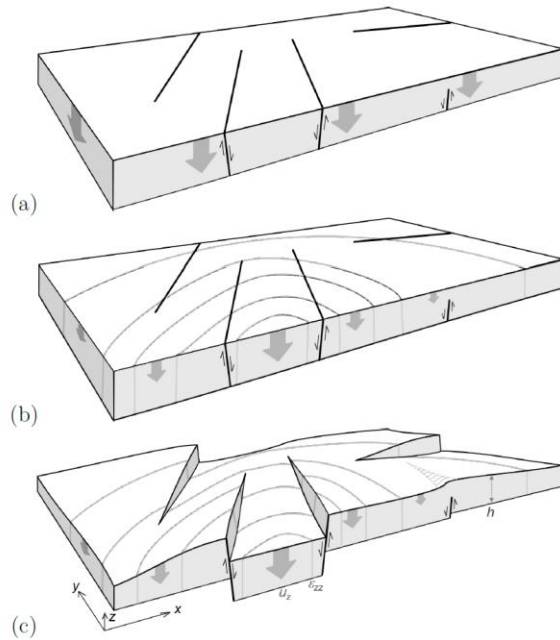


Figure 5.30 Models with increasing complexity and heterogeneity based on the elastic thin-sheet are used. (a) Model with uniform pressure depletion within a homogenous thin-sheet, (b) Model with laterally variable depletion and compressibility and homogenous geometry. (c) Model with laterally variable depletion, compressibility and geometry.

The laterally variable reservoir depletion is estimated using a well calibrated reservoir model (section xxxx). The laterally variable vertical compaction strains are derived from surface observations of subsidence (section xxx). The geological model, including faults in the reservoir formation, details the laterally varying geometry and topographic gradients (section xxx). These are three rich data sources for the seismological model used to estimate the stress development in the reservoir using the poro-elastic thin sheet theory (Fig. 5.31).

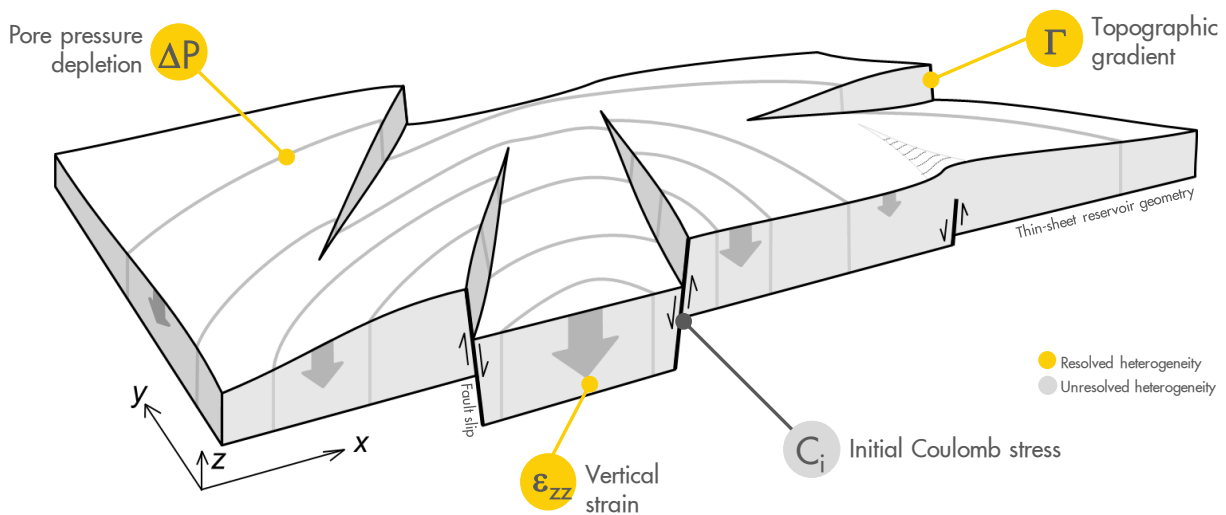


Figure 5.31 Elastic thin-sheet model with lateral heterogeneity of pressure ΔP , topographic gradients Γ . The vertical reservoir strain ϵ_{zz} reflects compaction.

During ongoing production, faults will become critically stressed and rupture. The extreme threshold theory is used to estimate the development of fault reactivation (Fig. 5.32). Application of the knowledge of the laterally varying

pressure depletion, vertical strains and topographic gradients results in estimations of earthquake density and magnitude distribution.

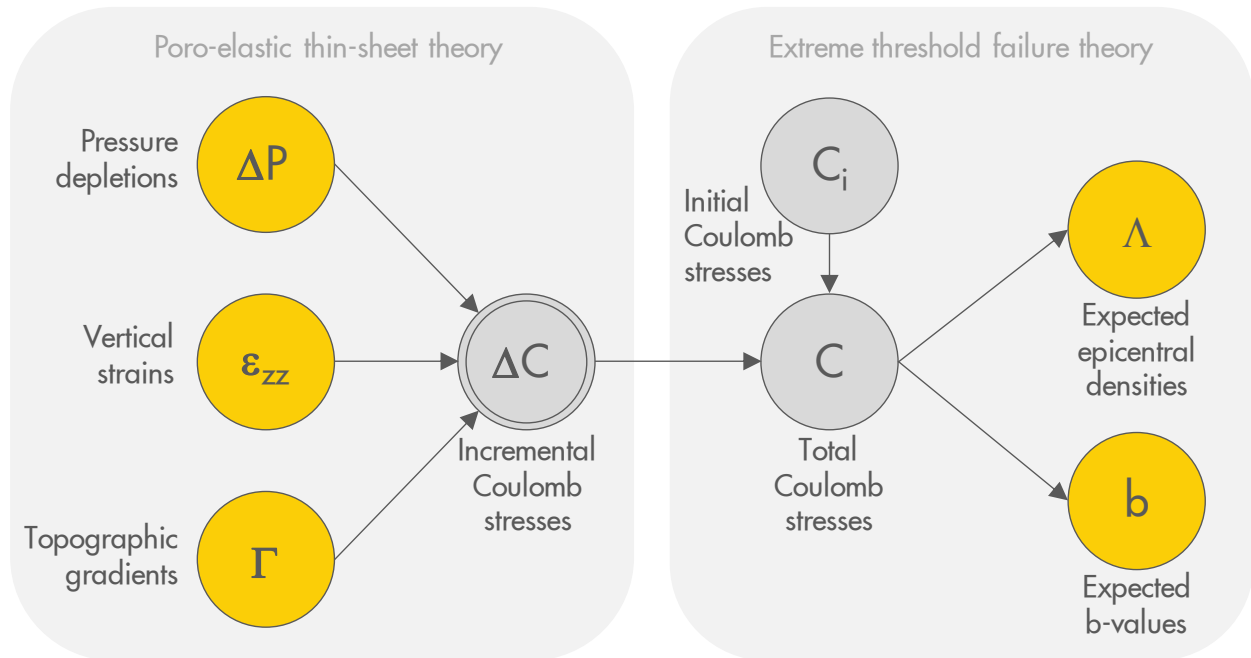


Figure 5.32 Seismological Model as a network of physical processes. The poro-elastic thin-sheet theory describes the built-up of stresses in the reservoir caused by pressure depletion. The extreme threshold failure theory describes the progressive rupture of fault.

In total seven different models with increasing complexity were developed. Each of these models was calibrated with the seismic data set for the learning period from 1995 to 2012. The models were then used to forecast seismicity for the “forecast period” from 2012 to 2017 (Fig 5.33).

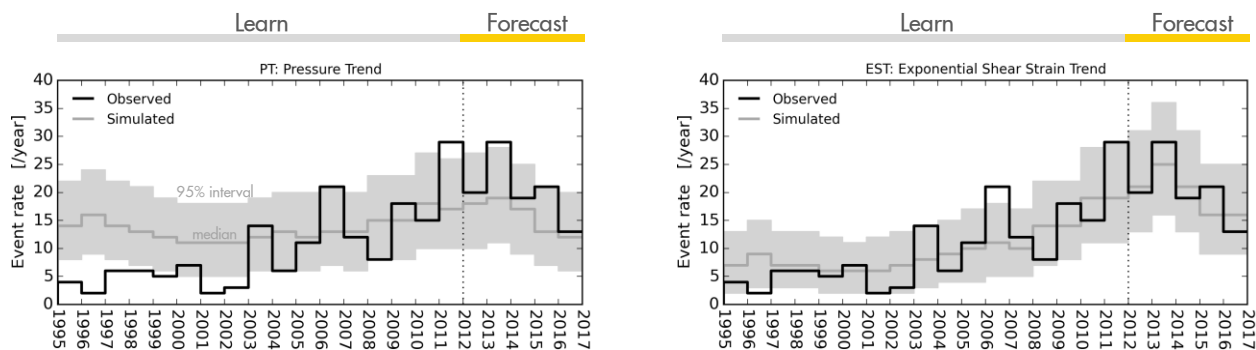


Figure 5.33 Calibration of two models over the learning period and forecasting over the forecast period. Left: the Pressure Trend Model (PT) and Right: Exponential Shear Strain Model (EST).

The performance of each model over the forecast period was tested against the observed seismicity during this period using likelihood prospective performance testing (Fig. 5.34).

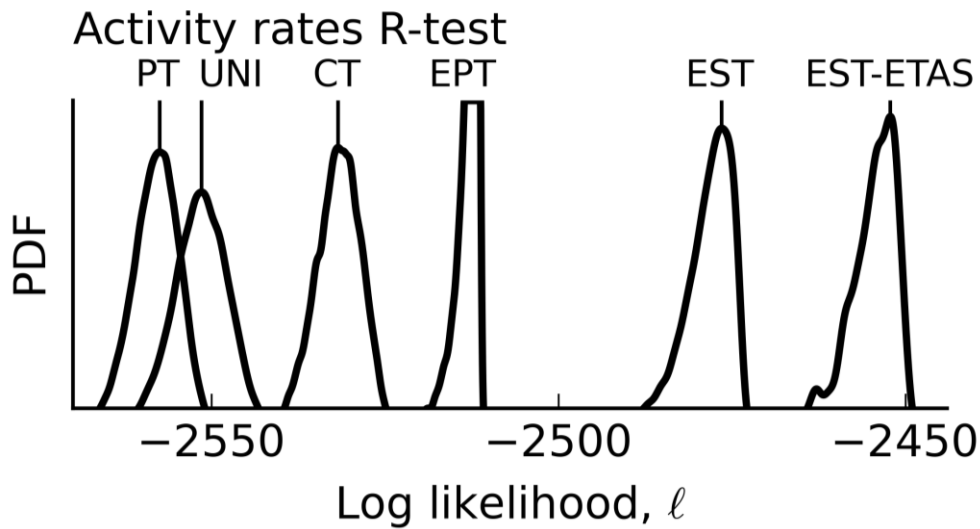


Figure 5.34 The performance of the seismological models using the likelihood prospective performance test. From left (poor) to right (improved):
 PT Pressure Trend,
 UNI Uniform Model,
 CT Lateral variability in compressibility.
 EPT Homogeneous reservoir with exponential failure trend
 EST geometric and elastic variability in reservoir properties in combination with the exponential failure trend
 EST-ETAS as the EST model, but with aftershocks

The model that incorporates both geometric and compressibility variability in reservoir properties in combination with the exponential failure trend and including aftershocks (EST-ETAS) performed best in this test and was therefore used for the hazard assessment in this report.

The seismological model is used to forecast the seismicity in terms of, the number location and magnitude of future earthquakes. The probability of an earthquake with a magnitude exceeding a given magnitude can be assessed. In table 5.3 the annual probability of an earthquake occurring with a magnitude exceeding the specified magnitude is given. For instance, the probability of an earthquake occurring in 2018 with a magnitude exceeding $M=3.6$ (the magnitude of the Huizinge earthquake) is equal to 16%.

YEAR	$M \geq 3.6$	$M \geq 4.0$	$M \geq 4.5$	$M \geq 5.0$
2018	16.0%	6.6%	1.6%	0.4%
2019	17.0%	7.0%	1.6%	0.4%
2020	17.8%	7.5%	1.8%	0.4%
2021	19.3%	8.0%	1.9%	0.5%
2022	20.2%	8.7%	2.2%	0.6%

Table 5.3 Table with annual probabilities for occurrence of earthquakes exceeding a set magnitude.

The probabilities for the occurrence of an earthquake with magnitude $ML \geq 3.6$, have not changed since the assessment for Winningsplan 2013. For the larger magnitudes, there is a slight reduction in the probability of occurrence since the assessment for Winningsplan 2013. Over time, these probabilities slightly increase when the field is produced at a constant gas production rate. However, over these longer time a-seismic relaxation of stresses in the reservoir might reduce seismicity below this forecast, as this effect has not been included in the model.

Improvements in subsequent updates of the Seismological Model

Since the Hazard Assessment of Winningsplan 2013, the Seismological Model has been improved with each subsequent update of the hazard and risk assessment. Table 5.4 provides an overview of the improvements of the models since Winningsplan 2013.

The table below gives an overview of the added features over the development phases of the Seismological Model:

Feature	Hazard Assessment Winningsplan 2013	Intermediary Hazard and Risk Assessment May 2015	Hazard and Risk Assessment November 2015	Mid -2016	Mid-2017	Hazard and Risk Assessment November 2017
	V0	V1	V2	V3	V4	V5
Model	Compaction Strain Partitioning Model	Strain Thickness Activity Rate Model	Strain Thickness Activity Rate Model	Strain Thickness Activity Rate Model	Strain Thickness Activity Rate Model	Coulomb Stress Extreme Threshold Failure Model
Compaction forecasts	Porosity model, time-decay forecast	Levelling inversion, linear forecast	Levelling & InSAR inversion, linear forecast	As V2, with geodetic data update	As V2, with geodetic data update	As V2, with geodetic data update
Deformation state variable	Compaction	Strain thickness	Strain thickness	Strain thickness	Strain thickness	Incremental Coulomb stress
Seismicity trend	Exponentials in strain partitioning	Exponentials in activity rate	Exponentials in activity rate	Exponentials in activity rate	Exponentials in activity rate	Exponentials in activity rate
Aftershocks	No	ETAS	ETAS	ETAS	ETAS	ETAS
<i>b</i> -value	Constant	Decreases as hyperbolic tangent of strain thickness	Decreases as inverse power-law of strain thickness	Decreases as inverse power-law of strain thickness	Decreases as inverse power-law of strain thickness	Decreases as inverse power-law of incremental Coulomb stress
Maximum magnitude	6.5	6.5	Preliminary distribution from 5 to 6.5	3-point sampling of SHAC M _{max} workshop outcome	3-point sampling of SHAC M _{max} workshop outcome	3-point sampling of SHAC M _{max} workshop outcome

Table 5.4 Key features of the six phases of Groningen Seismological Model development

Alternative Seismological Models

In the Technical Addendum to the Winningsplan 2013 (Ref. 2), a geomechanical model was presented. The first version of this model included a global model and two sub-models. The global model includes the entire Groningen field region but does not explicitly include faults. The pore pressure field is imposed and the model responds with deformations based on pore pressure changes and salt creep behaviour. The deformation of the reservoir rocks is modelled using porosity dependent elastic properties. Global model subsidence and predicted reservoir strains compare well with available data. The global model deformations are then used as boundary conditions to the sub-models, which have been developed to model regions of seismic activity in greater detail. The sub-models include detailed modelling of faults as contact surfaces, permitting slippage due to depletion-induced stress changes.

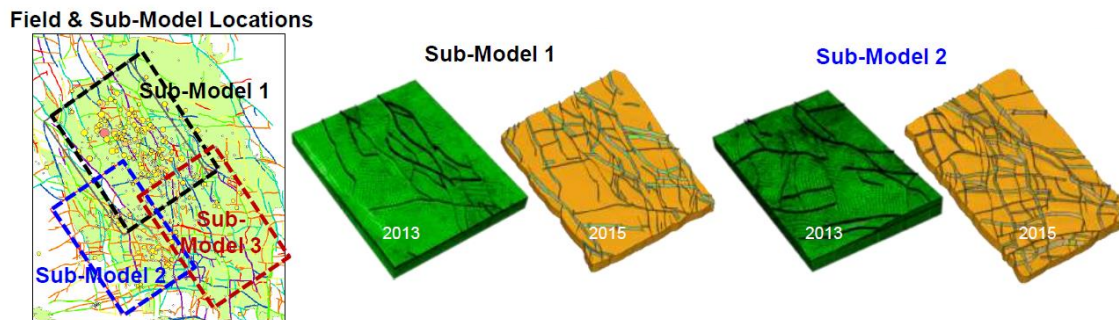


Figure 5.35 Large scale geomechanical model of the Groningen field. The additional complexity incorporated in this model since winningsplan 2013 in terms of faults and improved fault description with offsets is shown.

Currently, compaction from the global geomechanics model can be used as the basis of the seismological model (Ref. 9). Rather than using a strain partitioning model, a direct correlation is made between the compaction (change in reservoir thickness) and the number of events (activity). This approach directly produces an activity map that can be read into a PSHA analysis. A variety of functional forms can represent the correlation between compaction (relative to a point in time (e.g. 1995)) and the total number of earthquakes. A maximum likelihood estimation is used to build a Poisson process model, which incorporates the spatial and temporal components for each individual observed earthquake. Quadratic, predicted hazard for 2016-2021 between the cubic and the exponential forms. As alternatives to these models, slider block models and models based on Eshelby's inclusion theory are also being actively studied.

References

1. Winningsplan Groningen 2013, Nederlandse Aardolie Maatschappij BV, 29th November 2013.
2. Technical Addendum to the Winningsplan Groningen 2013; Subsidence, Induced Earthquakes and Seismic Hazard Analysis in the Groningen Field, Nederlandse Aardolie Maatschappij BV (Jan van Elk and Dirk Doornhof, eds), November 2013.
3. An activity rate model of induced seismicity within the Groningen Field, (Part 1), Stephen Bourne and Steve Oates, February 2015.
4. An activity rate model of induced seismicity within the Groningen Field, (Part 2), Stephen Bourne and Steve Oates, June 2015.
5. Maximum magnitude from induced earthquakes in the Groningen field, Nora Dedontney et.al., Exxonmobil Upstream Research Company, July 2016
6. Report on Mmax Expert Workshop, Mmax panel chairman Kevin Coppersmith, June 2016
7. Zöller G. and M. Holschneider, The Maximum Possible and the Maximum Expected Earthquake Magnitude for Production-Induced Earthquakes at the Gas Field in Groningen, The Netherlands, Bulletin of the Seismological Society of America December 2016 vol. 106 no. 6 2917-2921
8. Dempsey, D. and J. Suckale, (2017) Physics-based forecasting of induced seismicity at Groningen gas field, the Netherlands, Geophysical Research Letters, Accepted manuscript online: 25 July 2017

9. Groningen 2015 Geomechanical Analysis, Suvrat P. Lele, Jorge L. Garzon, Sheng-Yuan Hsu, Nora L. DeDontney, Kevin H. Searles and Pablo F. Sanz (ExxonMobil Upstream Research Company, Spring, TX), March 2016.

Ground Motion Prediction

The earthquakes in the Groningen area are induced by the production of gas from the Rotliegendes sandstone reservoir. These seismic events are described by their hypocentral location and local magnitude, M_L . Based on theoretical considerations, the depth of these events was initially assumed to be located within the reservoir, which is located at an average depth of 3,000 m. Studies analyzing the seismic data sets recorded by the extended geophone and accelerometer network operated by KNMI and the geophone arrays located in deep wells over the reservoir sections, have confirmed this.

An essential element of the causality chain from gas production to risk is the estimation of ground motions at any location at the surface in the field area resulting from earthquakes originating from the deep gas reservoir. This ground motion prediction is essential in order to understand how an earthquake at 3 km depth is felt at the surface and impacts the buildings that are founded on that surface. Detailed data from the complete rock and soil package underneath and above the gas fields is needed as input into the Ground Motion Prediction methodology. The Ground Motion Model (GMM) is tailored to the Groningen field area characteristics. This means that the Groningen GMM cannot, without modification, be applied to other areas.

The 5%-damped elastic response spectral acceleration, SA , is generally a good indicator of the seismic demand on a structure. Due to the variation on the building stock, the response spectral acceleration needs to cover a wide range of oscillator frequencies, from 0.2 Hz to 100 Hz. The latter is equivalent to peak ground acceleration (PGA). Building typologies like single or two storey houses as a rule of thumb have a response frequency in the range of 10 to 20 Hz, while high rise buildings and large infra-structure objects typically have a response period below one Hertz.

However, for unreinforced masonry buildings, the possibility of collapse can also depend on the duration of shaking due to reduced strength and stiffness under cyclic loading. Therefore, the duration of shaking (D_s) is also included. In other domains studying building vibrations, peak ground velocity (PGV) is used. To allow comparison with the alternative causes for building movement, a model for PGV was additionally included. Additionally, regulation regarding tolerable levels of vibration from anthropogenic sources are generally framed in terms of PGV.

Ground Acceleration Data

At the time of the preparation of Winningsplan 2013, in total 58 acceleration records from 15 earthquakes (with magnitude $M_L \geq 2.5$) were available from the Groningen field area for the development of the ground motion model (Fig. 5.36). This was caused by the relatively low number of earthquakes causing measurable ground accelerations and the relatively low number of accelerometers placed over the field to record these earthquake accelerations. The extended geophone network with accelerometers installed at some 70 locations has led to an increase in the available seismic earthquake data, with denser sampling of the ground-motion field during recent earthquakes. Prior to Winningsplan 2013, on average an earthquake with magnitude $M_L \geq 2.5$ resulted in four seismic acceleration records. In comparison, the recent earthquakes near Hellum ($M_L = 3.1$) and Slochteren ($M_L = 2.6$) were recorded by 42 and 68 accelerometers station respectively (Ref. 1). Although the number of earthquakes with significant accelerations measured at surface only increased from 15 to 23 from Winningsplan 2013 to this assessment, the number of acceleration records of these earthquakes increased from 58 to 246 (Fig. 5.37).

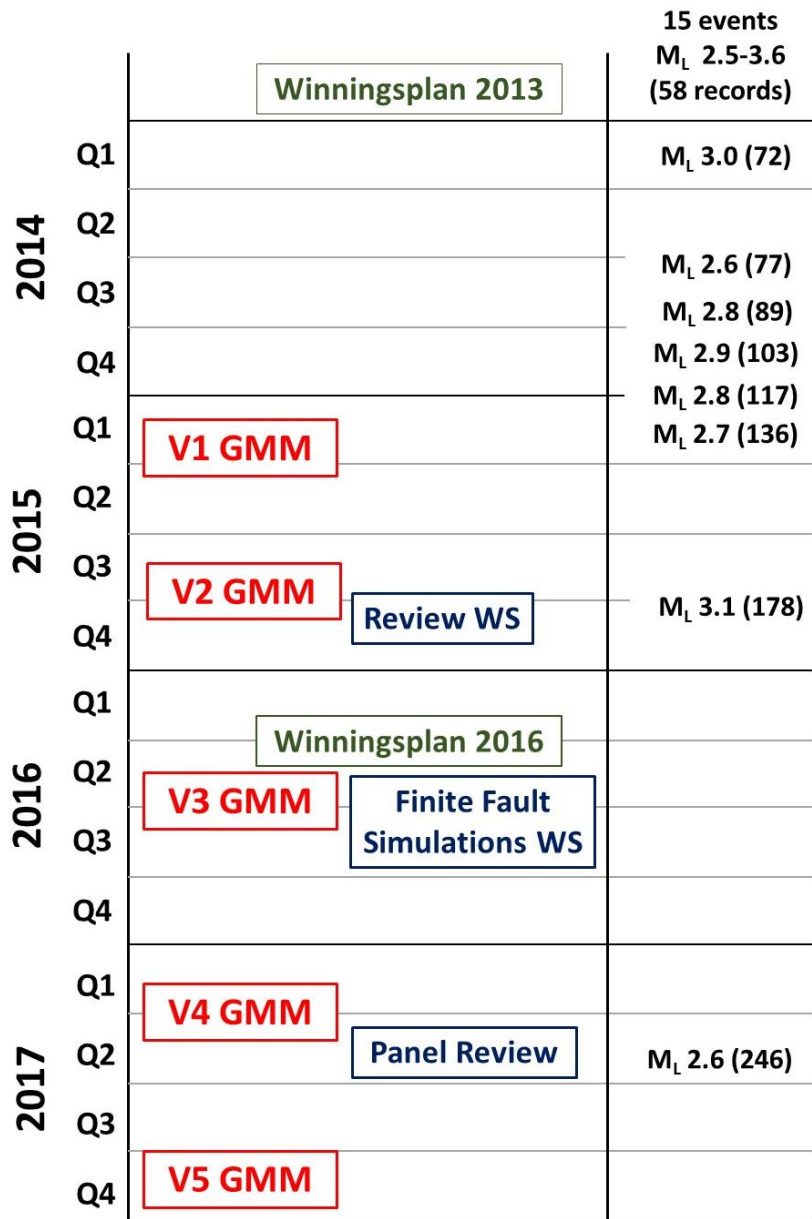


Figure 5.36 Timeline of GMM development for Groningen, with models indicated by date of issue of first report. The right-hand side indicates the growth of the ground-motion database in terms of acceleration record from events of $M_L \geq 2.5$.

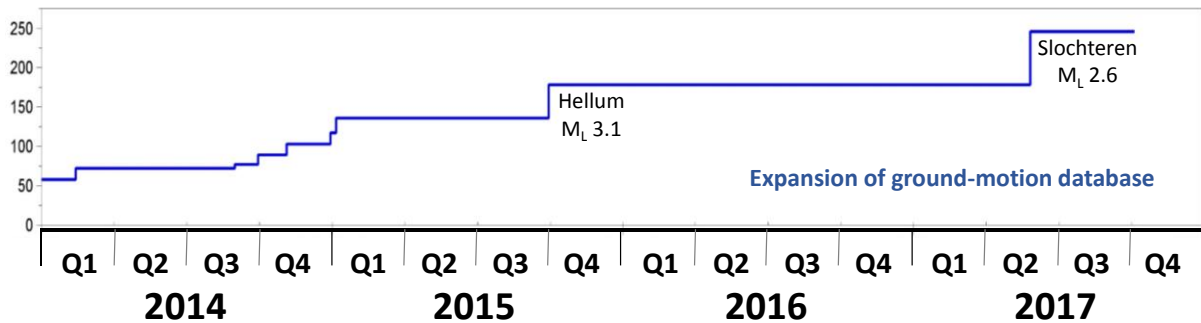


Figure 5.37 Timeline of GMM development for Groningen, with models indicated by date of issue of first report. The right-hand side indicates the growth of the ground-motion database in terms of recordings from events of $M_L \geq 2.5$.

In addition to the data obtained with the geophone and accelerometer network operated by KNMI, the TNO building sensor network also record earthquake accelerations. Potentially this data (Fig. 5.38) can also be used in the derivation of the GMM. At some of the locations, the instruments are not installed at ground level but mounted on the lower parts of the walls, raising concerns about the extent to which building response may have influenced the recordings. To investigate this issue, the wall installations were mimicked in shake table tests on full-scale model houses conducted in Lisbon and the recordings from the floor and wall levels are now being analysed and compared.

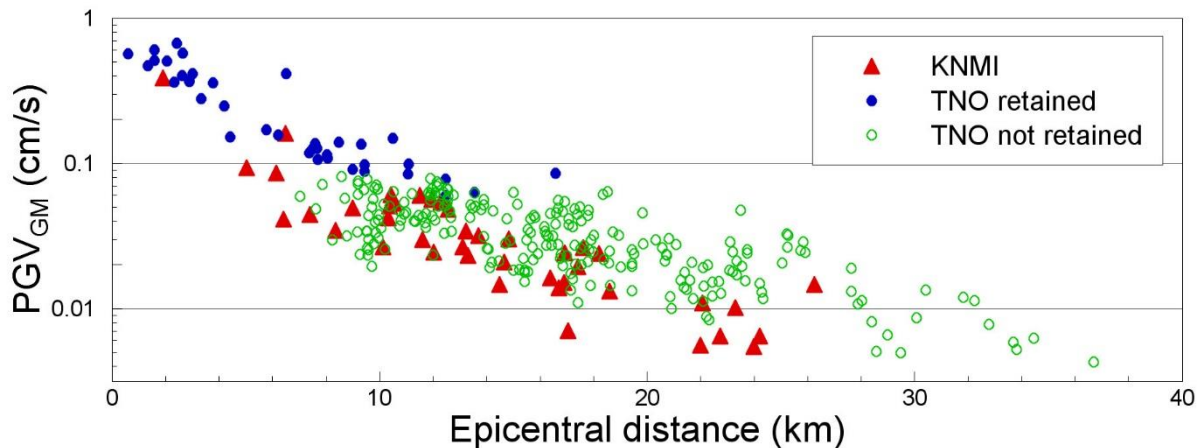
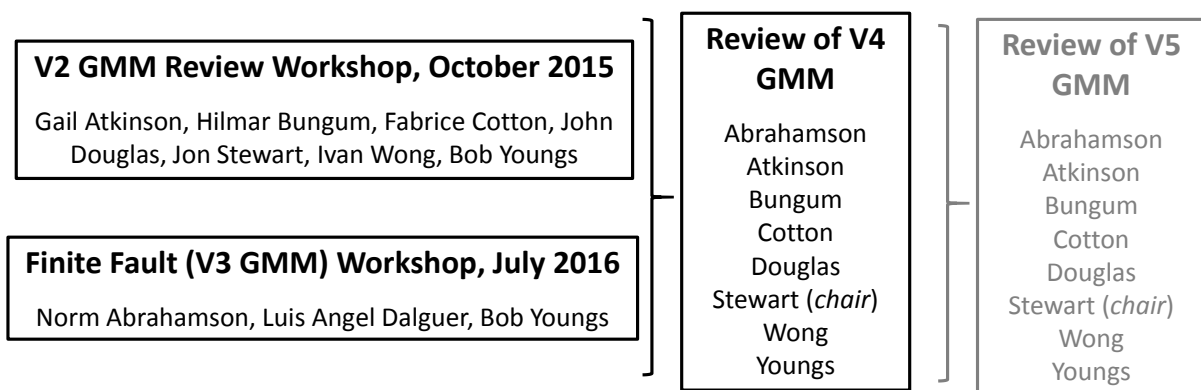


Figure 5.38 Geometric mean horizontal PGV values from the KNMI and TNO accelerographs from the $M_L = 3.1$ 2015 Hellum earthquake, showing the censoring effect of the trigger threshold on the household instruments. The green dots are PGV values reported as part of the ‘heartbeat’ monitoring that transmits the highest velocity value recorded in each minute; the time-histories corresponding to these records are not retained.

Model Development

Since 2012, several updates of the Ground Motion Models have been developed (Ref. 2, 7 and 12). Each with increasing complexity and calibrated to a larger seismic data set. Figure 3.36 and 5.36 show a timeline of the development of available seismic acceleration records and updates of the GMM. The time between updates of the GMM has on average been 7 months. Two large assurance events are also indicated in figure 5.36. Figure 5.39 shows the assurance events for the GMM.



Additional reviews as a result of submission of papers to journals
(*Bulletin of the Seismological Society of America*, *Earthquake Spectra*,
Bulletin of Earthquake Engineering and *Journal of Seismology*)

Figure 5.39 Peer Review Assurance Framework for GMM.

The acceleration records currently available in the Groningen area are for low-magnitude earthquakes ($M_L \leq 3.6$), which may cause aesthetic damage to buildings, but have proven to be too small to cause serious structural

damage. Figure 5.40 shows the available seismic records for epicentral distance and magnitude. The largest earthquake to date was only recorded by 6 accelerometers all located within 10 km from the epicentre. In contrast, the recent Slochteren earthquake was recorded by 68 stations up to a distance of 28 km from the epicentre. For the hazard and risk assessment, the ground motion forecasts for larger magnitude earthquakes need to be estimated. To achieve this, the available data needs to be extrapolated to larger magnitude earthquakes.

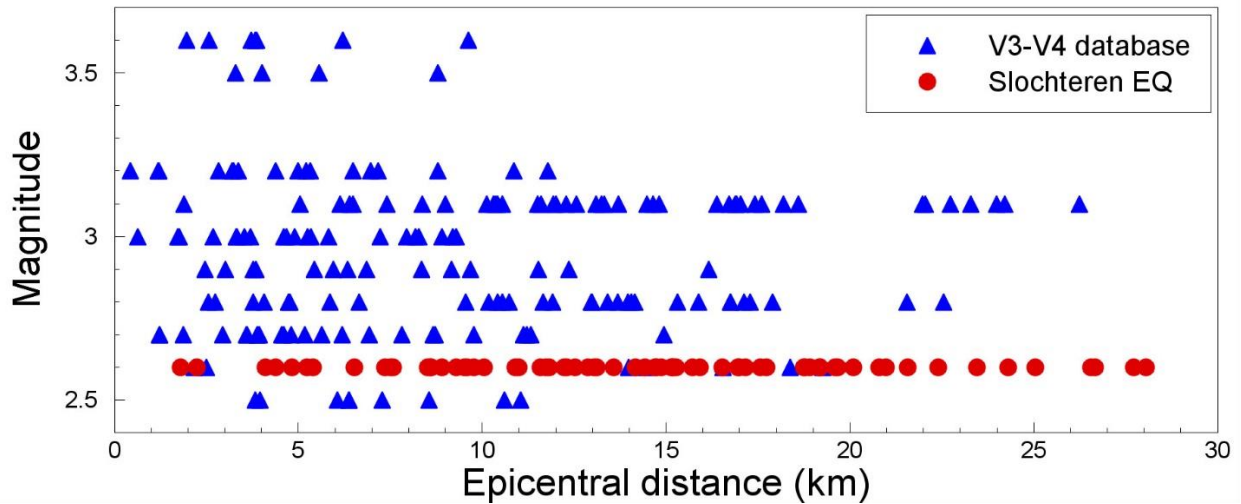


Figure 5.40 Distribution of the V5 Groningen ground-motion database in terms of local magnitude, M_L , and epicentral distance, R_{epi} .

Ground Motion Model

The framework for construction of the ground motion model is based on an inversion method to be able to extend the range of earthquake magnitudes from the current experience range to the full magnitude range required for the risk assessment (Ref. 12). The current experience range of magnitude is below $M_L = 3.6$. Disaggregation for risk of previous risk assessments showed that the earthquake magnitude range contributing most to risk was earthquakes with magnitude between $M_L = 4.5$ and 5.5 . The estimation of the maximum magnitude concluded that the limiting earthquake size for the field may lie in the range from $M_L = 4.5$ to 7.25 .

The inversion consists of two parts (Fig. 5.41). In the first part, using the existing seismic records and knowledge of the site where the recording was made, motions at the hard rock interface (NS_B) are deduced. Site amplification factors and damping at these sites are important factors in this process. In the second step, these motions at the hard rock interface, the source, path and site parameters are derived through inversion. The source parameters include the stress parameter and seismic moment (related to energy), while the path parameters include the geometric spreading model and the attenuation along the path.

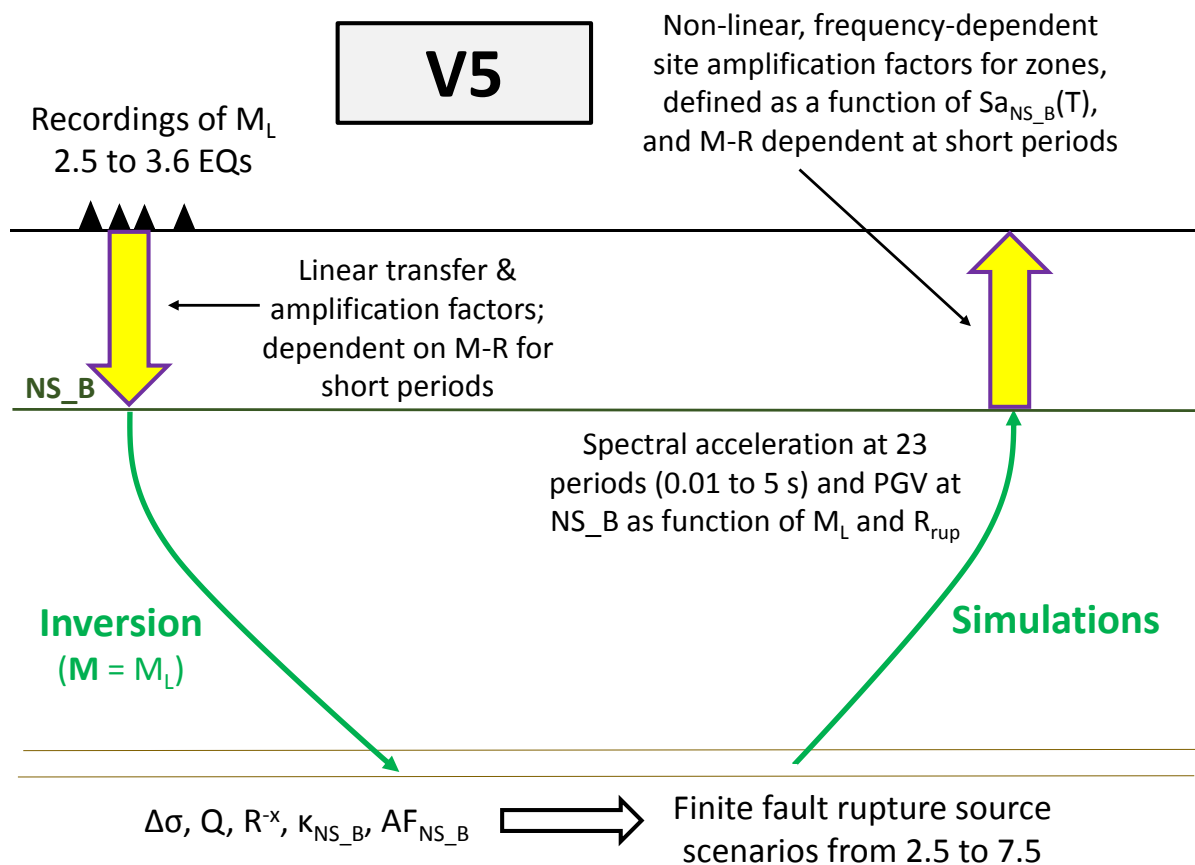


Figure 5.41 Schematic illustration of the development process adapted for the Version 5 update of the GMM.

Subsequently, the inverted source and path parameters are used in stochastic simulation to derive the motions at the reference hard rock interface. This can be done for a full range of values for these parameters also for much larger earthquake magnitude than observed in the Groningen field area. In the forward modelling to large magnitudes, multiple alternatives for the stress parameter—which controls the amplitude of the accelerations—are considered in order to capture the uncertainty associated with this extrapolation from the magnitude range of the data. This approach therefore allows for estimation of ground motions for a range of earthquake magnitudes required for the risk assessment.

Properties of the overburden (S-wave velocity and density)

To be able to predict ground motion at surface resulting from an earthquake originating from the Rotliegend reservoir located at 3 km depth, knowledge of the full rock and soil column from the surface down to the reservoir section and below is required (Fig. 5.42).

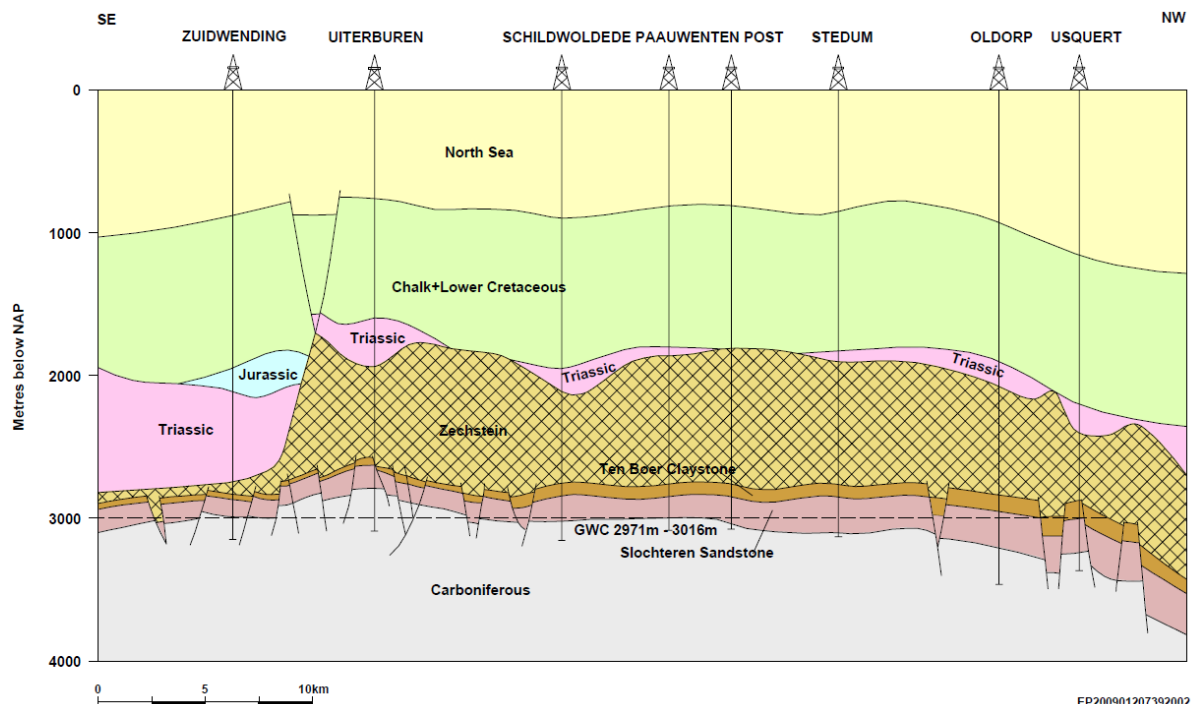


Figure 5.42 Simplified geological profile of the Groningen field. The thick Zechstein salt layers above the reservoir plays an important role in the transmission of seismic energy from the reservoir depth to the surface.

The model covers the full field area with an additional 5 km buffer zone and has an area of about 1,000 km². Rock property data, primarily density, P-wave velocity and S-wave velocity, were collected for different depths over the full area. Using different methods, data sets were acquired over different depth ranges (Fig. 5.43). The main data sets used to construct a model covering this full rock volume are:

- For the deeper section from below the reservoir up to some 60 m depth, the seismic data obtained during the 1980s supplemented by more recent well logging data was used. This includes density and sonic data (P- and S-wave velocity) obtained over the full well length in the most recently drilled three wells (BRW-5, BDM-5, ZRP-2 and ZRP-3A).
- The original seismic survey acquired in the 1980s was reprocessed and re-imaged using new inversion techniques to also obtain a detailed geological image of the shallow sub-surface. This technique improved the model over the depth range from 30 to 120 m depth.
- Well logs were obtained in 70 newly drilled wells of the geophone network. These wells are 200 m deep and provided log data over this depth range.
- Geophysical measurements of the response of the shallow subsurface and soil layers were carried out near the accelerometers that have been recording since the mid-1990's.
- A detailed geological model of the shallow sub-surface and soils was prepared. Main data source was the DINO and GEOTOP databases of TNO-NITG. These data were supplemented by additional data (primarily CPT data) from private parties acquired through Fugro and Wiertsema. A summary overview into the geology of the shallow underground of the Pleistocene was prepared.

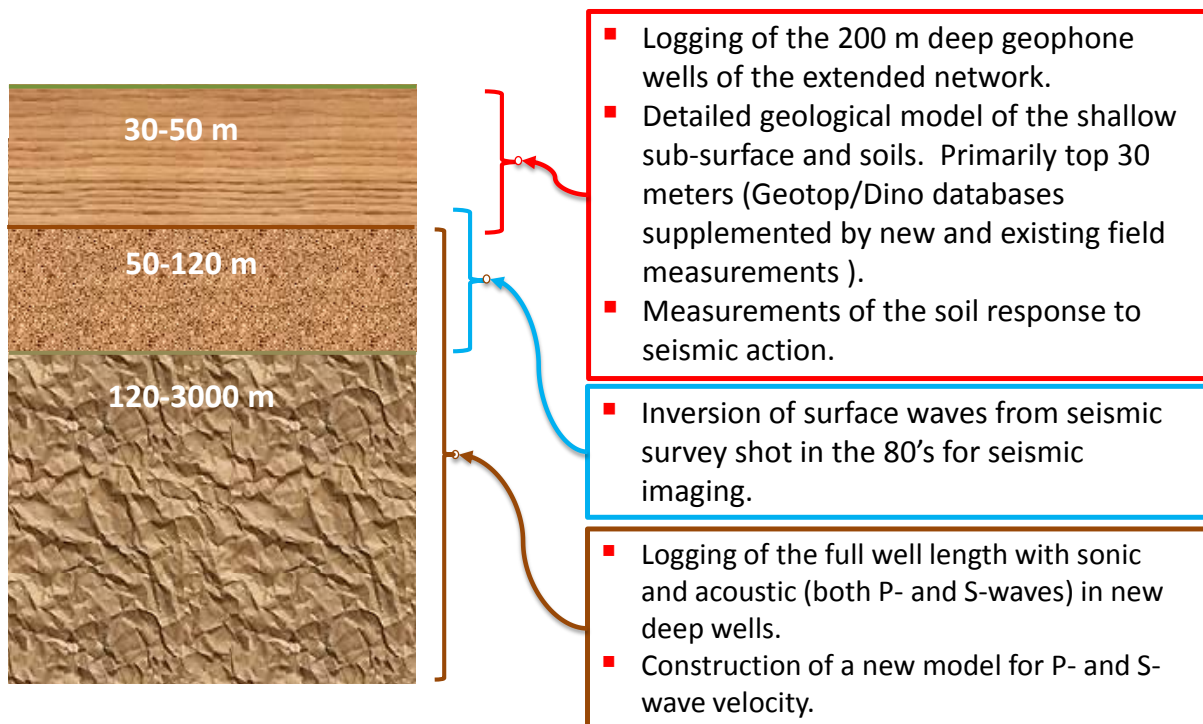


Figure 5.43 Rock column from the seismically active reservoir section to the surface (overburden), with the data gathering to improve our understanding of the progression of the seismic energy indicated in the boxes to the right.

Initiation in the Reservoir (Rotliegend Formation)

Geomechanical modeling and recorded earthquake data indicate that Groningen earthquakes originate in the Rotliegend reservoir section. This is particularly well demonstrated by data obtained from the geophones installed in the deep seismic observation wells in the Loppersum area. The GMM model is based on the simulation of finite ruptures in the Rotliegendes sandstone reservoir and for larger magnitude earthquakes also extending below the reservoir into the underlying Carboniferous rock.

Wave Propagation to the Near Surface (through Zechstein to Base Upper North Sea Formation)

Based on available seismic data from the surveys done in the 1980s, and supplemented by the density, P- and S-wave logs from the four new wells (Fig. 5.44), the model of the rock above and below the reservoir was updated. Figure 5.44 shows the P-wave velocity model and the different geological formations. Using this model, the spreading of the seismic energy as the earthquake wave progresses through the hard formations above the Rotliegend formation was modelled in detail. A snapshot of the simulated wavefield propagation is shown in Figure 5.45, with the seismic velocity structure in the background. The geologic layering in this deeper part of the Groningen subsurface has several geological interfaces, which have a significant impact on the spreading of the seismic energy as the waves travel upwards. Major interfaces such as those between the Rotliegend reservoir and the high-velocity Zechstein salt or the even higher velocity Zechstein anhydrites divide the wave energy through reflection and refraction. Other key geological interfaces, which further redistribute wave energy through reflection include the base of the Chalk and the base of the Lower North Sea Formation.

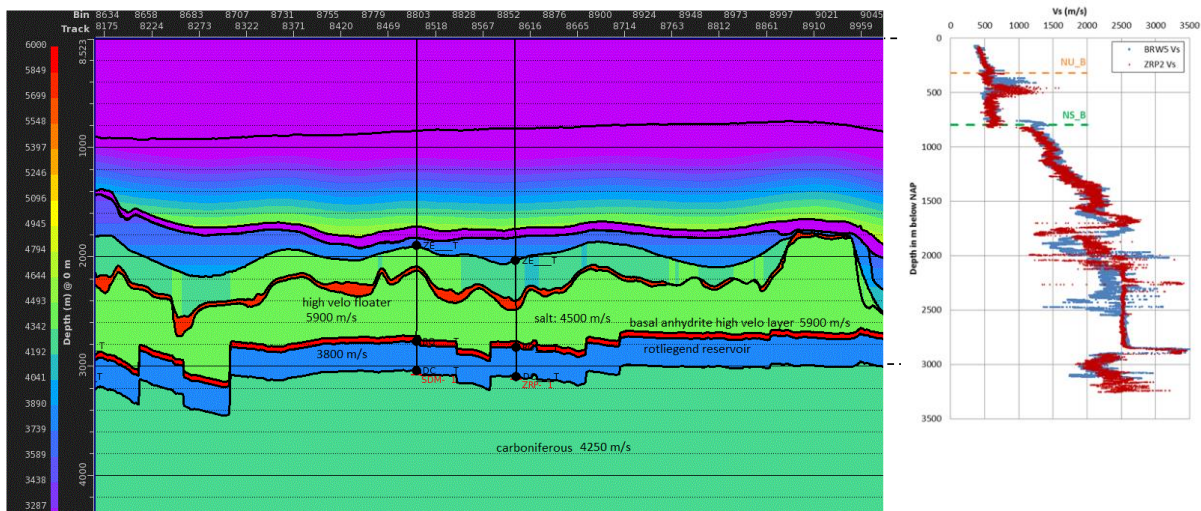


Figure 5.44 Left: P-wave model based on PSDM, DCAT and sonic logs S-wave model based on P – S sonic log relations per litho-stratigraphic unit. Right: Shear-wave velocity profiles from two deep borehole logs, indicating the location of the base of both the North Sea Supergroup Formation (NS_B) and the Upper North Sea Formation (NU_B) formations.

The progression of the seismic waves through the deeper formations is calculated up to the base of the North Sea supergroup (NS_B). This is across the field located at some 800 m depth. From this reference horizon upwards spatially-varying non-linear site amplification functions are used to estimate the ground motion at surface.

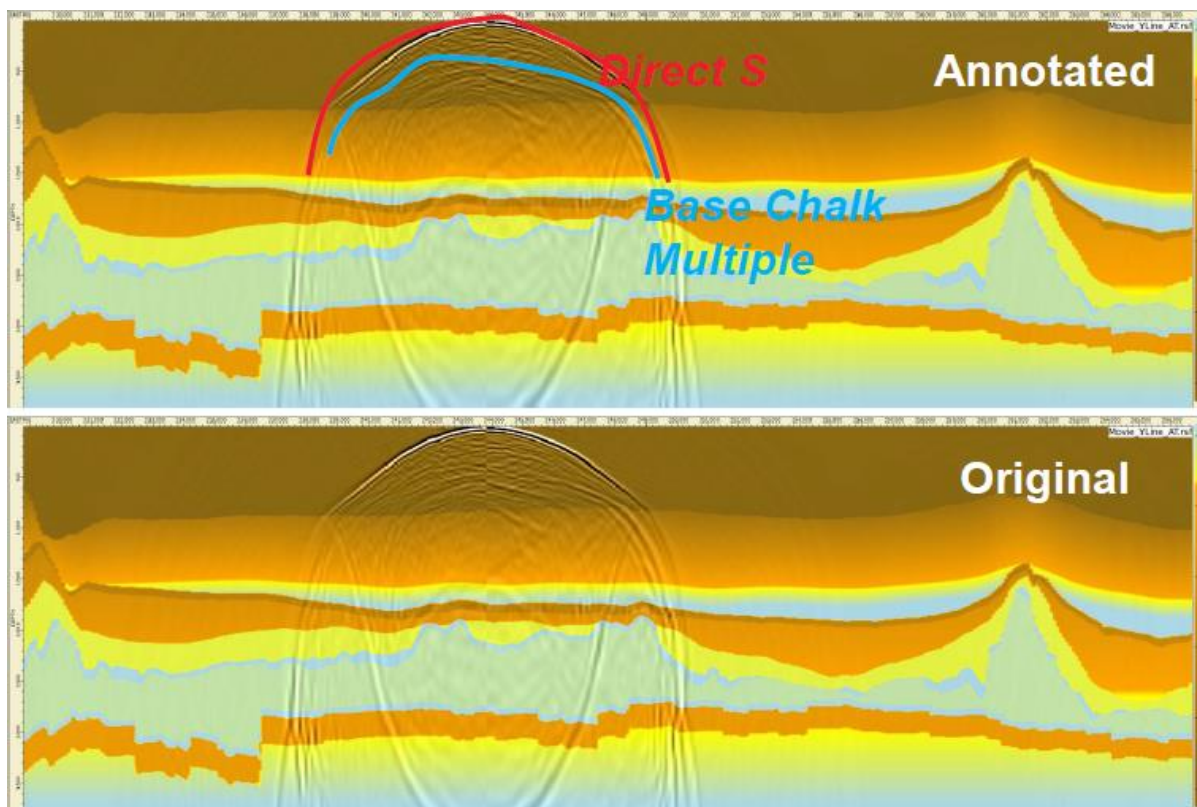


Figure 5.45 Image of the modelling of the progression of the seismic waves from the rupture area in the reservoir to the surface. This modelling does not include the effects of the approximately 350 m deep soil layer. The snapshot was taken 2.7 seconds after the rupture took place, when the S-waves reaches the surface.

While small-scale spatial variations in wave energy reaching the near surface are shown by elastic wave propagation modelling, a field-wide systematic reduction in wave energy has been independently predicted by two separate full elastic 3D wavefield modelling codes. This deviation is relative to the spherical $1/R$ -type spreading typical for a formation with homogenous and isotropic rock properties.

Wavefield analysis has shown that the primary source of the distance-dependent amplitude reduction is refraction of the up-going direct shear wave at the base of the Zechstein salt and anhydrites. The reduction does not depend on the continuous presence of these layers because of the many other strong velocity inversions in the Groningen stratigraphy. The reduction is robust to event location and source orientation, and is therefore incorporated as two distance-dependent terms. This phase of wave propagation, between the source and the near surface, is assumed to be linear, so this distance-dependent reduction in wave energy reaching the near surface is one aspect of the updated GMM which is independent of event magnitude.

To reflect the uncertainty in the resulting Spectral Acceleration predicted using Ground Motion Prediction methodology, a lower, central and upper model were prepared, straddling the uncertainty range. Figure 5.46 shows the Spectral Acceleration at 0.01 s.

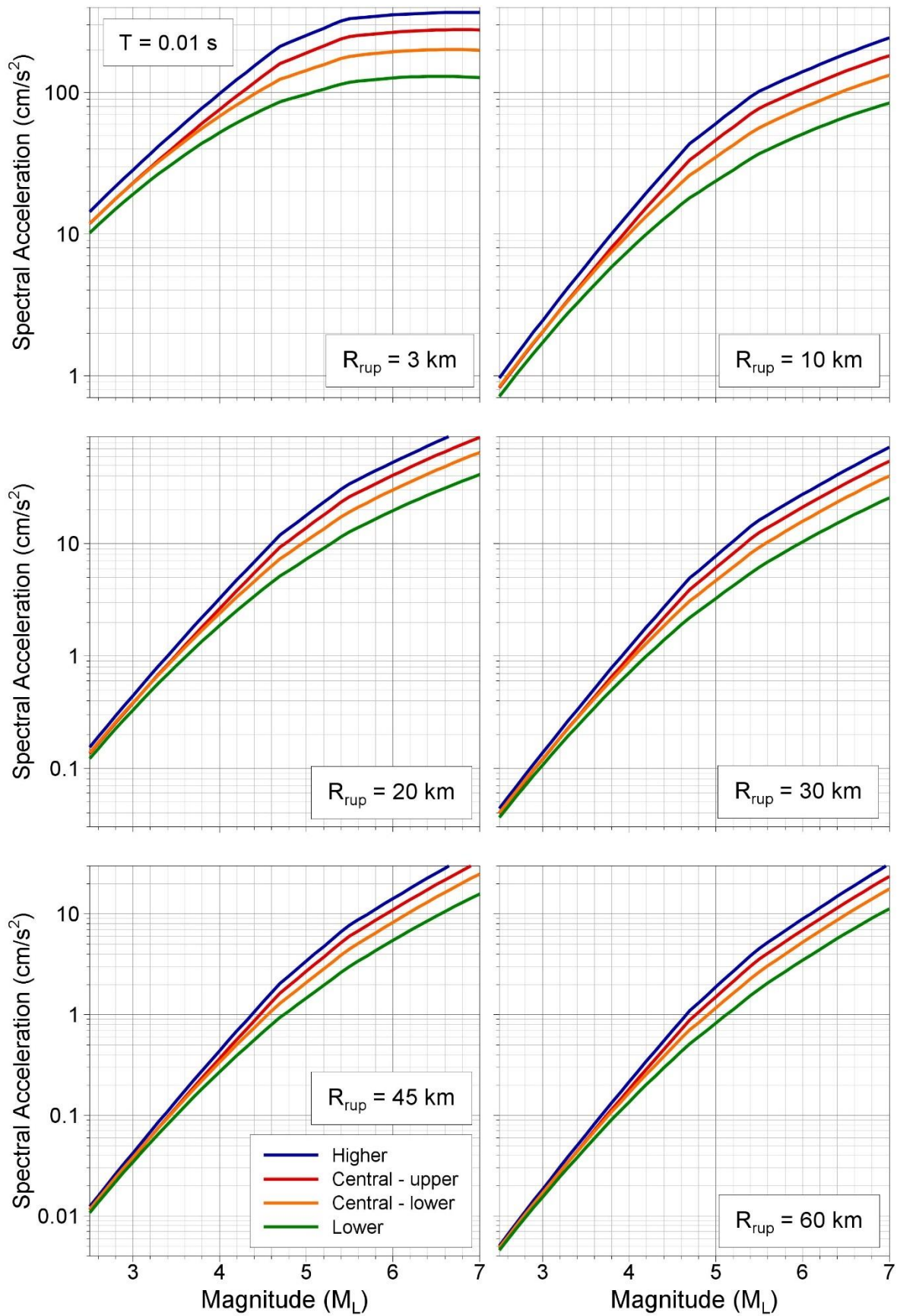


Figure 5.46 Spectral accelerations at 0.01 s from finite-rupture stochastic simulations for the four branches of the model at six rupture distances as a function of magnitude

Propagation to the Surface (from Base North Sea Formation to Surface)

A model of the shallow subsurface and soil was prepared by Deltares based on the GEOTOP model of TNO-NITG supplemented by additional data obtained from private owners through Wiertsema and Fugro (Ref. 4 to 6 and 9). This model assigns a lithostratigraphical unit and a lithological class to each voxel (small volume of rock in the model) in the Groningen area. This is required as V_s depends on both stratigraphy (i.e. formation, for instance Naaldwijk Formation) and lithology (i.e. sand, peat or clay). A description of the formations in the shallow Pleistocene geology of Groningen can be found in reference 3. Values of shear wave velocity (V_s) are assigned to geological formations present in the area of interest from published values of measured V_s in the Netherlands. In some cases, this assignment can be extended to lithological classes. Additionally, there are 60 seismic cone penetration tests (SCPTs) in the Groningen region that allow for determination of representative V_s values that are specific to this region. The SCPTs typically reach to a depth of approximately 30 m below the surface.

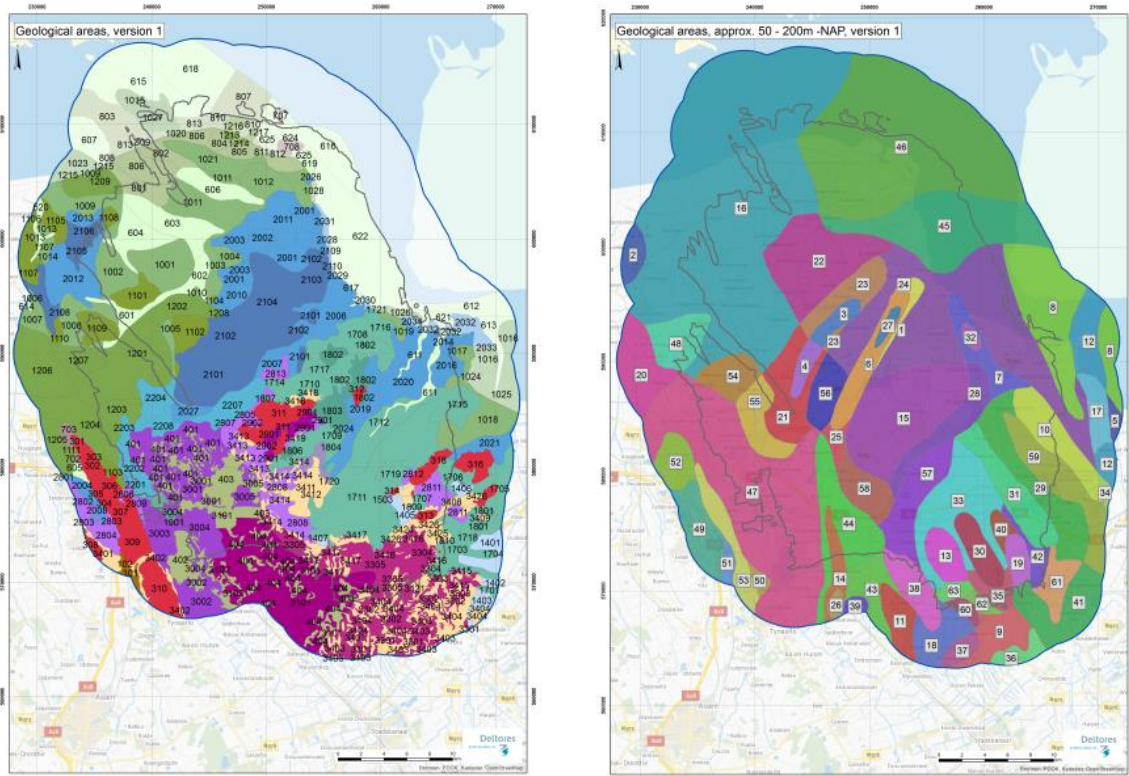


Figure 5.47 Left Surface to 50 m-NAP Map for entire field 225 geological areas sorted by profile type
 Right: 50 to 200 m-NAP Wider range for overlap with shallower part from top Peelo when shallower than 50 m-NAP and to at least base of Peelo when deeper than 200 m-NAP. This is for 3 geological areas, max depth is 235 m. Based on DGM, REGIS II, DINO, new borehole logs (15), geological expertise X-Y: map of geological areas Z: scenarios Wider range than 50 – 200 m-NAP < 50 m-NAP start at Peelo > 200 m-NAP when base of Peelo is deeper (max 235 m-NAP)

To extend the model deeper towards the reference level of the Base Upper North Sea, use was made of the large seismic survey campaigns conducted by NAM/Shell around 1988 to obtain a clear image of the deep gas reservoir. Legacy datasets were reinterpreted to extend the V_s distributions to depths beyond those measured by the SCPT. Using the at the time of acquisition unwanted surface waves (ground roll data) both V_p and V_s were derived using the Modal Elastic Inversion method (MEIDAS). Because of the acquisition setup, which tried to reduce ground roll, and the frequencies present in the data, the depth range for which the near surface model obtained from the MEIDAS inversions is considered to be reliable from approximately 30 to 120 m below the surface (Figure 5.48).

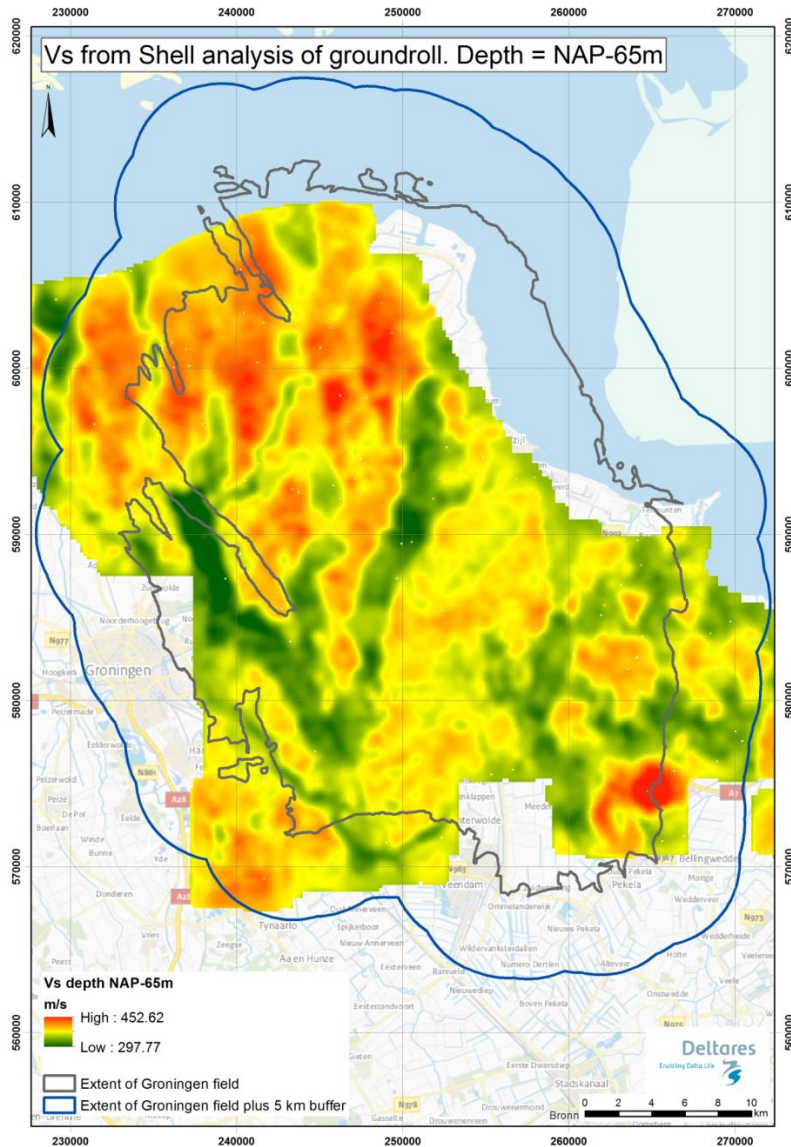


Figure 5.48 The V_s model from the inversion of the ground roll yielded depth slices of V_s at 10 m depth intervals. This figure shows a depth slice at NAP-65 m through the MEIDAS V_s model.

Overlapping with and extending below the depth range covered by the Model of the shallow Pleistocene geology and the MEIDAS model, the model based on the active seismic acquisition in the 1980s is used to reach the reference level of the Base Upper North Sea (Fig. 5.48).

Recognising the need to have reliably measured shear-wave velocity profiles at the recording stations, *in situ* measurements were conducted at the locations of the KNMI accelerometer stations (Ref. 10). The campaign of *in situ* measurements of site response applied a wide range of techniques at the first few stations in order to select those most suitable for general application across the networks. The multiple measurement approach was also designed to provide insight into the inherent uncertainty in the resulting V_s profiles and, to some extent, the degree of lateral heterogeneity at each site. The techniques included seismic CPT (with differing offsets), active MASW (with multiple sources), passive MASW, cross-hole measurements and PS suspension logging. Some of the borehole measurements, particularly the PS suspension logging, proved challenging in the Groningen ground conditions, but extensive measurements using seismic CPT and both active and passive MASW have been conducted at all of the 18 KNMI accelerograph stations.

The measured V_s profiles at accelerograph sites confirm the quality and reliability of the GeoTop-based near-surface profiles (Fig. 5.49).

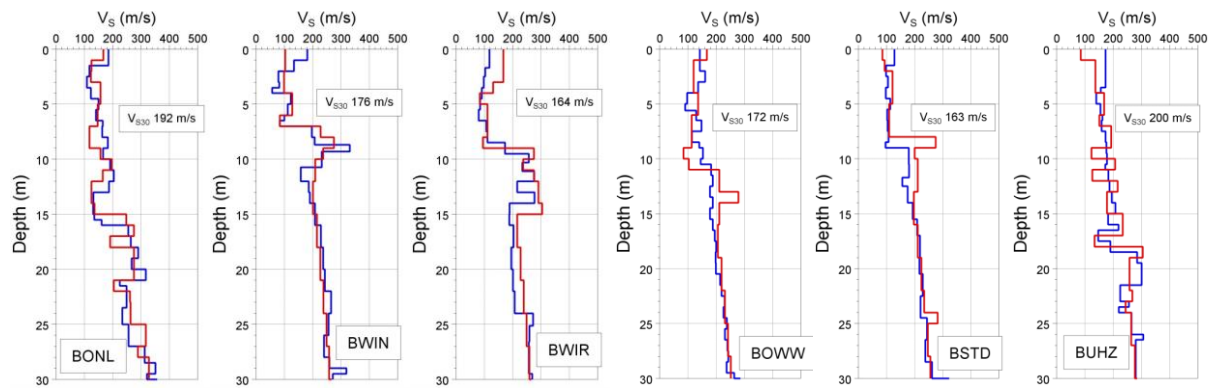


Figure 5.49 MASW, seismic CPT, cross-hole and PS suspension logging deployed to measure the shallow V_s profiles at the 18 permanent surface accelerograph (B-stations) sites operated by KNMI to constrain the part of the profile exerting greatest influence on the surface motions.

These measured V_s profiles will now replace the inferred profiles from the GEOTOP model and look-up tables, allowing more reliable deconvolution of the surface recordings to the NS_B horizon. For the site response modelling, the new measurements will enable a refinement of the empirical relationships used to define the look-up tables through which dynamic soil properties are assigned. Additionally, laboratory experiments are planned to better determine the stiffness and damping characteristics of the peat deposits in the Groningen field so that their influence on the site response can be more accurately modelled.

Based on this detailed description of the shallow geology, zone amplification factors were derived that define the change in amplitudes of the waves as they travel from the NS_B horizon to the ground surface (Fig. 5.50).

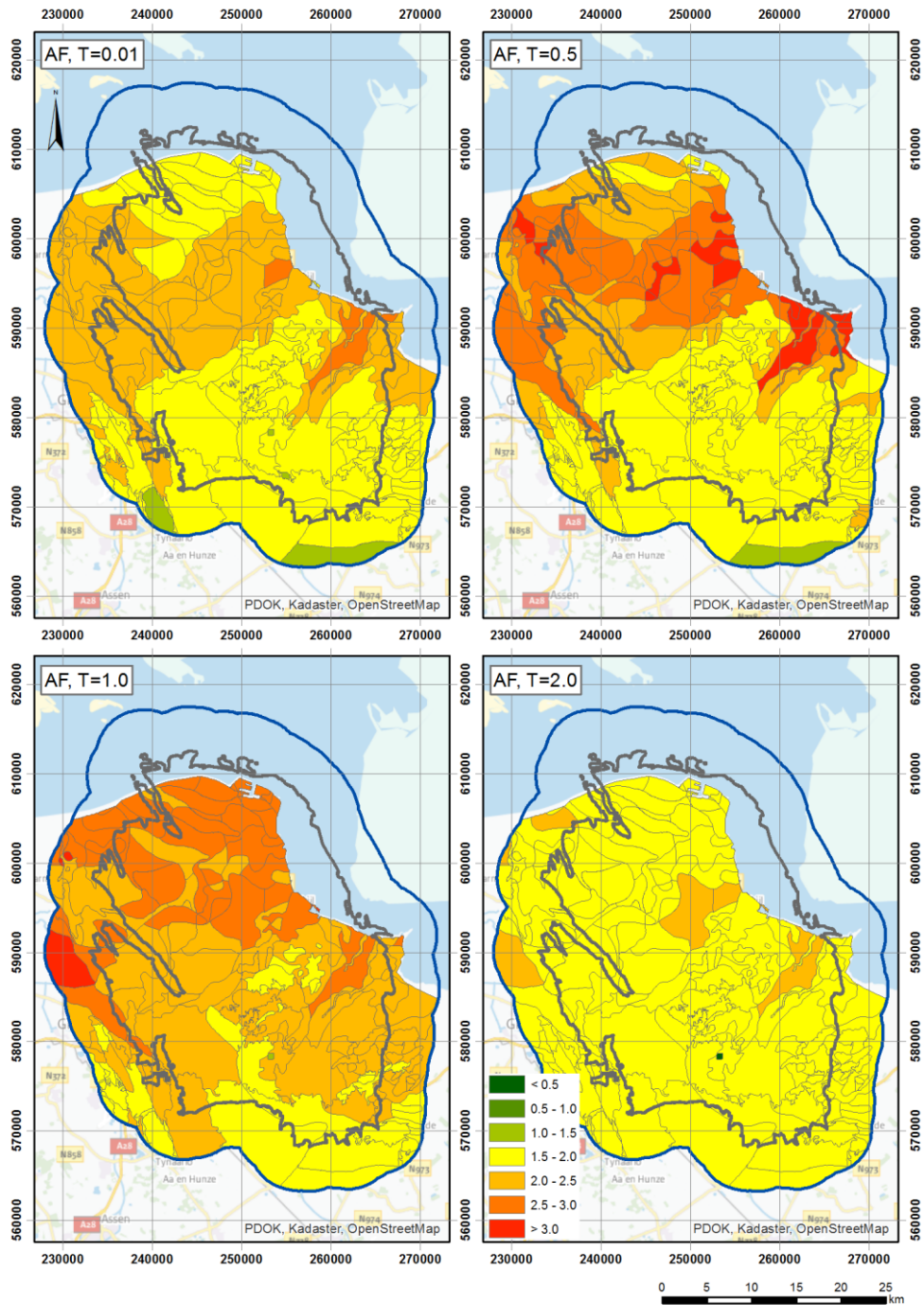


Figure 5.50 Amplification factors (AF) for the Groningen region for a scenario with $M 4.0$ and $R_{epi} 50$ km. AF for four periods are shown.

For the Groningen profiles, the nonlinearity of the soil properties with larger excitations implies a reduction in AF for shorter periods but an increase in the AFs at longer periods. This increase is expected as the resonant period of the sites shifts to longer periods as the soil softens (Figure 5.51).

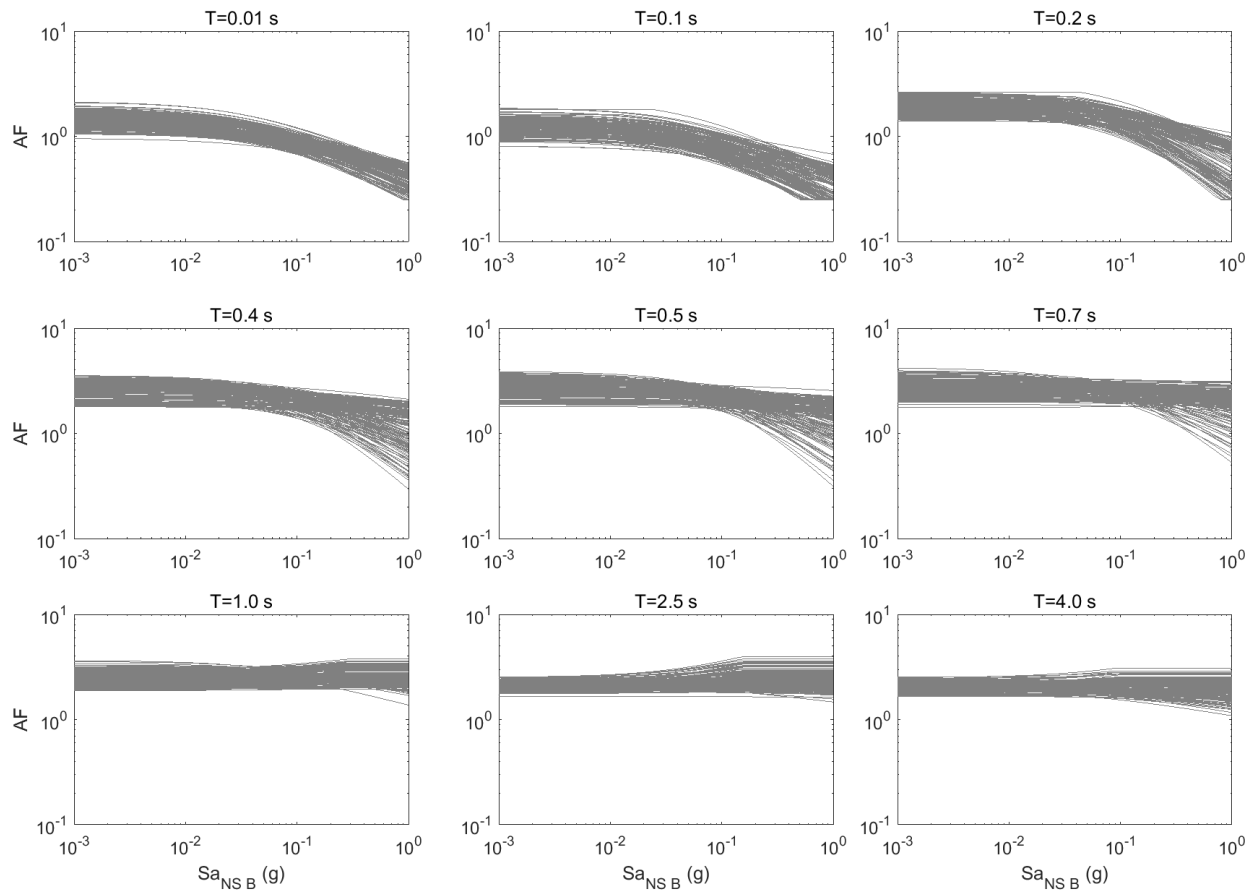


Figure 5.51 *Non-linear site amplification factors (ratios of acceleration at the ground surface to acceleration at the NS_B horizon) for spectral accelerations at selected oscillator periods*

These three steps allow prediction of the transmission of seismic energy from the reservoir to the surface and estimation Ground Motion resulting from an earthquake. Every step in the Ground Motion prediction methodology is supported by evidence collected in the Groningen area and bespoke models based on this evidence, and also consistent with well-established seismological theory while fully capturing all sources of uncertainty.

As well as predicting the median (or best estimate) values of the ground-motion amplitudes, the model also characterises the variability (or apparent randomness) in the predictions. These are represented by Gaussian or normal distributions of residuals, which are characterised by their standard deviation (sigma). The sigmas capture the earthquake-to-earthquake variability and the spatial variability of the ground motions at the NS_B horizon, as well as the variability of the site amplification factors within each of the 160 zones into which the field has been divided for the purposes of modelling the ground shaking.

Improvements in subsequent updates of the GMM

Since the Hazard Assessment of Winningsplan 2013, the Ground Motion Prediction Methodology has been continuously improved adding new features with each subsequent update. The two main areas of further study are the impact of anthropogenic soils like wierden/terpen (Ref. 8) and additional data acquisition using the flexible geophone network to establish an improved V_s characterisation for the top 500 to 800 m (Ref. 13). The response of the wierden would impact the assessment of the ground motion response locally for the building located on the wierden, but not lead to an update of the GMM. Recordings from the KNMI and TNO networks together with data from the flexible network will also be used to derive a Groningen-specific model for spatial correlation to check the implied spatial correlation imposed through the zoned approach to the ground motion prediction.

The table below gives an overview of the added features over the development phases:

GMPE Feature	Hazard Assessment Winningsplan 2013	Intermediary Hazard and Risk Assessment May 2015	Hazard and Risk Assessment November 2015	Mid -2016	Mid-2017	Hazard and Risk Assessment November 2017
	V0	V1	V2	V3	V4	V5
Predicted parameters	PGA, PGV	Sa(T) for 5 periods	Sa(T) for 16 periods	Sa(T) for 23 periods	Sa(T) for 23 periods, PGV	Sa(T) for 23 periods, PGV
Distance Metric	R_{epi}	R_{epi}	R_{epi}	R_{epi}	R_{rup}	R_{rup}
Sigma model (variability)	Akkar <i>et al.</i> (2014a)	Groningen-specific	Groningen-specific	Groningen-specific	Groningen-specific	Groningen-specific
Epistemic uncertainty	Single model	Three alternatives (Coupled μ and σ)	Three alternatives (Coupled μ and σ)	Three alternatives (Coupled μ and σ)	Eight alternatives (four μ and two σ)	Eight alternatives (four μ and two σ)
Target Horizon	Surface	NU_B and surface	NS_B and surface	NS_B and surface	NS_B and surface	NS_B and surface
Site classification	$V_{s30} = 200$ m/s across the field	Field-wide constant	Zonation based on amplification factors (167 zones)	Zonation based on amplification factors (161 zones)	Zonation based on amplification factors (160 zones)	Zonation based on amplification factors (160 zones)
Site amplification	Akkar <i>et al.</i> (2014a)	Network average, linear extrapolation	Zone-specific, non-linear frequency dependent AF's	Zone-specific, non-linear frequency dependent AF's	Zone-specific, non-linear frequency dependent AF's; M-R dependence at short periods	Zone-specific, non-linear frequency dependent AF's; M-R dependence at short periods
Components	Horizontal geometric mean	Horizontal geometric mean	Horizontal geometric mean and arbitrary components, the latter accounting for the component-to-component ratios (polarisation)	Horizontal geometric mean and arbitrary components, the latter accounting for the component-to-component ratios (polarisation)	Horizontal geometric mean and arbitrary components, the latter accounting for the component-to-component ratios (polarisation)	Horizontal geometric mean and arbitrary components, the latter accounting for the component-to-component ratios (polarisation)
Period-to-period correlations		Akkar <i>et al.</i> (2014b)	Akkar <i>et al.</i> (2014b)	Baker and Jayaram (2008)	Baker and Jayaram (2008)	Baker and Jayaram (2008)
Duration model	n/a	Adopted model from California	Adjusted California model to Groningen conditions	Adjusted new global model to Groningen conditions	Groningen-specific model based on finite fault simulations	Groningen-specific model based on finite fault simulations

Table 5.5 Key features of the three phases of Groningen GMM development

References

1. Ground Motions from the ML 2.6 Slochteren Earthquake of 27th May 2017, Julian J Bommer, Michail Ntinalexis, Ewoud van Dedem, Jelena Tomic, Leendert Geurtsen and Jeroen Uilenreef, June 2017
2. Technical Addendum to the Winningsplan Groningen 2013; Subsidence, Induced Earthquakes and Seismic Hazard Analysis in the Groningen Field, Nederlandse Aardolie Maatschappij BV (Jan van Elk and Dirk Doornhof, eds), November 2013.
3. De ondergrond van Groningen: een Geologische Geschiedenis, Erik Meijles, April 2015.
4. Geological schematisation of the shallow subsurface of Groningen (For site response to earthquakes for the Groningen gas field) – Part I, Deltares, Pauline Kruiver, Ger de Lange, Ane Wiersma, Piet Meijers, Mandy Korff, Jan Peeters, Jan Stafleu, Ronald Harting, Roula Dambrink, Freek Busschers, Jan Gunnink
5. Geological schematisation of the shallow subsurface of Groningen (For site response to earthquakes for the Groningen gas field) – Part II, Deltares, Pauline Kruiver, Ger de Lange, Ane Wiersma, Piet Meijers, Mandy Korff, Jan Peeters, Jan Stafleu, Ronald Harting, Roula Dambrink, Freek Busschers, Jan Gunnink
6. Geological schematisation of the shallow subsurface of Groningen (For site response to earthquakes for the Groningen gas field) – Part III, Deltares, Pauline Kruiver, Ger de Lange, Ane Wiersma, Piet Meijers, Mandy Korff, Jan Peeters, Jan Stafleu, Ronald Harting, Roula Dambrink, Freek Busschers, Jan Gunnink
7. Development of Version 2 GMPEs for Response Spectral Accelerations and Significant Durations for Induced Earthquakes in the Groningen field, Julian J Bommer, Bernard Dost, Benjamin Edwards, Pauline P Kruiver, Piet Meijers, Michail Ntinalexis, Barbara Polidoro, Adrian Rodriguez-Marek & Peter J Stafford, October 2015
8. Terp composition in respect to earthquake risk in Groningen, Dr. ir. E.W. Meijles, Dr. G. Aalbersberg and Prof. Dr. H.A. Groenendijk, March 2016.
9. Modifications of the Geological model for Site response at the Groningen field, Deltares, Pauline Kruiver, Ger de Lange, Ane Wiersma, Piet Meijers, Mandy Korff, Jan Peeters, Jan Stafleu, Ronald Harting, Roula Dambrink, Freek Busschers, Jan Gunnink
10. Geophysical Measurements of shear wave velocity at KNMI accelerograph stations in the Groningen field area, Deltares, Marco de Kleine, Rik Noorlandt, Ger de Lange, Marios Karaoulis and Pauline Kruiver, July 2016.
11. Empirical Ground-Motion Prediction Equations for Peak Ground Velocity from Small-Magnitude earthquakes in the Groningen field using multiple definitions for the Horizontal Component of Motion, Julian Bommer, Peter Stafford and Michail Ntinalexis, November 2016
12. V4 Ground-motion Model (GMM) for Response Spectral Accelerations, Peak Ground Velocity and Significant Duration in the Groningen field, Julian Bommer, Bernard Dost, Benjamin Edwards, Pauline Kruiver, Pier Meijers, Michail Ntinalexis, Adrian Rodriguez-Marek, Elmer Ruigrok, Jesper Spetzler and Peter Stafford, Independent Consultants, Deltares and KNMI, June 2017 with Parameter files - V4 Ground-Motion Model (GMM) for Response Spectral Accelerations, Peak Ground Velocity, and Significant Durations in the Groningen Field, Supplement to V4 GMM, Julian Bommer and Peter Stafford, Independent Consultants, June 2017
13. Wat gebeurt er met het Flexibele Geofoon Netwerk?, Stand van zake 1 maart 2017, Nederlandse Aardolie Maatschappij BV, February 2017, Jan van Elk & Dirk Doornhof

6 Hazard Assessment

Hazard Metric

Different metrics have been proposed to describe the hazard resulting from seismic activity. Most commonly used are the peak ground velocity (PGV) and peak ground acceleration (PGA). Because the focus of previous hazard studies was the assessment of risk, acceleration (PGA and spectral acceleration) was used as the prime metric for the hazard assessments. As this study will, for the first time, extend to the prediction of building damage, additional hazard metrics will be assessed (Ref. 1).

In the current report, the hazard assessment is based on Ground Motion Prediction Methodology (GMM) Version 5 (Ref. 3). This version of the GMM incorporates the minor comments from the assurance committee for ground motion prediction (see Table D.3 in Appendix D) on the previous release GMM version 4 (Ref. 2), which was prepared and assured May 2017, at the request of the NEN-NPR committee.

Risk Assessment

Peak Ground Acceleration (PGA) is a widely used metric for ground shaking intensity and was chosen as the most appropriate hazard metric for the seismic hazard assessment in support of the assessment of risk. Figure 6.1 shows the measured acceleration near the epicentre during the Huizinge earthquake of 16th August 2012. For the assessment of the response of a building to ground shaking spectral acceleration (SA) is used. This takes into account the response period of the building being considered. In addition to the peak PGA values, the duration of the event is also important for the seismic risk. Ground Motion Prediction methods have therefore focused on prediction of PGA, spectral acceleration at several periods and the significant ground shaking duration. These are the most important hazard parameters for the prediction of building collapse, failure of building elements and hence for personal risk.

Building Damage Assessment

For the assessment of the potential to cause building damage, velocity-based hazard metrics such as PGV (Peak Ground Velocity) are also important. Empirical evidence elsewhere has shown that building damage at lower damage states (damage states DS1 and DS2) correlates strongly with PGV. A Groningen-specific (induced) Ground Motion Prediction method to estimate the value of PGV at specific locations has therefore been developed as part of the Ground Motion Prediction Methodology Versions 4 and 5. The assessment of PGV is primarily in support of assessment of building damage due to historical earthquakes and expected future damage.

The official Dutch guidelines for assessing the impact of vibrations on buildings, as presented in the document “Building Damage: Measurement and Assessment” by the SBR (Ref. 4 and 5), are based on the ground velocity metric V_{TOP} . To ensure consistency with the SBR Guidelines, apart from the geometric mean velocity also a Ground Motion Prediction method for the V_{TOP} parameter (the ‘maximum’ value of PGV in any direction) was developed.

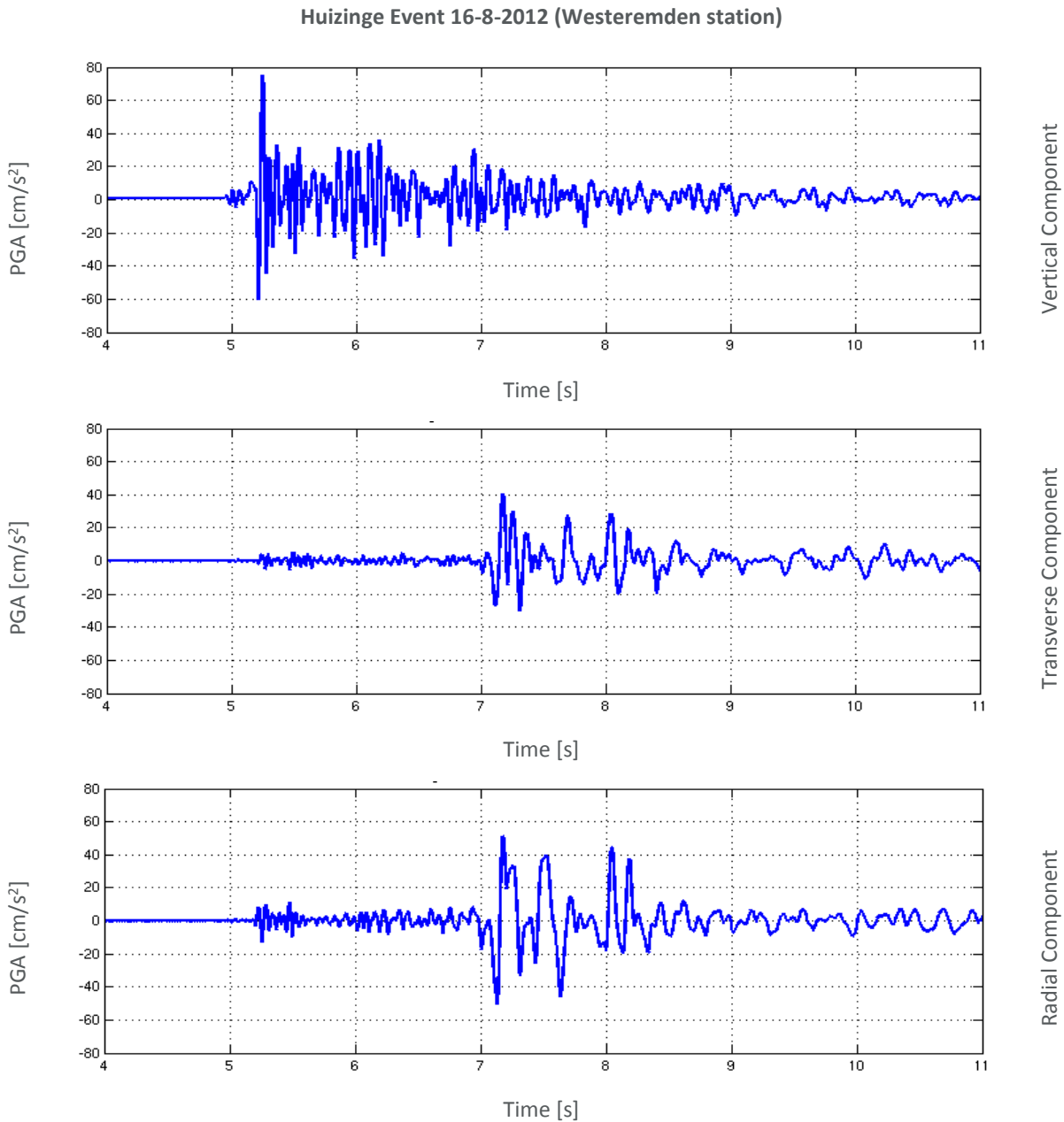


Figure 6.1 Accelerogram of the earthquake near Huizinge recorded at the 16th August 2012 by the accelerometer located near Westeremden (near the epicentre).

Hazard Map for Peak Ground Acceleration

For the probabilistic description of the ground accelerations (PGA, or generalised to Pseudo Spectral Acceleration, PSA), a hazard map is used. On this map for each location the acceleration is plotted that could occur, with a prescribed annualised probability of exceedance (exceedance level), during a prescribed analysis period. Hazard levels are shown using a gradual colour scale.

The hazard maps shown in this document were constructed according to the following procedure. Each location in the analysis area during the analysis period is subjected to ground motion accelerations resulting from induced

earthquakes. At some locations, e.g. near Loppersum, the chance of exceeding a given peak ground acceleration threshold is higher than at the periphery of the field. Equally, at any one location, the chance of exceeding some value of peak ground acceleration decreases with increasing peak ground acceleration. An example of a set of hazard curves is shown for a number of locations in figure 6.2. Each declining line indicates the hazard curve for a single location in the field.

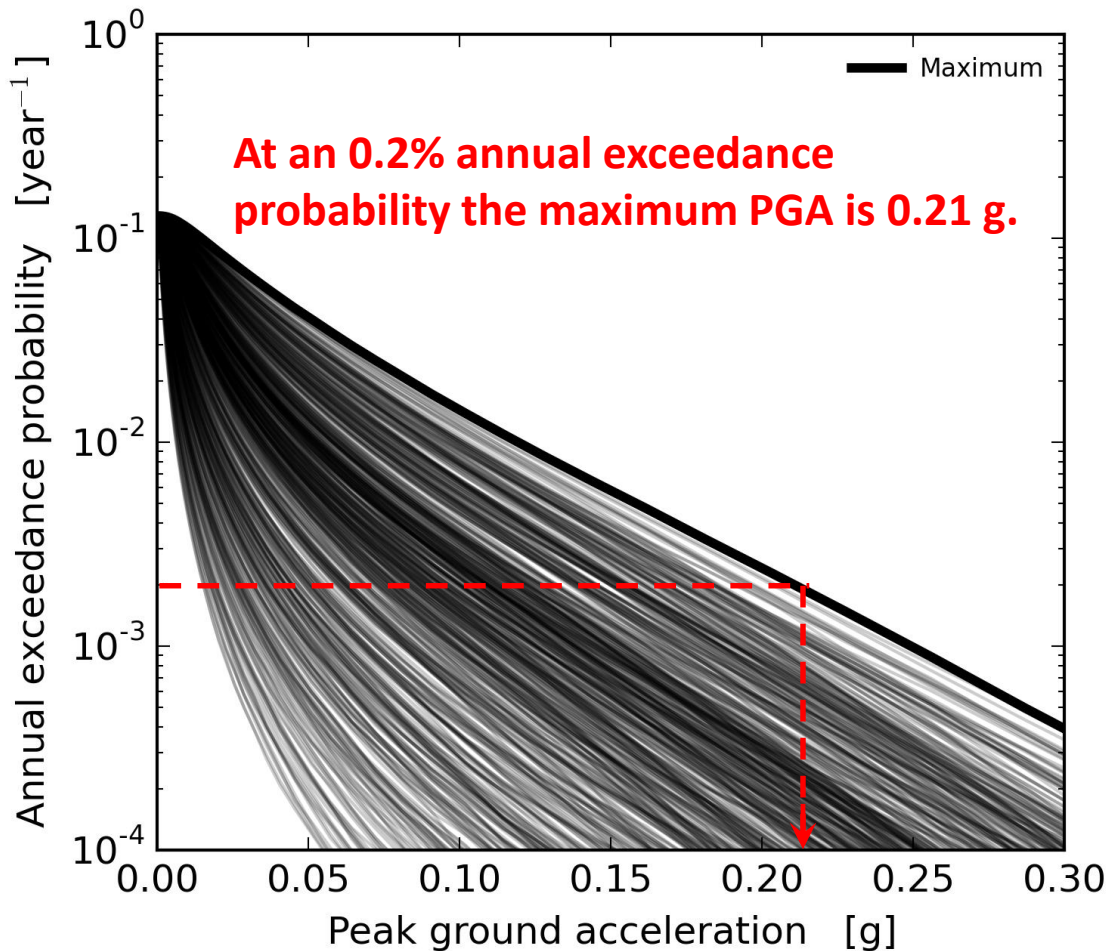


Figure 6.2 An example of a set of hazard curves showing average annual exceedance rate for peak ground acceleration at different locations in the field. Each line corresponds to a location in the field. The bold line indicates the maximum PGA anywhere within the field for a given exceedance level (bounding envelope). In this figure, the red line indicates that for an exceedance level of 0.2%/year the highest PGA in the field is 0.21g. Generic figure.

To prepare a hazard map, an exceedance level needs to be chosen. This is not a purely technical choice. However, inspired by Eurocode 8⁹, part of the current technical standards for structural design in Europe, it has become common practice to prepare hazard maps for an exceedance level of 0.2%/year. This exceedance level is equivalent to a 475-year return period for stationary seismicity. The same exceedance level is also used by KNMI for their hazard maps, which allows for comparison of these hazard maps. The choice of the exceedance levels (or return period) is

⁹ The Eurocodes are the current technical standards for structural design in Europe, and it is now compulsory for the 28 countries in the Eurocode zone to adopt these. Eurocode 8 specifically deals with earthquake-resistant design of structures (CEN, 2006). Each country adopting Eurocode 8 must develop a National Annex to indicate how the code is implemented; the National Annex for the Netherlands is being developed. Eurocode 8 uses a standard practice to represent seismic hazard via PGA maps associated with ground motions having a 10% probability of exceedance during 50 years, equivalent to 0.2%/year for a stationary process, or a return period of 475-years.

only for the representation of the hazard. This choice of exceedance level does not affect the subsequent assessment of risk. Hazard maps can also be prepared for spectral acceleration at a specified period. The standard PGA hazard map is the same as the spectral acceleration hazard map at shortest period, which for this assessment was chosen at 0.01 s.

Probabilistic Hazard Assessment

Seismic Event Rate and Total Seismic Moment Rate with time

Starting at the first step of the causal chain, from gas production via the resulting compaction, seismicity can be assessed. Seismicity is interpreted in this context as the event rate density of earthquakes larger than $M \geq 1.5$ and the frequency-magnitude distribution characterised by its slope (b-value) and upper bound (M_{max}). This minimum earthquake magnitude of $M = 1.5$ corresponds to the minimum magnitude of an earthquake, which the installed KNMI geophone network was historically able to record reliably (independent of its location within the field boundary or time of day). Earthquakes with smaller magnitude have not always been detected, because the signal might not have been distinguished from the background noise.

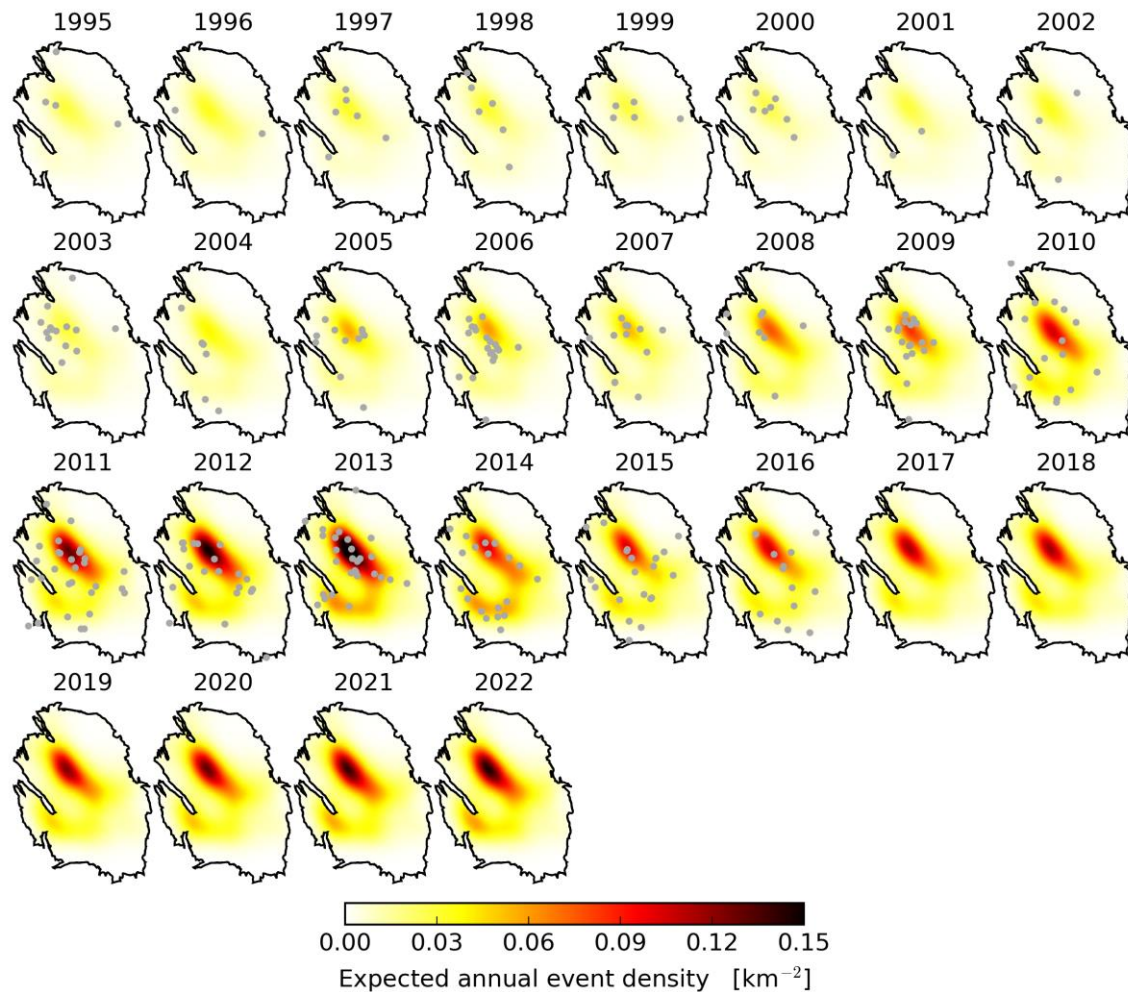


Figure 6.3 Expected annual event density maps over the period from 1995 to 2023 using the central branch of the seismological model. The forecast period is based on the production plan for 24.0 bcm/year and the linear compaction model. Grey dots denote the observed epicenters of $M \geq 1.5$ events.

Historical earthquake density maps for the period 1995 to 2016 are shown in figure 6.3. Clearly the increasing trend in the number of earthquakes each year can be seen. The earthquake density for later years shows the forecasted development of seismicity based on a production scenario of 24 Bcm/year.

Over the period from 1995 to 2016, the results of the Monte Carlo simulation and the observations for the annual event count and annual total seismic moments are shown in figure 6.4 and 6.5 respectively. The observed annual total seismic moment fluctuates around the median values of the simulated annual total seismic moments, but remains within the grey uncertainty band (the 95% confidence interval). This indicates the model is well calibrated. For the period 2017 to 2022, the forecasted annual total seismic moments and their confidence intervals are indicated. For this production scenario, the median annual total seismic moment is forecasted to remain in range similar to the actual observed seismic moment in the period 2012 – 2016.

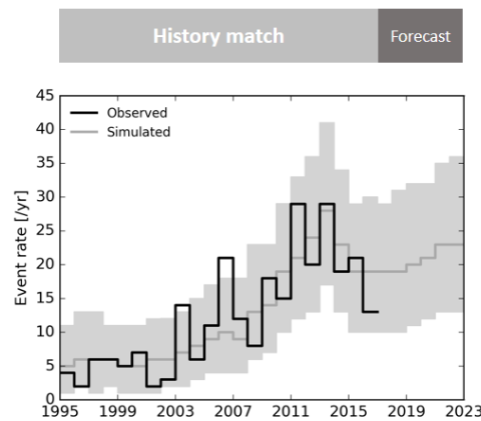


Figure 6.4 The annual number of $M \geq 1.5$ according to the seismological model with aftershocks for the 24BCM production scenario. Simulated results are based on 10,000 independent simulations; grey lines and regions denote the expected annual event count and its 95% confidence interval respectively. These simulations are based on Monte Carlo sampling of the distribution of estimated parameter values and includes aftershocks.

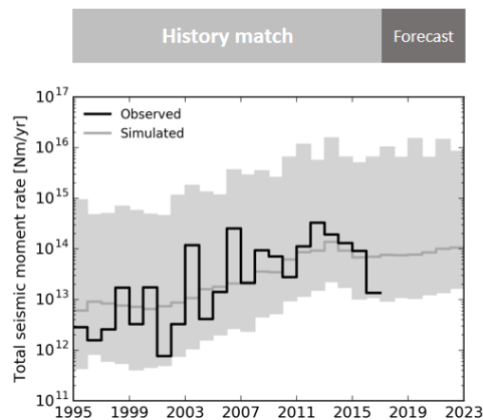


Figure 6.5 The annual total seismic moment according to the seismological model with aftershocks for the 24BCM production scenario. Simulated results are based on 10,000 independent simulations; grey lines and regions denote the expected annual total seismic moment and its 95% confidence interval respectively. These simulations are based on Monte Carlo sampling of the distribution of estimated parameter values and includes aftershocks.

Ground Acceleration incorporating Local Site Effects

The effects of the local shallow subsurface and soils on ground acceleration can be incorporated by subdividing the Groningen field area in smaller areas, based on the observed variation in the dynamic site response reflecting differences in the subsurface composition. The reference rock horizon is the base of the Base North Sea formation (NU_B), which is about 800 m below the ground surface. The motions are first predicted at this elevation, including random sampling from both the between-earthquake and within-earthquake components of variability, and then these rock motions are transferred to the ground surface via the site amplification factors.

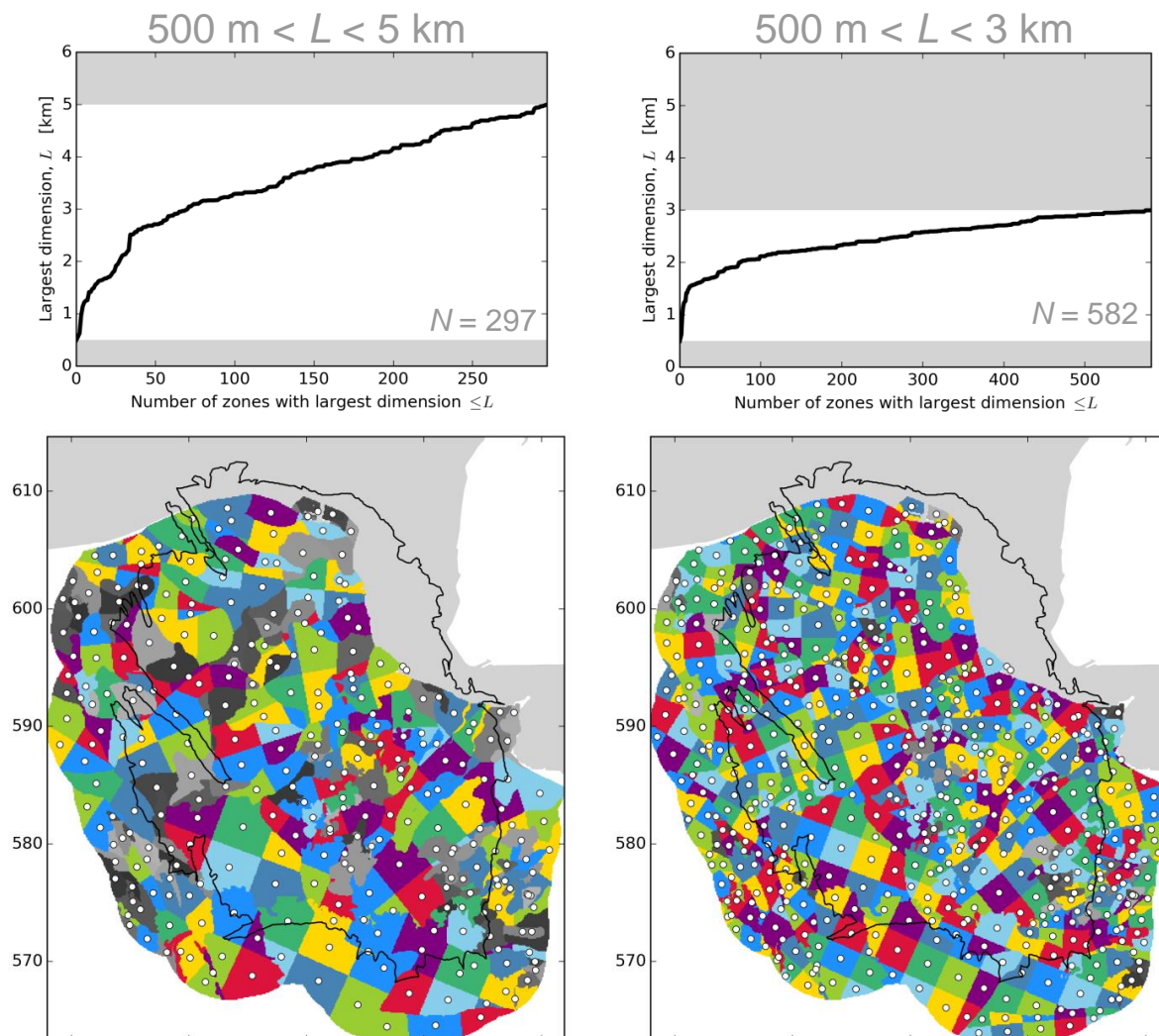


Figure 6.6 Zonation of the near-surface amplification of ground motion is represented by an irregular grid to honour the mapped geological boundaries: Left zonation with 300 zones. Right zonation with 500 zones. Note that colours do not represent any geological property but are randomly assigned to illustrate the topology of the grid.

Irregularly shaped zones were chosen to represent the complex local geological features in the shallow subsurface such as channel infills and peat areas, as realistically as possible. This causes an additional computational challenge, but leads to an improved result. Figure 6.6 shows two different zonation options. A sensitivity analysis comparing the results from using the two zonation schemes motivated the use of the zonation scheme with some 300 different soil response areas, within each which a single frequency-dependent amplification factor is applied together with a

site-to-site variability term that reflects, amongst other factors, the lateral variation in site response characteristics across the zone.

Prior to 2015, simulations of the acceleration caused by a single earthquake resulted in concentric PGA contours. In later hazard assessments, the effect of the soft soils is visible in the hazard (and PSA) maps.

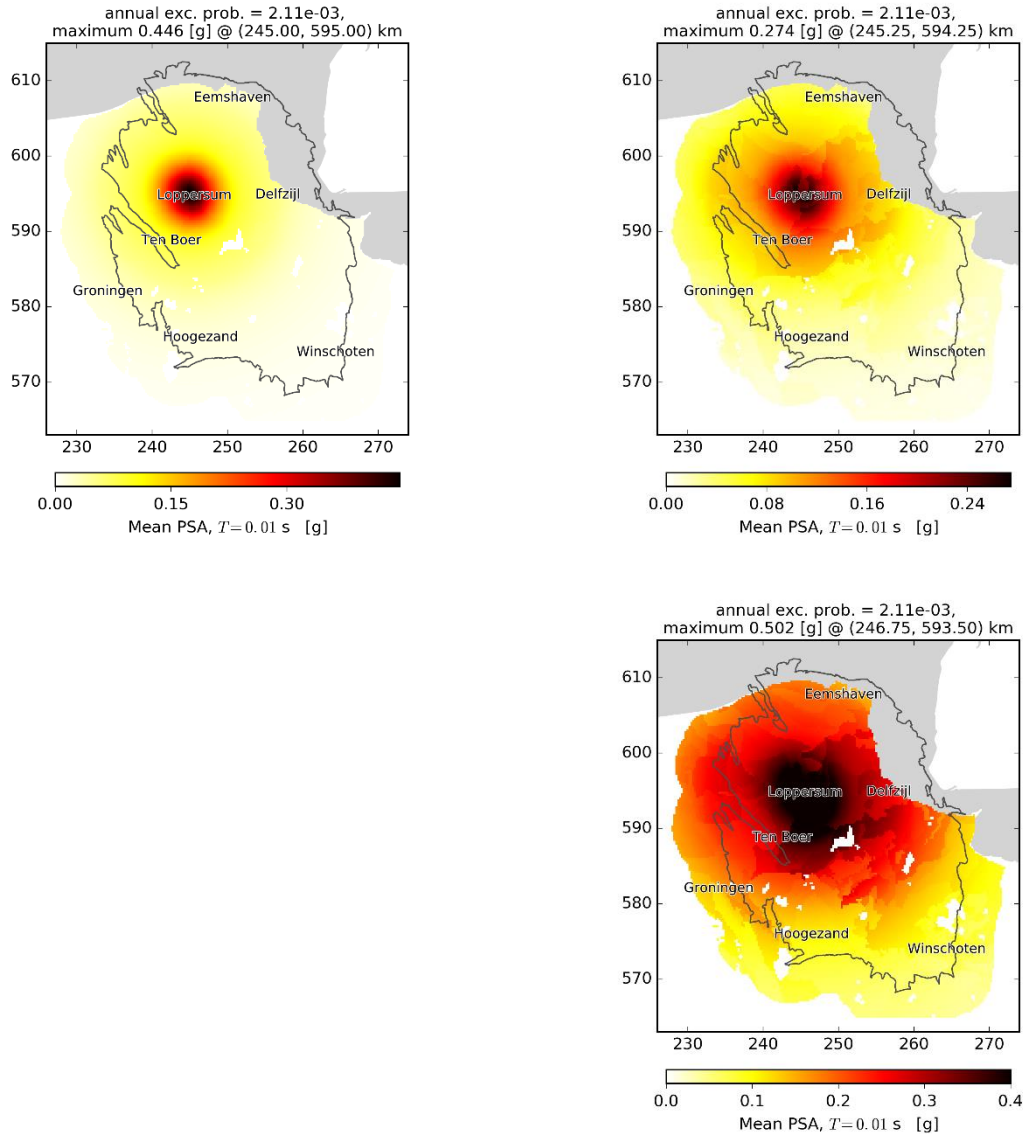


Figure 6.7 Ground motion prediction for a single event located at (245.0, 595.0, 3.0). (a) base-rock PGA for $M=4.0$, (b) surface PGA for $M=4.0$, (c) surface PGA for $M=5.0$ (clockwise from the top)

This effect is most clearly shown by comparing the PSA map at the base rock interface (Base Upper North Sea; NU-B) with the PGA (i.e. PSA at $T=0.01$) map at surface. Figure 6.7 shows on the left the concentric pattern of the PSA at the Base North Sea at some 800 m depth. The right-hand map shows the PSA at surface with the irregular imprint of the local soils, with the highest simulated PSA away from the earthquake epicentre.

Another important feature of the site amplification factors is that the site amplification factors include the non-linear behaviour of these soft soil deposits, when subjected to stronger levels of rock acceleration. For each zone and each

response period, the site amplification factors are defined as a function of rock acceleration; as a result of the Monte Carlo approach, the site response factors are conditioned on the actual realisation of the rock motions rather than the median motions. At shorter response periods, the amplification factors decrease with increasing rock acceleration due to the softening of the soil and the increase damping associated with larger shear strains; at long response periods, the pattern is reversed as a result of the elongation of the fundamental site period.

Hazard Logic Tree

In preparing the hazard maps, the uncertainty in the most important parameters has been incorporated by using scenarios. These scenarios are captured in the logic tree. The logic tree for the hazard is shown in figure 6.8. These scenarios are combined using the weights in the logic tree to provide the mean hazard map. The logic tree for the hazard assessment was extended with three branches. The first branch will be for the seismic model (based on M_{max}), the second on GMPE (median) and the third for GMPE (sigma).

The scenarios for maximum magnitude have equal weights. This part of the logic tree is based on the results from the workshop on maximum magnitude (held March 2016), where a panel of internationally recognised experts was asked to provide their assessment of the distribution of the maximum magnitude (Ref. 6).

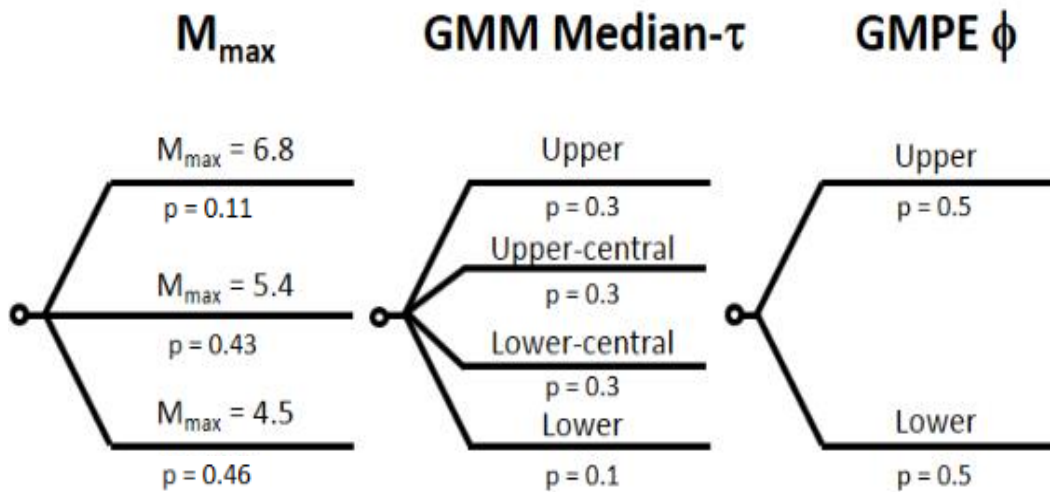
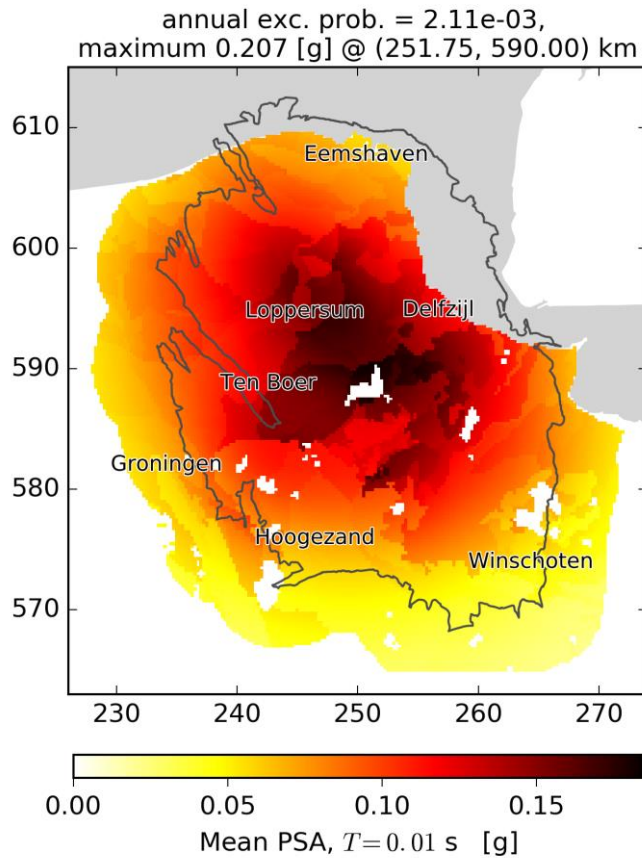


Figure 6.8 Logic tree used for assessing seismic hazard.

The weights for the different GMPE branches on the logic tree are based on the development of the Ground Motion Prediction Methodology and confirmed by the assurance committee.

Hazard Assessment

The impact of lateral heterogeneity in the composition of the shallow subsurface on the hazard map is less apparent in the mean hazard map, than in the acceleration response at surface to a single earthquake. This is because the mean hazard map combines the effects of all forecasted earthquakes in the evaluation period (2017-2022) which span a wide range of locations, magnitudes and all branches of the logic tree. The PGA hazard map for the scenario of an annual field production of 24 cm/year and the current offtake distribution is shown in figure 6.9.



2018/1 – 2023/1

Figure 6.9 PGA hazard maps Period: 2018 – 2023, Production: 24 bcm/year, Compaction: Inversion, Activity Rate Model: Version V2, Metric: 0.2% year-1 chance of exceedance (10% chance in 50 years), corresponding to a return period of 475 years. Mean hazard from logic tree.

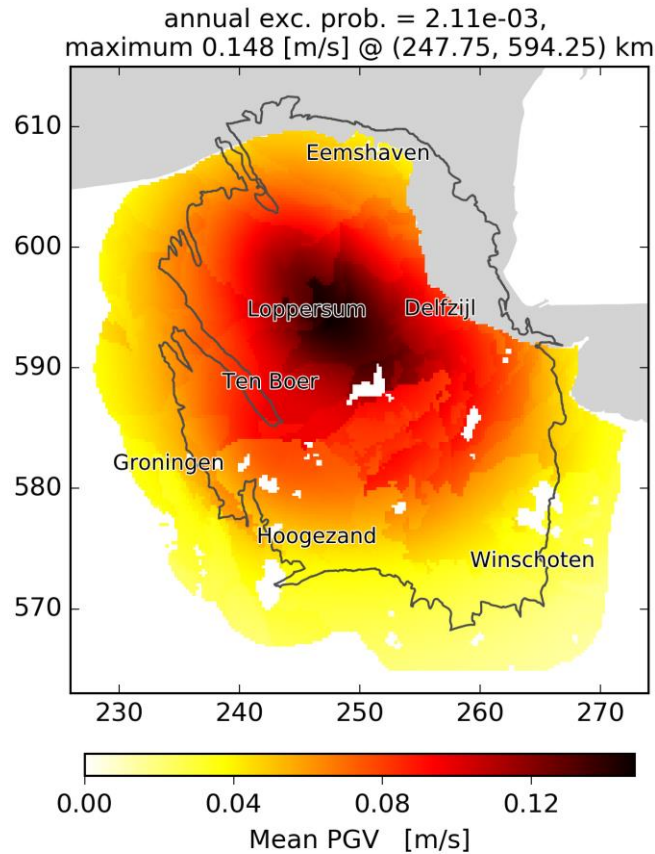


Figure 6.10 PGV hazard maps Period: 2018 – 2023, Production: 24 bcm/year, Compaction: Inversion, Activity Rate Model: Version V2, Metric: 0.2% year-1 chance of exceedance (10% chance in 50 years) corresponding to a return period of 475 years. Mean hazard from logic tree.

Although the return period chosen for plotting the hazard map is not a technical choice and does not impact the subsequent assessment of building damage and risk, sometimes hazard maps are also prepared for other return periods. These are for instance used in discussions around building codes. In Figure 6.11 hazard maps for different return periods are shown. Maps for return periods of 95, 800, 1500 and 3000 years are shown. The hazard map with the shorter return period of 95 years could for instance be of use in a discussion on building damage (Eurocode 8), and a map with a longer return period of 3000 years in a discussion on the seismic resistance of an infra-structure object.

The hazard maps show the peak ground acceleration (i.e. at the shortest spectral period of $T = 0.01$ s). However, in the assessment of building response the spectral acceleration at the, for the building, relevant periods is used. Figure 6.12 shows hazard maps for spectral acceleration at different periods. At the top left the hazard map for the very short spectral period $T = 0.01$ s is shown. This is the standard PGA hazard map. Moving to the right and down, hazard maps with larger spectral periods are shown relevant for larger and taller buildings with longer resonance frequency. As a rule of thumb, many of the two-story dwellings respond most to spectral accelerations with a period between 0.2 s and 0.3 s. Taller buildings, like high rise apartment buildings, typically respond to spectral accelerations with longer periods.

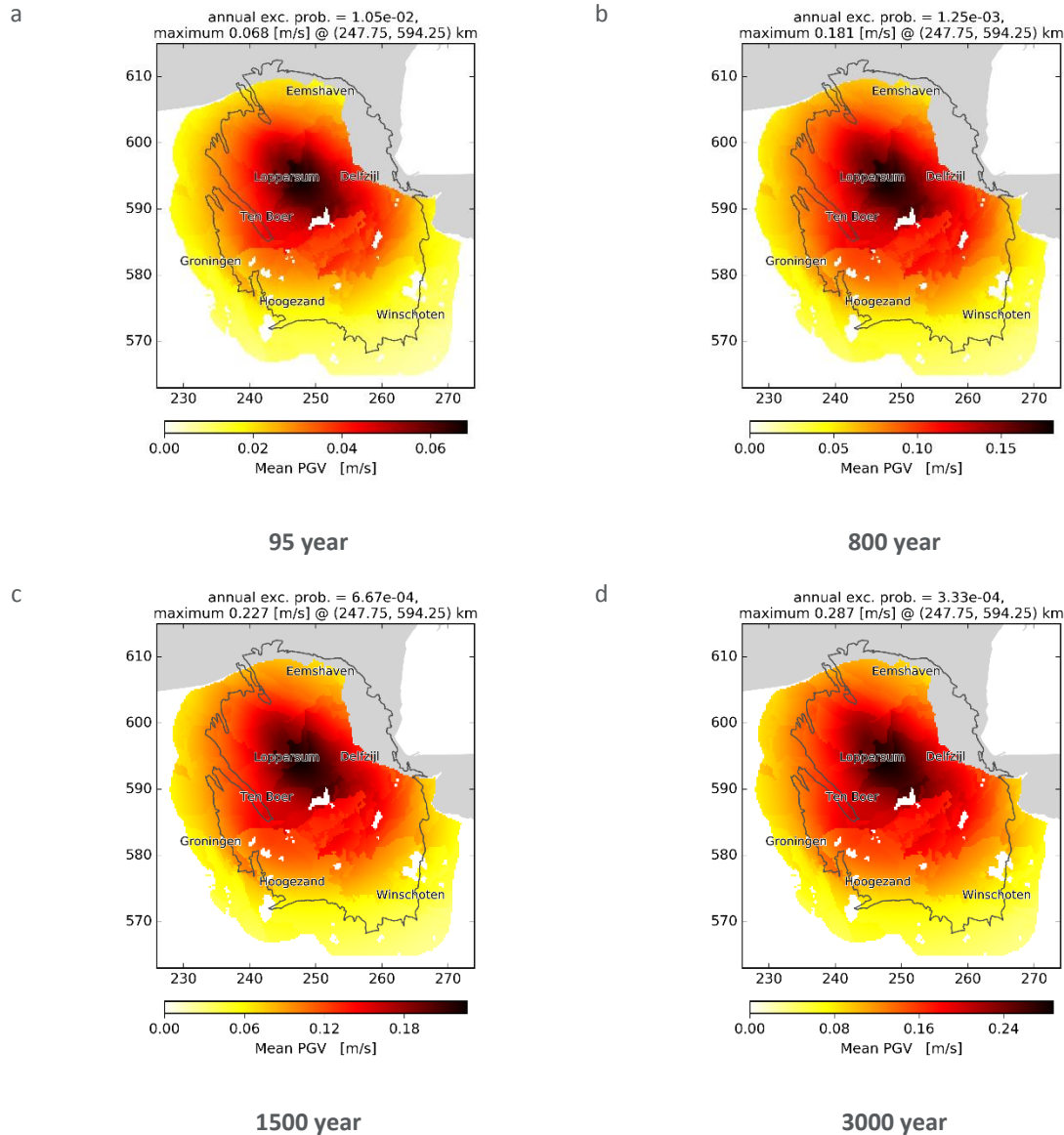


Figure 6.11 PGV hazard maps Period: 2018 – 2023, Production: 24 bcm/year, Compaction: Inversion, Activity Rate Model: Version V2, Metric: return periods of (a) 95, (b) 800, (c) 1500 and (d) 3000 years are shown. Mean hazard from logic tree.

Comparison of Hazard Maps

Since the hazard assessment of Winningsplan 2013, several updates of the hazard map have been prepared. The most important hazard maps are those for Winningsplan 2013 prepared November 2013, the maps of May and November 2015, the hazard map for Winningsplan 2016 and the current hazard map of November 2017. In figure 6.13 the hazard maps are shown with a consistent colour scheme.

The sequence of hazard maps shows a declining trend in the hazard assessment. This is in part the result of declining production rates the hazard was assessed for and in part due to the acquisition of Groningen data and studies based on this data (chapter 4).

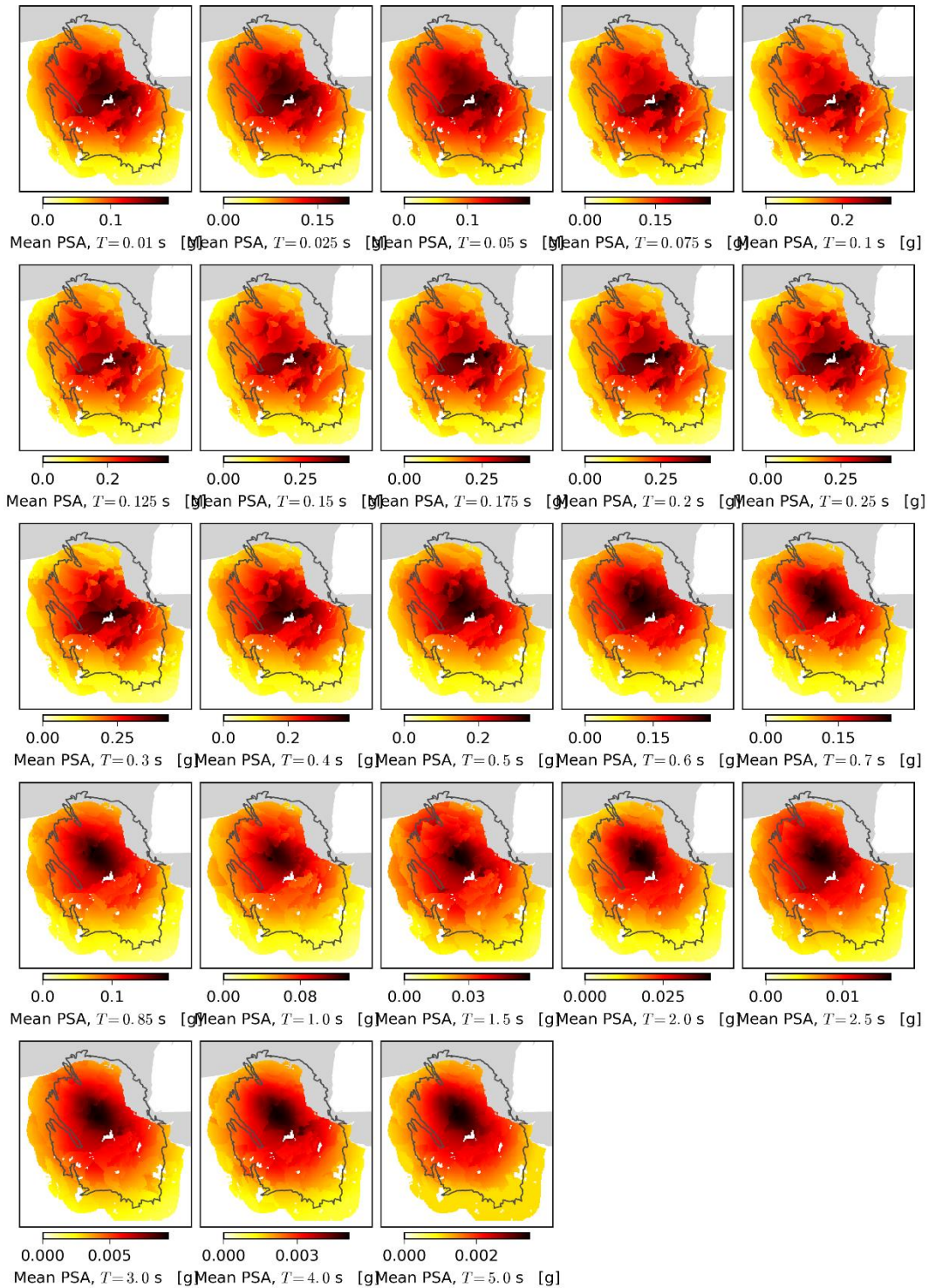


Figure 6.12

Hazard maps for different spectral periods from 0.01 s to 5.0 s. Production: 24 bcm/year, Compaction: Inversion, Activity Rate Model: Version V2, Metric: 0.2% year-1 chance of exceedance (10% chance in 50 years); return period of 475 years. Mean hazard from logic tree.

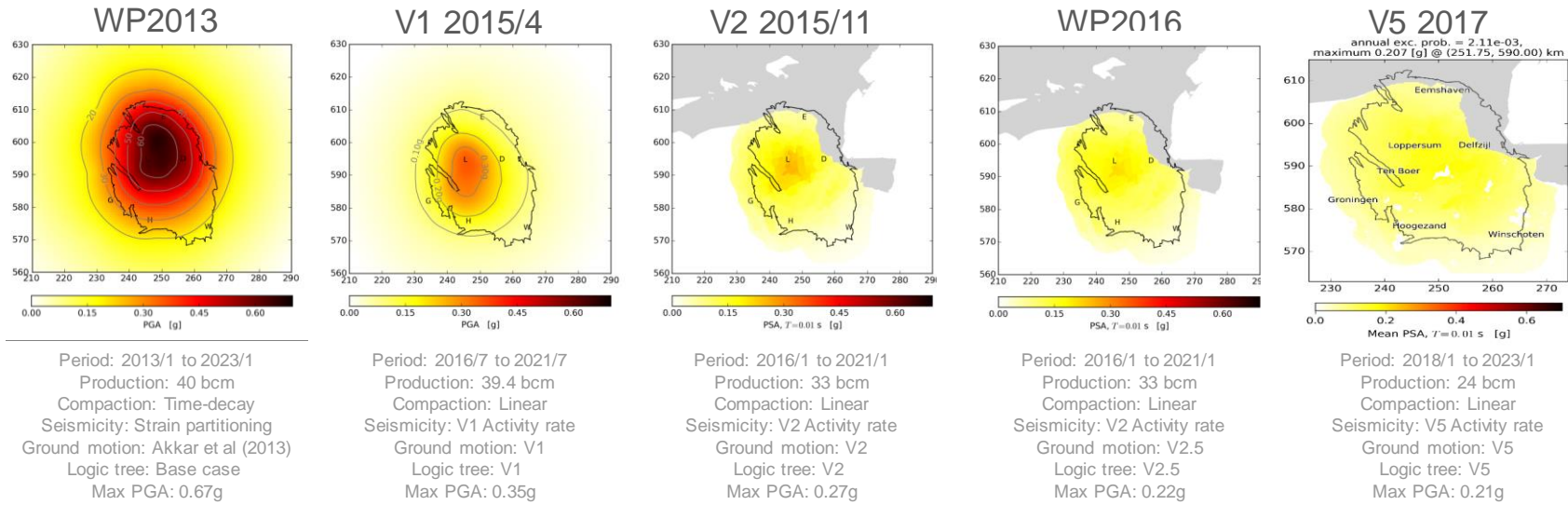


Figure 6.13 Comparison of the hazard maps prepared for the hazard and risk assessments for Groningen from 2013 to 2017.

Disaggregation of Seismic Hazard

The question which earthquakes have most impact on the hazard assessment was studied through a disaggregation of the hazard. Two disaggregations are shown; one for the hazard in the Loppersum area (Fig 6.14) and one for the city of Groningen (Fig. 6.15).

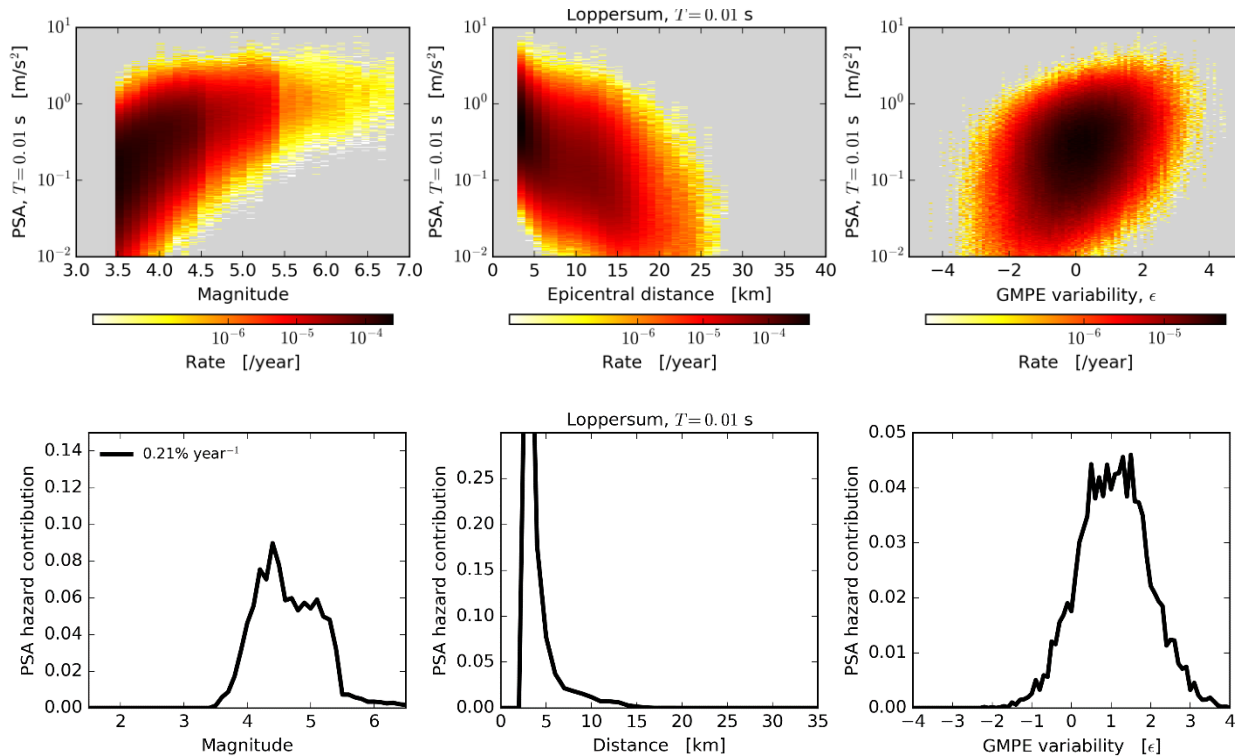


Figure 6.14 (a) Occurrence rates for peak spectral acceleration at 0.01 s as a function of magnitude, distance, and GMPE epsilon, ϵ , for a single surface location directly above the region of maximum reservoir compaction. Grey denotes no occurrence in any of the simulations. (b) The fractional contribution to the ground motion with a 0.2% annual probability of exceedance from January 2017 to January 2022.

The disaggregation of the hazard for the Loppersum area shows that the largest contribution to the hazard is from earthquakes within the Loppersum area (small distance of less than 5 km away with a magnitude ranging from 4 to 5). In contrast the largest contribution to the hazard in the Groningen city is from earthquakes with an epicenter approximately 10 km away from the city (towards the Loppersum area). To cause significant ground acceleration in the city of Groningen, these earthquakes located further away require a larger magnitude or GMPE epsilon to cause similar ground motions.

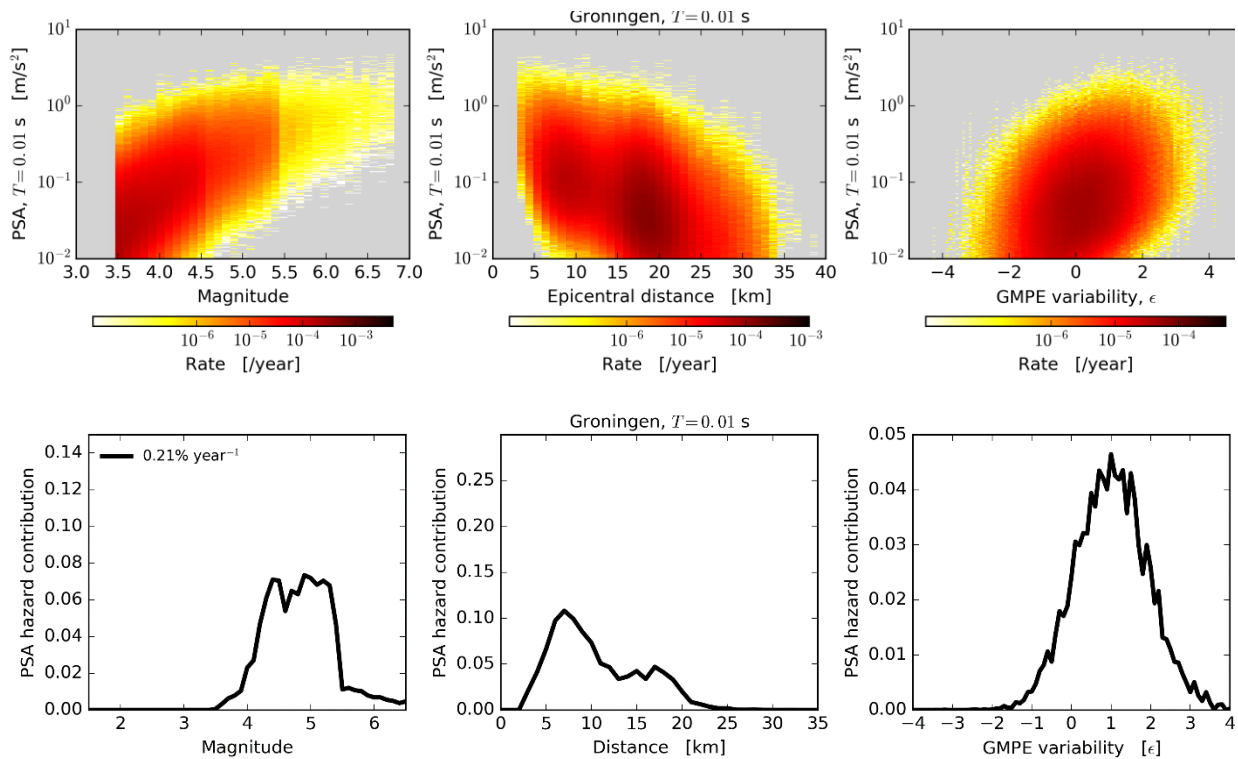


Figure 6.15 As previous figure, except for a surface location in the center of Groningen city.

Sites with poor site response ($\epsilon \geq 0$) contribute most to the hazard for the Loppersum area and the city of Groningen, with the largest contribution for $\epsilon = 1$.

Insight into the disaggregation for the Groningen area is shown in figure 6.16. It confirms that the largest contribution to the hazard in the Loppersum area comes from earthquakes with a magnitude 4 to 5. Away from the Loppersum area, in Groningen stad, Delfzijl and Eemshaven, the largest contribution comes from larger earthquakes.

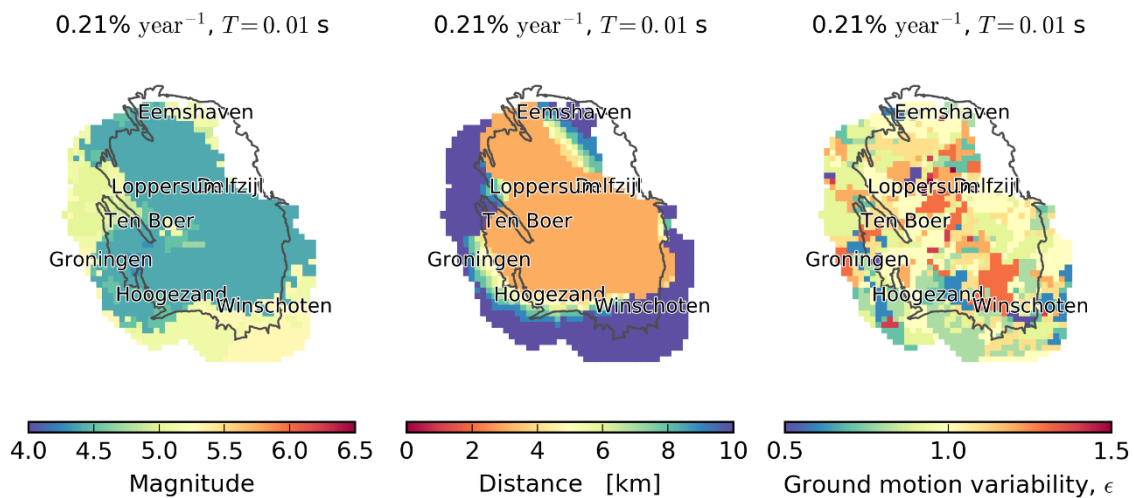


Figure 6.16 Maps of the magnitude, epicentral distance, GMPE epsilon that contribute most to the PGA hazard with a 0.2% annual chance of exceedance at that location.

References

1. NAM (Jeroen Uilenreef and Jan van Elk), Technical Addendum to the Winningsplan Groningen 2016, Production, Subsidence, Induced Earthquakes and Seismic Hazard and Risk Assessment in the Groningen Field, PART V – Building Damage, April 2016.
2. Development of Version 2 GMPEs for Response Spectral Accelerations and Significant Durations for Induced Earthquakes in the Groningen field, Julian J Bommer, Bernard Dost, Benjamin Edwards, Pauline P Kruiver, Piet Meijers, Michail Ntinalexis, Barbara Polidoro, Adrian Rodriguez-Marek & Peter J Stafford, October 2015
3. V4 Ground-motion Model (GMM) for Response Spectral Accelerations, Peak Ground Velocity and Significant Duration in the Groningen field, Julian Bommer, Bernard Dost, Benjamin Edwards, Pauline P Kruiver, Pier Meijers, Michail Ntinalexis, Adrian Rodriguez-Marek, Elmer Ruigrok, Jesper Spetzler and Peter Stafford, Independent Consultants, Deltares and KNMI, June 2017
4. SBR, Richtlijn Schade aan Gebouwen, Meet- en beoordelingsrichtlijn – Part A, August 2002
5. SBR, Trillingsrichtlijn deel A – Schade aan Gebouwen, Stichting Bouw Research, Rotterdam, 52 pp., 2010.
6. Report on Mmax Expert Workshop, Mmax panel chairman Kevin Coppersmith, June 2016

7 From Hazard to Building Damage and Risk

Exposure Database

Building Taxonomy based on Structural System

The exposure database combines a number of existing public and proprietary datasets containing information related to the buildings and population within the seismically affected area, with proper care to privacy regulations. The area currently extends 5 km (in all directions) from the boundary of the Groningen gas field. The datasets include:

- Basisregistratie Adressen en Gebouwen (BAG) (Kadaster – Dutch Land Register)
- AHN Actueel Hoogtebestand Nederland (Heights of buildings)
- DataLand address usage data
- CBS StatLine - Inhabitants per hectare 2014/ Education per municipality 2014 - 2015/ Time use data
- LISA – Landelijk Administratiesysteem Arbeidsplaatsen/ Number of jobs per category per postcode

Merging all this data into a single Geographical Information System (GIS) allows for the identification of the coordinates of each individual building (some 257,859 of which over 148,174 are regularly occupied by people) within the region and an estimate of the inside and nearby occupancy of each building during the day and night. An example of a building not occupied by people is a garden shed, bicycle rack, single car garage or an electricity transformer building. Barns, offices and industrial buildings are examples of buildings with a higher day-time than night-time occupancy. The database identifies individual buildings. An apartment complex is one building, but may contain several tens of addresses. By combining different datasets, the buildings are then grouped into categories as a function of their expected seismic performance.

The most important characteristic for the seismic response of a building is the construction material of the walls, frames and floors that make up the structural system of the building, i.e. the “lateral load resistive system”. These construction materials can be unreinforced masonry (URM), steel (S), reinforced concrete (RC), or wood (W). Unfortunately, there is no database with information on the construction material and system for each property, nor with information on the foundation. In the most seismically active area, the core area, inspections of buildings have been carried out to establish the main characteristics of the buildings that can be established without entering the building or excavating the foundation (Fig. 7.1).

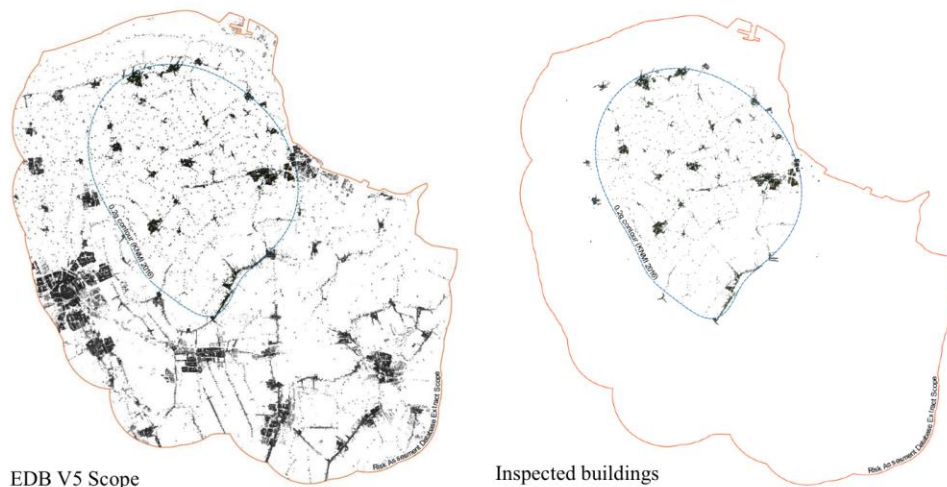


Figure 7.1 Left: The model area within which the all buildings are contained in the exposure database. Right: The area within which all buildings have been inspected.

The GEM building taxonomy system (Ref. 1) has been used to classify the different structural systems for the buildings, based on a combination of:

- Lateral load resisting system (LLRS)
- Material of lateral load resisting system
- External wall presence
- Floor material
- Height (<3 and >= 3 storeys)

The GEM building taxonomy serves a similar purpose to the set of building typologies used in Winningsplan 2016. However, the GEM taxonomy uses a consistent set of attributes, allowing information from inspections to be more easily incorporated into updates of the exposure database. For the Groningen area, a final set of 54 structural systems was used (Table 7.1a and b). Of these 54 structural systems, 15 are for buildings constructed with URM and 39 for buildings constructed with concrete, steel and wood; the non-URM buildings.

GEM Taxonomy Code	Short code	Short Description
CR+PC/LPB/CR+PC/LPB/EWN/FN/HBET:1,2	PC1L	Precast RC post and beam low-rise
CR+PC/LPB/CR+PC/LPB/EWN/FN/HBET:3,20	PC1M	Precast RC post and beam mid-to-high-rise
CR+PC/LWAL/CR+PC/LN/EWN/FC/HBET:1,2	PC2L	Precast RC wall-slab-wall low-rise no cladding
CR+PC/LWAL/CR+PC/LN/EWN/FC/HBET:1,2	PC3L	Precast RC wall-slab-wall low-rise with cladding
CR+PC/LWAL/CR+PC/LN/EWN/FC/HBET:3,20	PC3M	Precast RC wall-slab-wall mid-to-high-rise with cladding
CR+PC/LWAL/CR+PC/LWAL/EWN/FC/HBET:1,2	PC4L	Precast RC wall-wall low-rise no cladding
CR+PC/LWAL/CR+PC/LWAL/EWN/FC/HBET:3,20	PC4M	Precast RC wall-wall mid-to-high-rise no cladding
CR+PC/LWAL/CR+PC/LWAL/EWN/FC/HBET:1,2	PC5L	Precast RC wall-wall low-rise with cladding
CR+CIP/LPB/CR+CIP/LPB/EWN/FN/HBET:1,2	RC1L	Cast-in-place RC post and beam low-rise
CR+CIP/LPB/CR+CIP/LPB/EWN/FN/HBET:3,20	RC1M	Cast-in-place RC post and beam mid-to-high-rise
CR+CIP/LFM/CR+CIP/LFM/EWN/FC/HBET:1,2	RC2L	Cast-in-place RC frame low-rise
CR+CIP/LFM/CR+CIP/LFM/EWN/FC/HBET:3,20	RC2M	Cast-in-place RC frame mid-to-high-rise
CR+CIP/LWAL/CR+CIP/LN/EWN/FC/HBET:1,2	RC3L	Cast-in-place RC wall-slab-wall low-rise with cladding
CR+CIP/LWAL/CR+CIP/LN/EWN/FC/HBET:3,20	RC3M	Cast-in-place RC wall-slab-wall mid-to-high-rise with cladding
CR+CIP/LWAL/CR+CIP/LWAL/EWN/FC/HBET:1,2	RC4L	Cast-in-place RC wall-wall low-rise no cladding
CR+CIP/LWAL/CR+CIP/LWAL/EWN/FC/HBET:3,20	RC4M	Cast-in-place RC wall-wall mid-to-high-rise no cladding
MUR/LH/MUR/LH/EWN/FW/HBET:1,2	URM1L	URM house and timber post and beam low-rise
MUR/LH/MUR/LH/EWN/FW/HBET:3,20	URM1M	URM house and timber post and beam mid-to-high-rise
MUR/LWAL/MUR/LN/EWN/FW/HBET:1,2	URM2L	URM wall-slab-wall with solid walls and timber floors low-rise
MUR/LWAL/MUR/LN/EWN/FW/HBET:3,20	URM2M	URM wall-slab-wall with solid walls and timber floors mid-to-high-rise
MUR/LWAL/MUR/LN/EWN/FC/HBET:1,2	URM3L	URM wall-slab-wall with cavity walls and concrete floors low-rise
MUR/LWAL/MUR/LN/EWN/FC/HBET:1,2/IRIR+IRVP:CHV	URM4L	URM wall-slab-wall with cavity walls and concrete floors low-rise and large openings in ground floor walls
MUR/LWAL/MUR/LN/EWN/FC/HBET:3,20	URM3M	URM wall-slab-wall with cavity walls and concrete floors mid-to-high-rise
MUR/LWAL/MUR/LN/EWN/FW/HBET:1,2	URM5L	URM wall-slab-wall with cavity walls and timber floors low-rise
MUR/LWAL/MUR/LN/EWN/FW/HBET:3,20	URM5M	URM wall-slab-wall with cavity walls and timber floors mid-to-high-rise
MUR/LWAL/MUR/LWAL/EWN/FW/HBET:1,2	URM6L	URM wall-wall with solid walls and timber floors low-rise
MUR/LWAL/MUR/LWAL/EWN/FW/HBET:3,20	URM6M	URM wall-wall with solid walls and timber floors mid-to-high-rise

Table 7.1a GEM Taxonomy Code for each structural system with a short code (used in figures) and a brief description for each system (continued on the next page).

GEM Taxonomy Code	Short Code	Short Description
MUR/LWAL/MUR/LWAL/EW/FC/HBET:1,2	URM7L	URM wall-wall with cavity walls and concrete floors low-rise
MUR/LWAL/MUR/LWAL/EW/FC/HBET:3,20	URM7M	URM wall-wall with cavity walls and concrete floors mid-to-high-rise
MUR/LWAL/MUR/LWAL/EW/FW/HBET:1,2	URM8L	URM wall-wall with cavity walls and timber floors low-rise
MUR/LWAL/MUR/LWAL/EW/FW/HBET:3,20	URM8M	URM wall-wall with cavity walls and timber floors mid-to-high-rise
MUR/LWAL/W/LPB/EWN/FN/HBET:1,2	W1L	Timber (glulam) post and beam with masonry infill walls low-rise
MUR/LWAL/W/LPB/EWN/FN/HBET:3,20	W1M	Timber (glulam) post and beam with masonry infill walls mid-to-high-rise
W/LPB/W/LPB/EW/FN/HBET:1,2	W2L	Timber post and beam low-rise
W/LPB/W/LPB/EW/FN/HBET:3,20	W2M	Timber post and beam mid-to-high-rise
W/LWAL/W/LN/EWN/FW/HBET:1,2	W3L	Timber wall-slab-wall without ladding low-rise
W/LWAL/W/LN/EWN/FW/HBET:3,20	W4L	Timber wall-slab-wall with ladding low-rise
W/LWAL/W/LN/EWN/FW/HBET:3,20	W4M	Timber wall-slab-wall with ladding mid-to-high-rise
W/LWAL/W/LWAL/EWN/FW/HBET:1,2	W5L	Timber wall-wall without ladding low-rise
W/LWAL/W/LWAL/EWN/FW/HBET:3,20	W5M	Timber wall-wall without ladding mid-to-high-rise
W/LWAL/W/LWAL/EW/FW/HBET:1,2	W6L	Timber wall-wall with ladding low-rise
W/LWAL/W/LWAL/EW/FW/HBET:3,20	W6M	Timber wall-wall with ladding mid-to-high-rise
S/LPB/S/LPB/EWN/FN/HBET:1,2	S1L	Steel post and beam with no floor low-rise
S/LPB/S/LPB/EWN/FN/HBET:3,20	S1M	Steel post and beam with no floor mid-rise
S/LFM/S/LFM/EWN/FC/HBET:1,2	S2L	Steel frame with concrete floor low-rise
S/LFM/S/LFM/EWN/FC/HBET:3,20	S2M	Steel frame with concrete floor mid-to-high-rise
S/LFBR/W/LPB/EWN/FN/HBET:1,2	W7L	Timber (glulam) post and beam with steel bracing low-rise
S/LFBR/W/LPB/EWN/FN/HBET:3,20	W7M	Timber (glulam) post and beam with steel bracing mid-to-high-rise
S/LFBR/S/LPB/EWN/FN/HBET:1,2	S3L	Steel portal frame with bracing in one direction low-rise
S/LFBR/S/LPB/EWN/FN/HBET:3,20	S3M	Steel portal frame with bracing in one direction mid-to-high-rise
S/LFBR/S/LFBR/EWN/FN/HBET:1,2	S4L	Steel braced frame with no floor low-rise
S/LFBR/S/LFBR/EWN/FN/HBET:3,20	S4M	Steel braced frame with no floor mid-to-high-rise
S/LFBR/S/LFBR/EWN/FC/HBET:1,2	S5L	Steel braced frame with concrete floor low-rise
S/LFBR/S/LFBR/EWN/FC/HBET:3,20	S5M	Steel braced frame with concrete floor mid-to-high-rise

Table 7.1b GEM Taxonomy Code for each structural system with a short code (used in figures) and a brief description for each system (continued from previous page).

In the core area, indicated in Figure 7.1, 26,847 buildings have been inspected through various sources (Table 7.2). For 10,555 buildings, these inspections provided all of the above attributes necessary to fully describe the structural system of the building. For 14,605 inspections, not all building attributes could be identified. Expert judgement and data-driven inference rules based on structural layout (Figure 7.2), function and age of the construction were used to infer the remaining attributes that were not obtained during the inspections. Outside this core area, fewer inspections have been conducted and inference rules have been used more extensively to establish the most probable characteristics for each building.

Data Source	Building Count
Drawings Data	9,442
EVS Inspection (Extensive Visual Inspections)	283
Desk Study, ARUP (index buildings)	13
Desk Study, JBG	10,555
RVS Inspection (Rapid Visual Inspections)	4,308
Farmhouses, DataLand Description	2,246
	26,847

Table 7.2 Sources of data for the buildings inspected within the core area.

The structural system according to the GEM taxonomy described above is pieced together (inferred) from available data that includes structural layout, age, usage, location and attributes from inspections (where available). This piecing together is done using inference rules defined with the help of structural engineers with many years of experience in the region, who have provided information on the local Groningen construction practices over the last century, together with the results of the building inspections in the core area. The result of this analysis is that an individual building is assigned a probability that it belongs to a certain structural system. The sum of all the probabilities for each unique building is unity, but may consist of probabilities for several structural systems.

It is noted that the structural layout of the buildings, together with the function and age of construction, provides a better constraint on the inferred structural system than function and age alone, as was previously used in the exposure model for Winningsplan 2016.

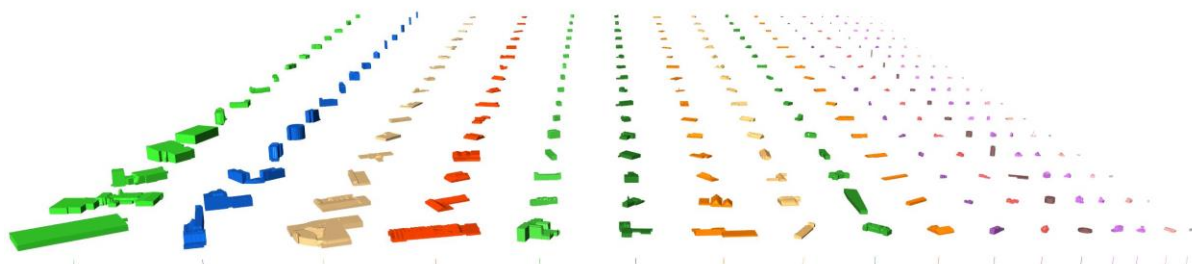


Figure 7.2 Examples of buildings for each structural layout from towers and blocks (on the left) to small detached houses and sheds (on the right)

Below an example is given of the use of inference rules:

DataLand usage label “Residential” and the structural layout obtained through GIS spatial analysis of Kadaster data combined with height data from AHN (Figure 7.3a and 7.3b) determines this building is a 2-storey detached house. After this first step, it is reasonably certain that this building is a detached house, but whether it has cavity walls or solid walls, wooden or concrete floors is unknown and will depend on location and age of the building and requires inference rules to be applied. Inference rules lead to a probability that the building belongs to a certain structural system. For example, it has a 60% probability of being a detached house with cavity walls and concrete floors, 20% probability of being a detached house with cavity walls and wooden floors, and 20% probability of being a detached house with solid walls and wooden floors. If inspection data is available that specifies that this building has cavity walls (which can typically be observed from outside the building) then the inference rules would be adapted accordingly and the building would have a 75% probability of being a detached house with cavity walls and concrete floors, and a 25% probability of being a detached house with cavity walls and wooden floors. There are around 150,000 populated buildings in the database and careful inspection inside a building is often required to get all of the information necessary to reliably (and uniquely) identify the structural system of the building.



Figure 7.3a ANH height data, to help evaluate number of stories: it also shows some of the problems that may arise.

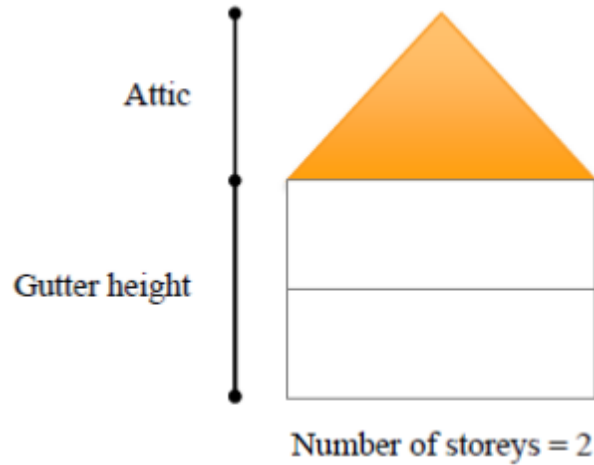


Figure 7.3b Use of ANH height data to identify total height, gutter height and number of storeys

Figure 7.4 shows the frequency distribution of buildings and average day/night inside occupants of each structural system. There are around 150,000 regularly populated buildings in the exposure database, and over 85% of the buildings are constructed in unreinforced masonry (URM). Figure 7.5 shows the most predominant URM structural system is well distributed across the region, with higher density in many of the villages. However, despite the abundance of masonry buildings, it can be seen from Figure 7.4 that a large proportion of the population live and work in higher rise reinforced concrete buildings (i.e. RC4M), though Figure 7.5 shows that they are mainly concentrated in the city of Groningen.

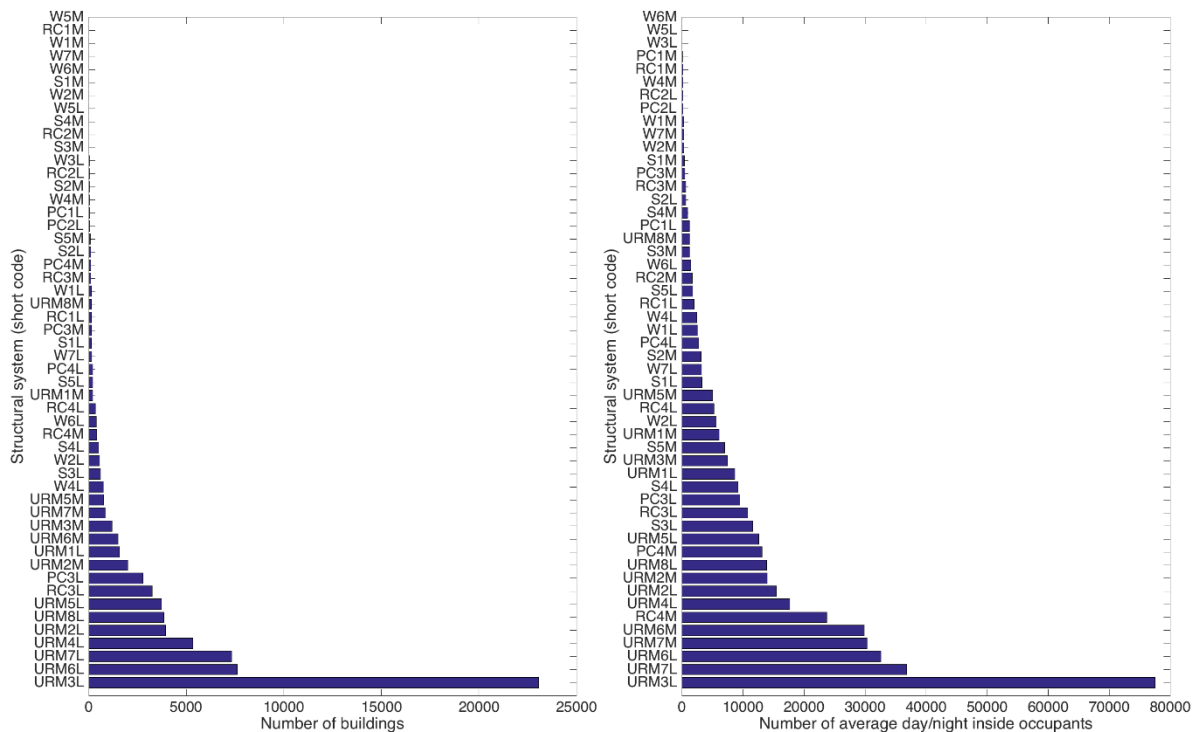


Figure 7.4 The frequency distribution of buildings and average day/night inside occupants within each structural system taxonomy class.

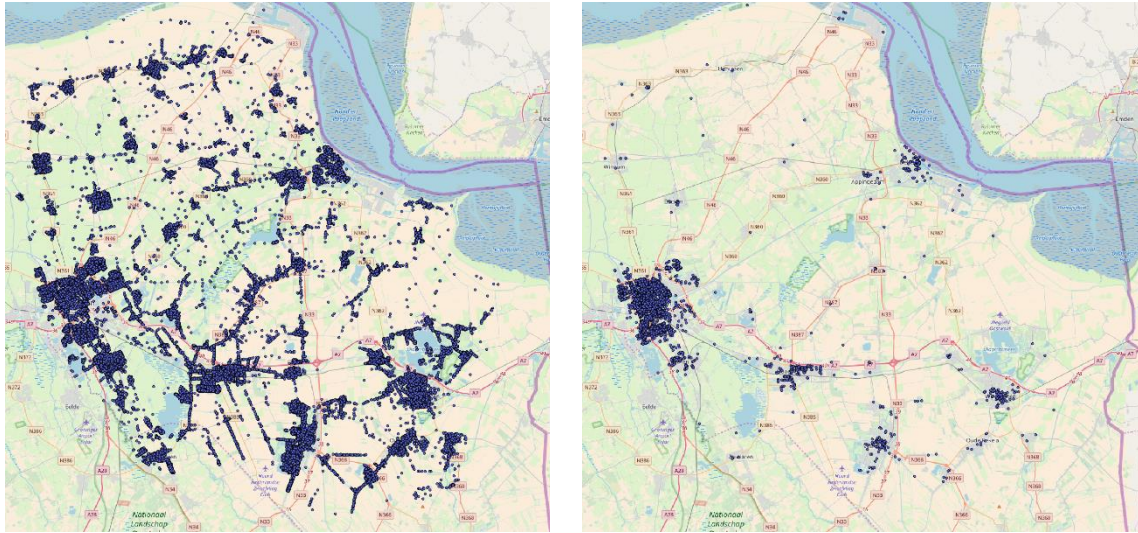


Figure 7.5 Maps showing the location of two very different structural systems within the exposure model (left: URM3L and right: RC4M) on an Open Street Map layer of the region

Building Occupancy

Using a number of datasets (CBS, LISA, DataLand) the exposure database provides an estimate of the average number of occupants per building during the day and during the night. It also contains an estimate of the number of people outside, and close to a building. To analyse the risk to people outside a building (due to the collapse of non-structural elements such as chimneys, the collapse of larger structural members such as gable or façade walls, as well as the full collapse of the structure) it is important to know the chance that someone will be in a location where they might be hit by the collapsed debris. The number of people outside and close to a building (Figure 7.6) consists of an estimate of pedestrians walking past the building and an estimate of a percentage of the occupants of a building that could run outside in the event of an earthquake and be in the location where they might be hit by collapsed debris falling outside.

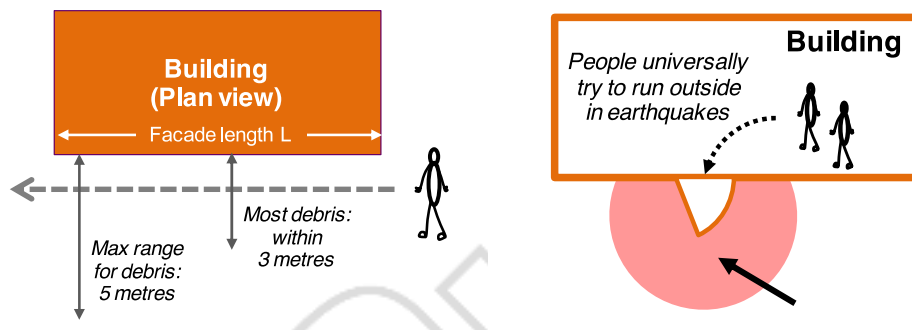


Figure 7.6 Illustration of the outside population: passers-by (left) and people running out of the building (right).

The occupancy has been analysed for many types of occupants: factory workers, government workers, office workers, teachers, nurses, patients, inmates, hotel guests, holiday home occupants, visitors to theatre/bar/sport facility or museum, church or mosque visitors, inhabitants of care homes, pupils in primary and secondary schools and university students. An analysis of time use data has provided estimates of the amount of time that people spend inside different buildings and footfall data has been used to estimate the people walking past buildings close to the street (Figure 7.6). Using CBS StatLine data on inhabitants per hectare, the inhabitants are evenly distributed over

the residential properties in a particular postal code and with the time use information the percentage of inhabitants at home during day/night can be estimated.

Development and Calibration of Seismic Building Response

Overview of program

To be able to assess the response of buildings to seismic motions, all buildings in the Groningen region have been categorised in a number of different building typologies (or structural systems). The buildings in a typology have similar resistance to earthquake-induced accelerations and specific usage and occupancy characteristics. Fragility curves describe the progression of damage, through the different damage states, with increasing ground motions. Damage and collapse fragility curves for input to risk assessments are developed considering the building materials and practices specific for the Groningen area over the past decades and centuries.

Many of the residential buildings in the Groningen area were built using unreinforced masonry, a highly heterogeneous material. These buildings have been given significant attention in the Study and Data Acquisition Plan (Ref. 2) and a special work program was prepared for them. Therefore, the research into building typologies is split into (1) masonry buildings and (2) non-masonry buildings. The latter category includes reinforced concrete, steel and timber constructions.



Figure 7.7 Examples of some of the typical unreinforced masonry building typologies found in the Groningen region

Following the development of numerical models and subsequent calibration of these models through in-situ and laboratory testing of materials, connections, structural components and even full-scale buildings, fragility curves

were developed that are specific to the buildings in the Groningen field area. These curves provide an estimate of the probability of damage and structural failure, given a specific level of ground shaking, and include the variability between buildings (due to different geometrical and material properties, which can be accounted for in the numerical models) and between the ground shaking characteristics of earthquakes with the same magnitude.

Experimental test program

Modelling of masonry buildings requires in-depth knowledge of the properties of materials manufactured and used locally, and the ability to capture these properties in numerical models. Therefore, the program to assess the fragility of masonry buildings has started with (1) a program to measure these properties through in-situ and laboratory tests, and (2) a program to validate the numerical methods by assessing the response of masonry buildings to ground shaking.

Non-masonry buildings are, due to the nature of the materials, more readily modelled with standard methods and software tools. As these building materials are less location specific, experimental tests from around the world can be used to calibrate the corresponding numerical models. However, since some of the cast-in-place and precast concrete buildings in the Groningen region featured particular structural configurations, additional tests have been performed to gain more confidence in the models for these buildings.

The program to test the performance of building materials, building elements and full-scale buildings and to calibrate models on these laboratory experiments was carried out by many scientific institutes and civil engineering companies spread over several locations (Fig. 7.8).

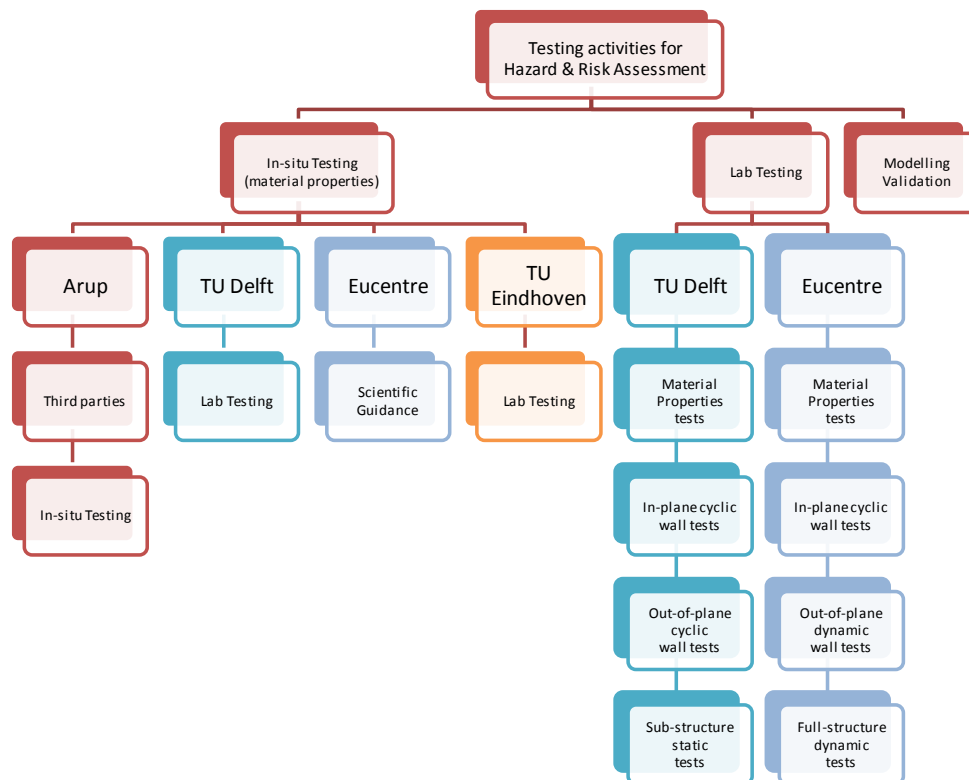


Figure 7.8 The different scientific institutes, laboratories and companies involved in the testing program.

The large shake-table tests were conducted under supervision of Eucentre at their laboratory in Pavia (Italy) and at LNEC in Lisbon (Portugal). Table 7.3 gives an overview of the most important material tests and experiments carried out.

				Testing Activities		
In-situ (in collaboration with TU Delft and TU Eindhoven)	material	characterisation	13 URM houses 2 RC buildings			
Lab (in collaboration with TU Delft and TU Eindhoven)	material	characterisation	≈ 200 (taken from actual houses)	test		specimens
Components testing			7 URM walls in-plane (cyclic, damage & collapse) 8 RC 2-way precast connections (cyclic, damage & collapse) 3 URM walls OOP one-way (shake-table, damage & collapse) 5 URM walls OOP two-way (shake-table, damage & collapse)			
Full-structure testing			2 URM houses (shake-table, damage) 1 URM house (shake-table, damage & collapse) 1 roof + gables (shake-table, damage & collapse) 1 roof (cyclic, collapse) 2 RC structures (cyclic, damage) 1 RC structure (shake-table, damage & collapse)			

Table 7.3 Overview of tests carried out by Eucentre in Pavia and LNEC in Lisbon. Tests indicated in red have been carried out since Winningsplan 2016.

Modelling program

An important objective of the tests is to provide experimental data for the calibration of models to simulate the response and damage of buildings in response to an earthquake. Several knowledge institutes and universities collaborate in the modelling studies. Especially modelling of URM buildings is challenging and required the development of new modelling techniques and incorporation of the complex behaviour of masonry material properties in modelling tools. The modelling studies were therefore initiated by a modelling and analysis cross validation study (Ref. 3), which was based on a set of benchmark experimental studies.

Typically, prior to each experiment a blind-prediction is prepared. This is also an important contribution to the design of the tests. The sequence of acceleration records the test sample or building is subjected to, depends on the outcome of the blind prediction modelling. After the experiments are completed the models are calibrated with the experimental results. Four partners have participated in the modelling effort, each with a dedicated software tool.

Participant in the Modelling Study	Modelling Software
ARUP	LS-Dyna
Mosayk	ELS (for URM) and Seismostruct (for non-URM)
Technical University Delft	Diana
Eucentre	Tremuri (academic version)

Table 7.4 Overview of participants in the modelling studies and modelling tools used.

For each building structural system, a number of index buildings were selected. These are buildings with characteristics typical for the set of similar buildings, with the same structural system. Understanding the seismic response of these index buildings will inform the seismic response to the population of buildings with this same structural system.

Calibrating numerical models with data from the field

A number of tests on masonry houses were carried out in-situ, i.e. inside the masonry buildings in the Groningen region (Ref. 4). Geophone tests to characterise the frequency characteristics of the buildings were used to compare with the mode shapes and frequencies of vibration obtained from the numerical models of these buildings.

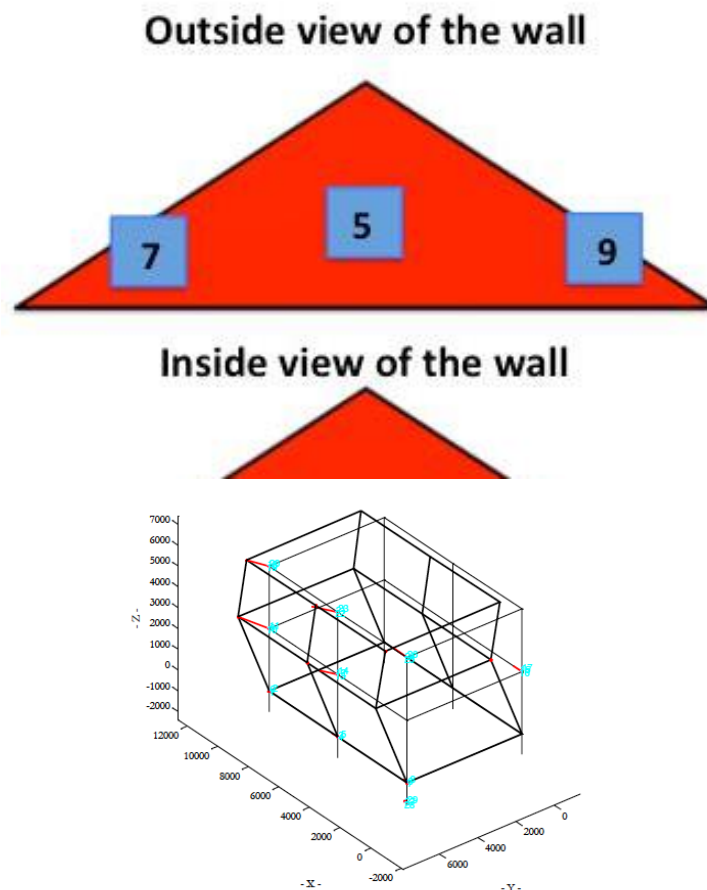


Figure 7.9 Geophones applied to a terraced masonry house to measure its frequency characteristics (Ref. 4).

Various tests on the walls of the buildings in Groningen provided insight into the material properties of masonry - combining bricks of either calcium silicate or clay with the mortar that binds them together - which can then be used as input to the numerical software.

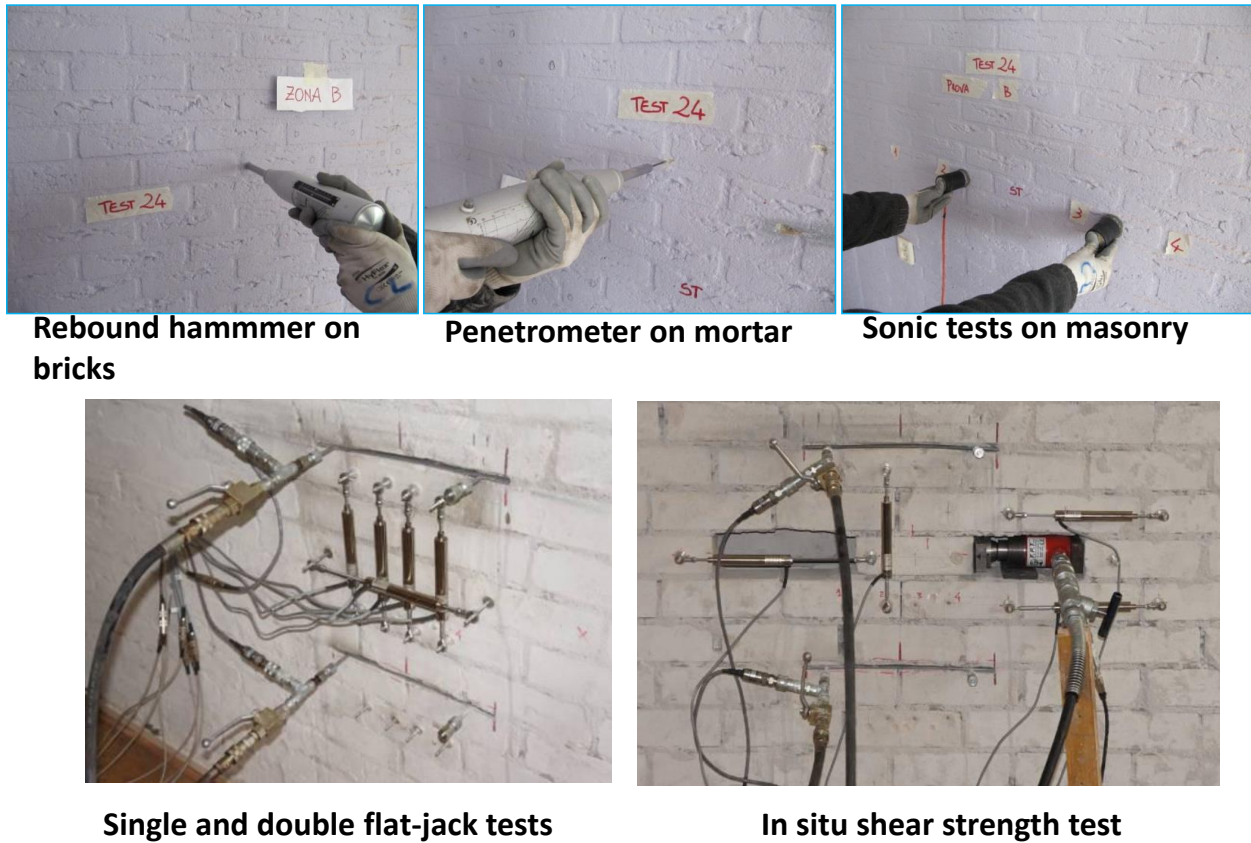


Figure 7.10 In-situ material tests on walls inside masonry houses in Groningen (Ref. 4).

Material Testing

The properties of both building material currently used in construction and materials historically used and taken from existing buildings (Fig. 7.11) have been assessed also through tests in the laboratory. More than 200 masonry specimens of both clay brick and calcium-silicate brick have been tested at the Technical University of Delft and at Eucentre in Pavia. These laboratory tests allow maximum control of properties and isolation of the factors affecting the mechanical response. As a result, experimental uncertainties were minimised making comparison and calibration with numerical models easier.

The results of these tests have been summarised in a building material characterisation report (Ref. 5), which was also used in the updating of the building norm (NEN-NPR).

To determine the properties of brick - mortar joint combination small walls were tested (Fig. 7.12).

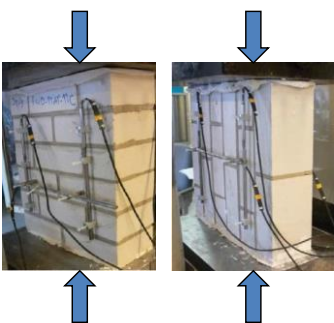


Figure 1 - Flexural test set-up.

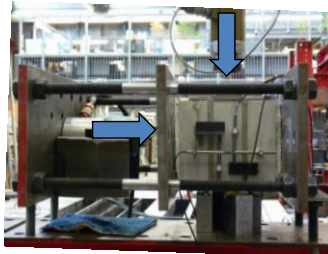
Figure 2 - Compression test set-up.

Figure 7.11 Material tests on building material; clay brick and calcium-silicate bricks.

Compression test



Triplet test



Pull-out test on connectors



Bond wrench test



Flexural tests

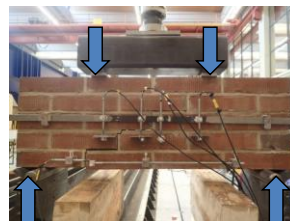
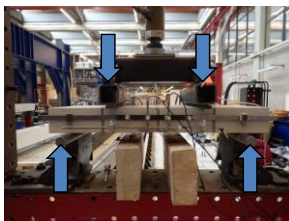
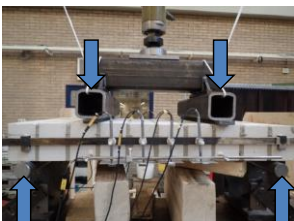


Figure 7.12 Material tests on small walls samples.

Calibrating numerical models with data from the laboratory

In-plane and out-of-plane testing of walls

For further calibration and testing of the numerical methods used to predict the response of masonry to ground shaking, sets of solid and cavity walls were constructed by Groningen masons and tested within laboratories in the Netherlands and Italy (e.g., Ref 8, 9).

These walls have been tested both in-plane and out-of-plane, and a number of modelling teams have attempted to predict the response of the tests (in terms of strength and stiffness of the walls, displacements at which failure occurs, crack patterns etc.) using various numerical software packages (ARUP et al., 2015). The lessons learned from the tests were then used to improve the modelling capabilities.

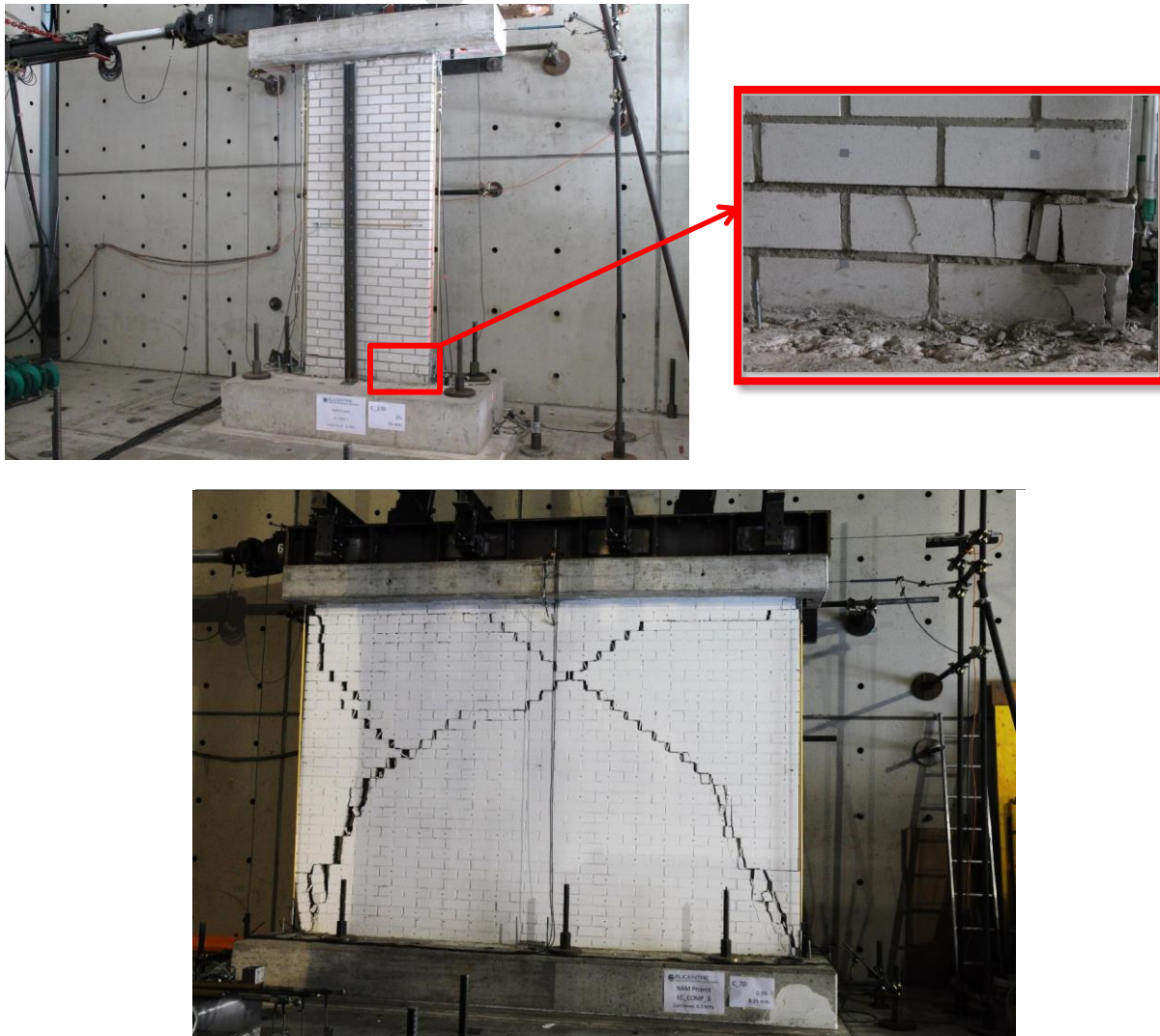


Figure 7.13 Masonry walls constructed by Groningen masons and tested in laboratories (Ref. 6). The slender wall (top) showed signs of “toe-crushing”, while the wider squad wall (below) shows “envelope fractures” typical for earthquake damage.

So far, the in-plane tests of slender walls have highlighted an important characteristic of the calcium silicate brick walls, which prove to have a much higher capability to dissipate energy than expected. With regards to squat walls,

comparisons with test results have indicated that current models are readily simulating the actual response of these masonry components as shown in the figure below.

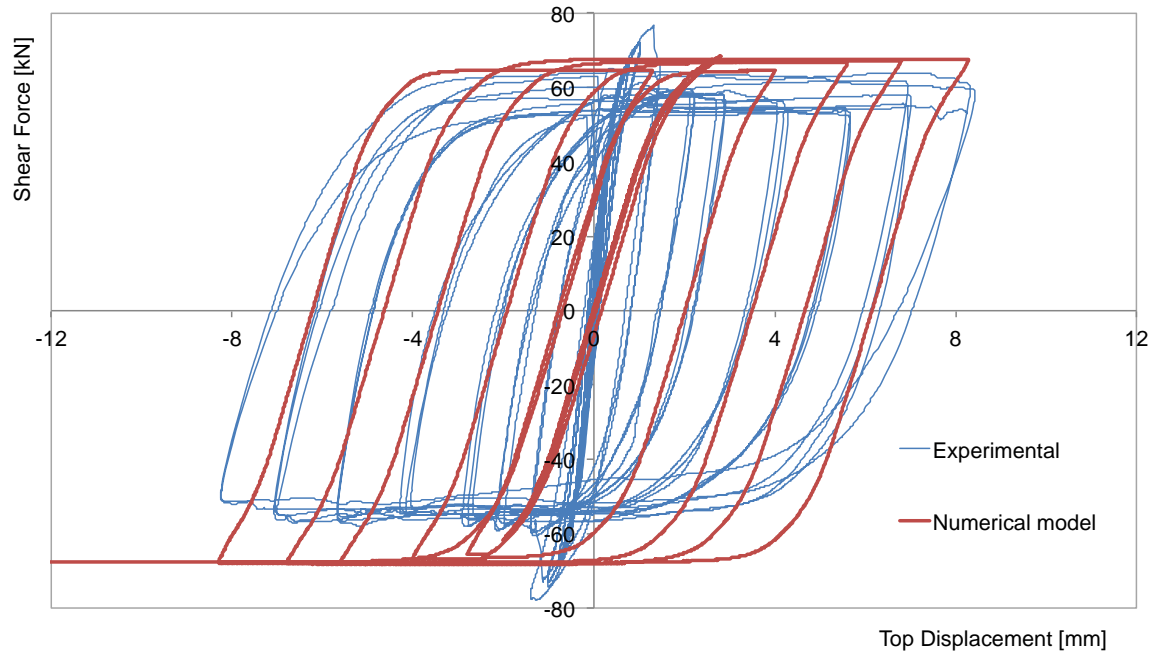


Figure 7.14 Example comparison of experimental in-plane response of calcium silicate wall and predictions by one of the modelling teams.

The results of the out-of-plane (OOP) tests on solid and cavity walls (with different numbers of ties) have also been compared with numerical models, which have also been seen to accurately predict the experimental results, as shown below.

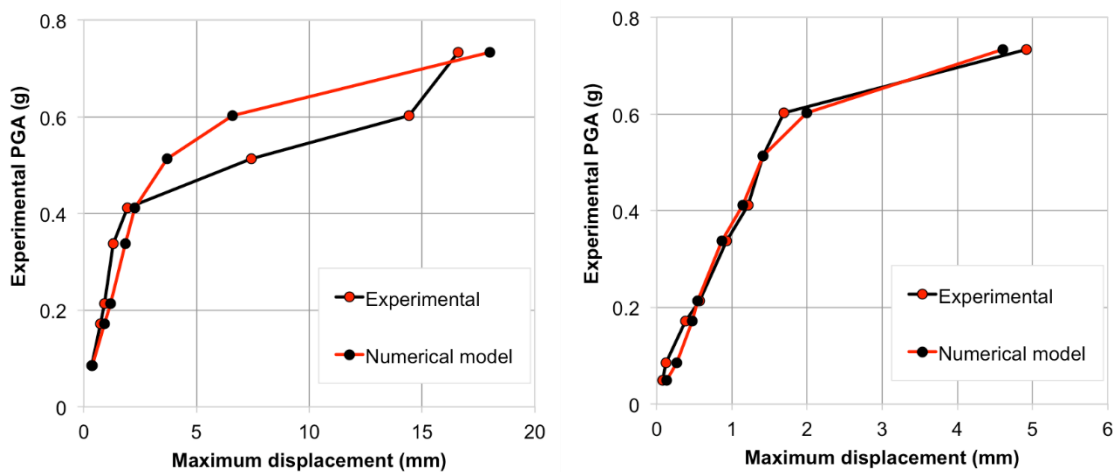


Figure 7.15 Comparisons of the predicted dynamic out-of-plane response of walls with the experimental results

Terraced House

To illustrate the practical calibration of the models with experiments and the preparation of fragility curves, four examples demonstrating the importance of the experimental results for the calibration of the models, are given. All examples are for important building typologies:

1. the terraced house,
2. detached house,
3. cast-in-place concrete building and
4. pre-cast concrete building.

A full-scale specimen of a terraced house (with one unit) was constructed on a shaking table by Groningen masons using local and historical materials and construction practice (Fig. 7.16). This type of house was chosen as it is one of the most prevalent in the area. This structure was tested by applying accelerations to the base of the structure, as would be the case during a real earthquake (Ref. 6). The accelerations have been scaled to values much higher than those that have already been experienced in the Groningen field, so that comprehensive calibration of the numerical models can be undertaken (examples of the latter are shown below). As per scientific practice, the tests were stopped before complete collapse of the structure, so as to prevent damage to the laboratory testing facilities.



Figure 7.16 Full-scale terraced house building on the shaking table

The building was subjected to several earthquakes of increasing intensity (largest PGA was 0.34g). After each earthquake, the house was subjected to small vibrations to establish the stiffness and detect (accumulated) structural damage. The building was after each earthquake experiment also visually inspected for damage to the structure (Fig. 7.17). The observed damage was carefully recorded (Fig. 7.18).



Figure 7.17 Careful inspection of the buildings after an earthquake experiment.

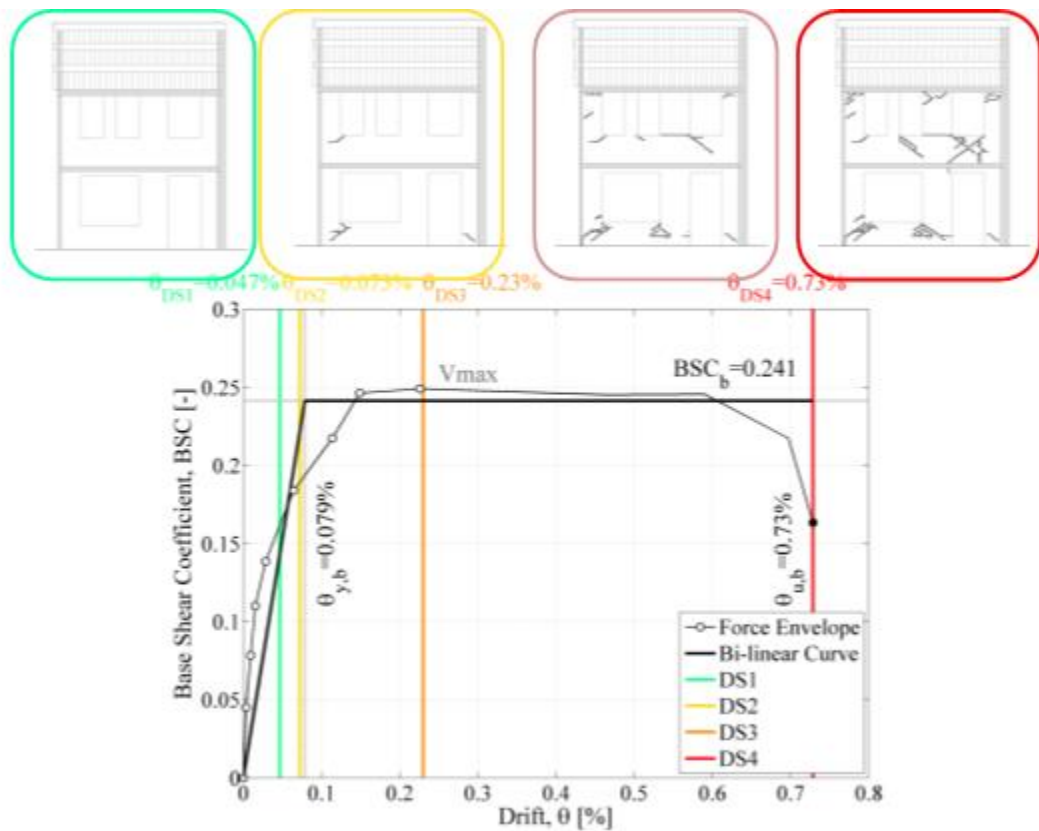


Figure 7.18 Record of the building damage for the terraced house identified during the post experiment inspections. This will be used in the preparation fragility curves for the damage states (DS2 to DS5).

Although the building had sustained serious damage after the experiments, it could not be taken to collapse during the testing at Eucentre in Pavia. Experimental evidence was thus missing on the remaining margin of resistance to partial collapse of elements of the building. Based on the damage observed during the test these were thought to first occur at the upper portion of the building (i.e. first floor and roof+gables). Such part of the building was therefore re-constructed at the LNEC laboratory in Lisbon (Ref. 10). This building specimen was subjected to the accelerations measured in Pavia at the base of the first floor (Fig. 7.19). The experiments done in Pavia on the full

scale two-storey house were repeated with the top floor building in Lisbon, and showed very similar behaviour for the two experiments for the first floor.

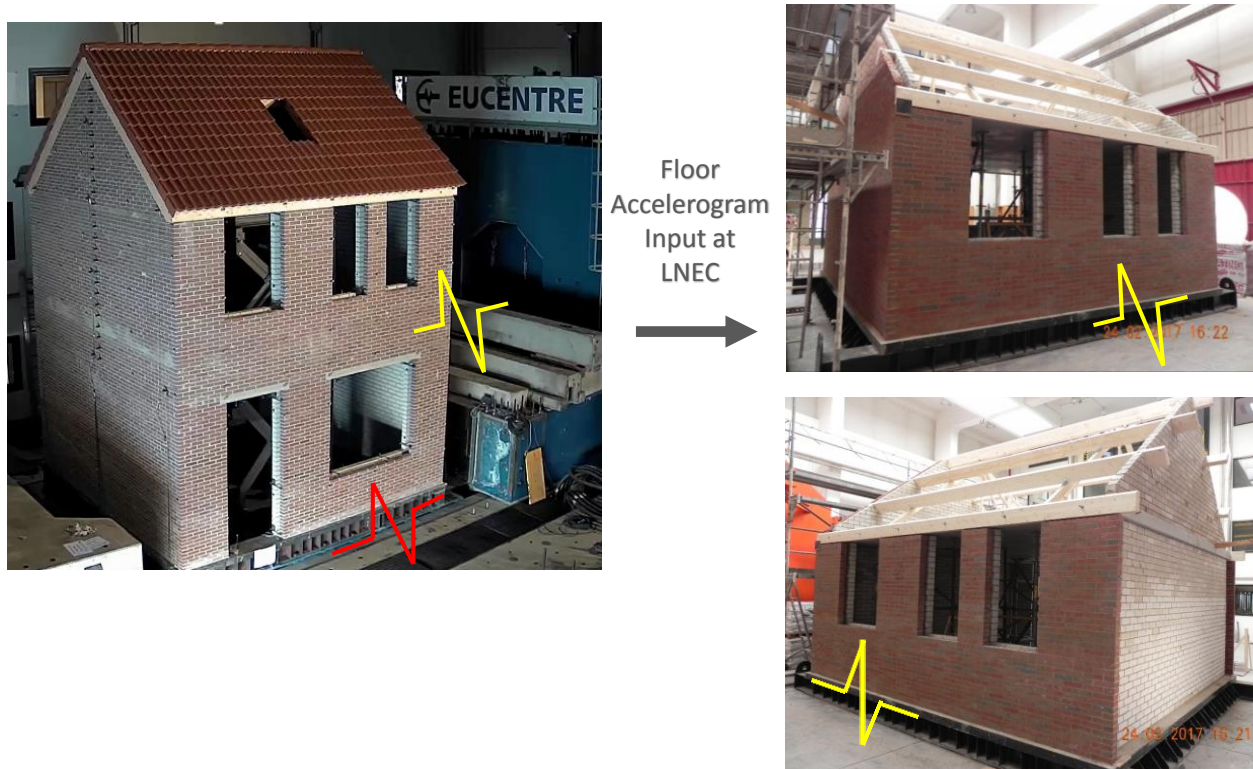


Figure 7.19 Left: Two-storey terraced house at the shake-table of Eucentre in Pavia.

Right: First floor (plus roof and gables) of the terraced house re-built at LNEC in Lisbon.

However, in the laboratory of LNEC the experiments could be continued with the structure exposed to further increasing earthquake accelerations. When the building showed serious signs of structural damage with partial collapse the accelerations the building was subjected to exceeded 0.6 PGA, which is in the range for large tectonic earthquakes and not expected to occur in Groningen. Finally, to study the response of the roof construction and gable, a roof structure was also tested (Fig. 7.20).

The recorded damage patterns and loss of structural integrity have been used to calibrate models for the terraced building. Models have been calibrated by ARUP using LS-Dyna software, TU Delft using Diana software, Eucentre using the Tremuri package and Mosayk using ELS software (Ref. 11). These calibrated models were used in sensitivity studies where the structure of the building (e.g. the size of windows and other openings) and properties of building material were varied. Based on these model results, fragility curves were constructed for the terraced buildings.



Figure 7.20 Roof structure of a terraced house building on the shaking table (Ref. 12)

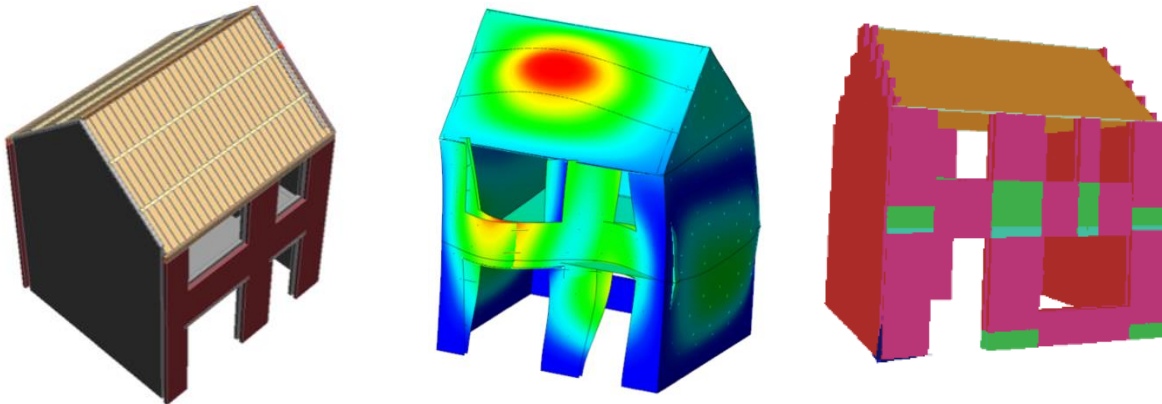


Figure 7.21 Numerical models (developed by Arup, TU Delft, Eucentre) of full-scale terraced house building tested on the shaking table (Ref. 9).

Detached house

Next a small detached building was tested at the Eucentre laboratory in Pavia (Fig. 7.22). The building was chosen to test the response of construction features often seen in small farmhouses and buildings from the 1930s. Special attention was given to the roof construction (Fig. 7.23). A roof construction typical for detached houses from this period was chosen.

Also this building was subjected to a number of simulated earthquake accelerations (Ref. 7). This building proved stronger than expected for the ground motions used in the shake table tests and there was no requirement to test the upper floor or roof further to collapse at LNEC in Lisbon. Building damage was carefully recorded after each earthquake (Fig. 7.24 and 7.25).



Figure 7.22 Detached house on the shake-table in the Eucentre laboratory (Ref. 7).

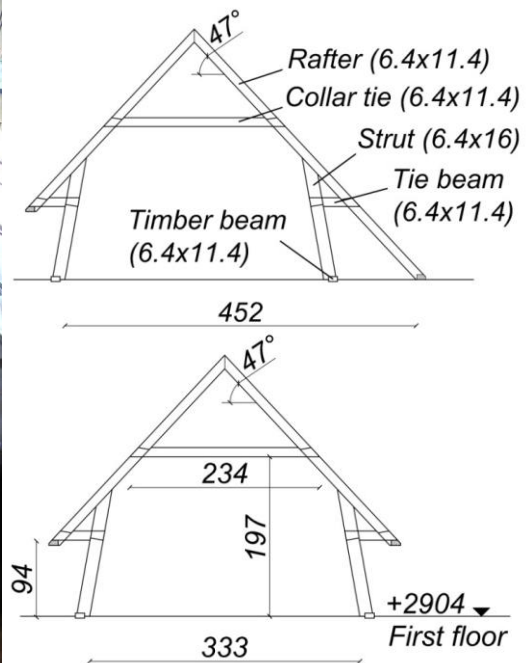


Figure 7.23 Roof construction of the detached house on the shake-table in the Eucentre laboratory (Ref. 7).

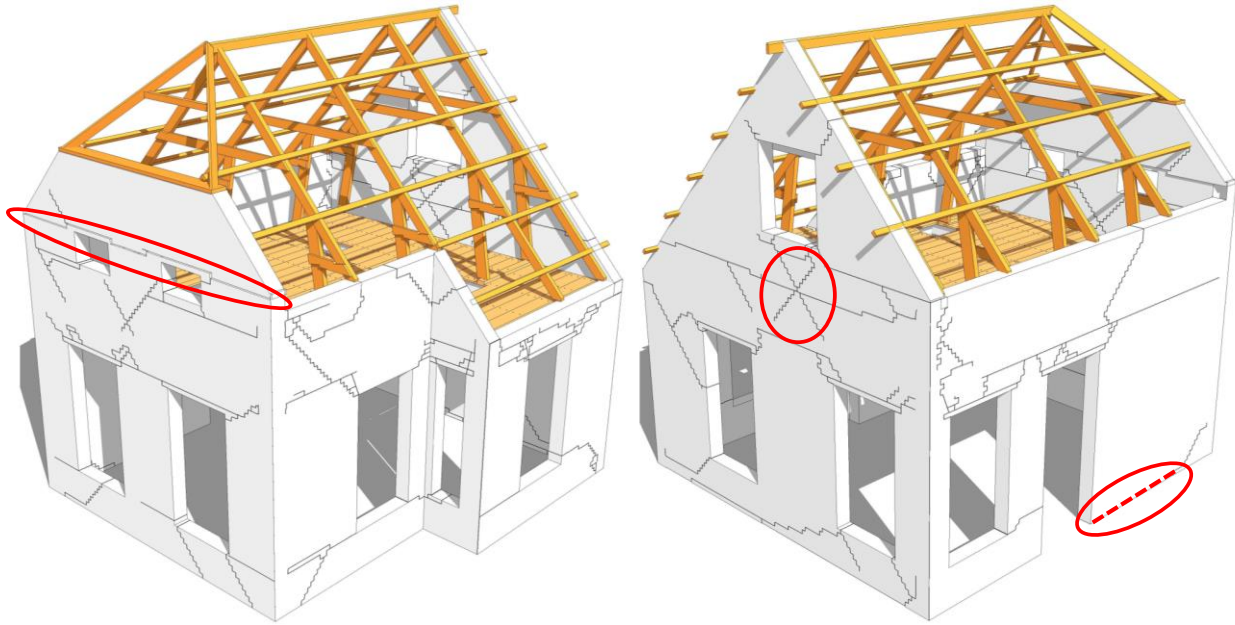
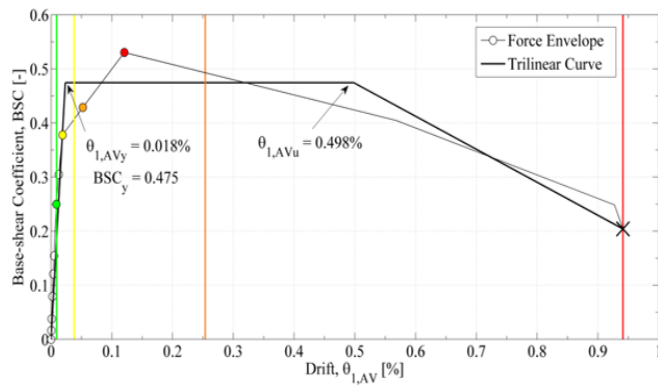


Figure 7.24 Detached house with building damage after final experiment indicated (Ref. 7).



Definition of **four damage limit states**:

- **DL1: no visible damage**
- **DL2: slight damage** (*cracking initiation in some West piers*)
- **DL3: significant damage** (*development of cracks at both ends of all West piers*)
- **DL4: near collapse** (*spread structural damage in all the facades*)

DL1: $\theta_{1,max} = 0.01\%$ DL2: $\theta_{1,max} = 0.04\%$ DL3: $\theta_{1,max} = 0.25\%$ DL4: $\theta_{1,max} = 0.94\%$

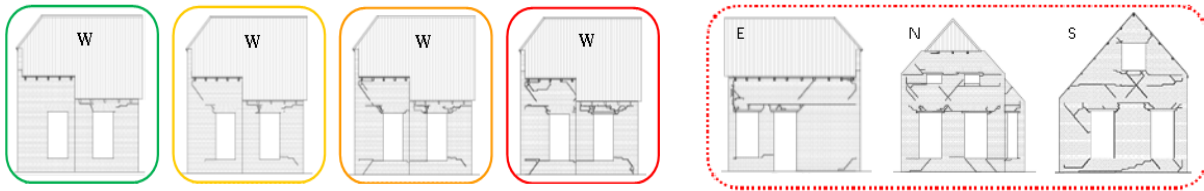


Figure 7.25 Record of the building damage for the detached house identified during the post experiment inspections. This will be used in the preparation fragility curves for the damage states (DS2 to DS5).

Pre-fab Concrete Buildings

Both pre-fabricated concrete and cast-in-place concrete are modern building construction methods. The buildings constructed with these methods are often difficult to identify. Often clay-brick walls are used as an outer veneer giving the impression the building is a URM building. However, the load-bearing construction hidden by the clay-brick veneer consists of concrete. Figure 7.26 shows a pre-fab concrete building being constructed. Large wall and floor elements fabricated off-site and hoisted in place at the construction site. For the seismic response of the

building, the material properties of the building elements are typically less important than the strength of the connections between these elements.



Figure 7.26 A pre-fab concrete building under construction.

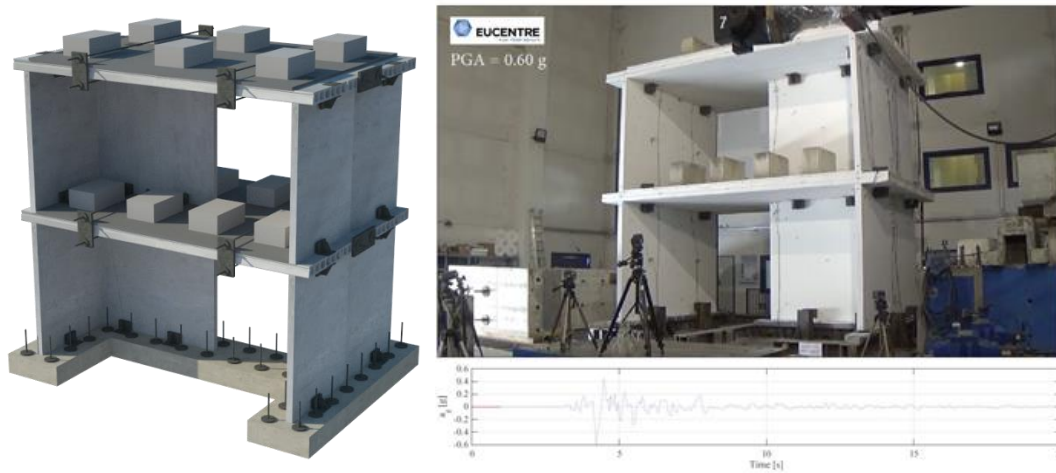


Figure 7.27 Pre-fab concrete building being tested in the Eucentre laboratory (Ref. 13).

As this construction method is also used to build multi-storey buildings, the construction tested in the laboratory was two-storeys tall. Two separate tests have been performed in the laboratory on the pre-fab construction (1) a cyclic test (Ref. 13), where large actuators laterally move the floors of the construction and (2) a shake-table test (Ref. 14).

Also the pre-fab construction was subjected to a series of earthquake acceleration records with an increasing strength. The construction was tested up to a PGA of 0.6 g. This is an acceleration only experienced with large tectonic earthquakes and not anticipated in Groningen. As for the URM test specimens, this was done to assess the strength of the building (and calibrate numerical models accordingly). However, when subjected to this series of earthquakes of which the last two had a PGA of 0.6 g, the building showed serious structural damage.

Cast-in-place building

Figure 7.28 shows the construction of a cast-in-place concrete structure. When finished, this building will look like the buildings in the background. Due to the clay-brick veneer, it is sometimes difficult to identify the building as having a cast-in-place concrete construction.



Figure 7.28 A cast-in-place concrete building under construction.

At the Eucentre laboratory, the cast-in-place construction was built by the Groningen construction company Bouwborg using local specifications (Fig. 7.29). The construction was subjected to a cyclic test (Ref. 15). Large actuators were used to push the floors in first the longitudinal and later transverse direction (Fig. 7.30).

The results from the modelling of the cost-in-place structure are shown in figure 7.32. For both the blind prediction carried out before the experiment and the post-test calibration of the model to the experimental data, the force of the actuators is plotted against the displacement of the top floor.



Figure 7.29 The cast-in-place concrete building under construction in the laboratory (Ref. 15). The specimen was built in the laboratory by the Groningen construction company Bouwborg.



Figure 7.30 The cast-in-place concrete structure with the actuators for the dynamic push-over tests clearly visible (Ref. 15).

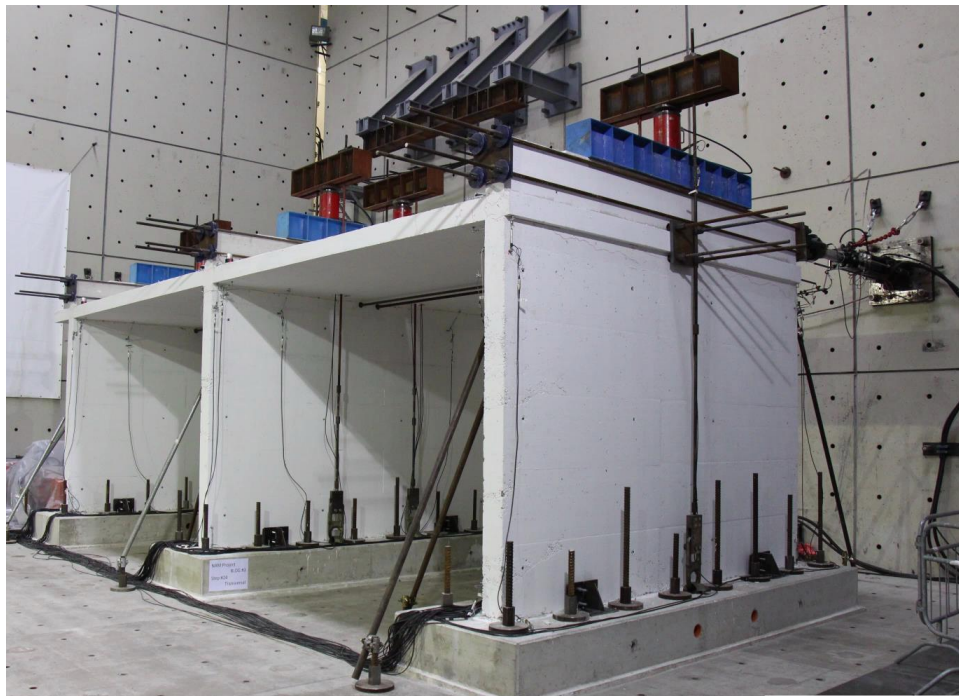
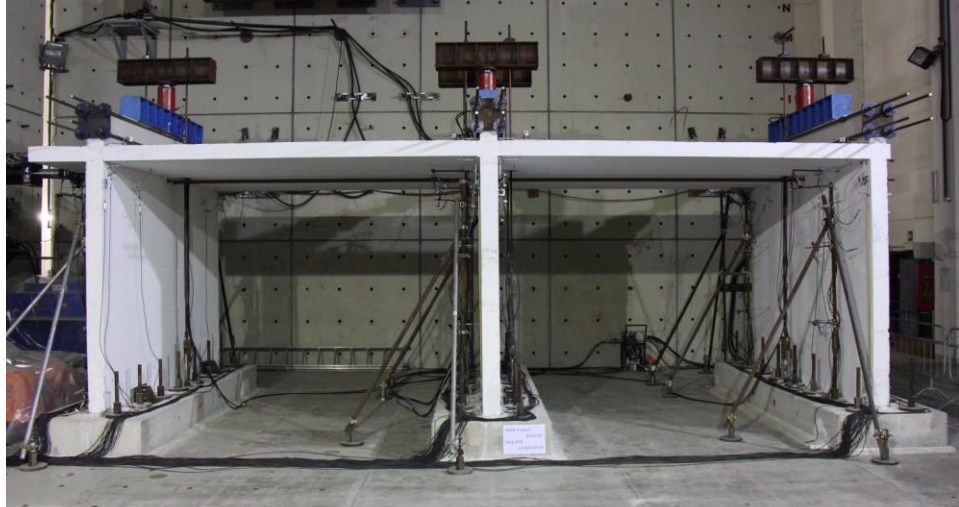


Figure 7.31 A cast-in-place concrete building under cyclic testing in the laboratory (Ref. 15).

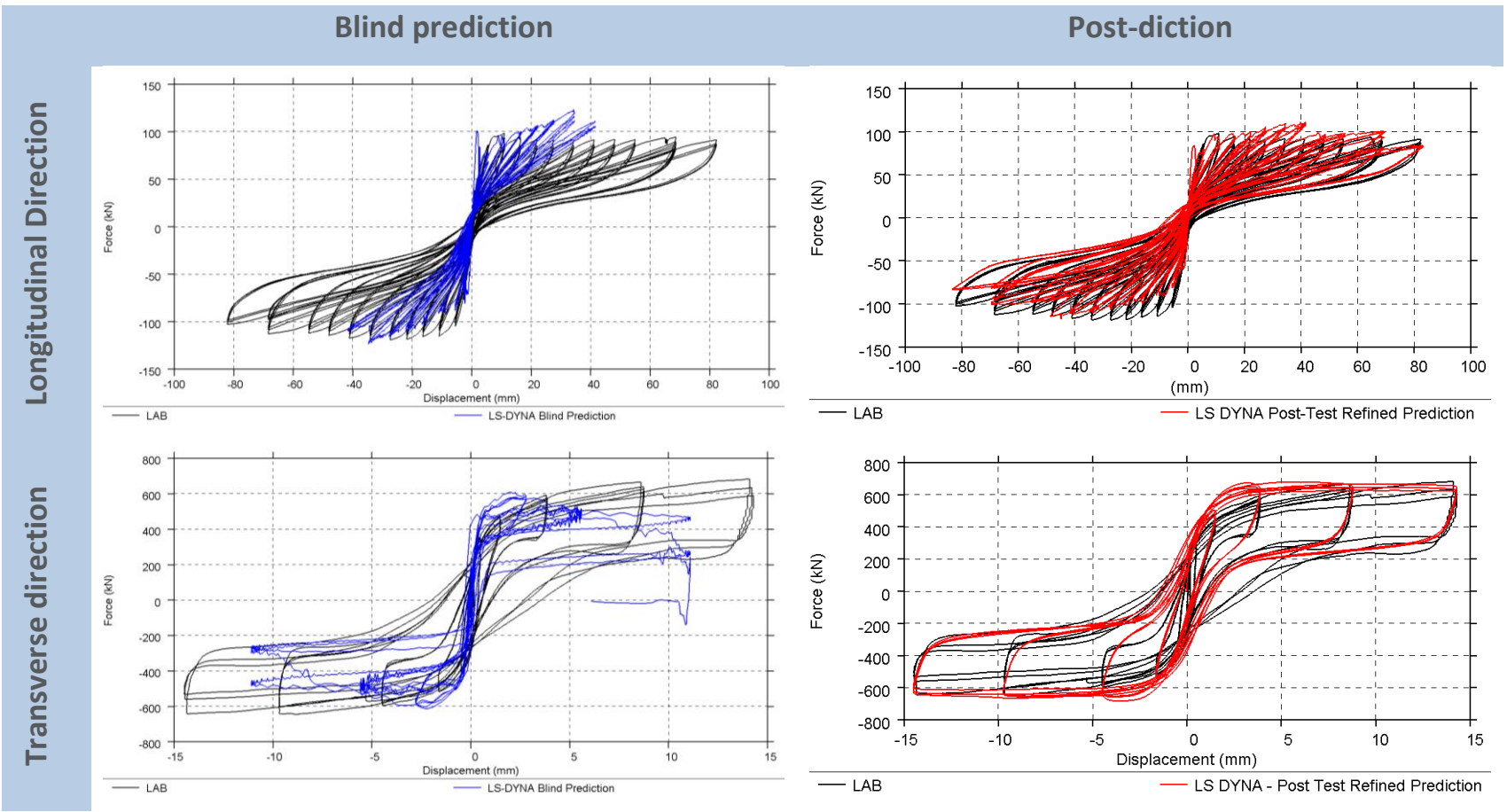


Figure 7.32 Modelling results for the cast-in-place test specimen. Experimental results of the cyclic test are shown in black. The blind-prediction is shown in blue and the post-diction in red.

Development of fragility functions

Following the calibration of numerical software for the seismic assessment of masonry and reinforced concrete buildings, a number of buildings that represent each structural system in the exposure model (so-called 'index buildings') have been identified and numerically modelled. These numerical models (some of which are shown in Fig. 7.33) are subjected to around 10 earthquake accelerograms with different characteristics in terms of magnitude, duration, and ground shaking intensity. The results of these detailed analyses are used to calibrate the backbone and hysteretic response of simpler single-degree-of-freedom (SDOF) systems, that are then used to estimate the nonlinear response of the building to hundreds of accelerograms, which are required for a robust derivation of fragility functions (Fig. 7.34) (Ref. 16, 17). The effects of soil-structure interaction (i.e. foundation-soil flexibility and damping) were also accounted for by adding springs and dashpot dampers at the base of the SDOFs, to represent the presence of either shallow foundations or piles on the different soils found within the Groningen field (Ref. 18).

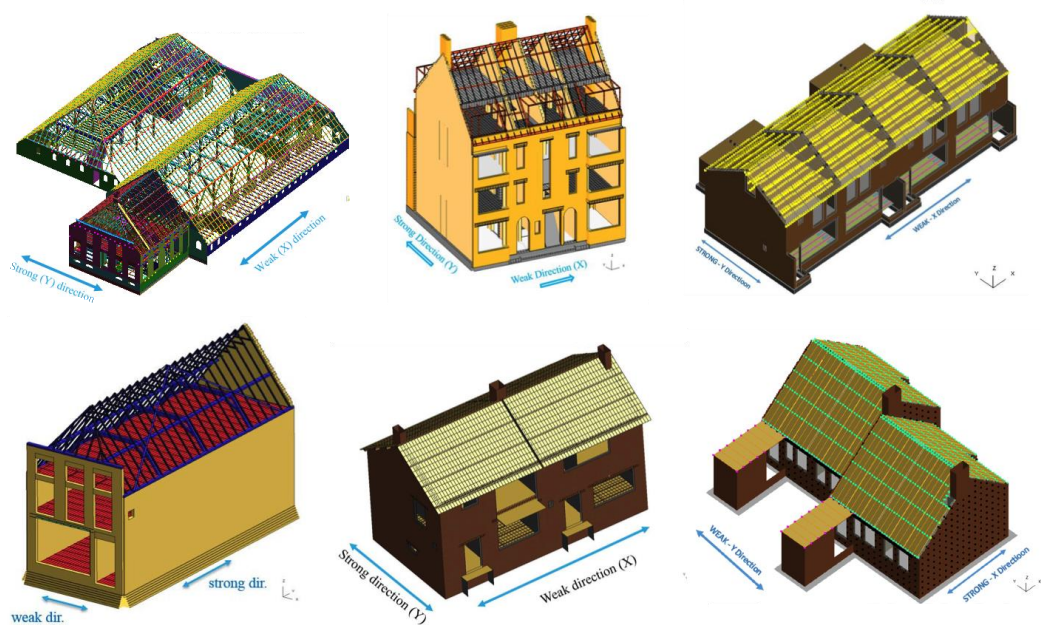


Figure 7.33 Screenshots of the numerical models of URM index buildings

Fragility functions that describe the probability of exceeding a given threshold to damage conditional on a level of ground shaking (Fig. 7.35) can be developed from the response of the SDOF models, by identifying the value of displacement at which different damage and collapse states occur. The thresholds for the damage states DS2, DS3 and DS4 have been obtained from the experimental activities described previously, whereas the collapse states are explicitly modelled in the numerical software. In addition to structural collapse, chimney collapse fragility functions have also been developed using empirical data from a number of earthquakes including Liege (1983) and Roermond (1992) (Ref. 19 and 20).

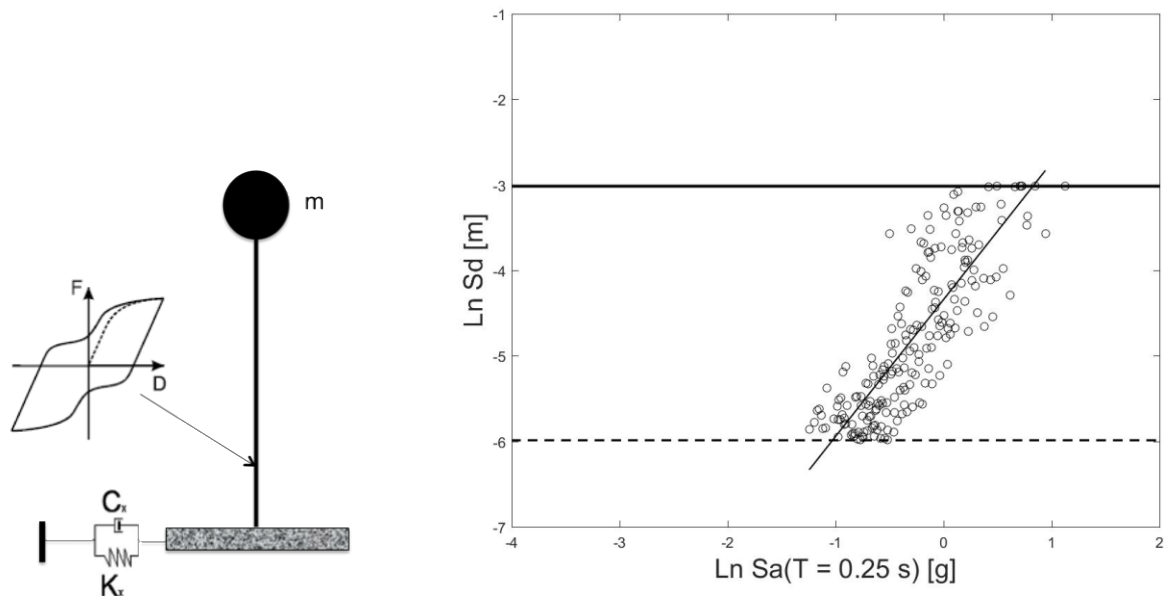


Figure 7.34 (Left) Single degree of freedom (SDOF) model, (Right) Log-log plot showing the displacement response of an SDOF model (vertical axis) against the ground shaking intensity (horizontal axis) of hundreds of accelerograms (each shown by a circle on the plot).

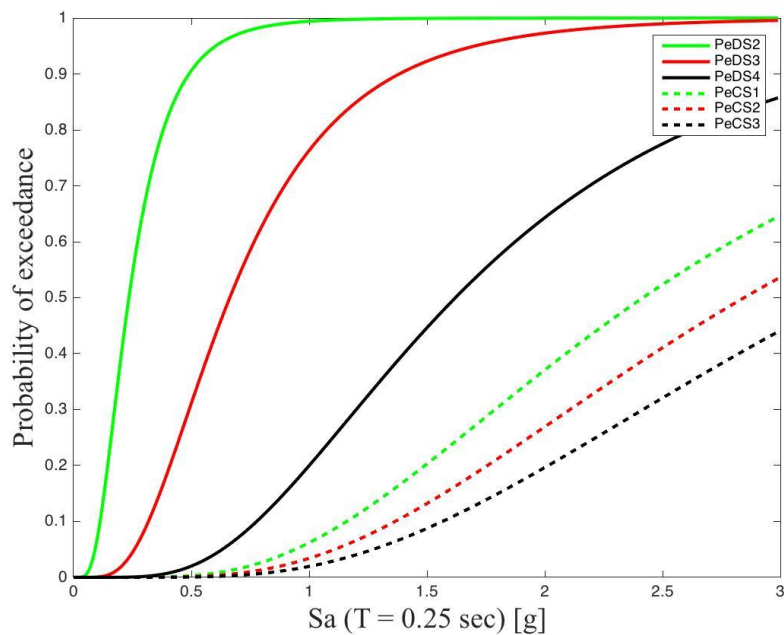


Figure 7.35 Fragility functions for different damage (DS) and collapse (CS) states. The parameter of ground shaking for this structural system is the spectral acceleration at 0.25 seconds.

Further Plans

The extensive experimental programme for buildings described above enabled a solid calibration of the structural modelling tools that were then employed in the development of the fragility functions used in the risk assessment

calculations. In other words, a relatively high level of confidence on the adequacy of these structural modelling for assessing the seismic capacity of buildings in the Groningen region has now been gained.

Therefore, it can be considered now timely to shift the focus of future experimental activities onto (i) the verification of the efficiency of seismic retrofitting techniques, (ii) the seismic vulnerability of non-structural or non-seismic resistant elements (e.g. chimneys, parapets, floor slabs), and (iii) the further verification of the seismic behaviour of connections in prefabricated buildings (e.g. felt layers applied between walls and slabs, 3-way connectors used to connect load-bearing walls to stability walls). This plan is evidenced in Table 7.5 below.

Testing Activities	
In-situ material characterisation	13 URM houses 2 RC buildings
Lab material characterisation	≈ 200 test specimens (taken from actual houses)
Components testing	7 URM walls in-plane 8 URM walls out-of-plane 8 RC precast connections (2-way) 4 URM walls in-plane (seismic retrofitting) 4 timber floors (stiffness, seismic retrofitting) 2 URM chimneys + 2 parapets (collapse capacity, retrofitting) 6 RC precast connections; felt material and 3-way connectors 4 URM walls OOP (vertical action effects, triaxial loading)
Full-structure testing	3 URM houses 2 Roofs 3 RC structures 2 URM houses (seismic retrofitting) 2 URM houses with non-structural elements (collapse capacity) 2 URM houses with non-structural elements (triaxial loading)

Table 7.5 Overview of tests carried out by Eucentre and plan for 2018 and 2019 in *red*.

On the structural modelling front, advantage will be taken of the availability now of solidly calibrated structural analysis tools to undertake an extensive parametric study aimed at providing robust insight on the effects that building characteristics such as the one list below have on the base shear and displacement capacities of URM houses:

- percentage of openings
- number of stories (i.e. vertical load/mass and dynamic amplification)
- ties between inner and outer leaves in cavity walls (i.e. number/corrosion of ties)
- diaphragm flexibility (i.e. timber vs. concrete floors)
- roof configuration (i.e. one/two-way framing, presence of dormer, etc)
- connections between floors/roof and walls
- any other that might be in the meantime identified

Naturally, the prototypes that will be considered in this parametric study will continue to correspond to Groningen-representative index buildings, and the obtained results will cater for the further attuning of the fragility functions.

In addition, the outcomes of such a numerical parametric study may also be of pertinent relevance in the fine-tuning of methodologies for prioritisation of seismic retrofitting activities.

References

1. URM Modelling and Analysis Cross Validation – Arup, Eucentre, TU Delft, Reference 229746_032.0_REP127_Rev.0.03, April 2015.
2. Hazard and Risk Assessment for Induced Seismicity in Groningen Interim Update November 2015, Nederlandse Aardolie Maatschappij BV (Jan van Elk and Dirk Doornhof, eds), 1st November 2015.
3. Material Characterisation – Version 1.3, Eucentre, P&P, TU-Delft, TU-Eindhoven, October 2015.
4. Eucentre Shake-table Test of Terraced House Modelling Predictions and Analysis Cross Validation, staff from ARUP, Eucentre (Pavia) and TU Delft, November 2015 [this document also includes; (1) Instruments full-scale test-house Eucentre Laboratory, (2) Protocol for Shaking Table Test on Full Scale Building (Eucentre) V_1, and (3) Selection of Acceleration Time-Series for Shake Table Testing of Groningen Masonry Building at the EUCENTRE, Pavia, all three by staff from Eucentre (Pavia)],
5. Methodology Prognosis of Building Damage and Study and Data Acquisition Plan for Building Damage, Nederlandse Aardolie Maatschappij BV, Jan van Elk, Jeroen Uilenreef and Dirk Doornhof, February 2017
6. Crowley H., Polidoro B., Pinho R., van Elk J. (2017) “Framework for Developing Fragility and Consequence Models for Local Personal Risk,” *Earthquake Spectra*, in press.
7. Crowley H. and Pinho R. (2017) “Report on the v5 Fragility and Consequence Models for the Groningen Gas Field,” NAM Platform.
8. Mosayk (2015) “Report on soil-structure interaction (SSI) impedance functions for SDOF systems” NAM Platform
9. Risk Assessment of Falling Hazards in Earthquakes in the Groningen region, Tony Taig and Florence Pickup (TTAC Ltd.), March 2016.
10. Risk Assessment of Falling Hazards in Earthquakes in the Groningen region (Appendices), Tony Taig and Florence Pickup (TTAC Ltd.), March 2016.

Consequence Modelling

For the risk metrics that focus on loss of life (see Section 9), a model is needed to predict the probability of loss of life given different levels of ground shaking. Methodologies for estimating fatalities from earthquakes range from those that directly attempt to predict the number of deaths from the magnitude of the earthquake (Ref. 21) or a level of ground shaking such as macroseismic intensity (Ref. 22), to those that propose ratios between the mean number of deaths (or injured persons) and the number of people exposed to a building with a given level of damage, so-called mean fatality ratios (Ref. 23).

The latter approach has been selected for the Groningen risk model, given that it has been observed in past earthquakes that the number of earthquake shaking fatalities is clearly related to the number of buildings that fully or partially collapse (Ref. 24). Furthermore, by estimating the fatality risk for different typologies of buildings, it will be possible to guide the strengthening efforts that are currently being applied to the buildings in the region.

The percentage of the structure that collapses will influence the number of people within the building that are affected (Ref. 25, 26, 27 and 23). So has shown (Figure 7.36) that mean fatality ratios are directly correlated with the volume loss and construction material of collapsed buildings (Ref. 28).

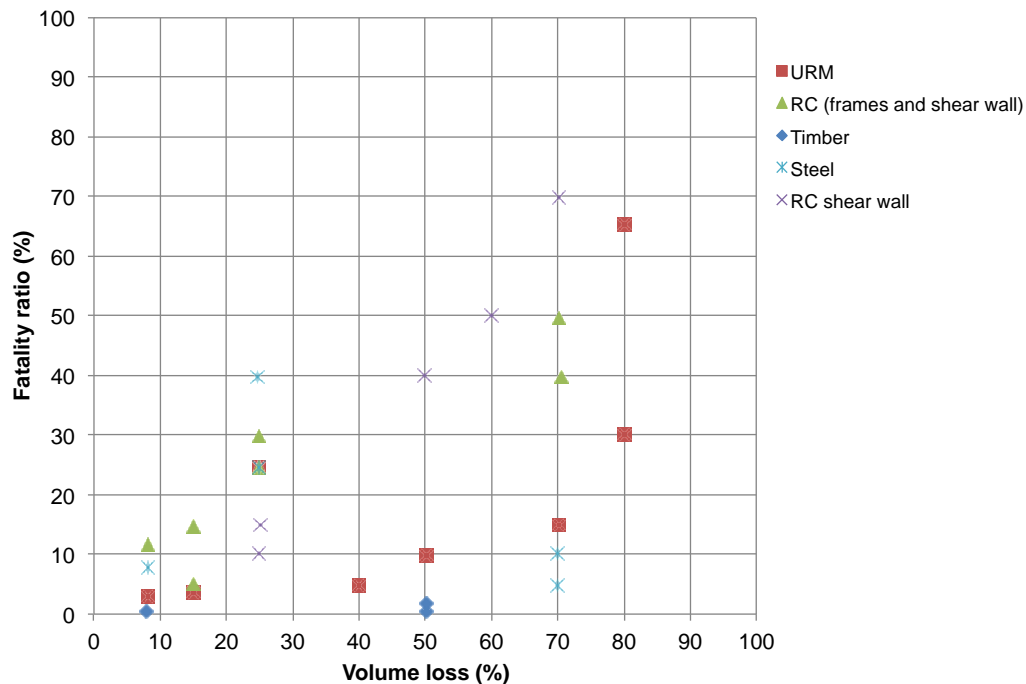


Figure 7.36 Relationship between fatality ratios and volume loss (Ref. 28)

Collapsed buildings are typically defined as having the same “damage level” in post-earthquake reconnaissance missions, despite very large differences in the percentage of the building that has collapsed (Fig. 7.37). This is one of the drawbacks in using empirical data to develop consequence models for fatality risk. This can be overcome by using analytical models that allow different collapse states and associated collapsed debris to be estimated, as employed herein.

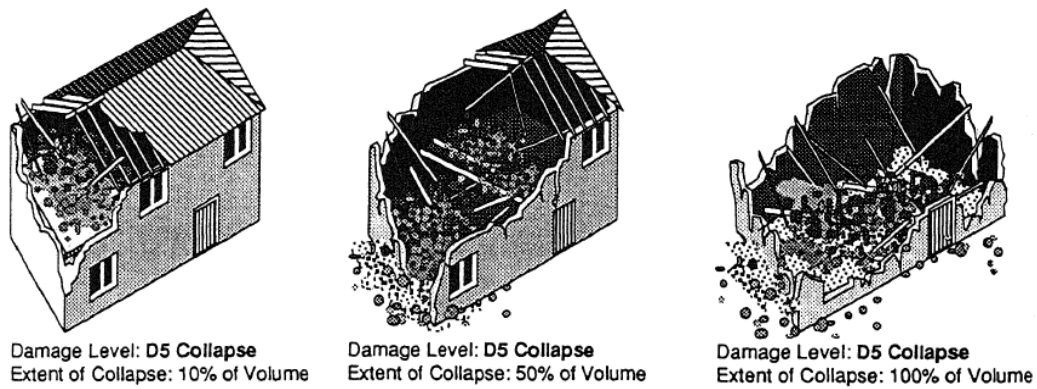


Figure 7.37 Varying volumetric reduction of a building defined as having a “collapse” damage level (Ref. 29)

As discussed previously, an analytical approach (calibrated using experimental evidence) has been adopted for the development of collapse fragility functions in the Groningen risk model. These advanced numerical models also provide insight into the different collapse states that structures with different characteristics will experience under different levels of ground shaking (Fig. 7.39b and Fig. 7.39c), and the associated collapsed debris (both inside and outside the building) that would thus be expected. However, empirical evidence from past events with similar characteristics (in terms of seismicity and structural systems) should also be used to support the results from these numerical models (e.g. Figure 8.10b and 8.10c). The final consequence model is thus based on a combination of analytical modelling and extensive empirical evidence related to fatality risk, as documented by Coburn and Spence (Ref. 23).

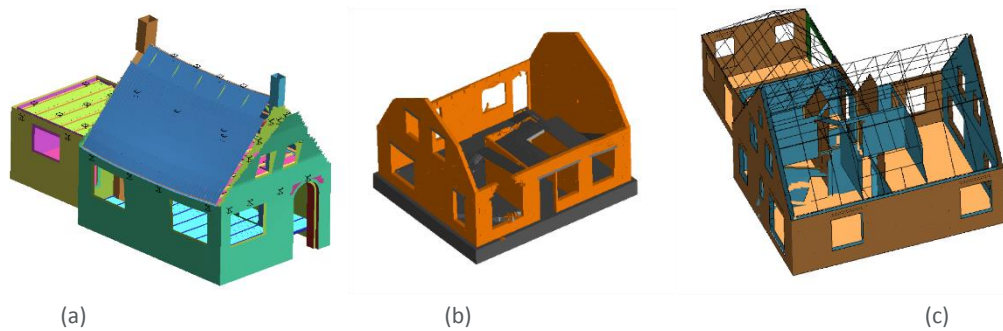


Figure 7.38 Examples of advanced numerical modelling of collapse states a) external gable façade collapse, b) floor collapse, c) internal partition wall collapse

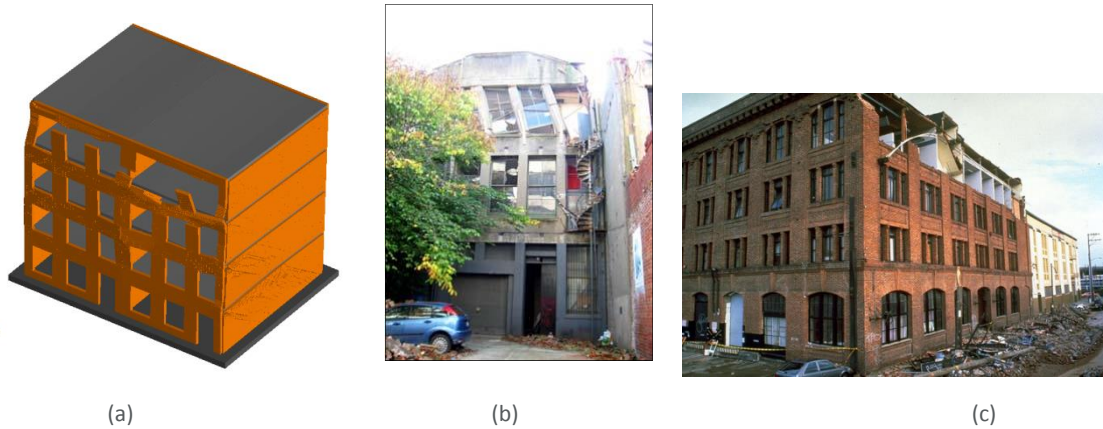


Figure 7.39 (a) Advanced numerical models for collapse modelling and comparisons with empirical evidence from (b) 2011 Christchurch earthquake and (c) 1989 Loma Prieta earthquake

References

7. Brzev S., C. Scawthorn, A.W. Charleson, L. Allen, M. Greene, K. Jaiswal, and V. Silva (2013), GEM Building Taxonomy Version 2.0, GEM Technical Report 2013-02 V1.0.0, 182 pp., GEM Foundation, Pavia, Italy, doi: 10.13117/GEM.EXP-MOD.TR2013.02.
8. Hazard and Risk Assessment for Induced Seismicity in Groningen Interim Update November 2015, Nederlandse Aardolie Maatschappij BV (Jan van Elk and Dirk Doornhof, eds), 1st November 2015.
9. URM Modelling and Analysis Cross Validation – Arup, Eucentre, TU Delft, 229746_032.0_REP127_Rev.0.03, April 2015.
10. In-situ testing of URM houses (building unit: Loppersum, Zijlvest 25), Eucentre, December 2014.
11. Material Characterisation – Version 1.3, Eucentre, P&P, TU-Delft, TU-Eindhoven, October 2015.
12. Experimental campaign on cavity walls systems representative of the Groningen building stock, Eucentre (F. Graziotti, U. Tomassetti, A. Rossi, S. Kallioras, M. Mandirola, E. Cenja, A. Penna, G. Magenes), 16th June 2016.
13. Experimental campaign on a clay URM full-scale specimen representative of the Groningen building stock, Eucentre (F. Graziotti, U. Tomassetti, A. Rossi, B. Marchesi, S. Kallioras, M. Mandirola, A. Fragomeli, E. Mellia, S. Peloso, F. Cuppari, G. Guerrini, A. Penna, G. Magenes, G), 20th July 2016.
14. Eucentre Shake-table Test of Terraced House Modelling Predictions and Analysis Cross Validation, staff from ARUP, Eucentre (Pavia) and TU Delft, November 2015.
15. Modelling predictions and analysis cross-validation of detached single-storey URM Building, ARUP, TU Delft, Eucentre and Arcadis (several staff members from all four institutions), 30th September 2016.
16. Collapse shake-table testing of terraced house (LNEC-BUILD1), Eucentre and LNEC (U. Tomassetti, A. A. Correia, F. Graziotti, A.I. Marques, M. Mandirola, P.X. Candeias), 1st September 2017.
17. LNEC-BUILD1: Modelling predictions and analysis cross-validation, ARUP, TU Delft, Eucentre and Mosayk (several staff members from all four institutions), 8th September 2017.
18. Shake-table test up to collapse on a roof substructure of a Dutch terraced house (LNEC-BUILD2), Eucentre and LNEC (A.A. Correia, A.I. Marques, V. Bernardo, L. Grotoli, U. Tomassetti, F. Graziotti), 31st October 2017.
19. 20. Cyclic testing of RC precast building (EUC-BUILD4), Eucentre (E. Brunesi, S. Peloso, R. Pinho, R. Nascimbene), 22nd June 2017.
20. Shake-table testing of RC precast building (EUC-BUILD5), Eucentre (E. Brunesi, S. Peloso, R. Pinho, R. Nascimbene), 31st October 2017.

21. Cyclic testing of RC precast building (EUC-BUILD4), Eucentre (E. Brunesi, S. Peloso, R. Pinho, R. Nascimbene), 22nd June 2017.
22. Shake-table testing of RC precast building (EUC-BUILD5), Eucentre (E. Brunesi, S. Peloso, R. Pinho, R. Nascimbene), 31st October 2017.
23. Cyclic testing of RC tunnel building (EUC-BUILD3), Eucentre (E. Brunesi, S. Peloso, R. Pinho, R. Nascimbene), 8th May 2017.
24. Crowley H., Polidoro B., Pinho R., van Elk J. (2017) "Framework for Developing Fragility and Consequence Models for Local Personal Risk," *Earthquake Spectra*, *in press*.
25. Crowley H. and Pinho R. (2017) "Report on the v5 Fragility and Consequence Models for the Groningen Gas Field," NAM Platform
26. Mosayk (2015) "Report on soil-structure interaction (SSI) impedance functions for SDOF systems" NAM Platform
27. Risk Assessment of Falling Hazards in Earthquakes in the Groningen region, Tony Taig and Florence Pickup (TTAC Ltd.), March 2016.
28. Risk Assessment of Falling Hazards in Earthquakes in the Groningen region (Appendices), Tony Taig and Florence Pickup (TTAC Ltd.), March 2016.
29. Samardjieva E. and Badal J. (2002) "Estimation of the expected number of casualties caused by strong earthquakes," *Bulletin of Seismological Society of America*, 92, pp. 2310–2322.
30. Jaiswal K., Wald D.J. and Hearne M. (2009) "Estimating Casualties for Large Worldwide Earthquakes using an Empirical Approach," US Geological Survey Open-File Report 1136.
31. Coburn A. and Spence R. (2002) *Earthquake Protection*, 2nd Edition, John Wiley & Sons Ltd, Chichester.
32. Alexander D. (1996) "The Health Effects of Earthquakes in the Mid-1990s," *Disasters* 20(3), pp. 231-247.
33. Seligson H.A. (2008) "Casualty Consequence Function and Building Population Model Development," Primary resource document for the "FEMA P-58 Seismic Performance Assessment of Buildings", FEMA, Washington.
34. Spence R., So E. (2009) *Estimating Shaking-Induced Casualties and Building Damage for Global Earthquake Events*, NEHRP Grant number 08HQGR0102, Final Technical Report
35. So E. and Pomonis, A. (2012) "Derivation of globally applicable casualty rates for use in earthquake loss estimation models," *Proceedings of the 15th World Conference on Earthquake Engineering*, Lisbon, Portugal, Paper no. 1164.
36. So (2015) Personal communication.
37. Coburn A.W., Spence R.J.S. and Pomonis, A. (1992) "Factors Determining Casualty Levels in Earthquakes: Mortality Prediction in Building Collapse," *Proceedings of the 10th World Conference on Earthquake Engineering*, Madrid, Spain.

8 Building Damage Forecasting

Introduction

This chapter starts with an introduction into the classification of damage states and into the Monte Carlo method used for forecasting building damage and fatality risk. Initially, the studies program focused on the assessment of risk. The risk assessment methodology was extended to also include assessment of building damage.

The report “Methodology Prognosis of Building Damage and Study and Data Acquisition Plan for Building Damage” (Ref. 1), issued February 2017, describes the studies program into building damage and the methodology for forecasting building damage.

The current chapter presents the forecast of building damage from DS 1 to DS3. The higher damage states DS4 and DS5 are relevant to risk and are addressed in the next chapter. For the assessment of DS1 building damage empirical methods based on analysis of historical damage data are used. The assessment of DS2 and DS3 building damage is based on analytical methods supported by laboratory experiments carried out in Eucentre and LNEC.

Classification of Building Damage; Building Damage States

European Seismological Commission, EMS-1998

Article 7 of the instemmingsbesluit refers to EMS-98, European Seismological Commission, 1998 (Ref. 8) for the assessment of building damage. The EMS-98 document provides guidelines for estimation of the intensity of an earthquake based on the damage assessment of buildings.

Damage of buildings is assessed on the basis of a damage classification. This is provided for two main categories: unreinforced masonry buildings (URM) and reinforced concrete (RC) buildings. Figure 8.2 describes the 5 distinguished damage grades for both main categories. The description of the damage states in this figure are purely qualitative. For instance, “negligible to slight damage” is termed DS1, “moderate damage” DS2, “substantial to heavy damage” DS3”. The EMS scale relates DS1 to “hairline cracks in very few walls”, DS2 to “cracks in many walls” and DS3 to “large and extensive cracks in most walls”. The qualitative descriptions of the building damage states form a very useful, practical and generally accepted and applied classification system for building damage.

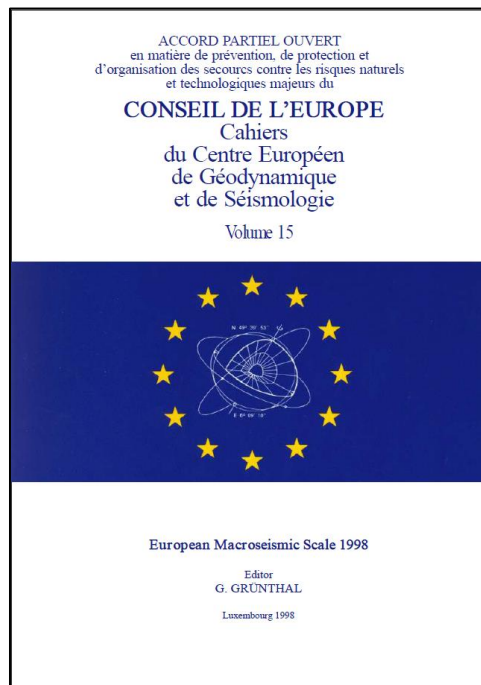


Figure 8.1 Cover of the “European Macroseismic Scale 1998, EMS-98” by the European Seismological Commission (G. Grünthal), 1998.

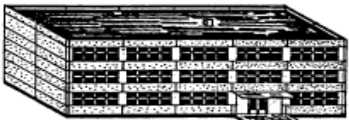
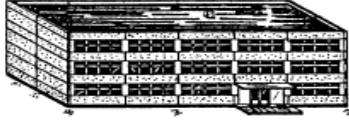
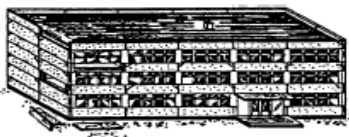
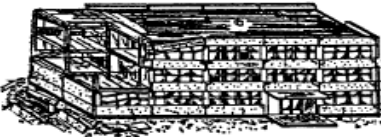
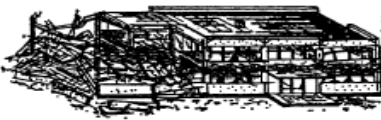
Classification of damage to masonry buildings		Classification of damage to buildings of reinforced concrete	
	<p>Grade 1: Negligible to slight damage (no structural damage, slight non-structural damage) Hair-line cracks in very few walls. Fall of small pieces of plaster only. Fall of loose stones from upper parts of buildings in very few cases.</p>		<p>Grade 1: Negligible to slight damage (no structural damage, slight non-structural damage) Fine cracks in plaster over frame members or in walls at the base. Fine cracks in partitions and infills.</p>
	<p>Grade 2: Moderate damage (slight structural damage, moderate non-structural damage) Cracks in many walls. Fall of fairly large pieces of plaster. Partial collapse of chimneys.</p>		<p>Grade 2: Moderate damage (slight structural damage, moderate non-structural damage) Cracks in columns and beams of frames and in structural walls. Cracks in partition and infill walls; fall of brittle cladding and plaster. Falling mortar from the joints of wall panels.</p>
	<p>Grade 3: Substantial to heavy damage (moderate structural damage, heavy non-structural damage) Large and extensive cracks in most walls. Roof tiles detach. Chimneys fracture at the roof line; failure of individual non-structural elements (partitions, gable walls).</p>		<p>Grade 3: Substantial to heavy damage (moderate structural damage, heavy non-structural damage) Cracks in columns and beam column joints of frames at the base and at joints of coupled walls. Spalling of concrete cover, buckling of reinforced rods. Large cracks in partition and infill walls, failure of individual infill panels.</p>
	<p>Grade 4: Very heavy damage (heavy structural damage, very heavy non-structural damage) Serious failure of walls; partial structural failure of roofs and floors.</p>		<p>Grade 4: Very heavy damage (heavy structural damage, very heavy non-structural damage) Large cracks in structural elements with compression failure of concrete and fracture of rebars; bond failure of beam reinforced bars; tilting of columns. Collapse of a few columns or of a single upper floor.</p>
	<p>Grade 5: Destruction (very heavy structural damage) Total or near total collapse.</p>		<p>Grade 5: Destruction (very heavy structural damage) Collapse of ground floor or parts (e. g. wings) of buildings.</p>

Figure 8.2 Classification of damage to masonry buildings (left) and classification of damage to reinforced concrete buildings (right). Illustration taken from EMS-98, European Seismological Commission, 1998 (Ref. 8).

Methodology for assessing Building Damage Forecasting

Monte Carlo Simulation

A typical Monte Carlo simulation repeats the model calculations many thousands of times, each time using different randomly selected input values, such that the stochastic variability of the output is small enough to ensure stability of the accumulated results at the probability levels required. The Monte Carlo methodology used for the seismic hazard and risk assessment is summarised in Figure 8.3. Full details of the method can be found in chapter 5, 6 and 7 of this report and references 2, 3 and 4.

Underlying model

- The underlying **seismological model** is an empirical relationship between reservoir compaction and geometry and the number of earthquakes induced by the gas production over a given time. This model considers the occurrence of earthquakes to be a (Poisson) random process, driven by the reservoir compaction due to production. Compaction is modelled for a range of gas production scenarios.
- The effects of spatial and temporal clustering of earthquakes were found to be statistically significant and have been incorporated in the model using the Epidemic Type After-shock Sequence (ETAS) formalism.
- The consequences of the individual synthetic earthquakes are calculated using probabilistic models for earthquake ground motion, building damage and risk of death or injury of the exposed population.
- The seismological model and ground motion prediction equations have been repeatedly calibrated using the earthquake catalogue (locations and magnitudes) and ground motion data available to date. The compaction model is calibrated with a wealth of geodetic data.

Input parameters

- **Synthetic earthquake catalogues.** In the Monte Carlo simulation process for the induced seismic hazard and risk assessment, repeated random sampling of a set of input distributions is used to build up a probabilistic output. So-called 'synthetic earthquake catalogues' (i.e. event locations and magnitudes for a specified time period) are generated from the input probability distributions of total seismic moment, number of events and event epicentres.
- **Aleatory uncertainties.** The inherently stochastic nature of earthquakes and the statistical variability of key properties determining earthquake ground motion, building damage and consequences of damage for inhabitants are captured by the properties of the input distributions sampled. In this way, the so-called aleatory uncertainties are modelled. Examples of such aleatory uncertainties in our simulation process are numbers of earthquakes in a catalogue and their locations, orientations and magnitudes, subsurface rock properties and small-scale near surface soil properties, strength and condition of buildings and the locations of inhabitants in relation to occurrences of building collapse.
- **Epistemic uncertainties.** Systematic uncertainties associated with a lack of knowledge of key pieces of information, the so called epistemic uncertainties, are addressed by running separate simulations with different sets of input parameter values. The key epistemic uncertainties are identified and likely ranges of values for these parameters with associated probabilities are estimated. Examples of key epistemic uncertainties identified are: i) the earthquake stress drops; ii) the maximum possible earthquake magnitude; iii) the set of medians and standards deviations defining the fragility curves; iv) and the values of the coefficients determining the probabilities of death if building collapse occurs.

Design

- **Logic tree.** With a manageable set of epistemic uncertainties identified and quantified, a logic tree is built up by running a separate simulation for each distinct path through the set of all possible parameter choices. For example, if four key uncertain parameters have been identified, each with 3 possible values (low, mid and high cases) then a logic tree with $3^4=81$ distinct paths must be simulated. The final result is a set of output distributions from which summary statistics (mean, median, P10, P90 etc) can be calculated by combining results from the individual logic tree branches weighted by their input probabilities.
- **Fragility curves** are used to characterise the probabilities of building damage. A fragility curve gives the probability of a given building type exceeding a given damage state as a function of the seismic ground motion

(ideally spectral displacement at a given frequency). It is a cumulative distribution function characterising the capacity of buildings of a certain typology to withstand seismic loading (demand) and therefore reflects the spread of building properties within the defined typology class. Fragility curves have so far been developed only for the higher damage states characterising partial collapse (Damage State 4, DS4) and full collapse (Damage State 5, DS5), for the assessment of life safety risk. The assessment of lower states of building damage requires the development of fragility curves for the damage states DS1, DS2 and DS3 as shown schematically in Fig. 8.4.

Sample:

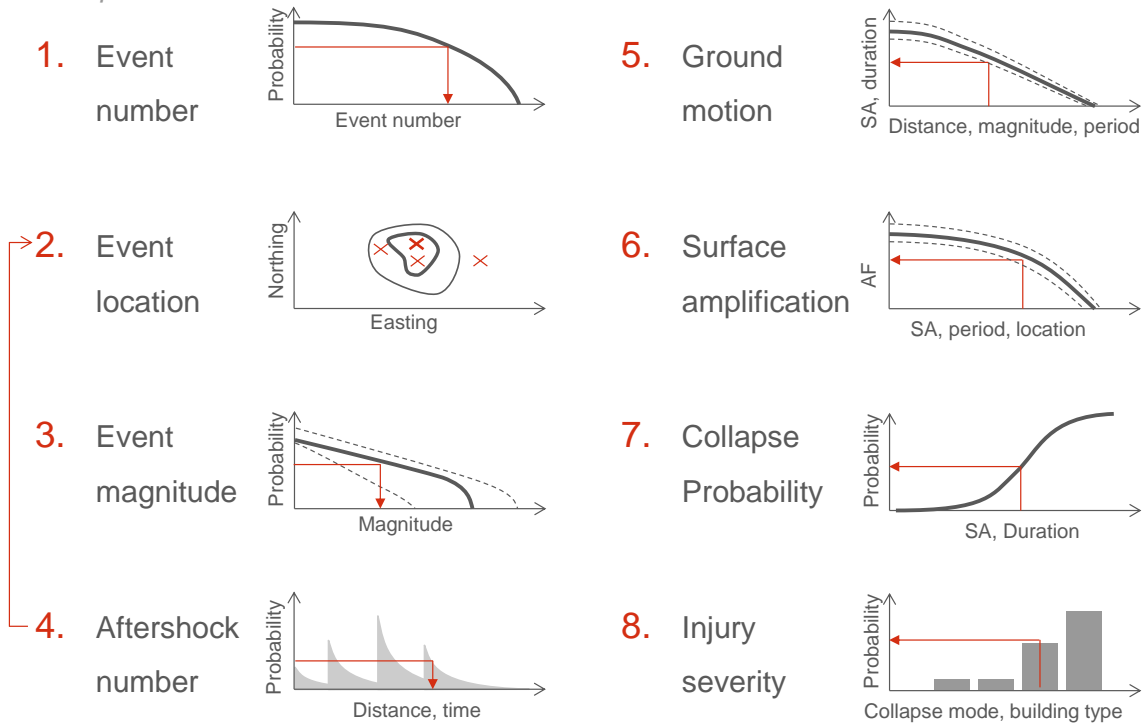


Figure 8.3 Monte Carlo simulation of the seismic hazard and risk model.

The procedure entails the following. Earthquake magnitudes are sampled from the frequency-magnitude distribution (usually assumed to follow a Gutenberg-Richter relationship). This distribution, then, will be truncated at the high end by the maximum magnitude, M_{max} , and at the low end by M_{min} . A value of M_{min} must be chosen such that it is low enough to ensure that all significant contributions to the ground motion hazard and risk are captured, but high enough to allow sufficiently fast simulations.

Fragility Curves for buildings in Groningen

Forecasting building damage (as well as life safety risk) requires fragility curves for the established set of building typologies covering lower damage states (DS1, DS2 and DS3) as well as the building collapse states (DS4 and 5).

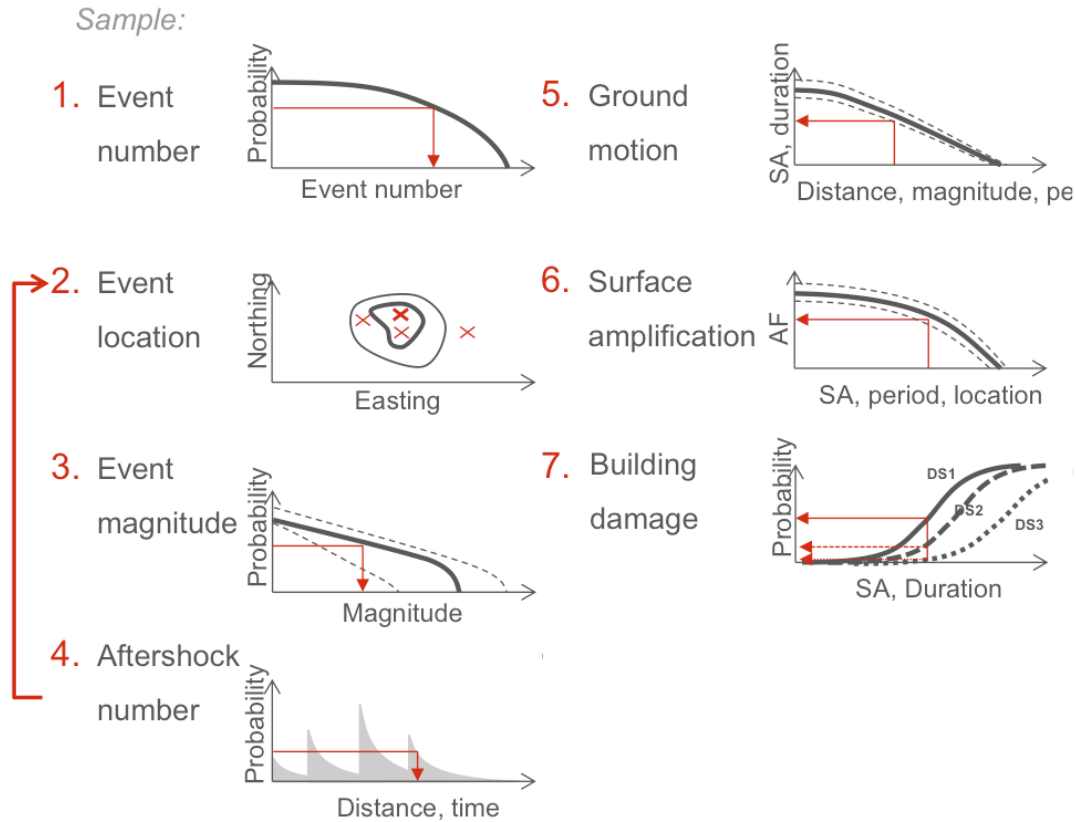


Figure 8.4 Monte Carlo simulation of the seismic hazard and risk model for the prognosis of building damage.

Fragility curves are typically constructed by considering building capacity within a population of buildings of a given typology class. They take the form of a log-normally distributed random variable. Capacity, A , of a building to withstand seismic ground motion demand, a , can be expressed in terms of a median capacity, A_m , and a log-normally distributed random variable, ε , with logarithmic standard deviation, β :

$$A = \varepsilon A_m$$

The fragility function gives the probability of failure – that is, the probability of experiencing a given level of damage – for demand, a , as

$$P_f(a) = \Phi \left[\frac{\ln a - \ln A_m}{\beta} \right]$$

where Φ is the cumulative normal distribution function. In other words, the fragility curve gives the probability that the building's capacity is less than the seismic demand for a specific damage state.

Figure 8.5 shows an example of a generic set of fragility curves for damage states DS1, DS2 and DS3. This set of curves belongs to a single building typology. Each curve allows us to derive the probability that a certain damage state is exceeded, given the ground motion.

For an exposure to a ground motion, the probability that a house of this typology would fall within each of the three building damage states (DS1, DS2 and DS3) can be read or extracted. Given that the fragility functions are applied to aggregations of buildings of a given typology within each zone at which the hazard is calculated, this probability can be interpreted as a proportion of those buildings that fall in each damage state. Figure 8.6 shows a generic example for buildings exposed to a peak ground acceleration of 0.15 g.

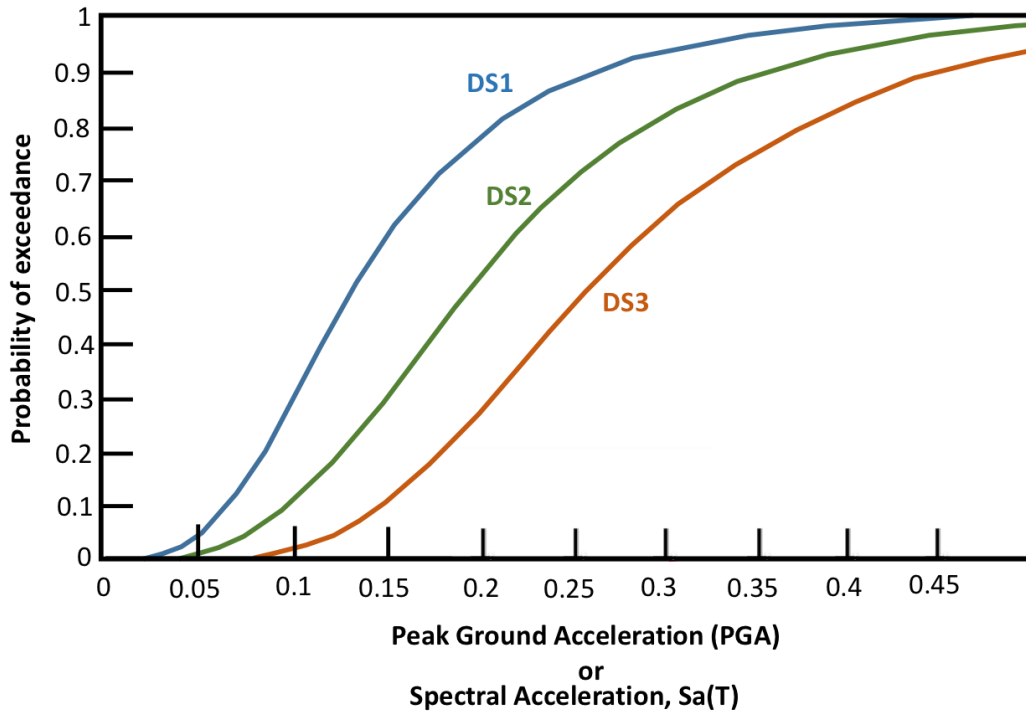


Figure 8.5 Generic example of fragility curves for the damage states DS1 – DS3, for a single building typology.

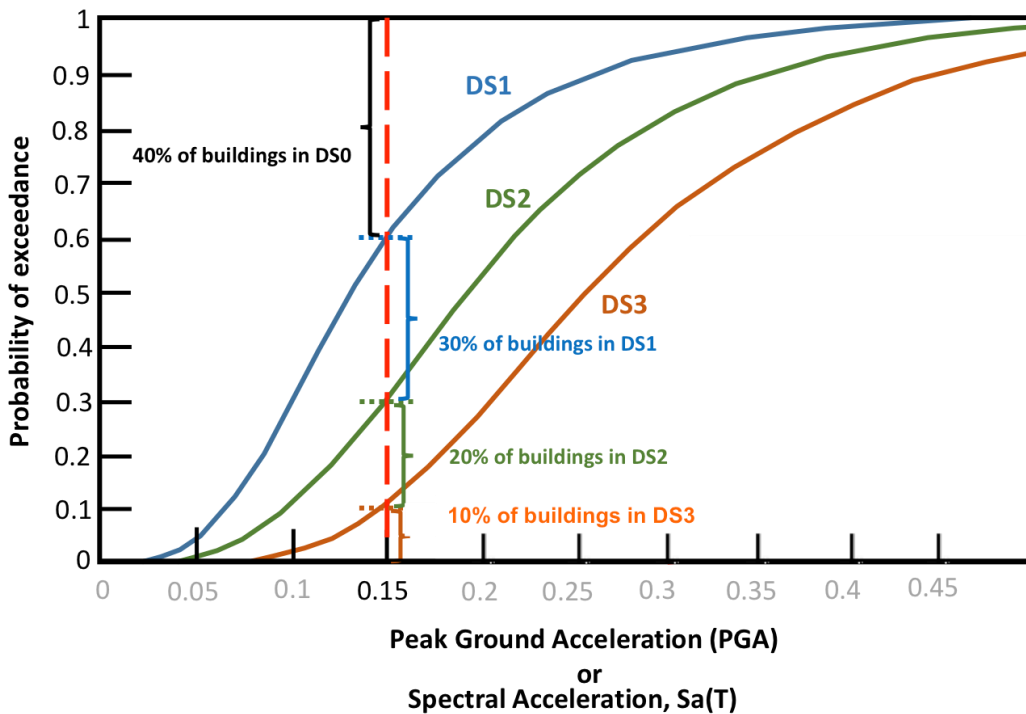


Figure 8.6 Generic example of a fragility curve for a building typology. The impact of an earthquake with a PGA (in this case of 0.15 g) on buildings of the relevant typology has been indicated. The damage state DS0 is used to indicate “no building damage”.

The lower damage states are much more likely to occur than partial or full building collapse. Different methods were used for the development of fragility curves for lower damage states:

Empirical: After an earthquake the building damage is assessed and recorded. From this field data, fragility curves can be constructed. In the literature, several damage assessments undertaken after an earthquake have been reported (Ref. 10, 14, and 15).

Also in The Netherlands, such an assessment of damage after earthquakes has been carried out by TNO (Ref. 5) and reported in the “kalibratie study”. As all damage was classified as DS1, only fragility curves for DS1 damage could be prepared. A forecast for building damage based on the TNO Kalibratie study is presented in chapter “Forecast of DS1 based on Observed Damage from Historical Earthquakes”.

Both NAM and CVW have recorded the building damage since August 2012 in a database. This building damage data source can also be analysed to gain insight into DS1 damage and prepare a forecast. A machine learning approach to forecasting DS1 building damage is described in the chapter “Damage analytics analysis and forecasts”.

Analytical: Using the empirical approach only a forecast for DS1 building damage in the Groningen area can be prepared. To prepare a forecast for the higher damage states DS2 and DS3, an analytical approach needed to be applied. This method makes use of the experimental results obtained in the laboratory in Eucentre and LNEC described in chapter 7.

Forecast of DS 1 based on Observed Damage from Historical Earthquakes

Background

A study of past building damage was carried out by TNO in the “Kalibratiestudie schade door aardbevingen” published in November 2009 (Ref. 5). This research into building damage started in 2006 and was commissioned by five oil and gas companies (NAM BV, BP Nederland Energy BV [later TAQA], Vermilion Oil & Gas Netherlands BV and Wintershall Noordzee BV). The objective of this study was to establish the maximum distance from the epicentre where damage could still be expected, given the earthquake’s local magnitude.

In document 5 chapter 9 of the Technical Addendum to the Winningsplan Groningen 2016 (Ref. 3) addressing building damage, the TNO methodology was used to estimate the number of damaged buildings after the Huizinge (August 16, 2012) and Hellum (September 30, 2015) earthquakes, respectively. These expectations were then compared with the number of damage claims received within 10 weeks after each seismic event. In this comparison, we should keep in mind that, in terms of energy release, the Huizinge earthquake was roughly 5.5 times stronger than the earthquake in Hellum.

For the Huizinge earthquake, the analysis showed a strong correlation between predicted impact on building damage and observed building damage (based on supported damage claims). That correlation is much weaker for the Hellum earthquake, where the number of damage claims is much higher than the predicted building damage. It was concluded that a damage claim does not necessarily correspond to actual earthquake damage. The relationship between seismic activity and damage claims appears to be more complex.

Based on a refinement of the TNO method in combination with improved knowledge regarding the hazard (described in chapter 6) and exposure (described in chapter 7) a forecast of building damage due to future earthquakes in Groningen can be made, within limitations and uncertainty ranges. Further research aimed at better understanding of building damage initiation and characteristics will provide more insights and possibly lead to more precise forecasts.

Introduction

This section describes the applied empirical methodology and provides the actual Damage State 1 (DS1) forecast, in line with section 5.1 of the “Methodology Prognosis of Building Damage and Study and Data Acquisition Plan for Building Damage” (Ref. 1).

Building damage was assessed and recorded for several historical earthquakes. From this field observation data, and using up-to-date empirical GMPEs, fragility functions were constructed for a number of building typologies. These fragility functions were then assigned to each building in the exposure area. Several possible future realizations (earthquake catalogues) were generated stochastically, based on the current production scenario and using the hazard tool. Finally, the total expected number of damaged buildings was calculated per event and per catalogue.

International experience from post-earthquake assessments (Ref. 7 and 8) shows that empirical methods are valuable in situations where the predictions are made for the same building stock and same levels of shaking at the observed data, but also have some limitations.

Limitations

The following limitations apply to this empirical approach in general and are therefore not unique to Groningen:

1. The first uncertainty relates to the local ground motion. For historical earthquakes, often the level of ground motion was not recorded or was sparsely recorded and therefore has a relatively large uncertainty. Even when recordings are available, the spatial variability of ground-motion fields is such that some of the uncertainty

associated with motions at a particular location remains. The extension of the KNMI geophone and accelerometer network has reduced this uncertainty.

2. Secondly, the focus is on the damaged buildings; the undamaged buildings are often not counted or recorded, making it difficult to assess the relative level of damage. The quality and consistency of the damage assessments often also limits their usefulness.
3. Another limitation is that this empirical method is restricted to the experience domain of earthquakes. In this case, smaller than magnitude 3.6 and primarily damage level DS1 has been encountered and there is very limited data for DS2. The method does not allow extrapolation of the observed building damage to larger earthquakes or higher damage states.
4. Finally, for lower damage states, the cause of the damage is very difficult to establish. Damage at these levels due to an earthquake is difficult to distinguish from damage due to other causes (e.g. thermal loads, creep and shrinkage of the mortar, differential foundation settlement or vibration from heavy road traffic, rail transport or construction work).

Compared to international experience the situation in Groningen with respect to items 1 and 2 is substantially improved because of the ongoing research effort, including the large dataset now available and detailed knowledge of the building stock. Limitations 3 and 4 remain particularly relevant. However, these limitations do not stand in the way of providing a methodology and practicable outcome as per article 7 of the “Instemmingsbesluit”.

Historical Building Damage Data

To be able to establish an accurate forecast of the damage to buildings caused by earthquakes, historical assessment data can in principle be used. The damage data underlying TNO reports “Kalibratiestudie schade door aardbevingen” (Ref. 5), and “Analyse van de gevolgen van de aardbeving te Huizinge d.d. 16 augustus 2012” (Ref. 9) was used for the forecasting of future building damage. Because detailed verification of damage assessment reports is no longer possible, the damage data shared by TNO was taken at face value.

The following Groningen field related earthquakes have been considered as input:

- Hoeksmeer 2003 M= 3.0
- Stedum 2003 M= 3.0
- Westeremden 2006 M= 3.5
- Huizinge 2012 M=3.6

The TNO study distinguished 4 different typologies for which damage was considered: “Boerderijen” (Farms), “Laagbouw voor 1940” (Low Rise buildings before 1940), “Laagbouw na 1940” (Low Rise buildings after 1940) and “Hoogbouw” (High-Rise Buildings). For High-Rise buildings, no damage was observed, most probably because these are primarily concrete structures as opposed to unreinforced masonry (URM) type construction (more vulnerable to vibrations). Since these earlier damage studies significant developments have been achieved in Ground Motion Modelling for Groningen.

Empirical GMPE for Peak Ground Velocity from Small-Magnitude Earthquakes

Ground Motion Prediction methods have initially focused on prediction of PGA (Peak Ground Acceleration), spectral acceleration at several periods and significant ground shaking duration. These are the most important hazard metrics for the prediction of failure of building elements and hence for risk. For the assessment of the potential to cause damage, the velocity-based hazard metrics such as PGV (Peak Ground Velocity) are also important. Empirical evidence elsewhere (Ref. 10) has shown that building damage (DS1 and DS2) correlates more strongly with PGV. In addition, most guidelines for tolerable shaking levels—implying disturbance to occupants and/or low damage levels—are specified in terms of PGV.

NAM has developed an empirical Groningen-specific (induced) Ground Motion Prediction method to estimate the value of PGV at specific locations (Ref. 11). The new PGV equation presented can be used with confidence to estimate peak ground velocity in the Groningen field for earthquakes with magnitudes from 2.5 to 3.6. The model could be extrapolated beyond these limits, perhaps to 2 at the lower end and 4 at the upper end (in which range the extrapolation is most likely slightly conservative), but certainly no further, due to the purely linear magnitude scaling in the model, which would not be appropriate for a broader magnitude range. The equation can be applied with confidence up to 30 km and probably with reasonable confidence to 50 km from the epicentre. The equations include coefficients for the prediction of the median values of PGV and also the standard deviations to allow values to be estimated at other exceedance values.

Fragility Functions

Building damage functions (Ref. 12) are in the form of lognormal fragility curves. The “output” of fragility curves is an estimate of the cumulative probability of being in, or exceeding, each damage state for the given level of ground shaking (or ground failure). Each fragility curve is defined by a median value of the hazard demand parameter (in this case PGV has been selected) that corresponds to the threshold of the damage state and by the variability associated with that damage state. The conditional probability of exceeding DS1 given the PGV is then given by the following function:

$$P[DS1|PGV] = \phi \left[\frac{\ln \frac{PGV}{\theta}}{\beta} \right]$$

where:

θ is the median value of PGV at which the building reaches the threshold of damage state DS1,

β is the standard deviation of the natural logarithm of PGV for damage state DS1, and

ϕ is the standard normal cumulative distribution function.

Fragility Functions (DS1) have been fitted for each of the typologies defined in TNO report using maximum likelihood estimation (Ref. 13), and shown in Figure 8.7.

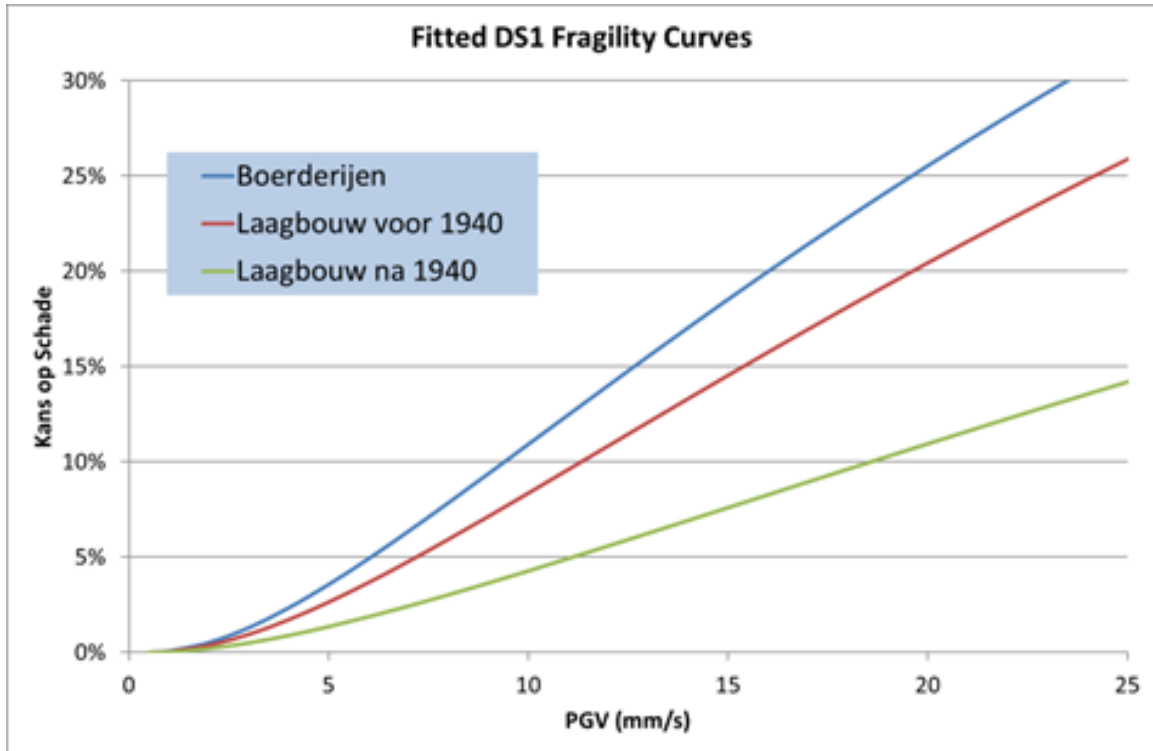


Figure 8.7 Fragility Functions (DS1) developed based on the TNO Kalibratiestudie for three building typologies.

A comparison with fragility functions available in earthquake literature (Ref. 10, 11, 15 and 16) is shown in Table 8.1 below:

	Type of Fragility function	Type of Structures in Scope	1% DS1 (mm/s)	10% DS1 (mm/s)
Okada and Takai (2000)	Empirical Japan / Tectonic	Wooden frame with infill walls	50	100
Hancilar et al. (2000)	Empirical Haiti / Tectonic	RC frames with infill walls; Wooden frame with infill walls	320	440
Bommer et al (2006)	Empirical El Salvador / Tectonic	Madera (wood); sistema mixto (masonry); adobe (sundried clay brick); bahareque (wattle-and-daub)	42	55
Gehl et al (2013)	Theoretical (non-linear dynamic analysis) / Tectonic	URM	38	46

Table 8.1 PGVs at 1% and 10% probability of DS1 exceedance from earthquake literature.

Except for work by Hancilar et al., the degree of agreement between these very different studies is quite remarkable. The non-structural damage classified by Hancilar as DS1 could be that of the brick infill walls, which is actually more like structural damage or DS2. This may explain the higher PGV at which damage is reported.

One might conclude that damage to Groningen buildings occurs at significantly lower vibration levels, therefore they would be much more susceptible to vibration damage than abroad. While the type of buildings and earthquake characteristics obviously do differ in Groningen, the very large difference of factor 10 or more would appear unrealistic. This possibly relates to difference in the actual definition of damage, and could be the result of limitation 4 stated above. Further research is needed to better understand the validity of the TNO observations. Nevertheless, only the “Kalibratiestudie” observations have been used as input to the forecast.

Exposure model

The exposure database (EDB V5 Ref. 14) is an extract of a project database and consists mainly of the building typology classifications and several other building related attributes, including the population, arranged per building. In addition to its use as input into the Hazard and Risk Modelling, the EDB deliverable also provides the necessary information to assign the TNO typologies to all 257,174 Buildings (“Basisregistratie adressen en gebouwen (BAG)” from the Kadaster) in the area considered for damage forecast.

The area of interest is the same for the Hazard and Risk assessment is and is based on the Groningen gas field outline. The extract boundary for the EDB V5 is a 5 km buffer around the gas field outline as seen in the assessment boundary in Figure 8.8.



Figure 8.8 Assessment boundary used for the exposure database scope.

Table 8.2 shows how the different type of buildings present in the Groningen building stock have been assigned to the typologies used by TNO.

TNO typology	EDB V5	Number of Buildings
“Niet gecategoriseerd” (Not categorised / Secondary)	Buildings with zero population (day and/or night)	108,315
“Boerderijen” (Farms)	WBB Barn WBH Barn with House WBC Barn Complex WBU Barn / Warehouse	5,908
“Hoogbouw” (High Rise Buildings)	Gutter height >10m	4,442
“Laagbouw voor 1940” (Low Rise Buildings before 1940)	Remaining year of construction before 1940	37,970
“Laagbouw na 1940” (Low Rise Buildings after 1940)	Remaining year of construction after 1940	100,539

Table 8.2 Assignment of EDB V5 typologies to the typologies used in the TNO Kalibratiestudie.

Although it has been recognized that secondary buildings representing ca. 40% of all buildings mainly consisting of sheds, garages and other small normally unoccupied buildings could also incur damage, they have been excluded from the forecast because damage data/reports are unavailable for such structures. A sensitivity analysis, with assumed fragility function like Low Rise buildings after 1940, shows that secondary buildings may perhaps add up to ca. 60% additional damage cases.

Due to the absence of damage observations in the earlier TNO studies, fragility function for Low Rise buildings after 1940 have also been assigned to all High-Rise buildings. This is believed to be a conservative assumption.

Earthquake catalogue of events

Finally, for the forecast several possible future realizations are needed that adequately represent the anticipated earthquake distribution both in terms of magnitude and location in the field.

These have been generated stochastically, using the hazard tool for the 24 Bcm depletion scenario. This is the same scenario as used for the full Hazard and risk assessment. In the Monte Carlo simulation process, repeated random sampling of a set of input distributions is used to build up a probabilistic output. So-called ‘synthetic earthquake catalogues’ (i.e. event locations and magnitudes for the period 2018-2022) are generated from the input probability distributions of total seismic moment, number of events and event epicentres. This forecast uses events between M_L 2.0 and 4.0.

Results

Figure 8.9 shows results of the DS1 damage forecast in the form of an F/N curve for the whole Groningen area.

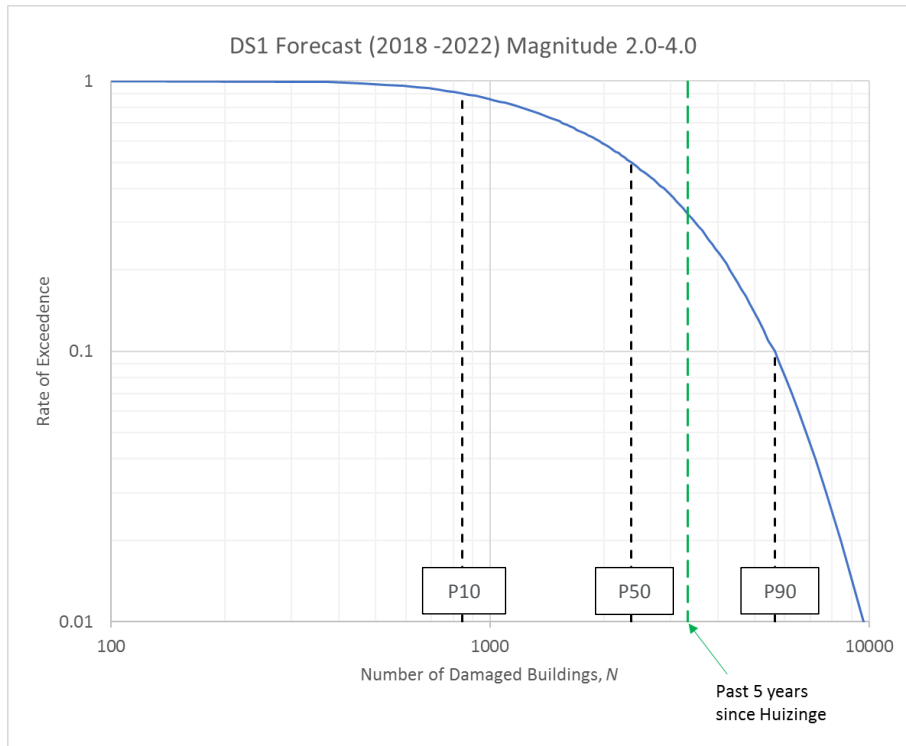


Figure 8.9 DS1 Forecast for period 2018-2022 based on the mean from the logic tree.

The median forecast (P50) is indicated as well as the 80% confidence interval (P10 to P90). Each building in the exposure area was assigned with relevant typology. It was assumed that any resulting building damage is repaired after the event and before the next one (instant repair). The green dashed line shows the same model applied to the past 5 years (since Huizinge earthquake).

In addition, sensitivities were run assuming all buildings are of weakest type as determined by TNO (i.e. farms) and assuming all buildings of the strongest type (i.e. Low Rise Buildings after 1940). Figure 8.10 shows the comparison of the central branch of the logic tree of the seismological model.

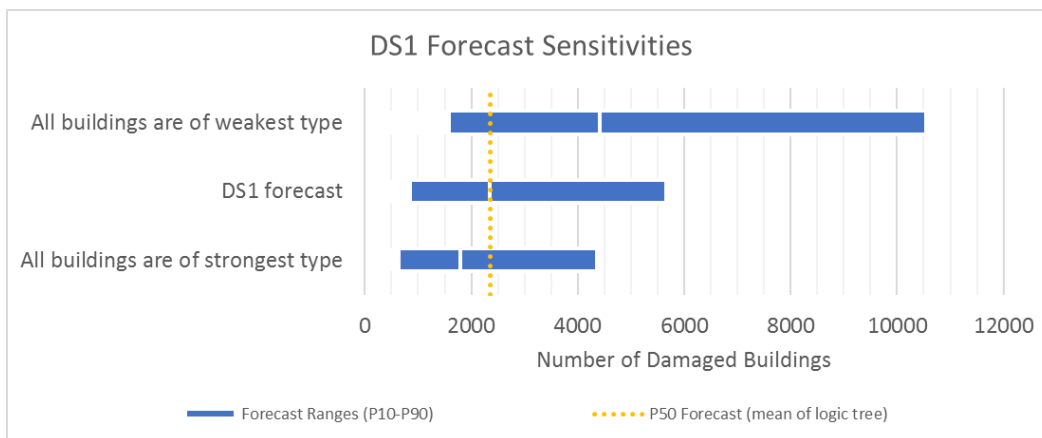


Figure 8.10 Tornado plot showing DS1 Forecast sensitivities for the central branch of the logic tree (seismological model)

The “schadedeel van de definitie van maatschappelijk risico” has been assessed for 7 communities. The DS1 F/N curves for maatschappelijk schaderisico for these seven communities are shown in figures 8.11 and 8.12.

DS1 F/N curves (2018-2022) Magnitude 2.0 -4.0

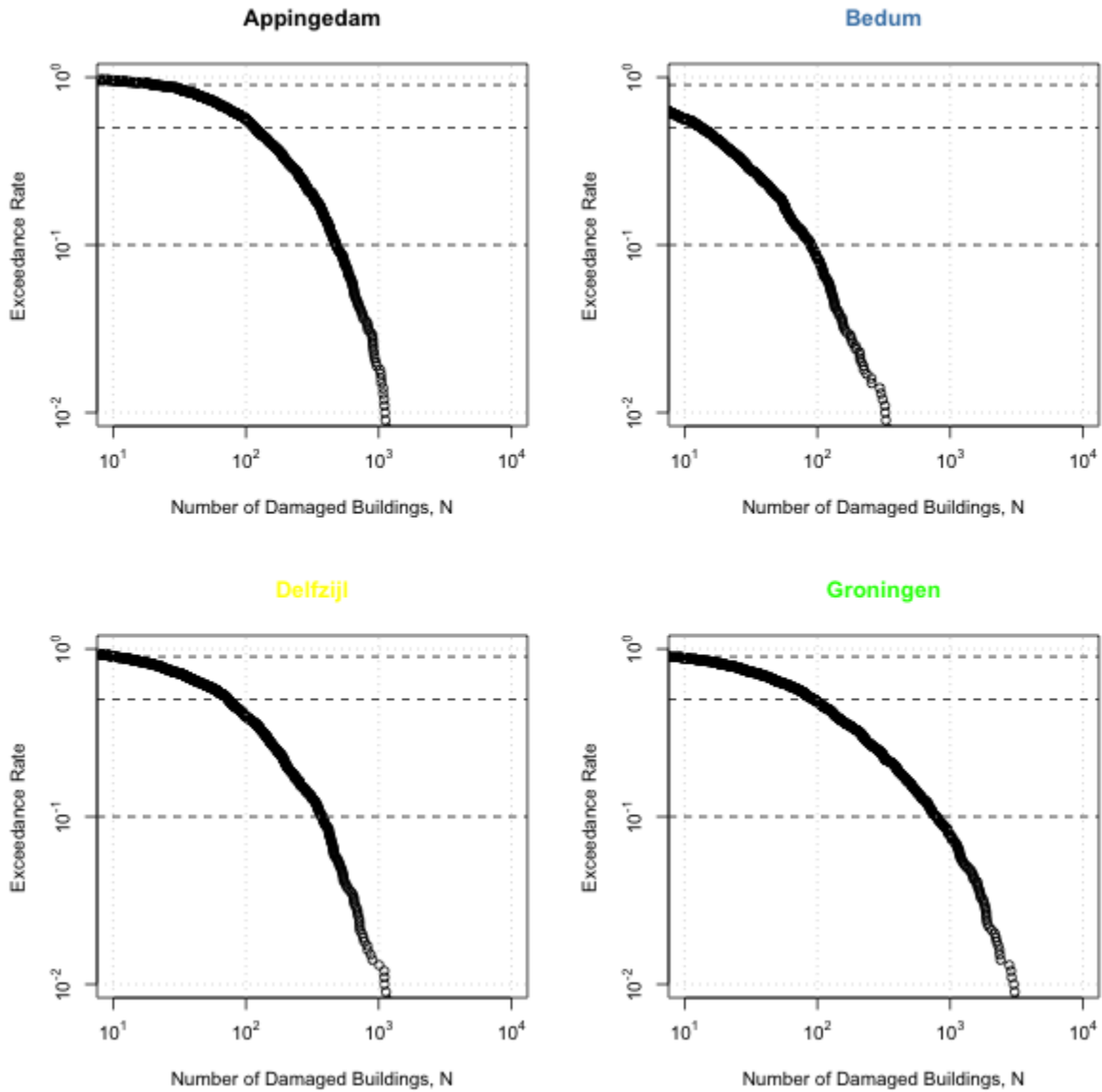


Figure 8.11 *Maatschappelijk risico for building damage DS1 (MR(S) for four communities; Appingedam, Bedum, Delfzijl and Groningen.*

DS1 F/N curves (2018-2022) Magnitude 2.0 -4.0

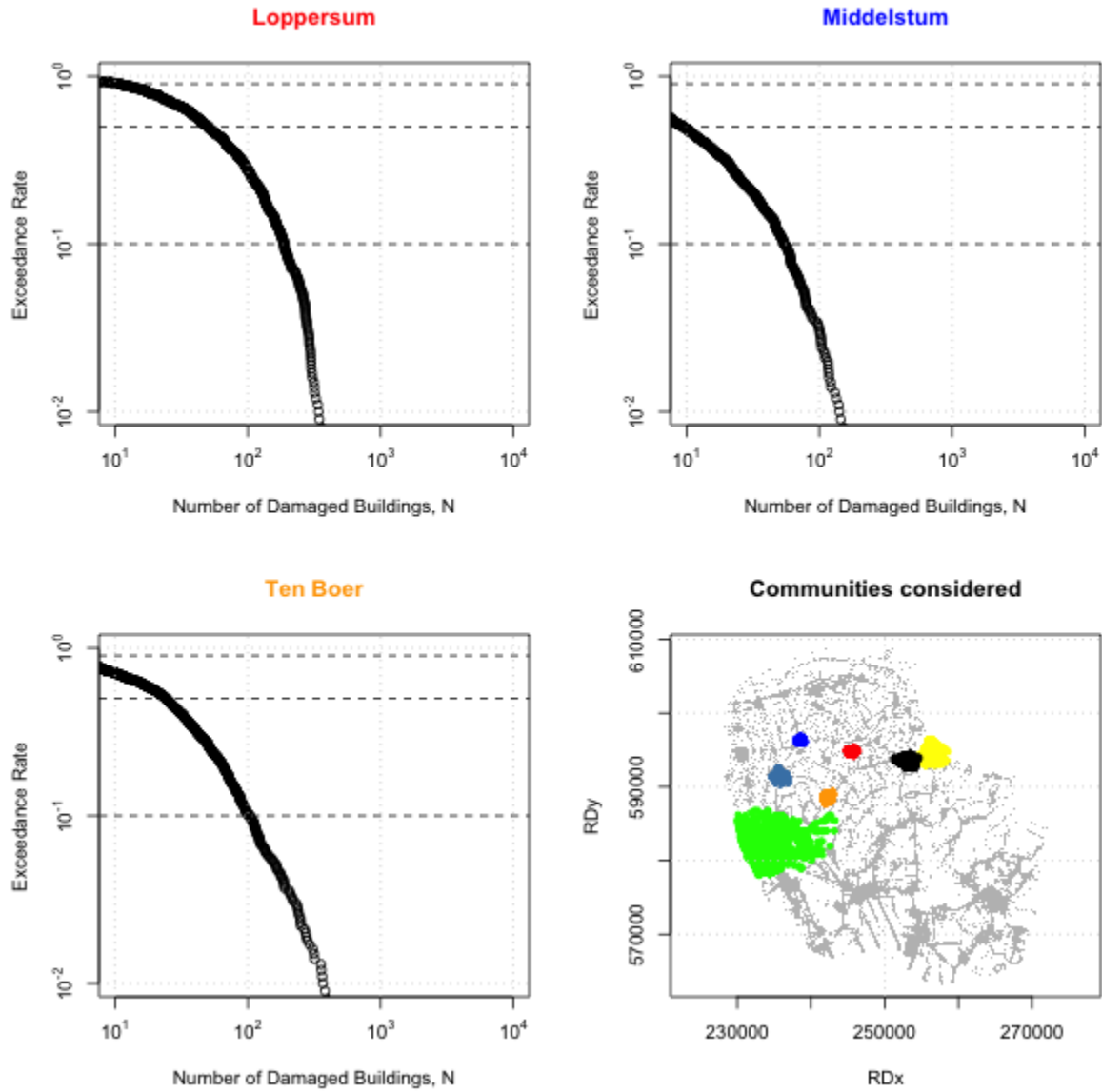


Figure 8.12 *Maatschappelijk risico for building damage DS1 (MR(S) for three communities; Loppersum, Middelstum and Ten Boer.*

Forecast based on Machine Learning Analysis

A complementary method to predict DS1 damage from induced earth-quakes has been developed based on analysis of historical claims received in the Groningen area since 2012. The central simple idea being that if a good statistical historical relationship can be developed between (e.g.) earthquake magnitude and the extent of damage claims, a comparison can be made with damage forecasts extrapolated from mechanical first principles (fragility curves). As also argued in the introduction above, however, pre-processing is needed to derive such a statistical relationship as the relationship between claims and (magnitude of) earthquakes is far from straight-forward; not all damage claims are related to earthquake damage, the amount of damage is not always proportional to earthquake magnitude and over time the number of claims varies not only as a function of the earthquake magnitude (i.e. a similar earthquake did result in quite a variable number of claims, unrelated to differences in number of houses potentially affected by the earthquake). All this required intensive analysis and pre-processing of the data before it could even be cautiously used for prediction and proper uncertainty assessment of the results. Outlined below is the approach that has been taken.

Definition of damage and data set used

The analytics study defines earthquake-related building damage as either new earthquake damage or a previous damage worsened by an earthquake. The damages were extracted from the claim's damage assessment result from the first-line assessor's building inspection (over 40,000 honoured claims).

Approach taken

The analytics scope of developing a DS1 forecast was divided into the following main work-streams:

1. Investigate the quality of previous damage assessment reports and incorporate learnings into the predictive model
2. Develop a building damage/claims predictive model using existing data sets
3. Applying above to generate the prediction based on 500 random earthquake catalogues from the Groningen earthquake hazard and risk model
4. Compare predictive model results to the results presented in previous section based on TNO Damage Calibration Study.

Damage assessment verification

The first work-stream (Damage Assessment Verification Study) is important to determine the accuracy level of the assessed damage category in previous damage assessments (basis for defining building damage in the model). A multi-functional verification study was carried out, with three independent damage assessors. Each independent damage assessors reviewed damage from 1,000 randomly-selected 1st-line damage assessment reports. The results were used to quantify the uncertainty in previous damage assessment results. Consequently, the assessed damage results were corrected to provide a better estimate of actual building damage. A few crude corrections were made as a first pass. First, the model filtered-out any assessed earthquake damage claim with less than 3mm/s historical ground motion as earthquake-related damage is considered unlikely based on guidelines established by the Dutch Building Research Foundation (SBR). Approximately 41% of damage assessment reports did not experience historical ground motion > 3mm/s. Second, it is realized that even above 3mm/s damage is yet certain. A part of that remaining set of claims will still be related to non-earthquake damage. However, that analysis is not yet fully finalized and, therefore, it is expected that the number predicted in the subsequent section will be on the high side. Future application of a correction factor to the damage building model results are likely to make the results more consistent with numbers derived from alternative methods (e.g. TNO kalibratiestudie).

Construction of a predictive model

The second work-stream (building damage/claims predictive model) started with fitting the model and then using 5-year earthquake catalogues to create 5-year building damage forecasts. The model fitting process included the evaluation of many variables including (but not limited to) building density around the earthquake, earthquake magnitude and location, estimated ground shaking at building, process/protocol changes, and media event frequency. A standard machine learning approach was followed where in and out sample test data were used to calibrate the model (illustrated in figure 8.13 below):

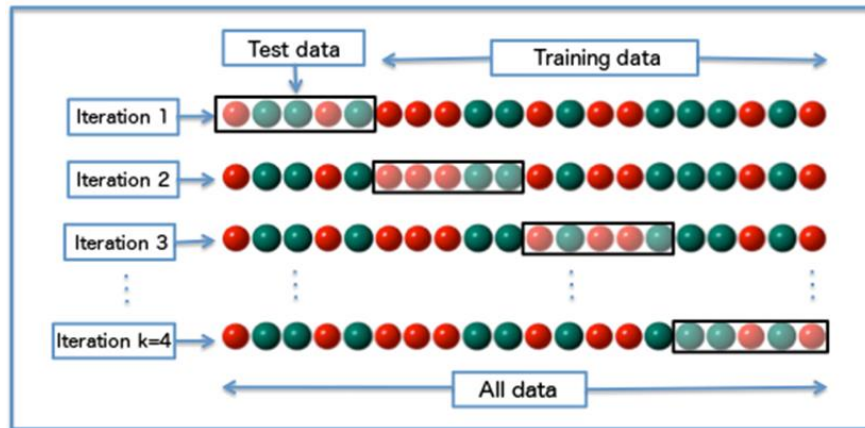


Figure 8.13 General machine learning approach.

The model produced acceptable results but large errors >50% were observed for some individual earthquakes as indicated in the cross-validation exercise. The damaged houses model showed no signs of bias, so the effects of under- and over-prediction will cancel out in the long term and the error in the predicted total number of damaged houses over 5 years should be small. A methodological uncertainty of +15%, -8% can be expected of the P50 values for the 5-year building damage forecasts.

Earthquake catalogue

To make a prediction of expected damage, first the number and magnitude of earthquakes will need to be predicted, as these are the two main parameters. This was done with the Groningen hazard model, in turn based on the latest as production scenario (24 Bcm) and production distribution. This model yields a probability distribution of expected number of earthquakes, per area and per magnitude class; 500 random earthquake catalogues were generated and from them the P10/P50/P90 scenarios for earthquake uncertainty were formulated.

Model results

Analytics modelling created a 5-year DS1 forecast for three earth-quake catalogues convoluted with the uncertainty in the machine-learning forecast itself (see figure 8.14). The 5-year building damage forecast ranges from some 24,000 houses to about 58,000 houses with a P50 of about 34,000. Key uncertainties in the building damage forecast are shown in the decision tree below in figure 8.14.

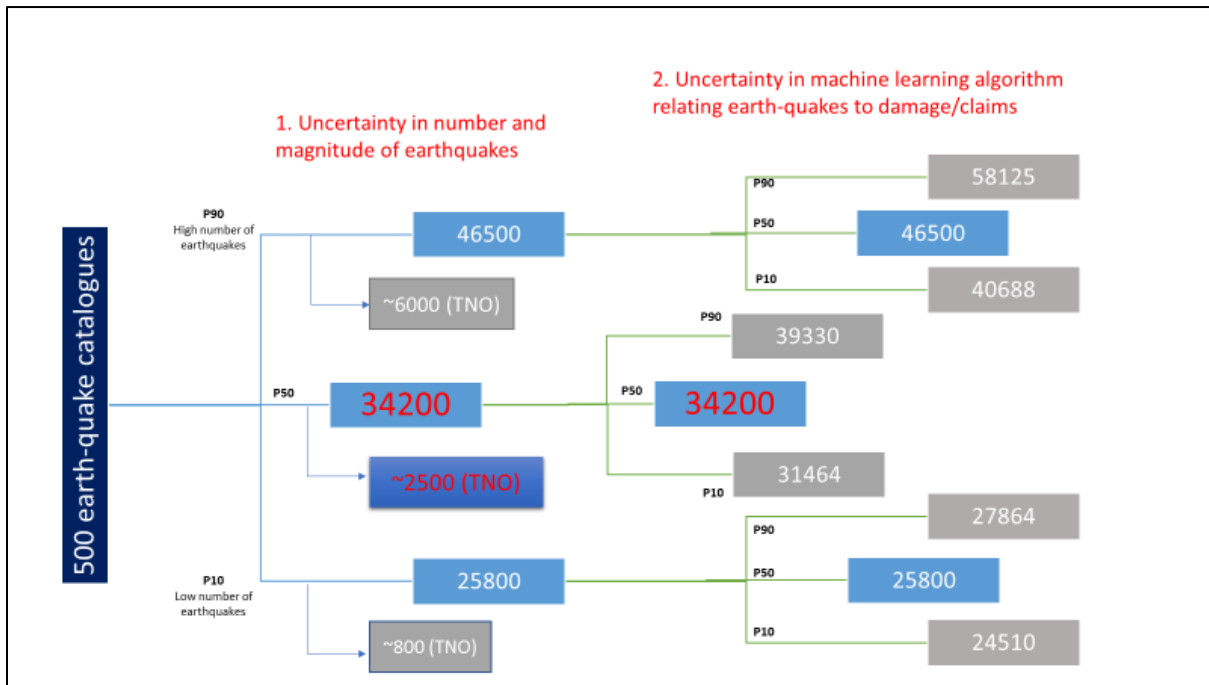


Figure 8.14 Overview of modelling results.

Comparison of results

The results from the analytics scope (machine learning methodology) are significantly higher than the empirical expectations (TNO Kalibratiestudie methodology) and points to a significant model discrepancy between the two methodologies. Since the EQ forecast uncertainty is captured by evaluating the P10/50/90 resulting forecasting building damage from 500 EQ catalogues and both models use the same building database, the most likely source of discrepancy between the two models is how the two methodologies define building damage. The TNO work defines DS1 damage as observed building damage for few historical earthquakes ($M > 2.5$) in the period up to and including the Aug 2012 Huizinge earthquake. On the other hand, the advanced analytics model (machine learning methodology) defines building damage based on the damage assessment result from claims submitted from the Aug 2012 to the end of 2016 for earthquakes $M > 1.5$.

To explain further, the periods of the two methodologies are uniquely different and the difference can be described as defining the damage basis before the 2012 Huizinge earthquake (TNO Kalibratiestudie methodology) and after the 2012 Huizinge earthquake (machine learning methodology). Prior to the 2012 Huizinge earthquake, less than 1200 total claims were received during the prior several years. In contrast, more than 1200 claims were received within the first two months following the 2012 Huizinge earthquake and the higher rate of claims continues today. The combination of high claims rates post 2012 Huizinge earthquake and evolving building damage knowledge (i.e., quality concerns/uncertainty of historical damage assessments) is the key source of uncertainty between the two methodologies. The combination of high claims rates post 2012 Huizinge earthquake and evolving building damage knowledge (i.e., quality concerns/uncertainty of historical damage assessments leading to assessed damage being greater than actual damage) will inherently lead to higher forecast values from the analytics models when compared to theoretical expectations (TNO Kalibratiestudie methodology).

These observed significant differences require further detailed analysis. Particularly completion of the historical damage assessment verification may provide additional clarity.

The conclusion remains that a damage claim does not necessarily correspond to actual earthquake damage and the relationship between seismic activity and damage claims appears to be more complex.

Forecast of DS 2 and DS3 based on Analytical Modelling and Experimental Tests

Fragility functions for DS2 and DS3 have been developed for each structural system identified in the exposure model using the extensive analytical modelling and experimental test campaign described in Chapter 7. F/N curves have been calculated with the Monte Carlo risk engine which show the annual frequency of exceedance (F) of different numbers of groups of buildings (N) which simultaneously reach DS2 or DS3. Figure 8.15 shows the F/N curve for the whole field, whilst those for each of the 7 communities (described further in Chapter 9) are shown in Figure 8.16.

Figure 8.15 shows that the annual frequency of exceedance of having anywhere 100 buildings simultaneously damaged to DS2 in a given earthquake is around 15%; in other words, the return period of having more than 100 buildings damaged to DS2 is around 7 years. This return period increases to around 20 years for a group of 1,000 buildings with DS2 damage. The return periods for DS3 are obviously higher.

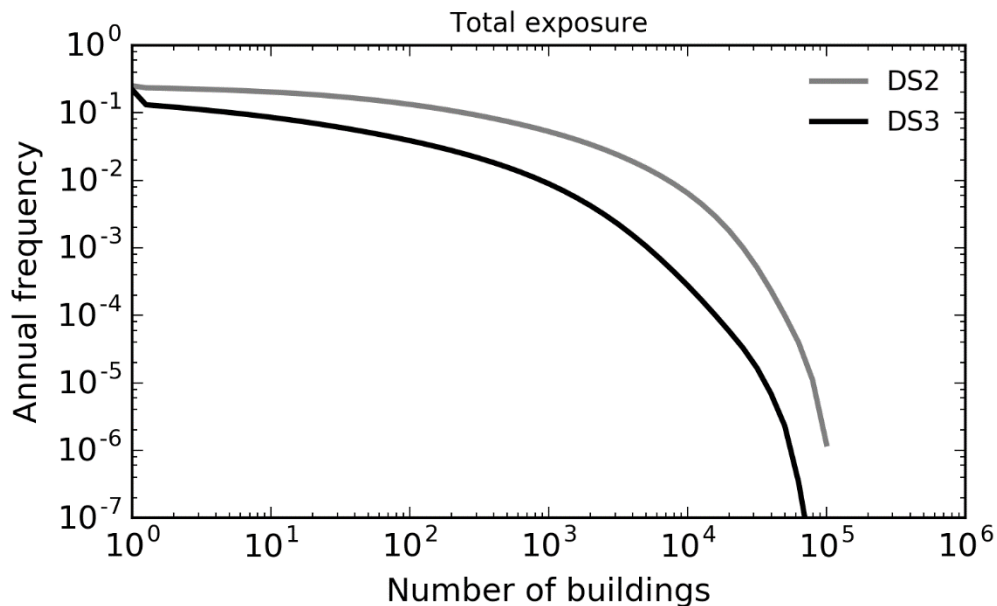


Figure 8.15 *Maatschappelijk risico for building damage DS2 and DS3 (MR(S)) for the whole field*

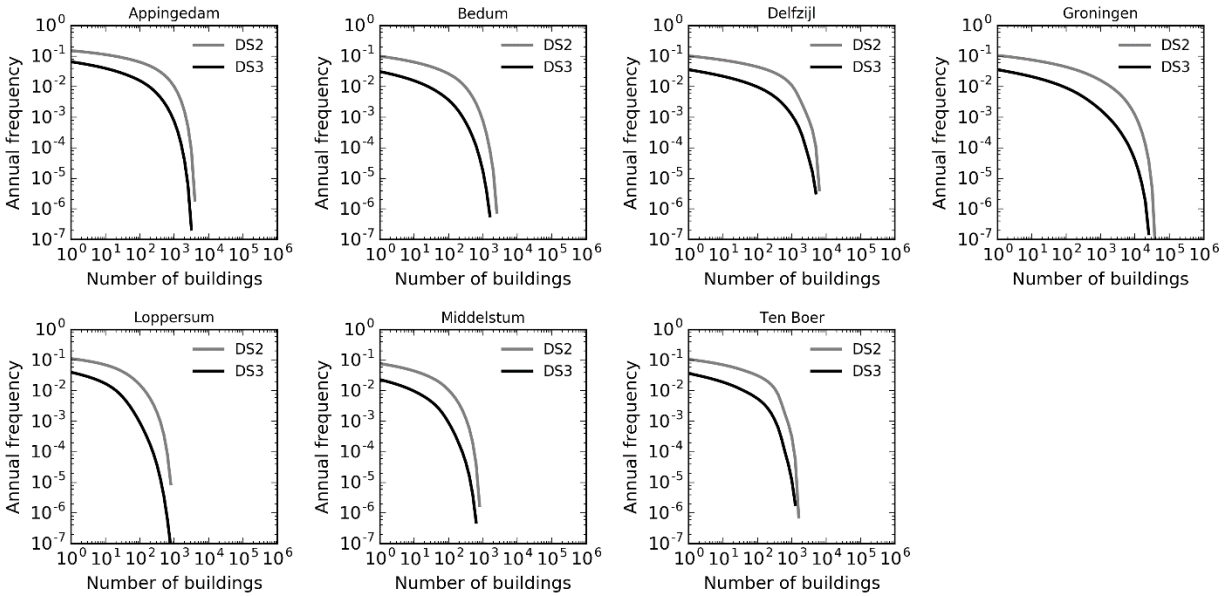


Figure 8.16 *Maatschappelijk risico for building damage DS2 and DS3 (MR(S)) for each of the 7 communities: Appingedam, Bedum, Delfzijl, Groningen, Loppersum, Middelstum, and Ten Boer*

Figure 8.17 provides some insight into the structural systems that are contributing most to the damage forecasts. These plots show the numbers of buildings exceeding a given average annual damage rate for DS2 and DS3. The interesting finding from these plots is that damage is not restricted to unreinforced masonry buildings (URM), but reinforced concrete buildings (RC2L, PC3L, PC4L) are also susceptible to damage.

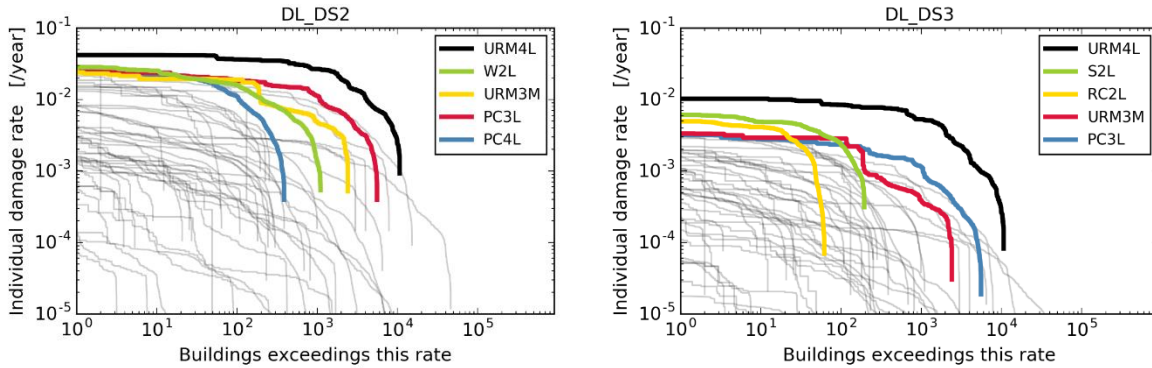


Figure 8.17 *Numbers of buildings exceeding a given average annual damage rate for DS2 and DS3, for the 24 bcm production scenario and 2018 – 2023 assessment period. The named structural systems denote the top-five ranked according to individual damage rate.*

References

1. Methodology Prognosis of Building Damage and Study and Data Acquisition Plan for Building Damage, Nederlandse Aardolie Maatschappij BV (Jan van Elk, Jeroen Uilenreef & Dirk Doornhof), 30 January 2017
2. NAM (Jeroen Uilenreef and Jan van Elk), Technical Addendum to the Winningsplan Groningen 2016, Production, Subsidence, Induced Earthquakes and Seismic Hazard and Risk Assessment in the Groningen Field, PART III – Hazard, April 2016.
3. NAM (Jeroen Uilenreef and Jan van Elk), Technical Addendum to the Winningsplan Groningen 2016, Production, Subsidence, Induced Earthquakes and Seismic Hazard and Risk Assessment in the Groningen Field, PART IV – Risk, April 2016.
4. Bourne, S.J., S.J. Oates, J.J. Bommer, B. Dost, J. van Elk, D. Doornhof, A Monte Carlo method for probabilistic hazard assessment of induced seismicity due to conventional natural gas production, February 13, 2015, BSSA-S-14-00354.
5. TNO-034-DTM-2009-04435, Kalibratiestudie schade door aardbevingen, 11 November 2009
6. NAM (Jeroen Uilenreef and Jan van Elk), Technical Addendum to the Winningsplan Groningen 2016, Production, Subsidence, Induced Earthquakes and Seismic Hazard and Risk Assessment in the Groningen Field, PART V - Damage and Appendices, April 2016.
7. European Seismological Commission (G. Grünthal), European Macroseismic Scale 1998, EMS-98, 1998
8. European Commission Joint Research Centre (JRC), Field Manual for post-earthquake damage and safety assessment and short term countermeasures (AeDEA), 2007
9. TNO 2012 R10227, Analyse van de gevolgen van de aardbeving te Huizinge d.d. 16 augustus 2012, 13 februari 2013
10. J.J. Bommer et al., Berlin HFR Project, Engineering Geology 83 P 287–306, 2006
11. Julian J Bommer, Peter J Stafford & Michail Ntinalexis, Empirical Ground-Motion Prediction Equations for Peak Ground Velocity from Small-Magnitude Earthquakes in the Groningen Field Using Multiple Definitions of the Horizontal Component of Motion, November 2016
12. FEMA, Multi-hazard Loss Estimation Methodology Earthquake Model HAZUS MR4 technical manual, 2003
13. Baker, J. W., "Efficient analytical fragility function fitting using dynamic structural analysis." Earthquake Spectra, 2013
14. Okada, S. and Takai, Classifications of structural types and damage patterns of buildings for earthquake field investigation, Journal of Structural and Construction Engineering (Transactions of AIJ) No. 524, October 1999
15. Hancilar et al., Empirical fragility assessment after the January 12, 2010 Haiti earthquake, Risk Analysis VII: Eighth international conference on simulation in risk analysis and hazard mitigation. WitPress ISBN 978-1-84564-620-2. P 353-365 Conference Paper · September 2012.
16. Gehl et al., Vector-valued fragility functions for seismic risk evaluation, Bul. Earthquake Eng. 11:365–384, 2013
17. Arup 229746_052.0_AUX2008, Exposure database V5 Extract Note, 27 September 2017

9 Risk and Personal Safety Assessment

Risk Metrics

The results from the probabilistic hazard and risk analysis (PHRA) are summarised via risk metrics, which are related to the annualised probability of fatality for an individual person or for groups of people, taken as an average across the forecast period of the PHRA. These risk metrics - “Inside Local Personal Risk”, “Outside Local Personal Risk” and “Maatschappelijk Veiligheidsrisico”¹⁰ – are defined below. “Inside Local Personal Risk” and “Outside Local Personal Risk” are individual risk metrics (related to probability of fatality for an individual continuously present in or near the building) that have been combined into a single “Local Personal Risk” metric, whereas the remaining metric is a measure of aggregate risk (related to probability of fatality for multiple people or for groups of people).

When measuring risk, it is important to select a risk metric that is appropriate given the purpose of the risk measurement. In many cases, there is more than one option available as to which metric to use. An advisory committee, Commissie Meijdam, was established in early 2015 to advise on risk policy related to Groningen earthquakes (Ref. 1, 2 and 3), including the selection of risk metrics. In December 2015, the Commissie Meijdam shared its third and final advice with the Minister of Economic Affairs. The selection of risk metrics for this PHRA reflects the final advice published by Commissie Meijdam.

The following table contains a summary of the risk metrics used in this PHRA along with the purpose of the risk metric:

Type of Metric	Risk Metric	Purpose(s)
Individual	Inside Local Personal Risk* (ILPR)	Individual risk metrics to measure fatality risk due to collapse of buildings and their non-structural elements both inside (ILPR) and outside (OLPR) the building, relative to the norm of 10^{-5} overall individual risk. Check if any buildings have Local Personal Risk above 10^{-4} (high priority for action).
	Outside Local Personal Risk (OLPR)	
	Local Personal Risk (LPR)	
Aggregate	Maatschappelijk Risico	Input towards prioritisation of buildings/non-structural elements (which don't comply with individual risk norm) within structural upgrading program. Provide risk insights for prioritisation of communities. Consider additional measures (where “reasonable”) beyond reducing individual risk to below 10^{-5}

Table 1.1 Overview of Risk Metric used for the probabilistic seismic risk assessment for induced seismicity in Groningen.

*For clarity, Dutch translations of these metrics in the final Commissie Meijdam advice are:

- Local Personal Risk = “Plaatsgebonden Risico”
- Outside Local Personal Risk¹¹ = “Objectgebonden Individueel Aardbevingsrisico”
- “Maatschappelijk Veiligheidsrisico” was not translated.

¹⁰ Both the terms “societal risk” and “group risk” have been used as translations of the Dutch term “groepsrisico”. In this document, we have therefore not translated the newly introduced term “Maatschappelijk Veiligheidsrisico” as this could lead to confusion.

¹¹ Outside local personal risk in this report does not only refer to “falling objects”, but also the risk outside due to collapse of parts or all of the structure itself.

Inside Local Personal Risk

“Local Personal Risk” (LPR) is generally defined as the annual probability of fatality for a fictional person, who is continuously present without protection at a specific at-risk location. For Groningen earthquakes, LPR is defined as follows: *“the probability of death of a fictional person who is permanently in or near a building”*. “Inside LPR” (ILPR) focuses on the risk to people inside of buildings, and assumes that the fictional person is present inside the building 100% of the time, and the location of the person is uniformly and randomly distributed inside the building i.e. if 10% of the building collapses there is a 10% probability that the fictional person will be in the collapsed part of the building. In this PHRA, ILPR is used to measure the fatality risk to people inside the building from building collapse. The mean value of the ILPR is the primary metric that has been used in previous risk assessments to compare against the 10^{-5} individual risk norm (as recommended by Commissie Meijdam and accepted by the Ministry of Economic Affairs, the fatality risk for a person inside a building should be less than 10^{-5} per year).

Outside Local Personal Risk

The Dutch term for Outside Local Personal Risk (OLPR) is “Objectgebonden Individueel Aardbevingsrisico”, OIA. Outside Local Personal Risk (OLPR) is used to measure the contribution to individual risk from both non-structural elements of buildings, such as chimneys, parapets and gables, as well as the collapse of the building itself, which poses a potential risk to people outside of buildings. In this context, OLPR is defined as the annual probability of fatality for a “representative person” that is present outside and within 5 m of the building 100% of the time.

Local Personal Risk

The Inside Local Personal Risk and Outside Local Personal Risk are aggregated to Local Personal Risk (LPR) assuming a *fictional person* is 99% of the time inside a building and 1% of the time outside the building, but in the direct vicinity of the building. Whereas LPR is normally calculated for a specific building, it can also be averaged across a number of buildings within a geographical area, such as within a map grid cell. In this report, the averaging of LPR uses weighting based on the estimated day/night population of each building.

Maatschappelijk Veiligheidsrisico

Aggregated risk metrics are available and are commonly applied for the evaluation and management of technical risks (e.g. chemical plant explosions) and natural risks (e.g. flooding) (Ref. 4). These group risk (GR) metrics were developed based on the concept that society has lower tolerance to accidents involving multiple fatalities in a single event than to multiple events involving single fatalities. However, there is no wide acceptance to use aggregate risk metrics. In its first advisory report, the committee Meijdam (Commissie-Meijdam) concluded: “The committee advises against the use of group risk on the grounds that this metric has not been given legal status in any safety domain, due to problems with the computability and the absence of any clear norms.”¹² (Ref. 1). The third and final advisory report from Commissie-Meijdam (Eindadvies Handlingsperspectief voor Groningen Adviescommissie ‘Omgaan met risico’s van geïnduceerde aardbevingen’) (Ref. 3) introduced the new aggregated risk metric of Maatschappelijk Veiligheidsrisico (MVR).

For Winningsplan 2016, Maatschappelijk Veiligheidsrisico was calculated for seven selected communities. The definition of the communities was based on the wijk- en buurten definition by CBS (Ref. 5). Maatschappelijk Veiligheidsrisico is an assessment of the frequency (f) with which defined numbers of fatalities (N) occur due to earthquakes, with an offset for “basic safety” (assuming everyone exposed to the earthquake risk is at uncorrelated

¹² Original text in Dutch: “Ook het gebruik van groepsrisico’s raadt de commissie af, omdat deze norm nergens een wettelijke status heeft gekregen, onder andere vanwege problemen met de berekenbaarheid.” (Ref. 2).

10^{-5} individual risk). The calculation procedure for Maatschappelijk Veiligheidsrisico is fully described in the final Commissie Meijdam advice, appendix 2.

Probabilistic Risk Assessment

In this section, an assessment is presented of the risk associated with the partial or full collapse of buildings and their non-structural elements. This includes different collapse states ranging from collapse of high-risk building elements (e.g. chimneys), to collapse of gable walls, to full collapse of the building.

While the Hazard Assessments issued by NAM have all been fully probabilistic since the Winningsplan of November 2013 (Ref. 6), the initial risk assessments were scenario based. In May 2015, NAM issued for the first time a fully probabilistic hazard and risk assessment (PHRA) (Ref. 7). At that time risk results were qualitative only, as these had not yet been fully calibrated to sufficient data obtained for the site-specific conditions of the Groningen field. The interim update of the hazard and risk assessment in November 2015, provided, for the first time, a quantified assessment of seismic risk.

Local Personal Risk (LPR)

With the aforementioned assumptions on the probability of the presence of people inside and outside buildings, the number of people exceeding a Local Personal Risk (LPR) can be estimated. The solid black line in figures 9.1 to 9.2 shows the number of people exposed to a certain level of local personal risk. During the 5-year period from 2018 to 2022, there are no buildings where the occupants are exposed to a mean local personal risk larger than 10^{-4} /year. People in and around of some 3,000 buildings are exposed to a mean local personal risk exceeding 10^{-5} /year in the period 2018 to 2022.

The distribution of buildings with a mean collapse rate (note this figure is not LPR as it does not yet take into account the likelihood of fatality if collapse occurs) over the different building typologies is shown in figure 9.3. These are predominantly terraced buildings with large openings at the ground floor, precast reinforced concrete buildings and barns. These estimates of buildings and people exposed to risk are aggregates over the total Groningen gas field area.

To obtain a sense of the areal spread of the higher risk buildings, a map of the LPR for individual buildings was prepared (Fig. 9.5). Each of the approximately 160,000 occupied buildings within the exposure area is represented by a single coloured dot. These are plotted in order of increasing risk so that the largest risks plot on top. The grey dots denote risks smaller than 10^{-5} /year. The coloured dots in the map of figure 9.5 shows all buildings with risk larger than 10^{-5} /year. These are the buildings that do not meet the norm of 10^{-5} /year and therefore need strengthening within the prescribed period of five years. As this is the result of a probabilistic assessment, it must be validated through inspections of buildings and seismic assessment against the NPR. A small number of buildings in the north-east of the city of Groningen do not meet the 10^{-5} /year norm in this assessment. These are primarily URM buildings with three storeys and an attic. The risk for these buildings is associated with the partial collapse of gables and chimneys.

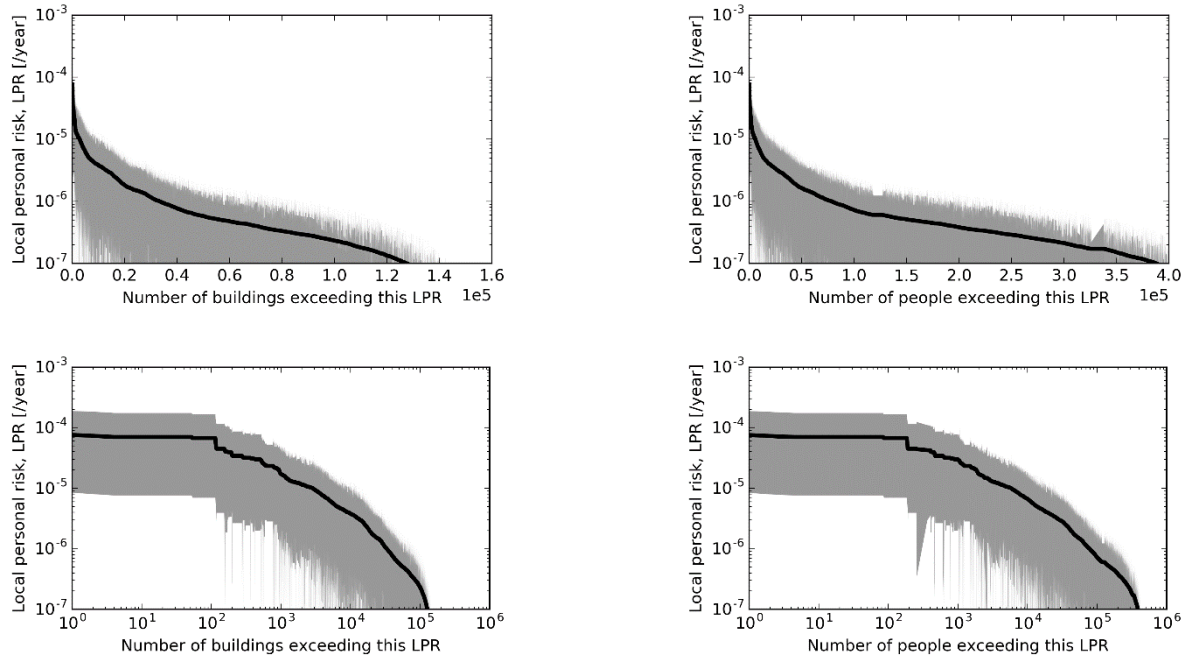


Figure 9.1 Number of buildings and people exceeding a given local personal risk shown on (top) a linear scale and (bottom) a log scale for the 24 bcm production scenario and the 2018-2023 assessment period.

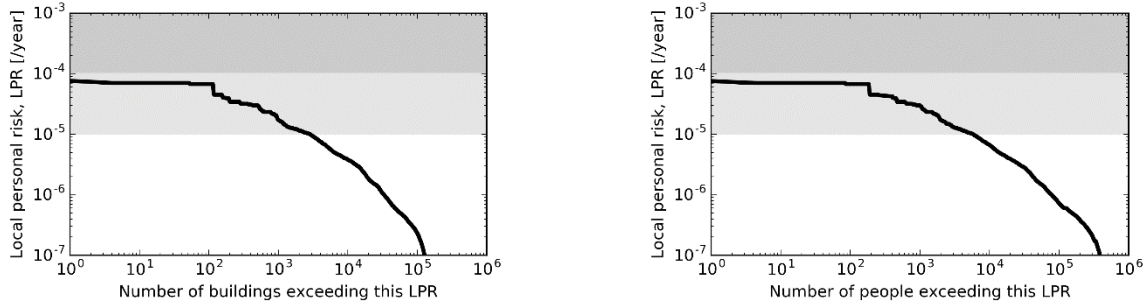


Figure 9.2 As Figure 9.1, except for just the mean local personal risk. The grey areas indicate the norm advised by the Committee Meijdam.

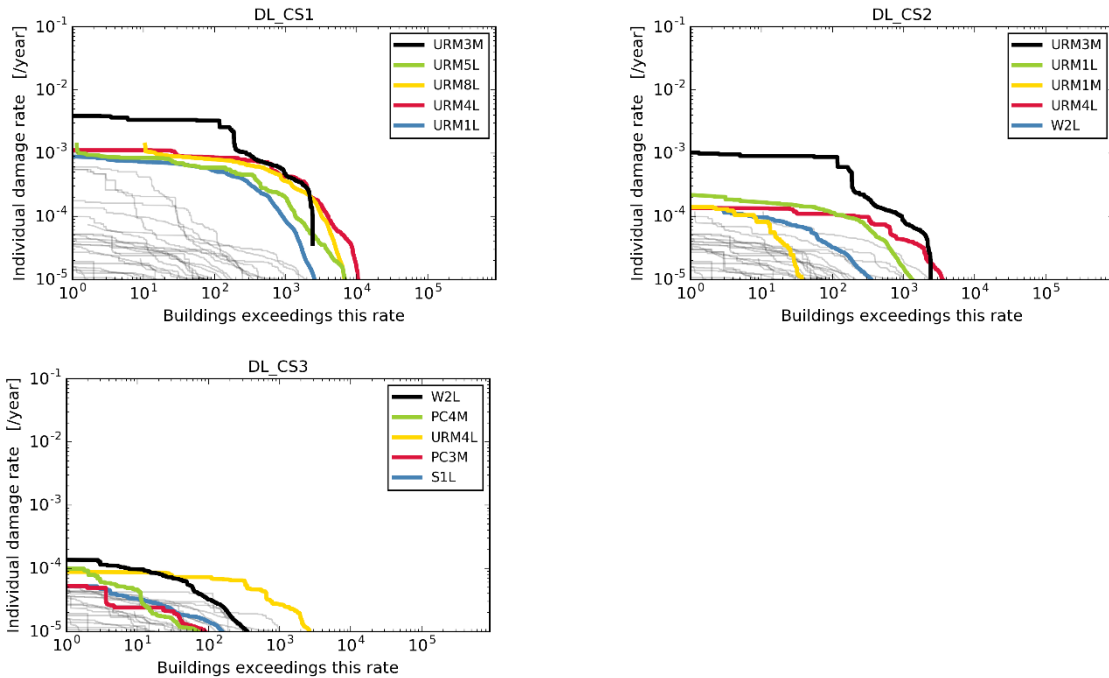


Figure 9.3 Numbers of buildings exceeding a given average annual collapse rate for CS1, CS, and CS3, for the 24 bcm production scenario and 2018 – 2023 assessment period. The named structural systems denote the top-five ranked according to the number of buildings with a collapse rate of at least 10^{-5} /year.

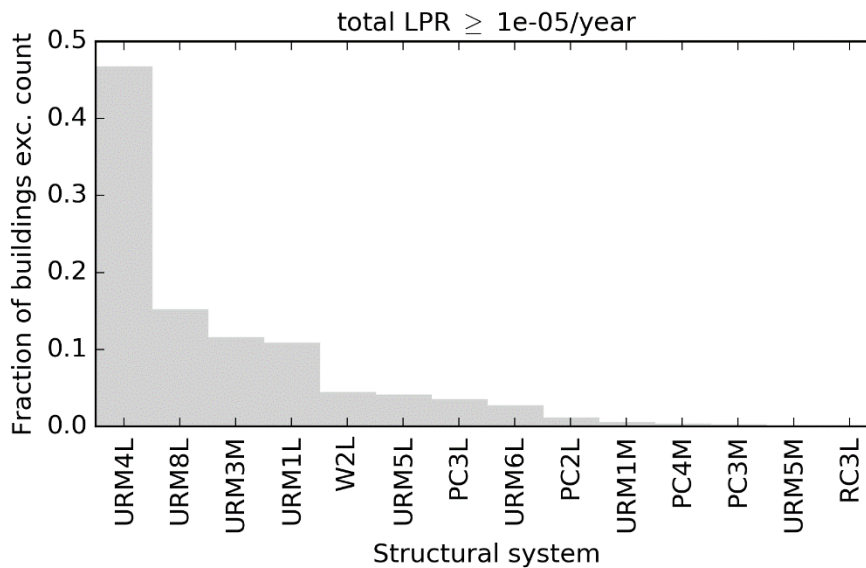


Figure 9.4 Breakdown of the structural systems contributing to LPR over the 10^{-5} /year threshold for the period 2018 – 2023 with a 24BCM p.a. production scenario.

$10^{-5} < \text{ILPR} < 10^{-4}$
(buildings c. 2,800)

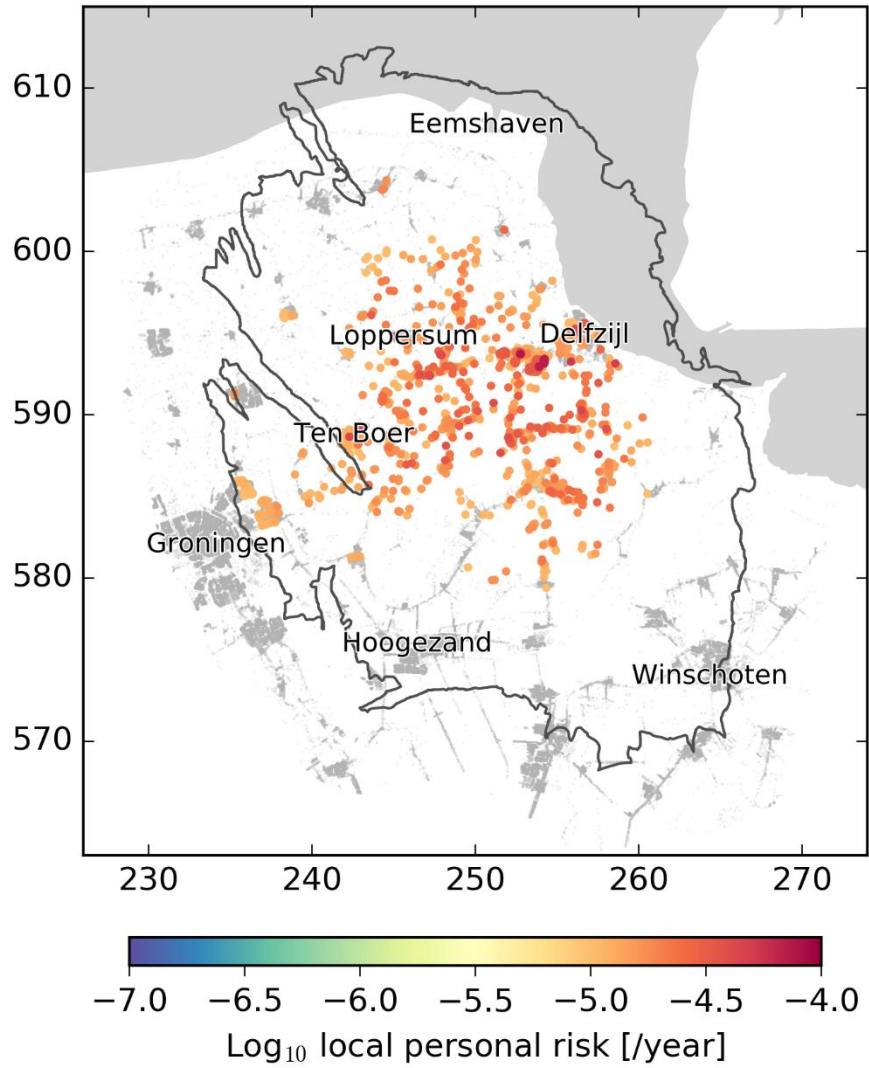


Figure 9.5

Map indicating individual building with Local Personal Risk exceeding 10^{-5} /year for the 5-year assessment period 2018 to 2023 under the 24 Bcm production scenario.

Disaggregation of Local Personal Risk (LPR)

A disaggregation of contributions to the base-case LPR was performed for magnitude, distance from the epicentre, the ground motion variability measure ϵ , and spectral acceleration causing building collapse.

Figure 9.6 shows the results for (URM4L) in the Loppersum area and the results for (URM3M) in Loppersum and Groningen city, respectively.

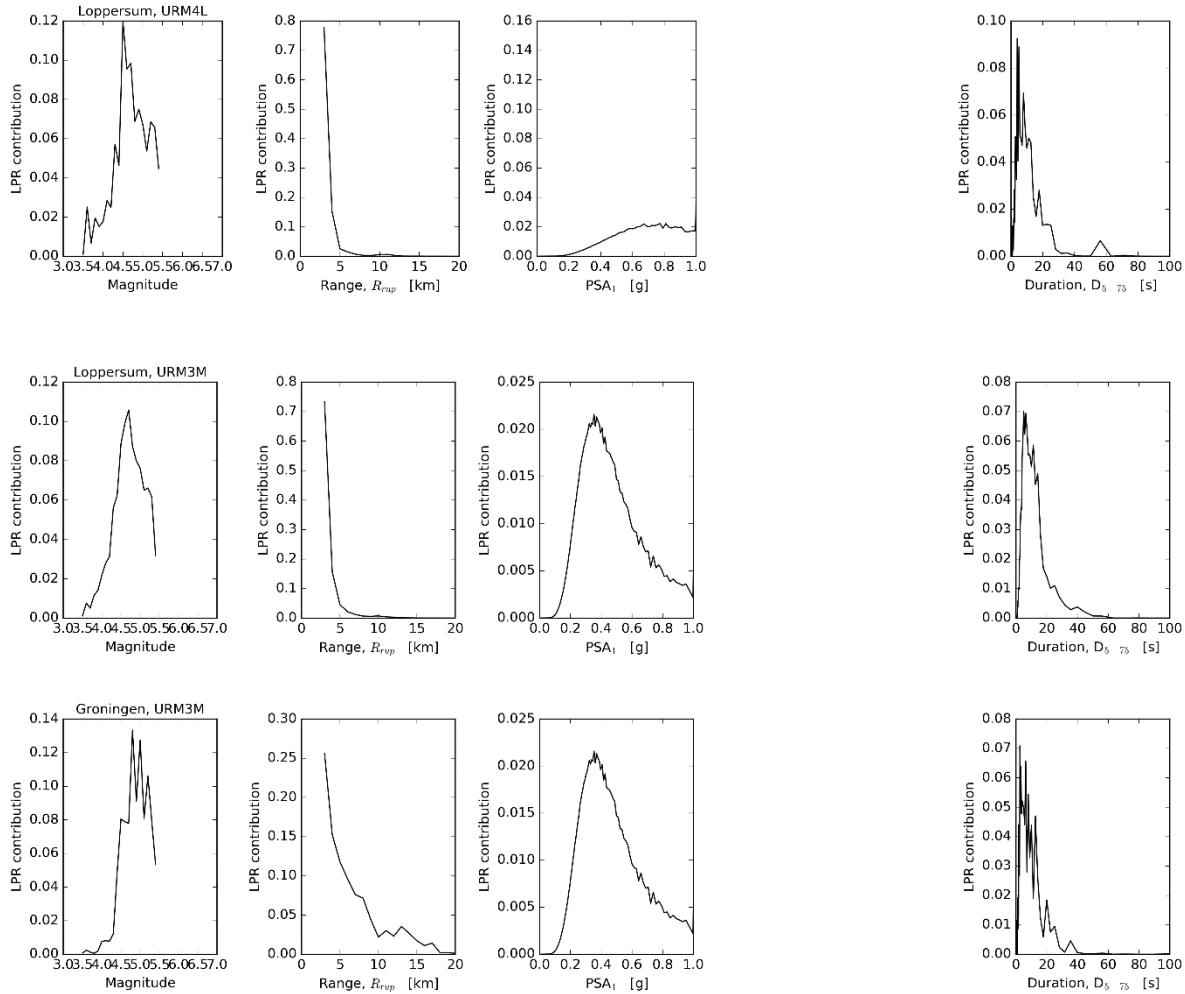


Figure 9.6 The fractional contribution to LPR for the URM4L building typology in Loppersum (top row) and the URM3M typology for Loppersum and Groningen city centre (bottom rows). This result was obtained for the 2018 to 2023 assessment period under the 24 bcm/year production scenario. Fluctuations between neighbouring points are due to finite sampling effects of the Monte Carlo procedure; nonetheless the underlying trends are clear.

As for hazard, earthquakes in the Loppersum area (i.e. at epicentral distances less than 5 km) contribute most to the risk for this area.

The areal representation of the risk disaggregation is shown in figures 9.7, 9.8 and 9.9. For areas with low risk (like the South East of the field) the risk disaggregation in this figure is less reliable due to finite sampling effects of the Monte Carlo process for these especially small values of LPR.

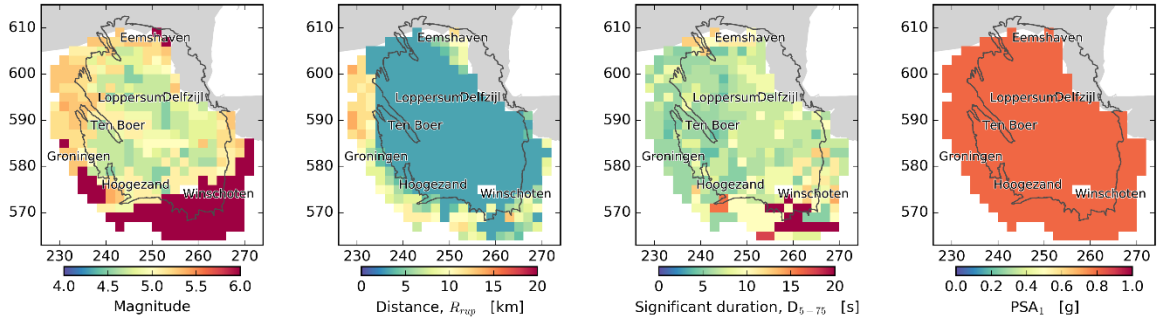


Figure 9.7 Risk disaggregation maps for the URM4L structural system showing the modal contribution to ILPR at each map location for the period 2018 to 2023 under the 24 bcm/year production scenario.

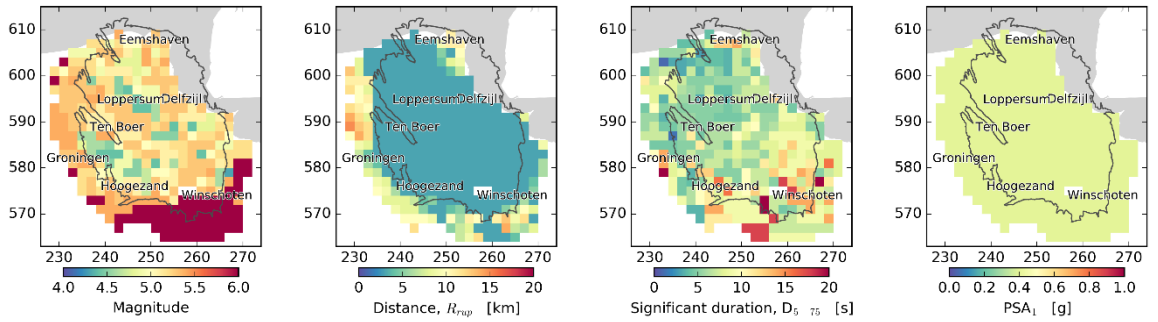


Figure 9.8 Same as figure 9.7 for the URM8L structural system

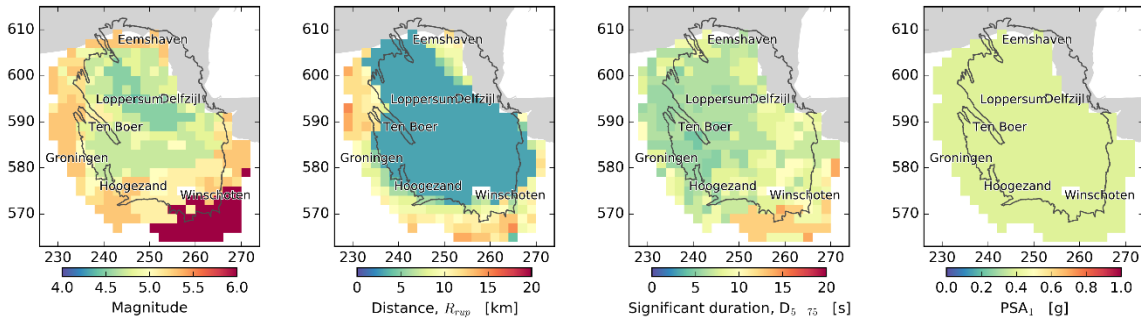


Figure 9.9 Same as figure 9.7 for the URM3M structural system

Sensitivity to epistemic uncertainties

The sensitivity of the assessed seismic risk to the epistemic uncertainties identified on the logic tree (fig. 9.10) is shown in figure 9.11. Four key factors have been identified: the seismicity model, ground motion prediction equation, building fragility model, and the consequence model. The extent of each grey bar denotes the average value of the risk metric for the subset of the logic tree where the given factor is constrained to the lower branch (lower limit) and then the upper branch (upper limit). Results are shown for 2018-2022 under the 24 bcm production scenario for two different risk metrics: (top figure) the mean local personal risk, computed as the weighted mean of the logic tree averaged over all populated buildings, (bottom figure) the number of populated buildings with a mean local personal risk exceeding 10^{-5} /year. Other assessment periods and production scenarios yield similar results.

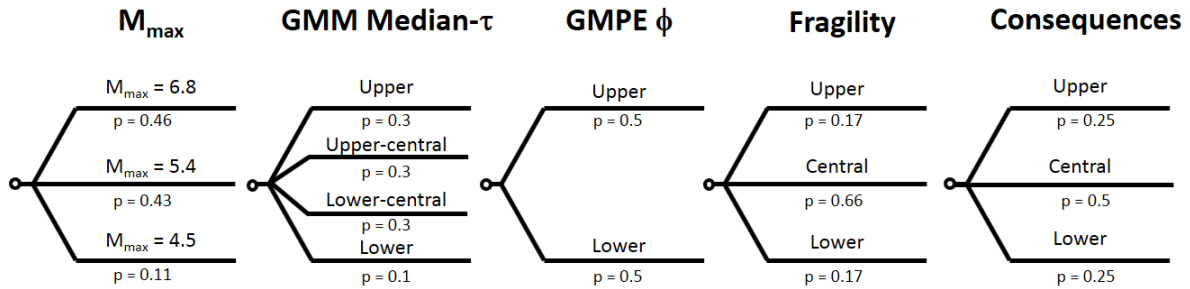


Figure 9.10 Logic tree for Risk.

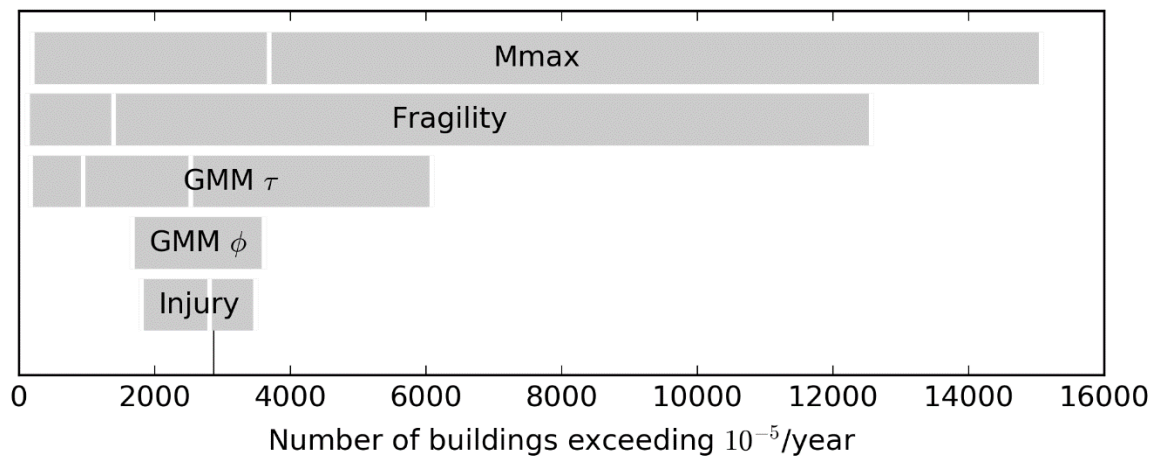
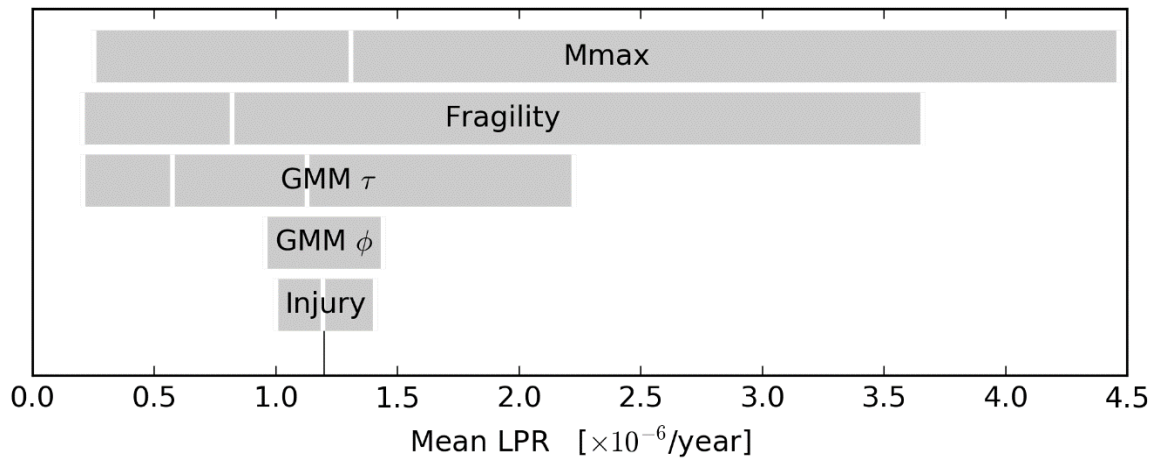


Figure 9.11 The sensitivity of the assessed seismic risk to the epistemic uncertainties identified on the logic tree.

Maatschappelijk veiligheidsrisico

The Maatschappelijk Veiligheidsrisico has been calculated for seven communities and for the area of the Groningen field (Fig. 9.12).

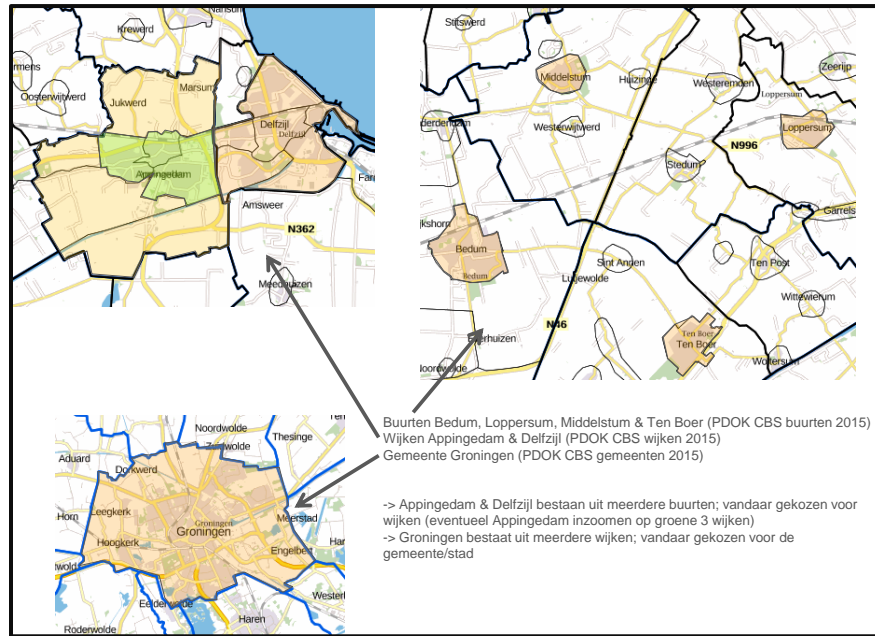


Figure 9.12 Extract from the advice by Ministry of Economic Affairs detailing the seven communities selected for calculation of Maatschappelijk Veiligheidsrisico.

This selection was based on the CBS buurtenkaart (Ref. 5). Table 9.1 shows has the seven selected communities are composed of several neighbourhods in the CBS buurtenkaart.

Community	Attribute Value	CBS Neighborhood/District
Appingedam	Appingedam-Centrum Appingedam-West Appingedam-Oost	Appingedam-Centrum Appingedam-West Appingedam-Oost
Delfzijl	Delfzijl-Centrum Delfzijl-Farmsum Delfzijl-Noord Delfzijl-West Delfzijl-Fivelzigt Delfzijl-Tuikwerd	Delfzijl-Centrum Farmsum Delfzijl-Noord Delfzijl-West Fivelzigt Tuikwerd
Groningen	Groningen-Binnenstad Groningen-Schilders- en Zeeheldenwijk Groningen-Oranjewijk Groningen-Korrewegwijk	Wijk 00 Binnenstad Wijk 01 Schilders- en Zeeheldenwijk Wijk 02 Oranjewijk Wijk 03 Korrewegwijk
	Groningen-Oosterparkwijk Groningen-Oosterpoortwijk Groningen-Herewegwijk en Helpman Groningen-Stadsparkwijk Groningen-Hoogkerk Groningen-Noorddijk	Wijk 04 Oosterparkwijk Wijk 05 Oosterpoortwijk Wijk 06 Herewegwijk en Helpman Wijk 07 Stadsparkwijk Wijk 08 Hoogkerk Wijk 09 Noorddijk
Bedum	Bedum	Bedum
Loppersum	Loppersum	Loppersum
Ten Boer	Ten Boer	Ten Boer
Middelstum	Middelstum	Middelstum

Table 9.1 The seven identified communities consist of one of more neighbourhods as defines in wijk- en buurten register by CBS. Community "gemeente Groningen" consists of 10 neighbourhods.

Reliable assessment of the contribution of the collapse of groups of buildings to Maatschappelijk Veiligheidsrisico requires detailed representation of the spatial correlations in the earthquake ground motions. In the current assessment, spatial correlation is represented as strong within each near-surface amplification zone up to a distance of 3 to 5 km with no correlation beyond this distance.

The Maatschappelijk Veiligheidsrisico assessments for all seven communities are shown in figure 9.13.

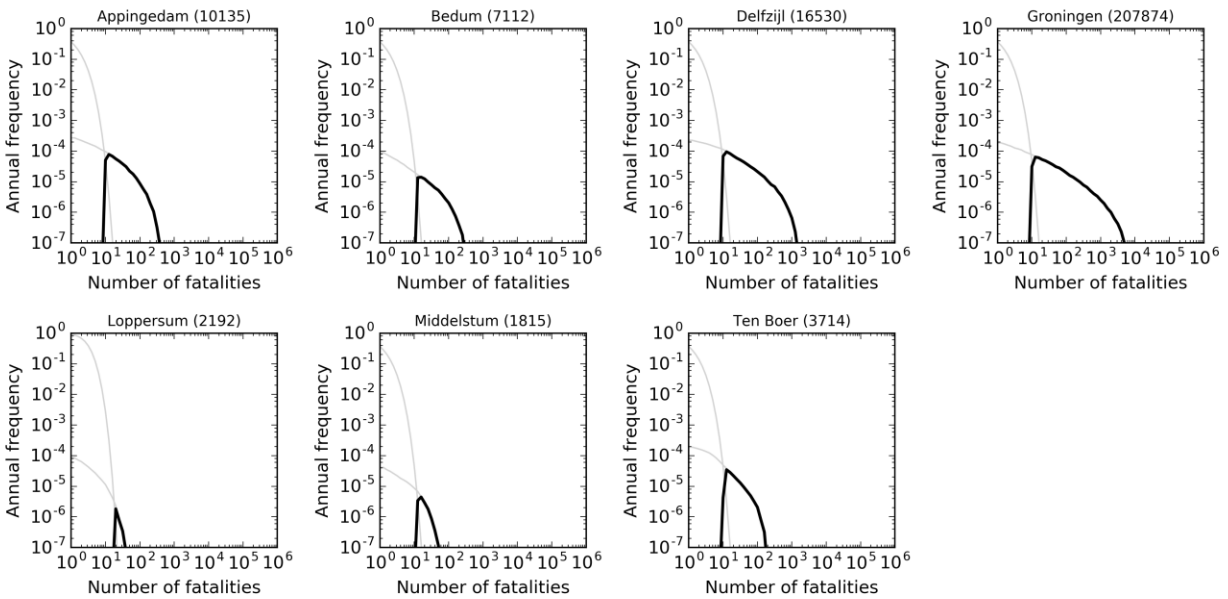


Figure 9.13 *Maatschappelijk Veiligheidsrisico based on the mean of the logic tree, for the seven communities (in alphabetical order) for a production scenario of 24 Bcm/year. Numbers after each community name denote the average day-night inside total population for that community.*

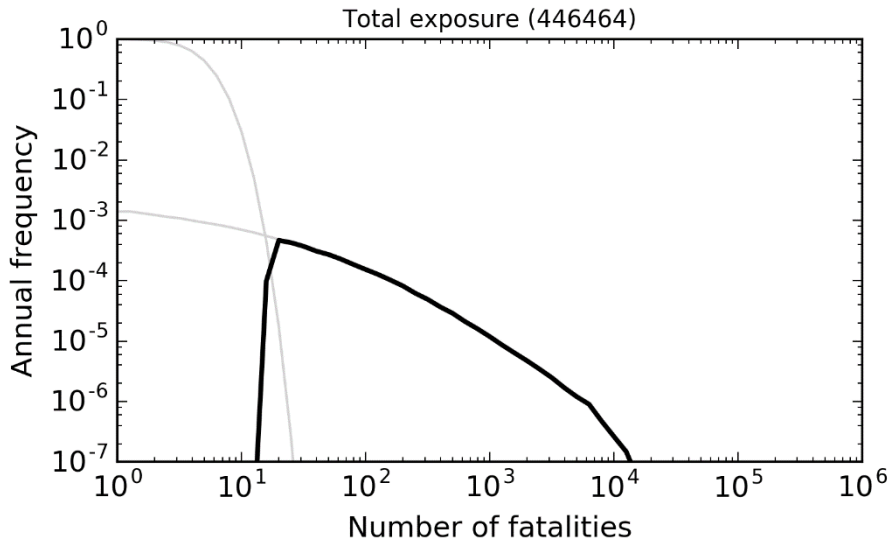


Figure 9.14 *Maatschappelijk Veiligheidsrisico based on the mean of the logic tree, for the Groningen field area for a production scenario of 24 Bcm/year*

For smaller N the Maatschappelijk Veiligheidsrisico is negative. The curves in fig. 9.13 show for the seven selected communities, that for N larger than about ten, the Maatschappelijk Veiligheidsrisico is about equivalent to Group Risk. The population (mean inside day-night population) is shown for each community. The Maatschappelijk

Veiligheidsrisico clearly depends on population size. The Maatschappelijk Veiligheidsrisico for the Groningen Field area as a whole is presented in fig. 9.14.

Structural Upgrading Program

A structural upgrading program is in progress in the Groningen Area. As of the end of September 2017, work carried out in this program includes more than 25,000 building inspections and 1,100 structural upgrades (including both temporary strengthening, and permanent measures to reduce building collapse risk and to secure potential falling objects). Additionally, 2,400 high-risk building elements have been secured.

The current risk assessment indicates that the number of buildings that do not meet the norm of 10^{-5} /year for LPR is some 2,800 buildings. This number is higher than previous assessments. The main reason for the increase in the number of buildings not meeting the norm is that the current risk assessment includes a more comprehensive assessment of the different collapse states that could affect people both inside and outside the building. In the assessment for Winningsplan 2016, the assessment for the high-risk building elements was performed and reported separately, while it is included in this current assessment.

The probabilistic assessment of the number of buildings that do not meet the Meijdam Norm does not immediately translate into an estimate of the structural strengthening scope. There are three main reasons why the scope of the structural upgrading plan is larger than the probabilistic assessment of the number of buildings that do not meet the Meijdam norm.

- Efficiency of identifying buildings with $ILPR > 10^{-5}$ has not yet been proven.
This is a probabilistic assessment and does not directly indicate every individual building that needs to be included in the structural upgrading plan. Through an inspection program these buildings will have to be identified. In time, with a well-designed and risk-based inspection program it is expected that buildings with $LPR > 10^{-5}$ can be found with reasonable efficiency, however this efficiency has not yet been proven.
- Remaining uncertainty in hazard and risk assessment.
Significant progress has been made towards assessing the risk from Groningen earthquakes, however considerable uncertainty remains in the estimate of the number of buildings that do not meet the norm based on mean $LPR > 10^{-5}$. Future updates of the hazard and risk assessment could result in a different mean value of the risk, for instance based on the results of shake table tests of a new typology of building, or where the small number of buildings subject to “special circumstances” (e.g. buildings located on “Wierden”) are taken into account.
- Differences between the hazard and risk assessment and NEN-NPR building code.
Ultimately the structural upgrading scope will be based on the NEN-NPR building code. However, the latest results for the seismic hazard have not yet been adopted in the NEN-NPR, and this along with other areas of technical difference between the hazard and risk assessment and the NEN-NPR could lead to a larger strengthening scope than the current LPR assessment.

Over time, as the efficiency of identifying buildings with mean $LPR > 10^{-5}$ is demonstrated, as the hazard and risk assessment is further matured and uncertainty reduced, and if/when the NEN-NPR building code is updated to reflect the latest seismic hazard assessment and calibration with the laboratory experimental results, then the required structural upgrading program may reduce towards a scope closer to the current risk assessment.

In the short-term, the structural upgrading program is expected to be in line with the current plan of the National Coordinator Groningen (NCG). The results of this risk assessment will be available as an input to help NCG define the scope for the medium to long-term and prioritisation of the structural upgrading program.

References

- 1 Eerste advies Adviescommissie 'Omgaan met risico's van geïnduceerde aardbevingen' 23 juni 2015,
- 2 Tweede advies Omgaan met hazard- en risicoberekeningen in het belang van handelingsperspectief voor Groningen Adviescommissie 'Omgaan met risico's van geïnduceerde aardbevingen' 29 oktober 2015,
- 3 Eindadvies Handelingsperspectief voor Groningen Adviescommissie 'Omgaan met risico's van geïnduceerde aardbevingen' (Commissie-Meijdam) 14 december 2015,
- 4 Guidelines for Developing Quantitative Safety Risk Criteria, Center for Chemical Process Safety, ISBN 978-0-470-26140-8,
- 5 Toelichting Wijk- en Buurtkaart 2013, 2014 en 2015 Respectievelijk Versie 3, 2 en 1, CBS, December 2015.
- 6 Winningsplan Groningen gas veld – 2013, November 2013, NAM
- 7 Interim Update of the Hazard and Risk Assessment for induced seismicity in Groningen, NAM, 7th November 2015.

Appendix A Research to gain a Fundamental Understanding of Earthquakes in the Groningen field

Introduction

One objective of the fundamental research program is to improve understanding of the physical mechanisms inducing earthquakes in the Groningen field. This requires integration of geophysical field data and laboratory rupture experiments on core material with geomechanical modelling. What we ultimately seek is a geomechanical model for seismogenesis with a basis in observed physical processes, validated by geophysical field data.

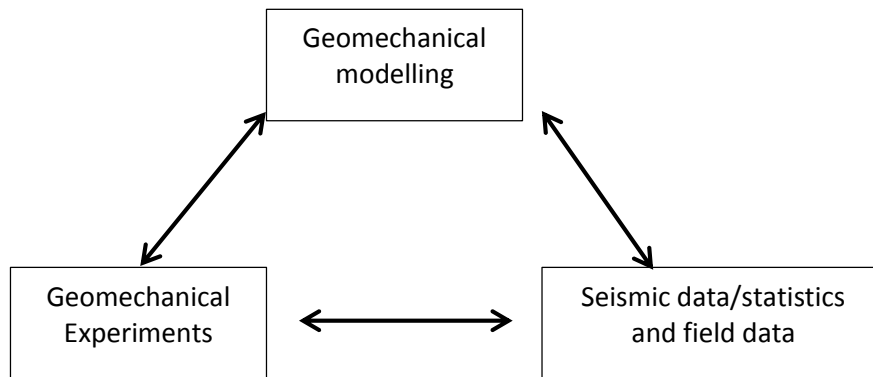


Figure A.1 Synthesis of laboratory experiments on core material, geophysical field data and geomechanical modelling.

Seismic events are characterised by acceleration and deceleration of the rock mass in the subsurface. Acceleration of a mass is proportional to the net resultant force acting on it. The fact that we measure acceleration and deceleration implies that stresses in the subsurface are temporarily not in equilibrium. For this fundamental reason, we are looking into stress-based failure criteria and fault laws that can explain and add to the understanding of seismicity in the Groningen field. We are focusing on stability of fault planes, because faults are planes of weakness relative to neighbouring rock. This is further supported by the interpretation of geophysical data which locates seismic events with increasing confidence on known, natural faults present in the reservoir rock.

It is important to realise that the assessment of fault stability and seismicity requires geomechanical evaluation at different scales. The length scale of a $M_w=1.0$ earthquake is about 30 m, while the nucleation length scale may be only a few meters or less. This implies that mechanical failure needs to be evaluated starting at the cm-scale, while reservoir depletion acts on the field scale of kilometres. The main study elements therefore include (1) the description of the faults, (2) evaluation of the production-induced loading and (3) failure on the reservoir scale.

Fault Interpretation & Modelling

The geological model (in the Petrel software) of the Groningen field (represented in the Petrel software) includes 1,037 mapped faults (Visser, 2012), which intersect with the depleting Slochteren reservoir formation (Fig. A.2). The fault model has been used to account for potential flow barriers in the history matching process of the dynamic reservoir model. A more detailed geometrical description of the faults is required to evaluate their mechanical stability. To this end, more than 35,000 cross-sections have been created across the 1,037 known faults, specifying the local fault dip and azimuth angle, as well as the thickness and depth of the ten Boer and Slochteren formations in the foot wall and hanging wall (Fig. A.2). The dominating fault dip angle (with the horizontal axis) is between 74 and 84 degrees, with most fault sampling points having an offset less than 30% of the reservoir thickness. Many more

faults are present within and intersecting the Slochteren reservoir, but have not been interpreted because their size or offset is too small to be detected on 3-D seismic.

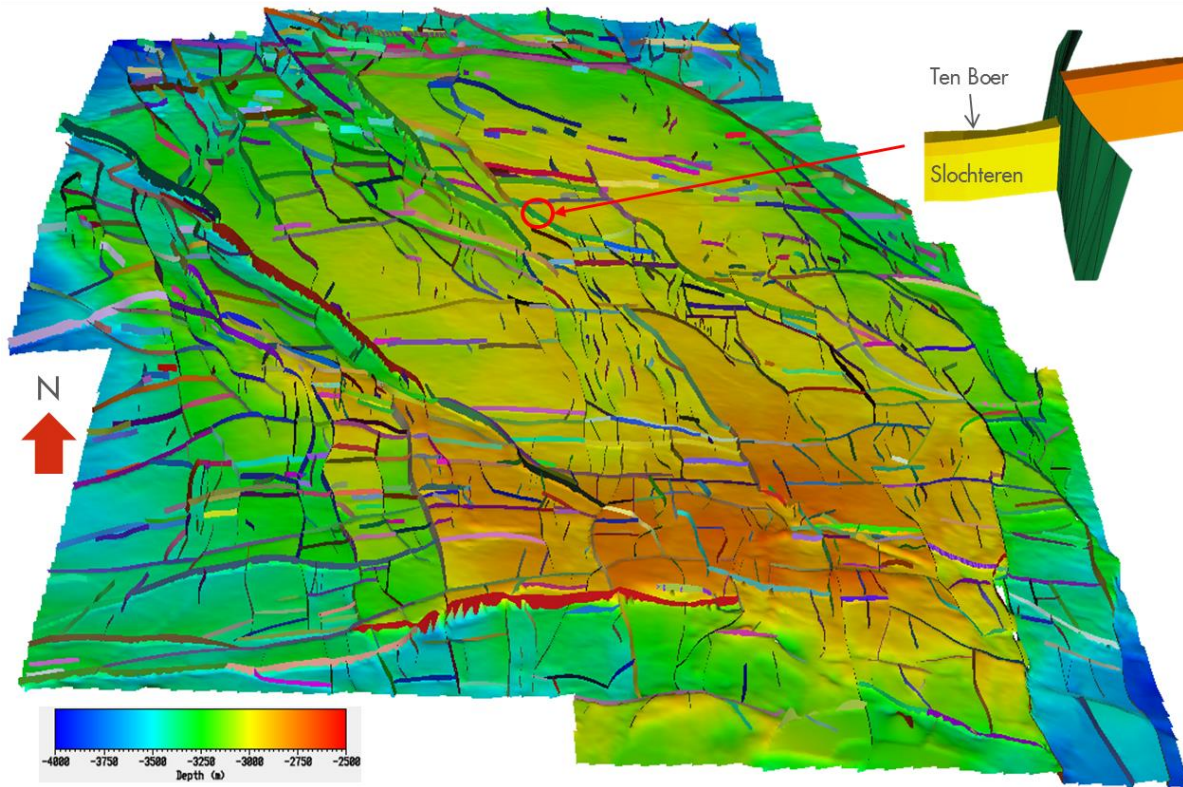


Figure A.2 The 1037 mapped faults in the Groningen field projected on the top Carboniferous depth map. The detail shows an example of vertical offset of the Slochteren formation across the fault.

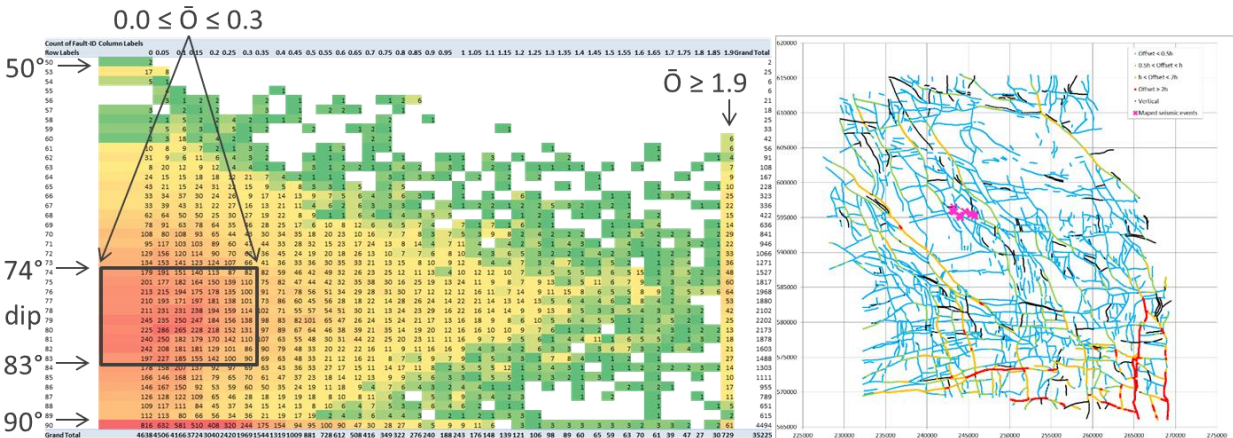


Figure A.3 Left Heat map (frequency distribution) of the 35,000 fault sampling points in terms of fault dip angle (vertically) and normalised reservoir offset (horizontally). Right: Normalised reservoir offset \bar{O} across the Groningen field (blue < 0.5, green < 1, yellow < 2, red > 2)

High resolution fault interpretation has been conducted to further improve the fault topography at smaller scales as fault rupture may nucleate at slip patches as small as a few meters. Three areas have been selected, each with an area of about 1.0 -1.5 km², based on seismic activity and the location of the deep down-hole geophone wells (Fig. A.4). Fault and horizon interpretations have been made concurrently using various techniques (ant-tracking, edge

detection, semblance Van Gogh, among others). Additional geological complexities have been incorporated in the structural framework built, such as fault topography, fault segmentation and low displacement faults.

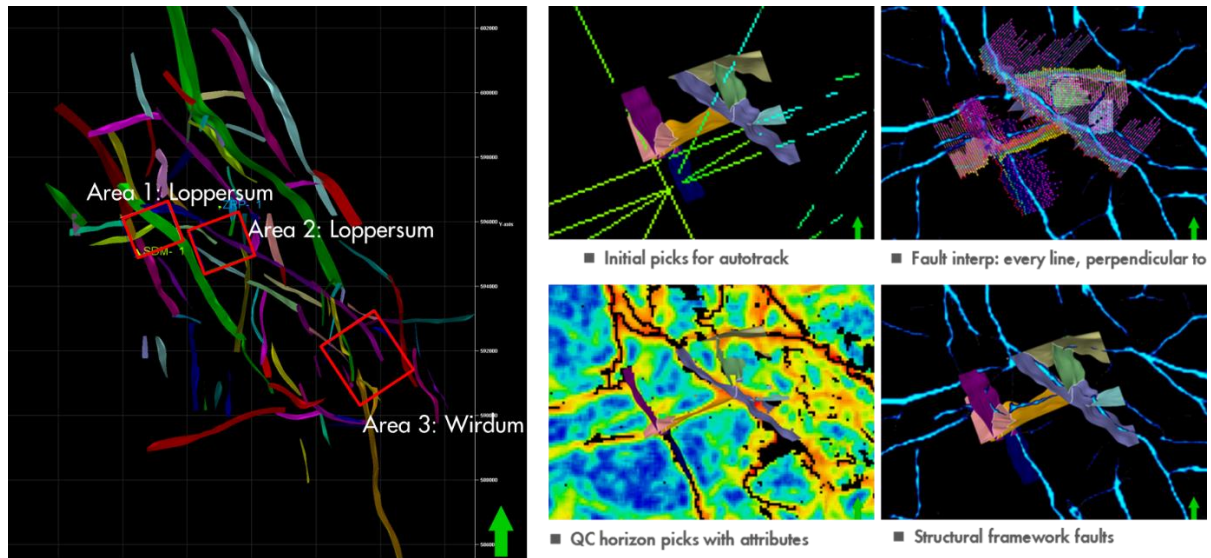


Fig. A.4 The three selected areas for high resolution fault interpretation

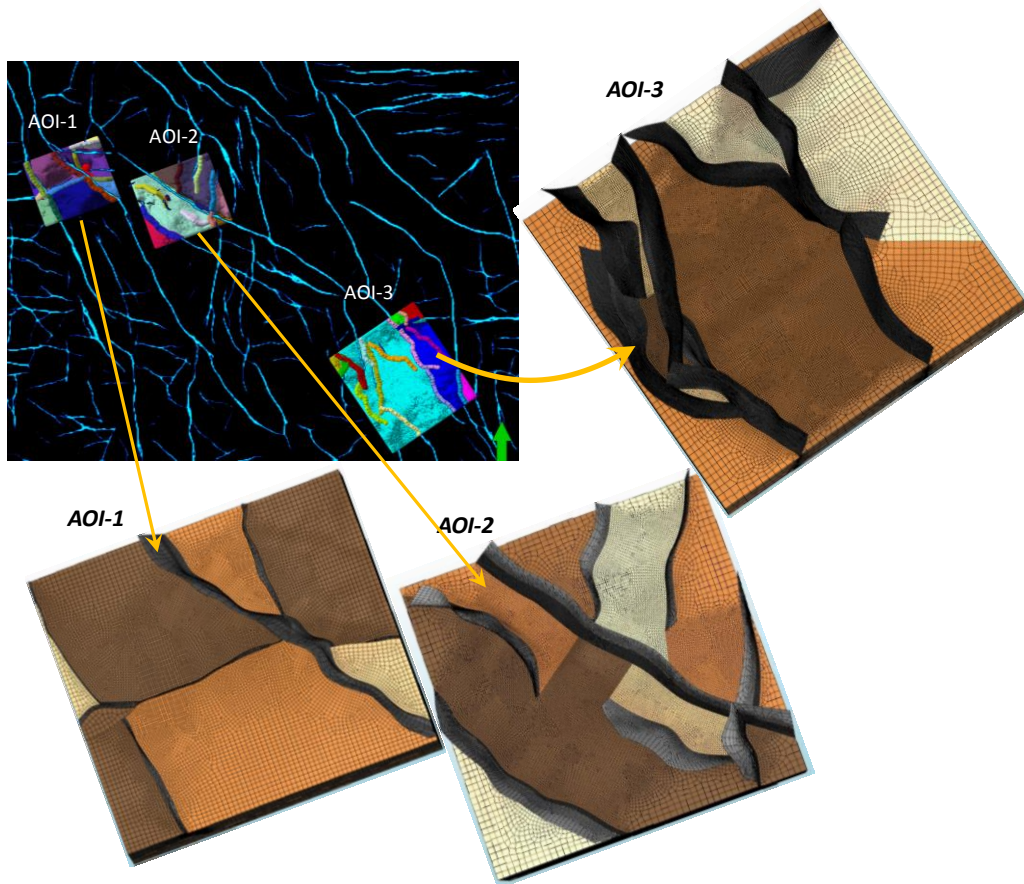


Fig. A.5 Sector-scale structural framework and dynamic rupture models and their mesh across the Loppersum area.

The structural framework also needs to take into account the requirements for domain discretisation (Fig. A.5). Fault interpretation and geomechanical modelling has been limited to selected parts of the Groningen field, because

development of 3-D meshes is complicated by variable reservoir juxtaposition along the strike of the faults and complex fault intersections.

Evaluation of production scenarios

Three-dimensional finite-element models have been built to evaluate (aseismic) fault slip across the Groningen field under different production scenarios. One, large-scale, 3D model without faults has been built to account for stress redistribution in the subsurface due to reservoir depletion. Three, smaller-scale sub-models have been constructed including virtually all known faults with reservoir offset represented as accurately as possible. The large-scale model, which has been calibrated against subsidence data, is used to impose the appropriate displacement and stress conditions as boundary conditions to the smaller-scale models. Sensitivity runs confirmed the importance of reservoir offset found earlier in the 2D modelling studies.

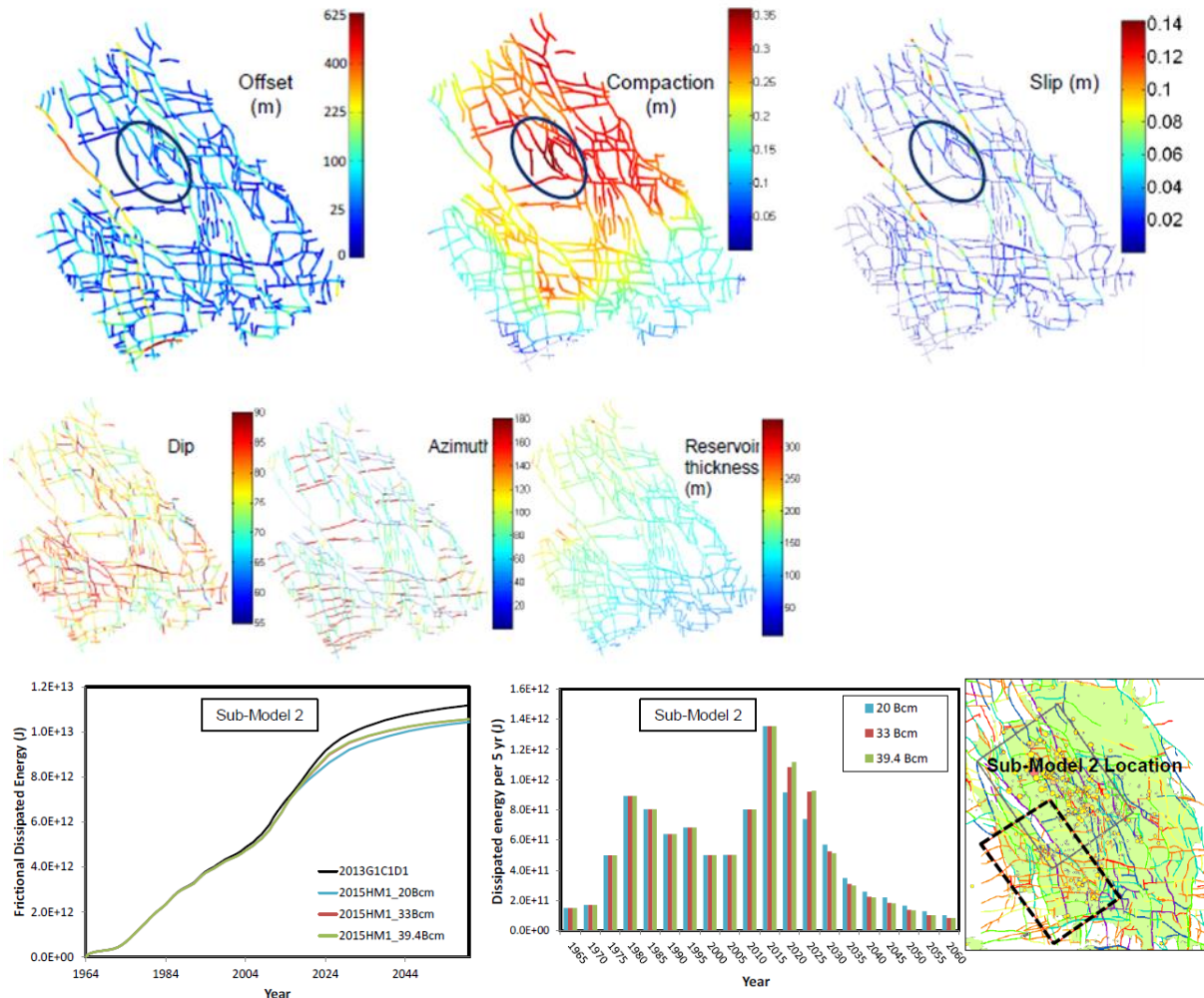


Figure A.6 Top: Fault dip, azimuth, offset & slip and reservoir thickness & compaction over the area covered by the three sub models. Bottom: the cumulative energy dissipated by fault slip as a function of time over sub-model 2 for different production scenarios.

The challenge in 3-D modelling is achieving adequate resolution (element size) in relation to the mechanical response simulated, within manageable computational effort. At least 20 elements (of about 10 m in Groningen) are required over the reservoir height to capture the onset of fault slip with reasonable accuracy. The element size required to simulate seismic events with $M_w \approx 1.0$ is in the order of 1 m, as the aseismic slip patch at the start of the rupture is in

the order of 5-10 m. This is the reason why sub-models are required to simulate fault slip in 3-D, and even smaller models are required to simulate seismic rupture (section 0).

The proposed way forward is to use the existing global 3-D geomechanical model to determine the stress paths along (known and/or hypothetical) fault planes, with attention for dip-slip and strike-slip loading conditions, considering different production scenarios. Variation and uncertainties in the in-situ stress and formation properties can be addressed in a manageable number of runs. Also, non-linear and time dependent (creep) behaviour of different formations can be assessed, and their potential impact on the stress paths evaluated.

2D Dynamic rupture simulation

The objective of dynamic rupture simulations is to better understand the mechanics and failure of faults that offset depleting reservoir formations. A two-dimensional dynamic rupture analysis capability has been developed to better understand why faults become unstable and cause seismic events, assuming a linear fault slip-weakening relationship. An algorithm has been developed to reliably and accurately determine the depletion level at which the fault reaches a condition of unstable equilibrium. This is important because unstable fault conditions and the associated seismic event can be missed, or the calculated moment magnitude is over-estimated, if analyses are not conducted carefully. Bifurcation analyses have been used to correctly determine the depletion level at which faults become unstable and generate seismic events (van den Bogert, 2017). The dynamic rupture simulation capability has been successfully benchmarked against a representative case from the Southern California Earthquake Centre (SCEC) portfolio (Buijze, 2015).

Initial two-dimensional studies (van den Bogert, 2015) showed that two aseismic slip patches can occur, if the fault strength is reached in a depleting reservoir with offset (Fig. A.7). One slip patch occurs at the top of the hanging wall and one slip patch occurs at the bottom of the foot wall. The depletion level that causes onset of fault slip (green line in Fig. A.7) is strongly dependent on the normalized reservoir offset (offset divided by reservoir thickness). The simulations indicate that the distribution of stress along the fault scales with the reservoir thickness.

Evaluation of a large number of fault configurations with different fault and reservoir properties has revealed that the normalised reservoir offset also dominates the depletion level that causes onset of seismic rupture (yellow line in Fig. 6). All cases evaluated exhibit one of the following three rupture mechanisms as the root cause of the seismic event (right-hand side of Fig. A.7):

1. Merging of the two aseismic slip patches
2. Instability of a single slip patch without merging with the second slip patch
3. Instability of a single slip patch followed by merging with a neighbouring slip patch

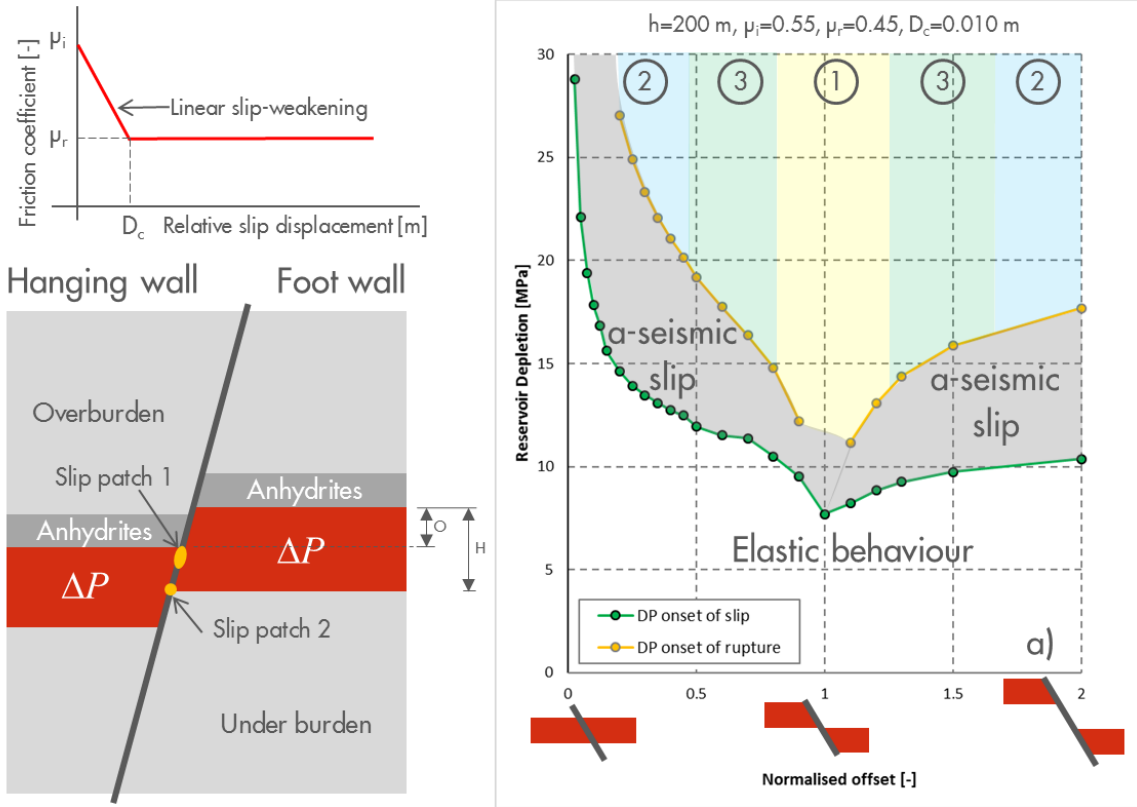


Figure A.7 Typical Groningen fault configuration with a reservoir offset O of about half the reservoir thickness H . Aseismic slip patches occur first at the top of the hanging wall and at the base of the foot wall. The depletion level at which fault slip occurs is strongly dependent on the normalized offset $h=O/H$ as indicated by the green line (right). In the model, seismic rupture occurs if the depletion is increased as indicated by the yellow line.

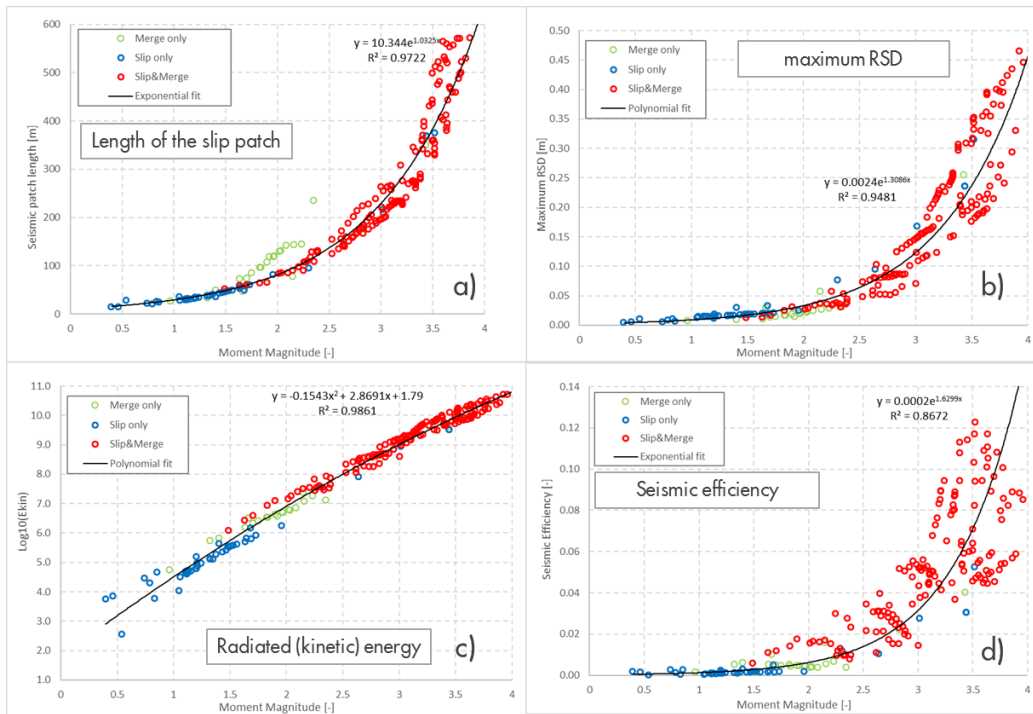


Figure A.8 Scaling relationships between the Moment Magnitude and different seismic parameters from the dynamic rupture simulation, discriminated by rupture mechanism.

Furthermore, it has been found that the depletion level at which onset of seismic rupture occurs reduces for smaller values of the critical fault slip displacement D_c (see slip-weakening diagram, top-left in Figure A.7). The length of the slip patch at the onset of seismic rupture observed in these geomechanical simulations is slightly lower, but close to the critical slip length analytically derived by Uenishi & Rice (2003).

The dynamic rupture simulations yield the size of the seismic slip patch, the (maximum) Relative Slip Displacement (RSD), the radiated (kinetic) energy, seismic efficiency, Moment Magnitude (MM) and other output data that can be compared to actual seismic events. Scaling relationships have been obtained between Moment Magnitude and other output data (Fig. A.8). These seem to be valid independently of the rupture mechanism. The stress drop over the seismic slip patch does not correlate well with Moment Magnitude. Moment Magnitude is strongly influenced by the difference between the initial and residual friction coefficient as well as the normalised reservoir offset (Fig. A.9, left).

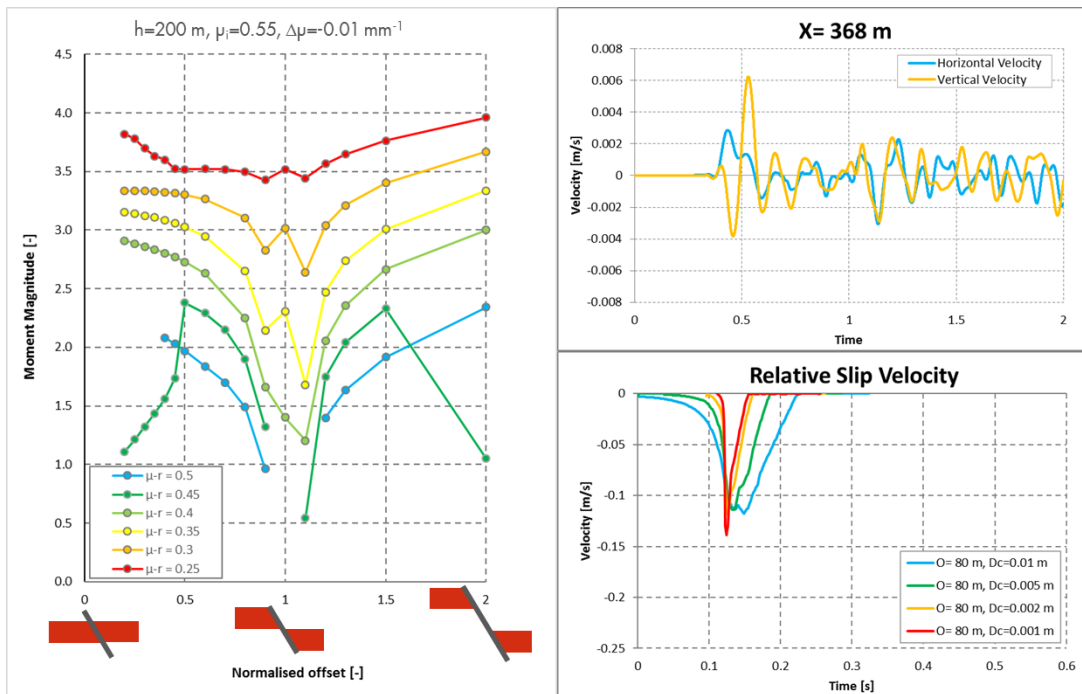


Figure A.9 Left: Moment Magnitude as a function of the normalised reservoir offset for different values of the residual friction coefficient (the initial friction coefficient is the same in all cases). Top-right: Simulated wave forms for a seismic station. Bottom-right: The source-time function has a shorter rise time for smaller values of D_c (Rupture Mechanism 2).

Dynamic rupture simulations generate displacement, velocity and acceleration vectors at every node of the geomechanical finite-element model. The velocity components calculate at a particular location (seismic station) provide waveforms for comparison with actual event data (top-right Fig. A.9). The slip velocity on the fault during seismic rupture is used to derive the synthetic Source-Time Function (STF, bottom-right Fig. A.9). The Source-Time Function (STF) and waveforms generated by each of the three rupture mechanisms are quite different. The critical slip displacement D_c determines the rise time and duration of the STF, thereby creating an opportunity for calibration against actual seismic event data.

3D Dynamic rupture simulation

The objective of the three-dimensional dynamic rupture simulations is to understand the impact of fault curvatures variations, along strike, on the onset of seismic rupture and the aspect ratio of the seismic slip patch. Also, the presence of fault intersections on rupture propagation is assessed. These aspects cannot be addressed in with a 2-D

model. We have developed three sector-scale dynamic rupture models focusing on the Loppersum region, where downhole and surface geophone arrays have been deployed to closely monitor the seismic activity (Fig. A.4 and A.5). The size of the sector models is in the order of 1.5 km to 2.0 km on each side of the fault studied. All the models are composed of four major mechanical stratigraphic units: 1) the deep overburden – lower Zeichstein anhydrites and carbonates; 2) the seal – Ten Boer claystones; 3) the reservoir – Rotliegend sandstones, and 4) the under-burden – Carboniferous.

These 3-D sector models generate the dynamics of rupture initiation, nucleation, propagation and arrest on a realistic fault network (Fig. A.10). As model calibration is an ongoing and interactive process, integrating existing geophysical, petrophysical, and reservoir/production data, these early results provide encouraging insights to the understanding of seismic fault rupture due to reservoir depletion. It is believed by many that the fault movement due to reservoir compaction in Normal Fault stress setting like Groningen is dip-slip. From the present 3-D models we see the rupture initiating at the fault-horizon intersects and converging dip over the fault juxtaposition, while widening along the strike as it propagates forward. The modelled slip distribution, however, does suggest numerous local events at the rupture front with strike-slip components when encountering heterogeneities in fault geometry (Fig. A.11). Such outcomes are qualitatively supported by focal mechanism analysis.

The locations where modelled ruptures nucleate in fair agreement with the seismic event clustering detected and interpreted using the current monitoring network. For the first time, we observe that curvature of faults baffles rupture propagation. Notably, rupture branching onto neighbouring splay and conjugate faults is apparent in most of these modelling cases. These ruptures generate distinctive wave forms that are received by monitoring stations relative to the seismic sources, which are being analysed in comparison with recorded field ground motions.

The 3-D dynamic rupture models provide additional insights that 2-D models cannot; e.g. into rupture width, rupture branching into intersecting faults, scaling with moment tensor and seismic magnitude, and the likely causes of complex rupture behaviour derived from focal mechanism analysis. While it is still premature to use these results to forecast the location, timing, and magnitudes of production-induced seismicity, we are hopeful that such modelling efforts will be able to shed lights on the fault reactivation mechanisms in Groningen.

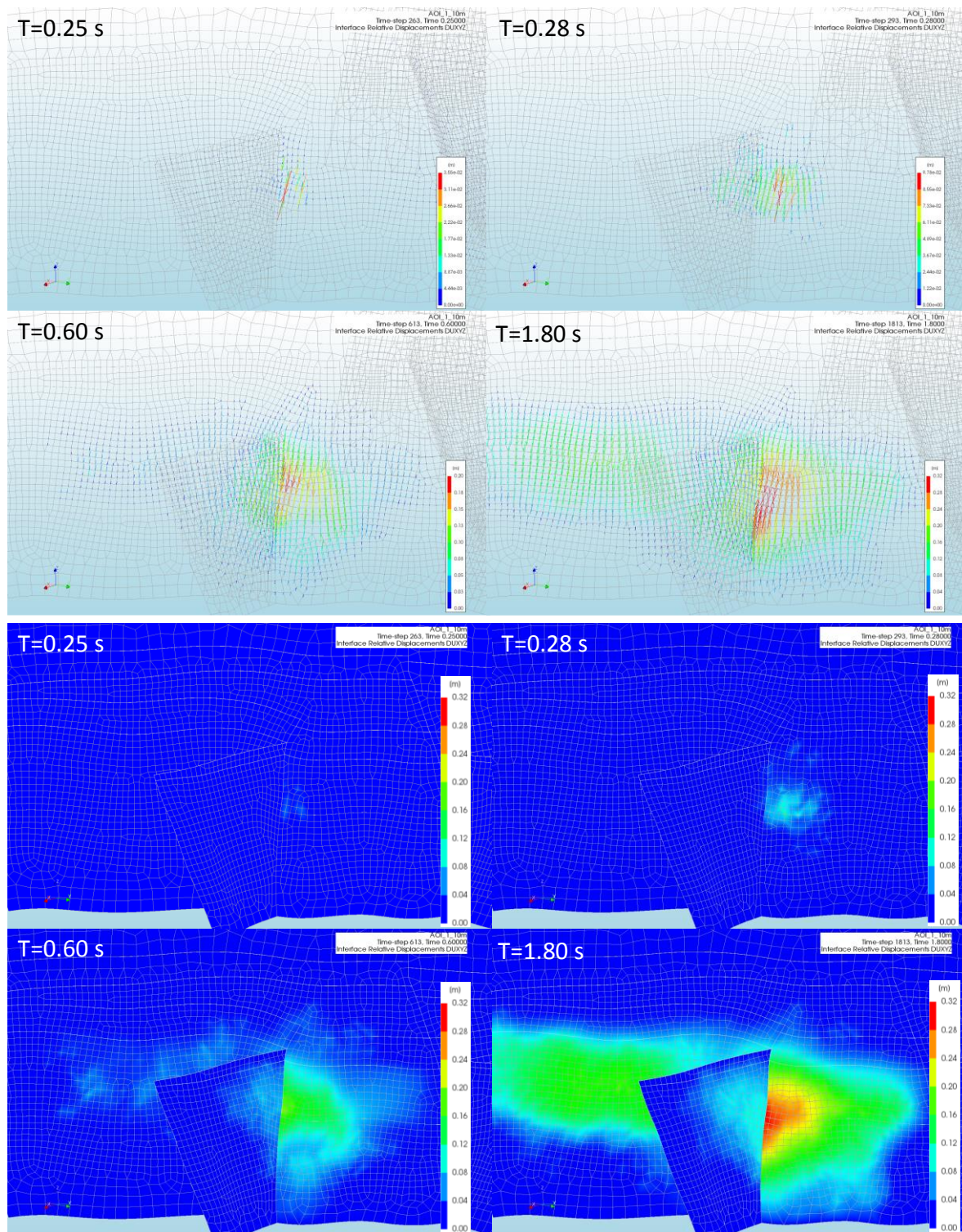


Figure A.10 Modelled total fault slip vector and magnitude over time snapshots, illustrating the rupture initiation, nucleation, and propagation of the Int8 fault in the AOI-1 sector model.

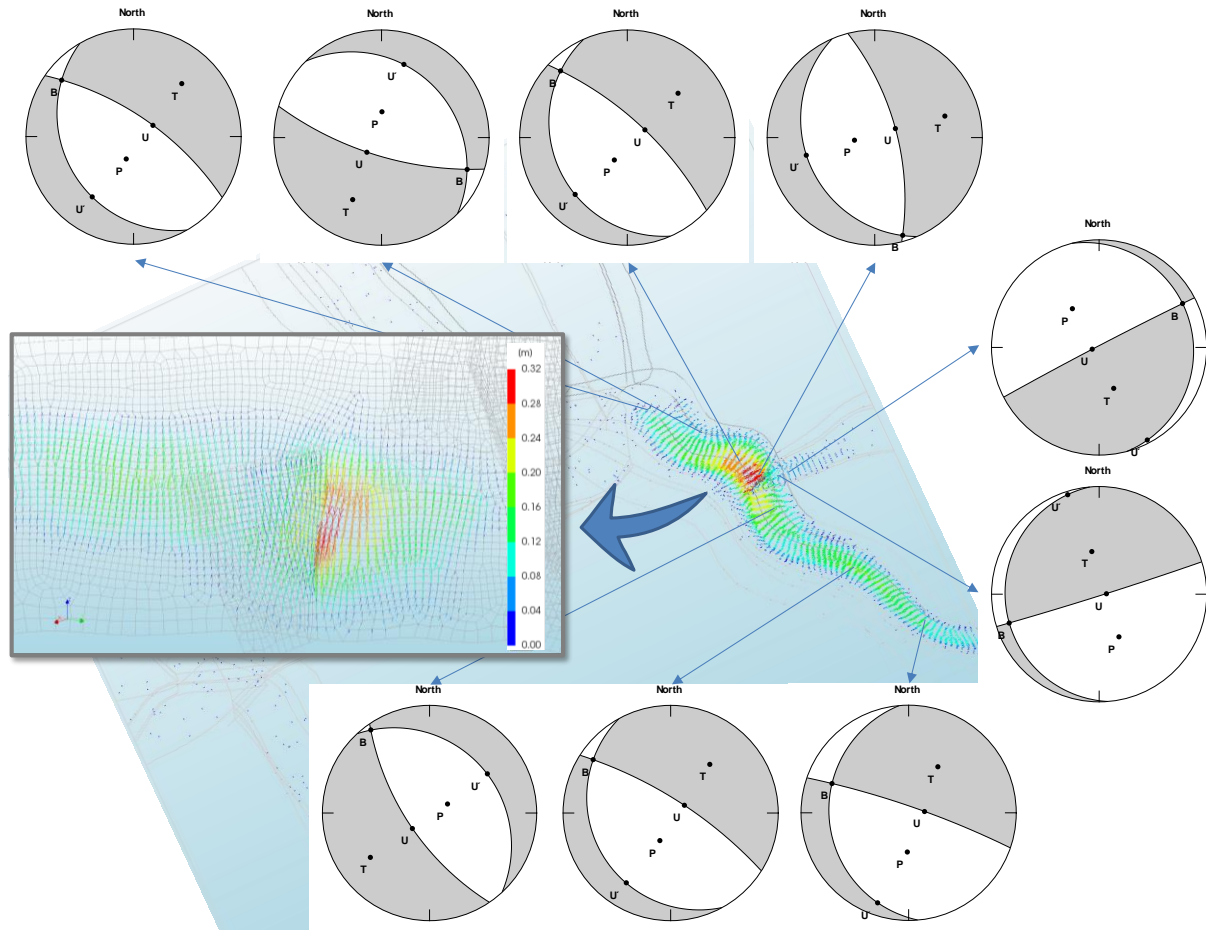


Figure A.11 Slip distribution (top view; side view as inset) across the modelled rupture of Int8 fault in the AOI-1 sector model and stereographic projections relative to local fault strike and dip.

Characterization of fault surface roughness

The objective of fault roughness characterization is to quantify the spatial waviness of the seismically imaged faults found to control rupture due to reservoir depletion. Insights gained from the 3-D dynamic rupture modelling of realistic fault networks indicate that competition between slip convergence in the dip direction and slip widening along strike determines the rupture propagation pattern and the eventual rupture shape and size, with propagation in both directions being significantly influenced by surface roughness, and the associated resistance to seismic slip.

Spectral analysis has been undertaken for two major faults, Int8 and M69, which are indicated to host a series of seismic event clusters in the Loppersum region (Fig. A.12). Surface roughness anisotropy is expressed by different Hurst exponents parallel and normal to the geological slip directions. Within the range of the sampling resolution, a Hurst exponent of about 0.5 is calculated from the averaged spectrum in strike direction, and about 0.4 in dip direction for fault M69. Preliminary comparison with published research, performed over the 0.1-10 m range of length scales on rock specimens and fault faces exposed at the surface (e.g. Candela et al., 2011), suggests that our findings at the 10-1000 meters scale are distinctive from those studied at smaller length scales.

For the first time, this study attempts to characterize seismically mapped fault geometry on the larger scale and to explore feasibility of applying such findings to smaller scale fault geometry relevant for seismogenic fault rupture. Continuing efforts are underway to utilize this result and understanding to further constrain 3-D dynamic rupture models which can numerically simulate depletion induced ruptures scalable to field observations.

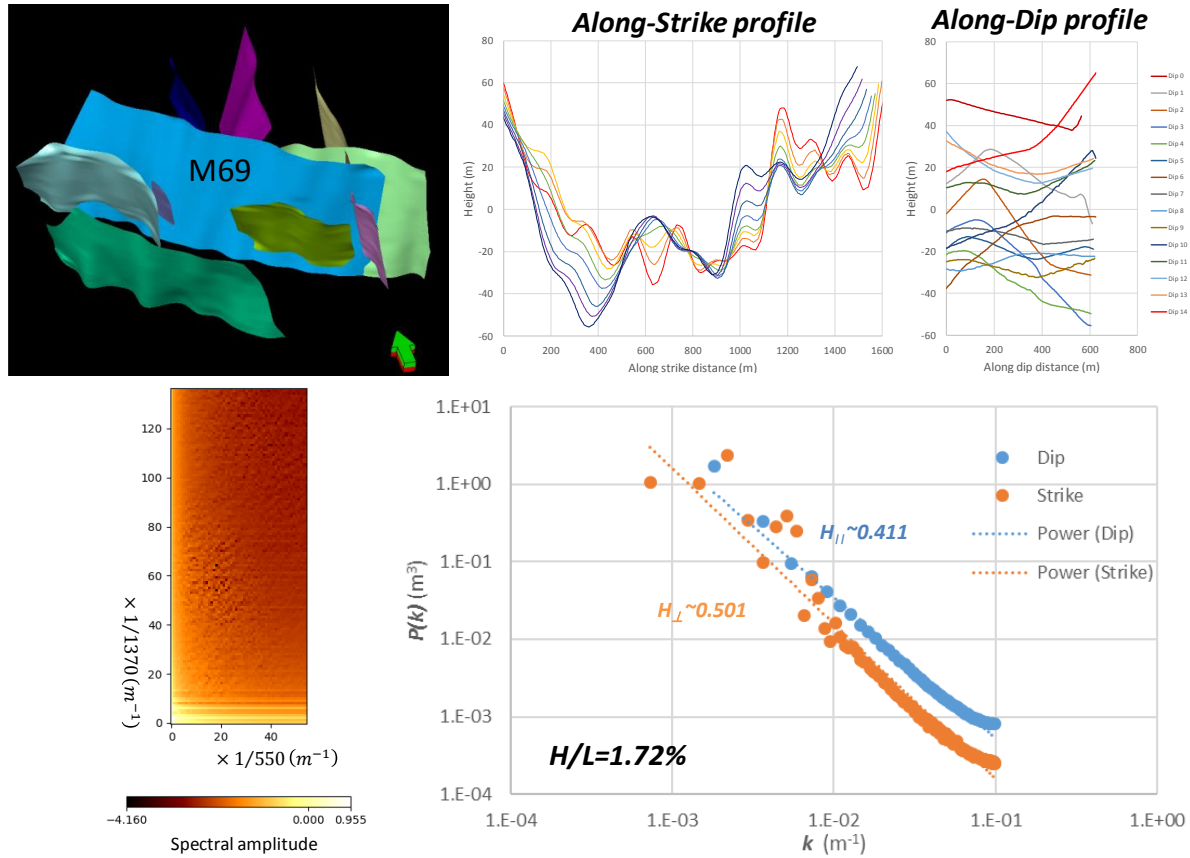


Figure A.12 Top left: M69 Fault in the AOI-2 sector that hosts a series of seismic events over time. Top right: Selected cross-sectional profiles of the M69 fault along the strike and dip directions. Lower left: Spectrum map of the M69 fault. Lower right: Relations of power spectra vs. wave number indicate anisotropy in fault roughness along strike and dip directions.

Geophysical data acquisition & Interpretation

The overarching objective of the geophysical data acquisition, analysis and interpretation is to detect and locate seismic events in the Groningen field and determine the moment tensor and moment magnitude as accurately as possible.

As a brief reminder from chapter 4, the main monitoring campaigns that feed seismicity data into the subsequent analysis in the Groningen are the following (described in more detail in chapter 4):

- 69 geophone wells and accelerometers; an extension of the existing passive seismic monitoring network, to improve the resolution over the whole Groningen field,
- 2 temporary monitoring wells with vertical geophone arrays, later replaced by,
- 2 dedicated deep monitoring wells with vertical geophone arrays (Zeerijp-2 and Zeerijp-3A): Installation over the reservoir section in deep wells located in the Loppersum area, to improve the determination of earthquake hypocenters:
 - a. Temporary geophone arrays were placed at and around the reservoir interval (at 3 km depth) in two deep observation wells in the Loppersum area (Zeerijp-1 and Stedum-1). These strings have been operational from late 2013 to early 2016.
 - b. Another temporary geophone array in a deep observation well near Harkstede (Harkstede-2A), operating from October 2016 to January 2017.

- c. The temporary geophone arrays in the Loppersum area were replaced in 2015 by permanent seismic monitoring arrays in two newly drilled wells (Zeerijp-2 and Zeerijp-3A) in this same area.
- Flexible geophone network: a roving array network consisting of ~400 geophone nodes, being deployed over the gas field in 11 configurations
- Real-time acoustic monitoring with a fibre optic cable (DAS interrogator still in research / pre-deployment stage)

The acquired data is analyzed internally by NAM, Shell and ExxonMobil research teams as well as continually shared with reputable research institutes and universities around the world to do their own independent research. Each research study carried out by or on behalf of NAM is subjected to both internal review and various types of external and fully independent reviews and verification.

Analysis and Interpretation research efforts

The recorded seismic events from these arrays have been studied to determine the micro-earthquake event locations and magnitudes. This information in turn has been used to investigate the geomechanical behaviour of the Groningen field and, in particular, the activity of several hundred faults that cross the area, which are the primary source of the earthquakes themselves. The driving mechanism in these cases are the stress changes induced in the reservoir by pressure depletion, which causes overburden compaction and activation of the faults. Bourne et al [8] analysed the relation between seismicity and compaction and determined empirically that seismic moment is an exponential function of cumulative compaction.

Induced seismicity in the Groningen reservoir is typically of small magnitude, difficult to observe and with a limited number of stations for detailed analysis. The events are also of much higher frequency than their tectonic counterparts. For instance, in global seismology surface waves between 0.025-0.1 Hz are used for full waveform based source mechanism analysis. In contrast, the frequency content of small magnitude induced seismicity usually ranges between 10 Hz-100 Hz and 2 to 3 orders of magnitude higher than the tectonic earthquakes. As discussed later, some of the induced seismicity data in this project is monitored with downhole arrays, where interbed multiples and guided waves quickly complicate the observed wave fields, making analysis even more challenging. In reservoirs with faults and strong horizontal velocity variations, the sub-surface illumination coverage from ray-trace travel times can be poor. Even when ray-tracing succeeds, it is possible that one particular phase is predicted while a different phase is interpreted in the observed data, resulting in phase mismatch and mis-location of events. For example, head waves can be picked in the observed data, while direct arrivals are calculated in the ray-tracing, resulting in location ambiguity and outlining reasons to approach the problem from multiple angles, i.e. the full waveform inversion as well as ray-based method.

Initial results of some previous studies of micro-earthquakes from a ray-based method suggested that the origin of the microearthquakes was due to the movement of several large basin bounding faults, strongly implying that the complexity of the sub-surface in and around the reservoir plays a significant role in the timing and magnitude of various wave modes propagating from the epicentre to the receivers. To better understand this behaviour, both a ray-based workflow as well as a wave equation based method were developed and implemented internally. The ray based method is robust but may be challenged around large structural heterogeneity, while a wave equation based workflow is highly computationally intensive.

Determining the fault(s) on which slip occurred and the nature of the deformation that occurred there can be constrained with the right analytical methods and then used to test and improve geomechanical models, wavefield simulations, seismicity forecasts, and estimates of the maximum earthquake magnitude in the Groningen field. A well-established **ray-tracing method** is adapted and applied to relocate events and determine their focal mechanisms. For this traditional method, it is recognized that the complex velocity structure immediately above the Groningen reservoir presents special challenges. Thus, several steps are taken to optimize the velocity data appropriately select

seismic stations to best constrain ray-traced earthquake locations. Further, the ray-traced method is combined with the conventional “focal mechanism” estimation, in which slip is assumed to be well represented by sliding along a fault surface. The resulting focal mechanisms and moment tensors indicate fault slip consistent with the compaction understood to drive seismicity in the Groningen reservoir, consistent with earlier work by Kraaijpoel and Dost (2012; figure x1 below). However, the results also demonstrate that even with an ideal velocity model the absolute depth is not as well constrained (figure x2 below).

Therefore the need exists for further analysis, and the raytracing method can be thought of as complementary to the full wavefield inversion method discussed below.

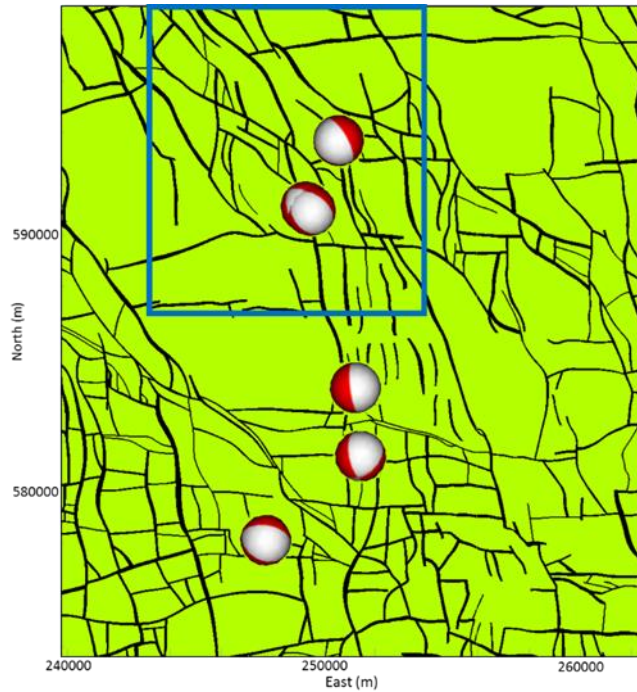


Figure A.13: Ray-tracing based focal mechanisms. Red portions represent compressional parts of fault slip projected onto a hemisphere viewed from below. The mechanisms indicate dominant normal faulting consistent with compaction of the reservoir.

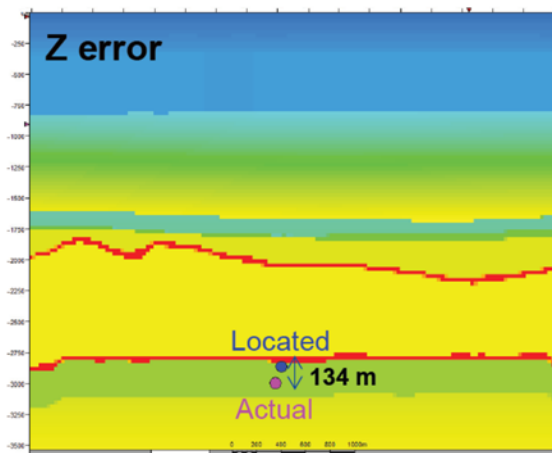


Figure A.14: Results of internal benchmarking of event location using wavefield simulation data. The map location is accurately recovered, but the depth error (shown above) is larger.

In parallel, a **full waveform inversion method** to (a) relocate KNMI-detected events and (b) compute focal mechanisms for each event. The method is originally developed for the analysis of the seismicity data recorded by the multiple deep downhole arrays and later adapted for the surface shallow borehole network. The full waveform inversion method is performed in near-real time: the results are ready within a day of the earthquake occurrence. The method is computationally intensive: it requires generation of a synthetic data library of approximately 8 Terra Bytes of waveforms, which is subsequently correlated with the high-fidelity field data recorded by the KNMI shallow borehole network for the best-match in the earthquake location and a best-fit of the focal mechanism inversion.

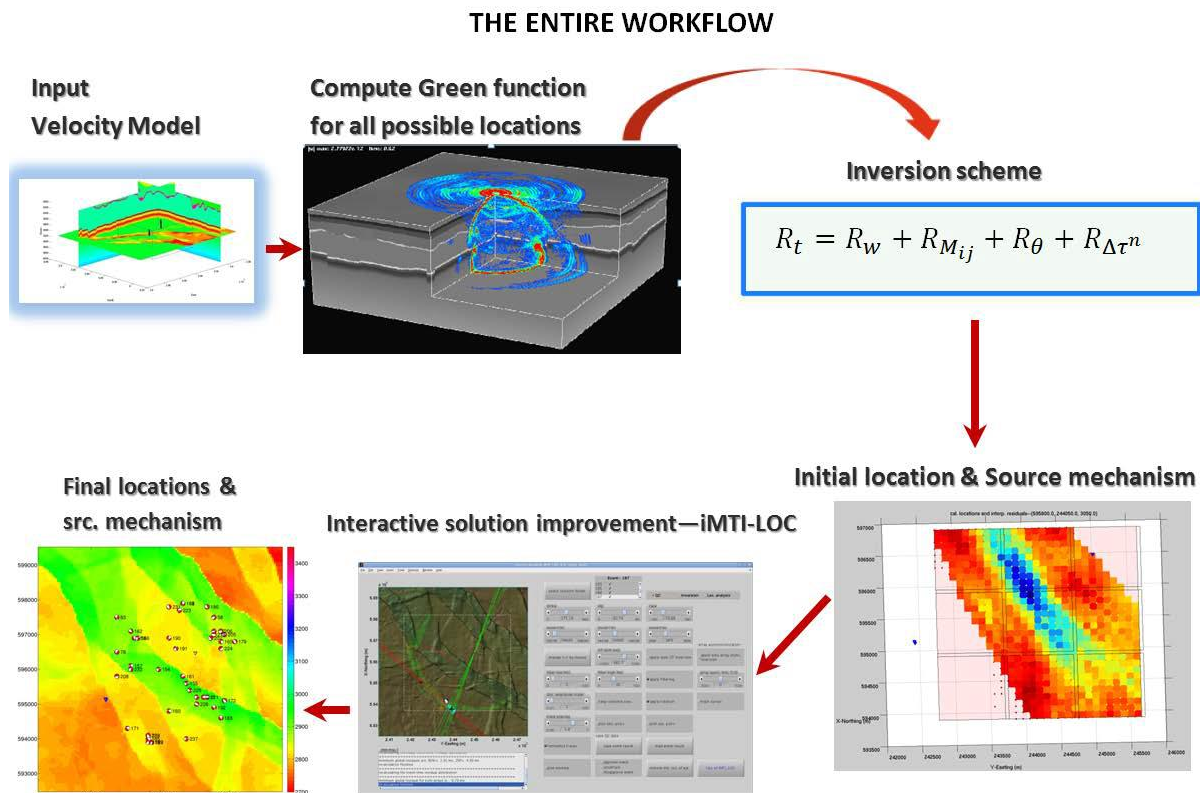


Figure A.13. the workflow describing full waveform based event location and moment tensor inversion.

The results from the analysis of the deep downhole arrays are invaluable and fundamentally change our understanding of the seismic wave arrivals. In summary, the event interpretation shows:

- the first breaks are head waves. However, these arrivals are weak and may be lost in the ambient noise.
- P and S arrivals are well distinguishable when the source to receiver distance is small. For larger offsets, the strongest arrivals are the P and S guided waves.
- Depth positioning although somewhat poorly resolved, suggests all events originate within the reservoir interval
- The event locations have a close correspondence to the position of major faults across the
 - study area.

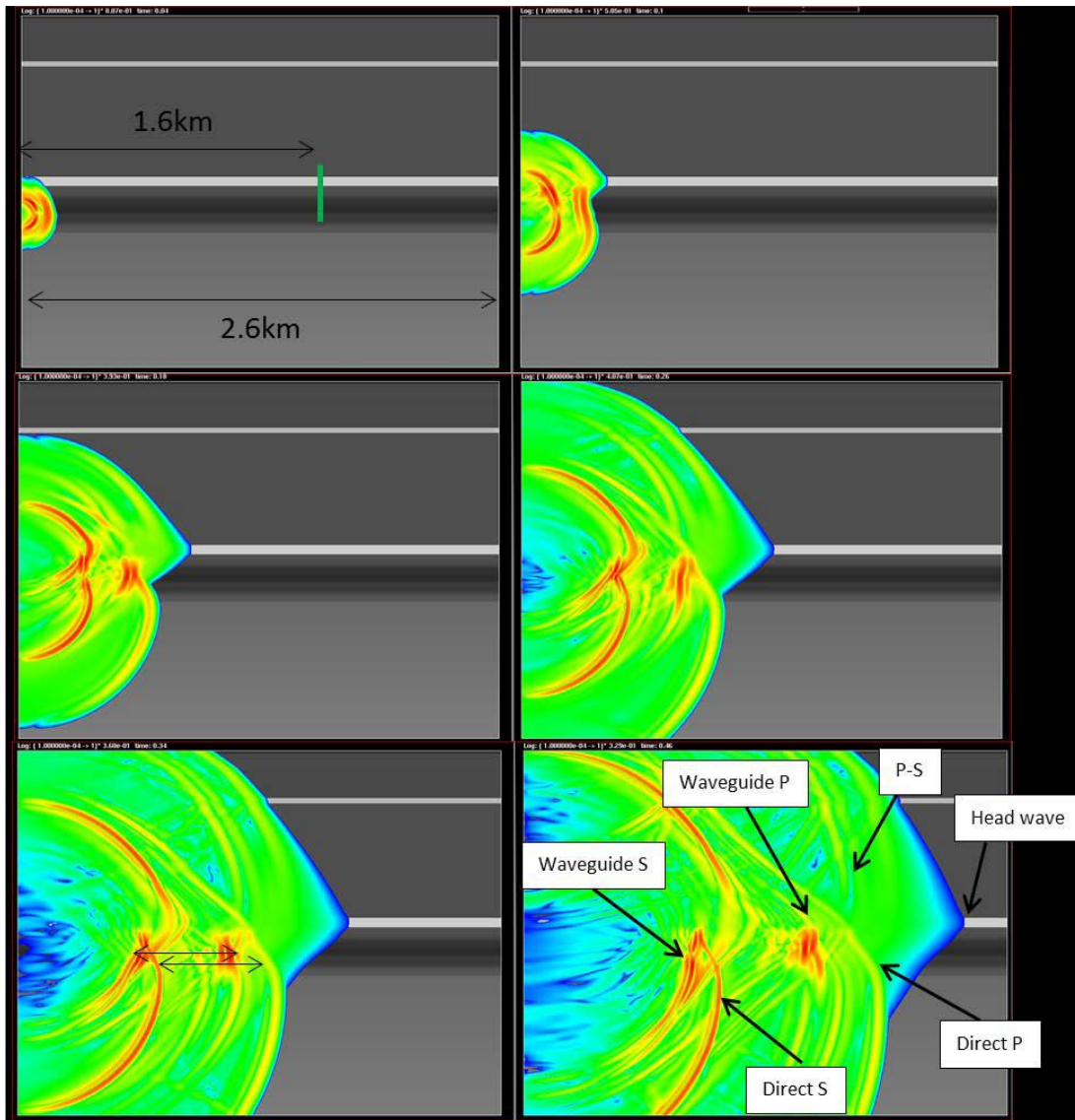


Figure A.14. Snapshots of the wave propagation field shown at 0.04, 0.1, 0.18, 0.26, 0.34 and 0.46 seconds from the firing time.

To better resolve the earthquake focal mechanisms as well as improve upon the earthquake positioning errors, the full wavefield inversion method was adapted and applied to the surface borehole network. The result is a set of improved earthquake locations that lie within a few hundred meters of the KNMI's original locations and align more precisely with the known faults (Fig. A.15 below). The focal mechanism solution results are remarkable and reveal that the events are predominantly the result of normal fault movement, with fault-strike aligning well with the known NW-SE striking faults. The method is currently undergoing internal assurance before being published in a peer-reviewed geophysical journal, with the future plan to integrate the results and analysis with geomechanics and solidify our understanding of the behavior of the field.

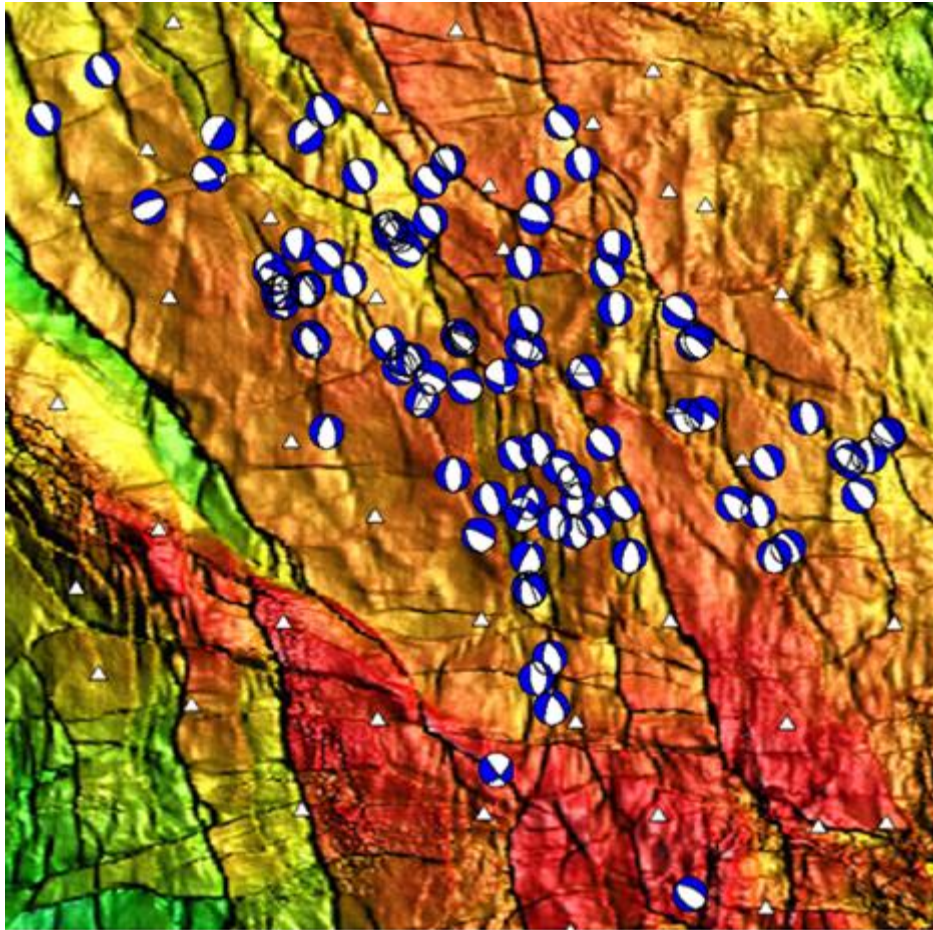


Figure A.15 Relocated earthquakes (a subset of 99 events) and the focal mechanism solutions (fault-slip orientation -first ever routine calculation for Groningen events)

Comparison of the Geophysical results with fault data has revealed that many seismic events occur on known faults and exhibit dip-slip displacement aligned with the fault azimuth (Fig. A.16, left). Furthermore, it is found that dynamic rupture simulations follow the same relationship between moment magnitude and corner frequency as actual seismic events (Fig. A.16, right).

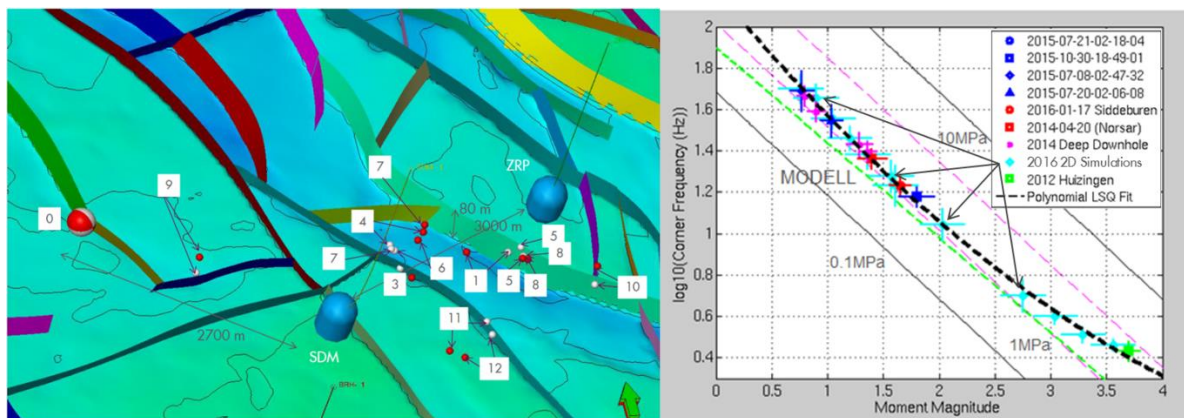


Figure A.16 Left: Selection of events recorded by the Stedum (STD) and Zeerijp (ZRP) deep geophone wells and their location relative to known natural faults Right: Moment Magnitude (M_w) versus corner frequency derived for various seismic events, compared with the results from 2D Geomechanical simulations.

More in-depth comparison of synthetic and observed waveform data may provide the opportunity to calibrate the critical slip displacement D_c in the dynamic rupture models. To this end, the STF in Figure 9 is convolved with full-waveform Green's function (path term) computed using the Wavefield Finite-Difference (WFD) code. Synthetic waveforms have been generated from dynamic rupture simulations with different values for D_c and compared with a selected event recorded by the deep down-hole geophone wells (Fig. 16). The amplitudes of each dynamic rupture simulation have been individually scaled to seismic moment ($N \cdot m$) for clarity. The goodness of fit is quantified through the Normalized Residual Sum of Squares (NRSS). The remaining waveform discrepancies could be related to WFD grid dispersion artefacts, velocity errors and possible inelastic attenuation effects that cause amplitude and phase fluctuations, and is subject of further work.

Some of the main findings:

- Many observed seismic events are located on known natural faults with a focal mechanism aligned with the local fault azimuth (taking data accuracy of into account, Fig. 12, left).
- Simulated ruptures show good correspondence with observed seismic events in terms of Moment Magnitude and corner frequency (Fig. 12, right).
- Promising results are obtained calibrating the critical slip displacement D_c for particular seismic events based on the dominant period in the observed waveforms.

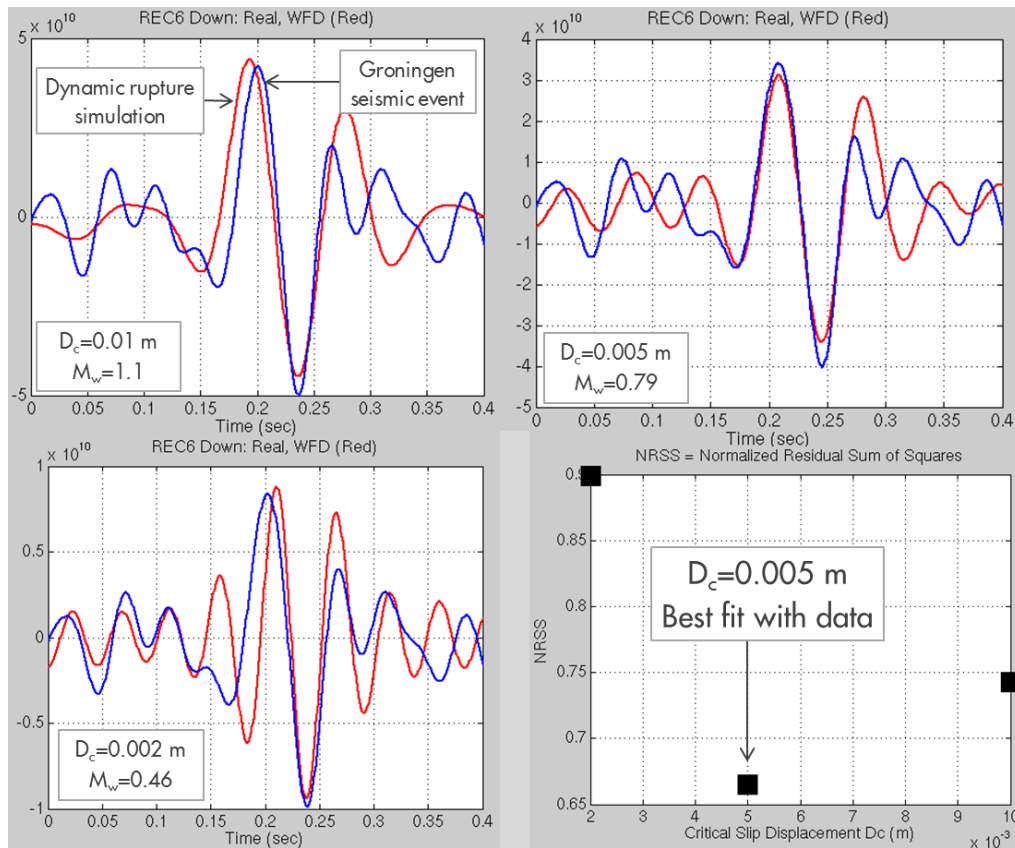


Figure A.17 Event 2014-04-22:03:14:10 ($M_L \sim 0.8$): windowed S arrival recorded by the deep downhole ZRP1 array (vertical component of receiver 6 with high signal-to-noise ratio). Waveform comparison between dynamic rupture simulation (red) and the actual Groningen seismic event (blue). Bottom-right: Smallest variance is found around a critical slip displacement $D_c = 0.005$ m

Identification of the three rupture mechanisms (section 0) in observed seismic events is a major challenge. Several issues need to be resolved before calibration of D_c from waveform data is proven and robust for a wider range of events.

Experimental and related results

As demonstrated by the dynamic rupture simulations described above (see Figs A.7 and A.9), characterization of fault strength and its evolution during fault slip is essential for understanding and modelling the response of faults to reservoir depletion, whether seismic or aseismic. Experimental efforts conducted at Utrecht University (UU) have focused on the determination of the (initial or static) friction coefficient of the frictional wear products, or fault gouge, generally found in upper crustal faults, and any (slip- or velocity-dependent) weakening behaviour as a result of slip. Post-slip healing (strength recovery) and its evolution upon reactivation has also been investigated. The rationale for investigating the frictional behaviour of fault gouge at the lab scale (using 1 mm thick by 45 mm x 35 mm layers of crushed Groningen core material) is based on surface field observations, which show that natural fault slip in reservoir systems is generally localised in narrow slip zones within a gouge-filled fault core (Figure A.18).

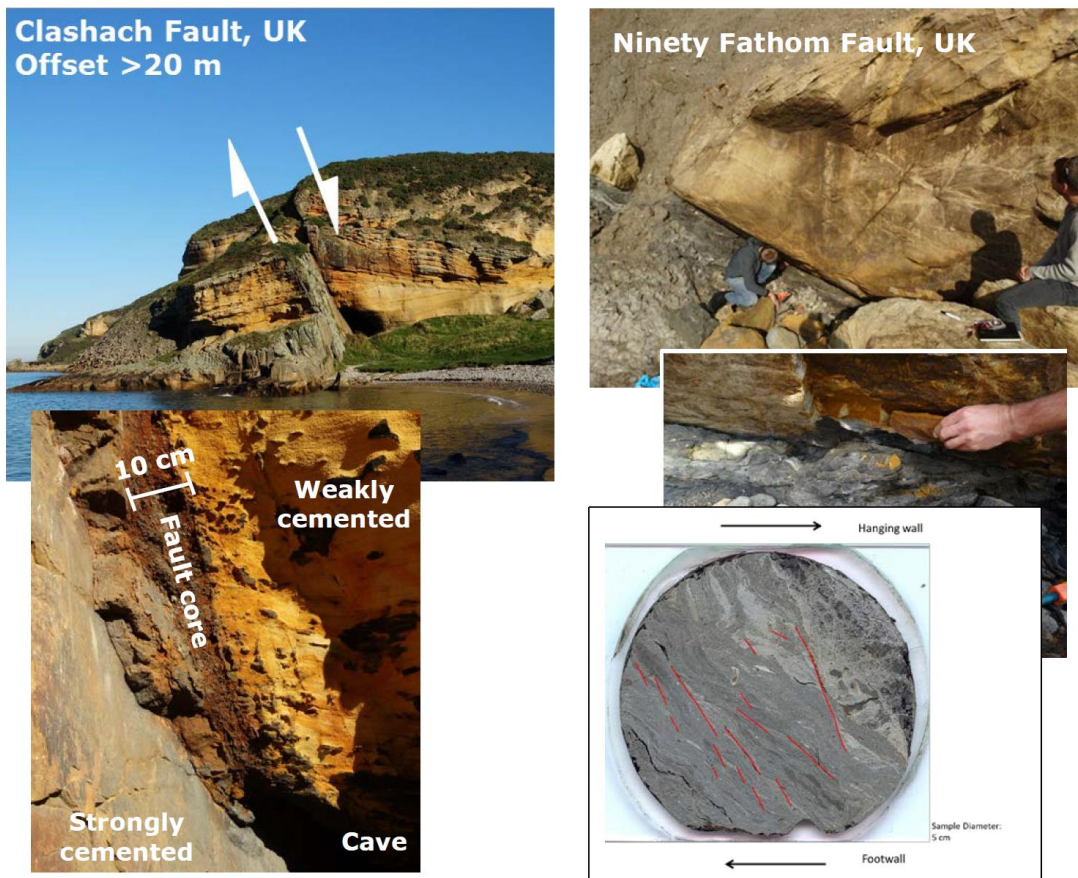


Figure A.18 *Field observations showing that natural fault slip in sandstone reservoir systems is generally localised in narrow slip zones within a gouge-filled fault core. Clashach Fault (Scotland) cuts lateral equivalent of Rotliegend sandstone. Ninety Fathom Fault (N.E. England) juxtaposes Rotliegend sandstone equivalent against grey Carboniferous shales and coals.*

To date, the so-called rate and state dependent frictional (RSF) behaviour of gouges, prepared from all four principal lithologies associated with the reservoir system (Basal Zechstein, Ten Boer Claystone, Slochteren Sandstone and Carboniferous shales/silts), has been fully characterized under reservoir stress, temperature and pore fluid pressure

conditions, employing pore fluids ranging from reservoir brine to methane. Slip velocities explored correspond to those associated with the onset of rupture nucleation. A key parameter in RSF laws for fault slip, the most widely used laws in modelling natural earthquake rupture (Marone, 1998), is the (a-b) parameter, which describes the velocity dependence of friction. A negative value of (a-b) is associated with velocity weakening material behaviour required to explain fault instability and nucleation of seismic events.

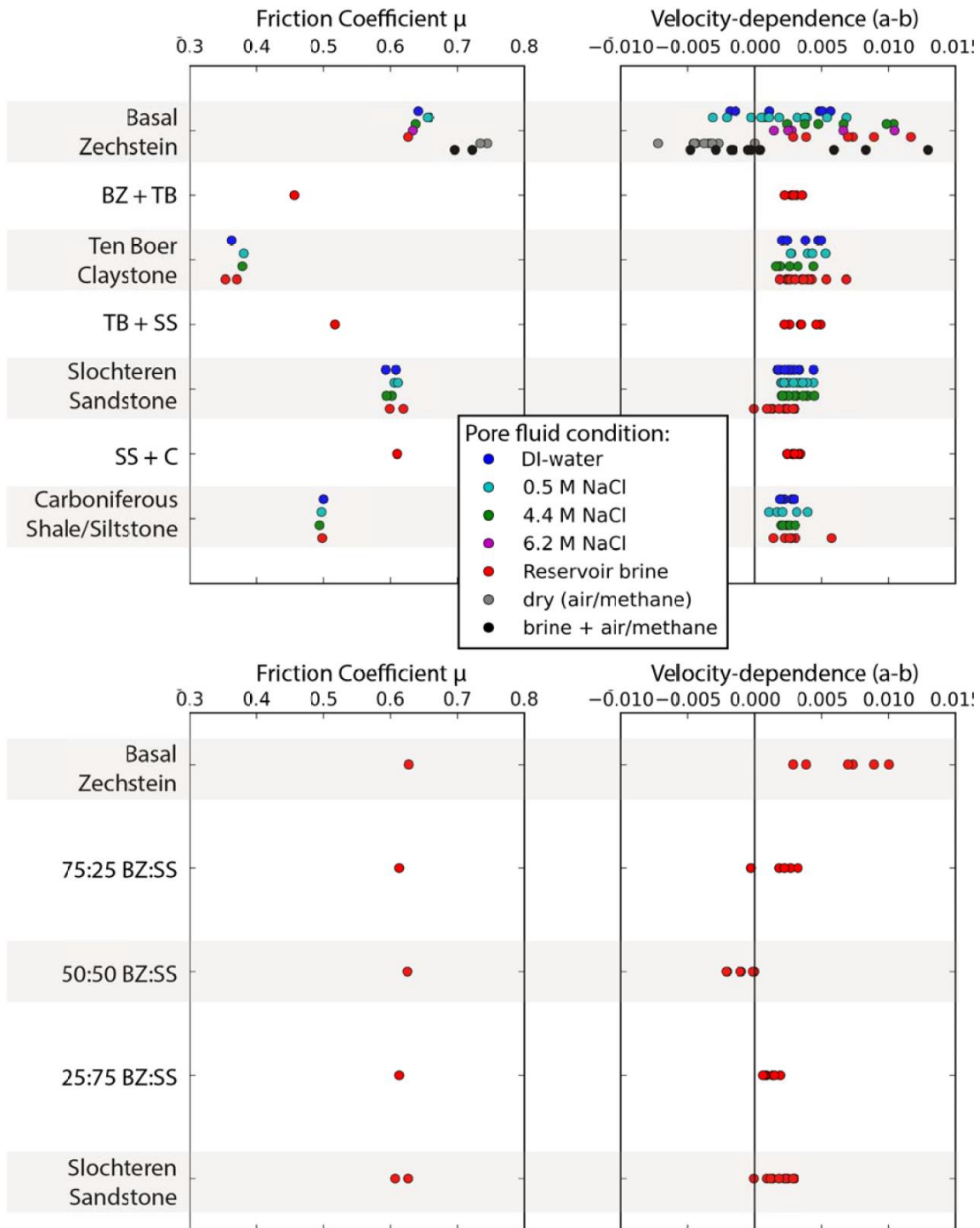


Figure A.19 The (initial or static) friction coefficient (left) and the (a-b) factor (right) measured for various mixtures and end-members of fault gouge material made from the stratigraphic elements in Groningen reservoir.

The experimental results so far, have demonstrated potentially seismogenic velocity weakening behaviour in Basal Zechstein gouges and in mixtures of Basal Zechstein with Slochteren Sandstone (Figure A.19). These respectively represent the gouge compositions expected in fault portions immediately above the reservoir and within the reservoir interval, where faults juxtapose and inter-mix (smear) the two formations. Experiments performed at decreasing slip rates further suggest that the even lower loading rate in the Groningen field may enhance velocity weakening and seismic event nucleation in the above gouge compositions. By contrast, gouges derived from the Slochteren Sandstone, Ten Boer Claystone and Carboniferous units, and smear-simulating mixtures of these, show no or little tendency for unstable velocity weakening, even towards the lowest slip rates explored. This may mean that seismic rupture nucleation purely within these units is dominated by a slip weakening component, caused by loss of cohesion from the static state, and possibly aided by minor thermal pressurization of the pore fluid due to frictional heating, or even weakening by local flash-heating (Figure A.20). The RSF parameters obtained for these materials offer important input for modelling stable slip (creep) on faults, and hence stress redistribution, during reservoir depletion. Dynamic slip weakening is currently being investigated via experiments in which fault gouge is allowed to heal under in-situ conditions for periods up to 3 months, to develop cohesion approaching that of gouge in natural static faults, followed by reactivation of slip. These show marked healing in Slochteren Sandstone and Basal Zechstein gouges (Figure A.21), but not in the Ten Boer or Carboniferous, pointing to significant potential for seismogenesis due to slip weakening in the former two units and their mixtures.

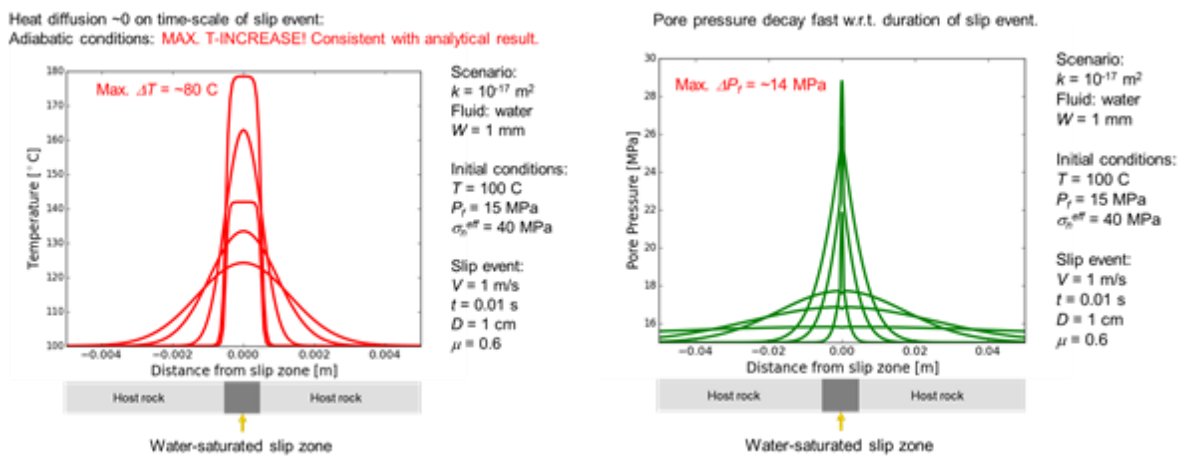


Figure A.20 Calculated thermal pulse and pressurization of the pore fluid due to frictional heating during seismic slip through a displacement of 1 cm, at a velocity of 1 m/s, on a 1 mm thick fault slip zone. Assumed rock/fluid properties appropriate for a gouge filled fault in the Slochteren reservoir under in situ conditions. Calculated using the model by Chen et al. (2013) following the broad approach of Rice (2006).

Integration of the experimental results, which are obtained on the mm to cm scale, into the dynamic rupture modelling that addresses the mechanics of failure on the 10 m scale, and on the 1m scale typical of the mesh dimension used in these models, is a significant challenge. The problem here is the mechanical heterogeneity caused by heterogeneities and irregularities in fault zone composition, internal structure and enveloping surface that occur in natural faults at the 0.1 to 100 m scale. One of the most important heterogeneities in faults in the Groningen field is the variation in fault rock composition that occur as individual faults transect and juxtapose the four reservoir and near-reservoir lithologies. The effects of lithology-related compositional variation and gouge smearing on base-level fault frictional (RSF) properties have already been addressed, to a substantial extent, via the experimental results illustrated in the mechanical stratigraphy presented in Fig. A.19.

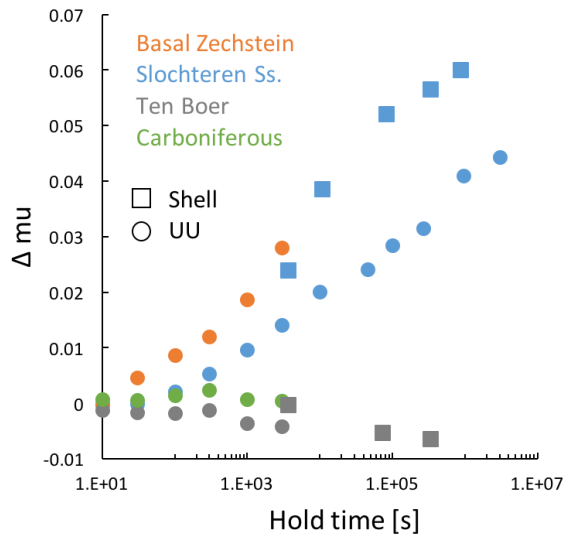


Figure A.21 Experimental results showing recovery of fault gouge frictional strength (healing $\Delta\mu$) versus log time in fault gouges prepared from Slochteren Sandstone and Basal Zechstein. Effect is absent in gouges prepared from the clay rich Ten Boer formation or Carboniferous underburden. Healing indicates potential for seismicogenesis due to slip weakening in the former two units and their mixtures

However, these data do not account for heterogeneity and anisotropy of frictional properties caused by irregular geometrical irregularities in internal and enveloping fault architecture. These factors are expected to play a role in both the occurrence and frequency of seismic events as well as their magnitude. Geometric irregularities and roughness in external fault zone form can be addressed at the 1-10 m scale and above by meshing the 2- or 3-D fault form accurately (as described in the foregoing sections), and by including inelastic deformation behaviour into the laws describing the mechanical behaviour of the wall rock “asperities” (a future target recently identified). Directly bridging the gap between the 50 mm lab scale and the 1-10 m or larger scales is an issue that remains an outstanding problem in modelling natural fault motion and seismicity. Barton and Bandis (1983) identified different scale dependent contributions to frictional resistance (Fig. A.22). This and similar concepts could help link the lab-measured friction data (e.g. Fig A.19), that seem most directly related to the base frictional component of Barton and Bandis (Fig. A.22) with the apparent friction simulated in our current geomechanical models and observed in the field. The search for quantitative upscaling rules based on such concepts is being pursued, in the present programme, by means of numerical modelling that aims to capture the mechanical effects of the anastomosing internal structure of gouge-rich shear bands, and intervening fragments, seen at all scales in both experimental and natural faults. The results points to a positive scaling relationship between slip weakening distance and fault segment length scale that should be useable in future rupture modelling. In addition, friction experiments have been performed, on 30-50 cm polymer blocks cut by gouge-filled faults, with scaled properties, to explore the effects of gouge compositional variations on unstable slip behaviour (Fig. A.23). Comparison with numerical rupture calculations shows broadly similar behaviour and is aimed at model validation.

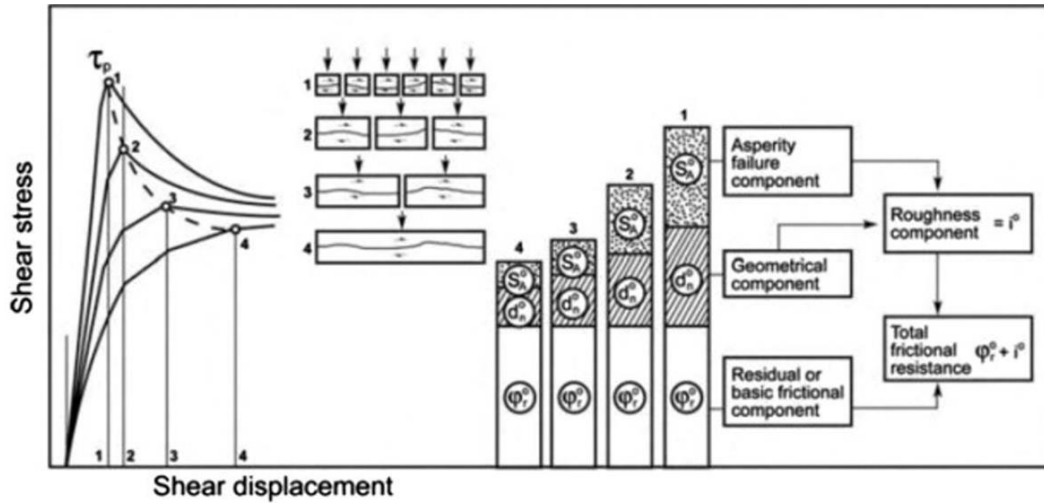


Figure A.22 The Barton & Bandis classification of frictional resistance

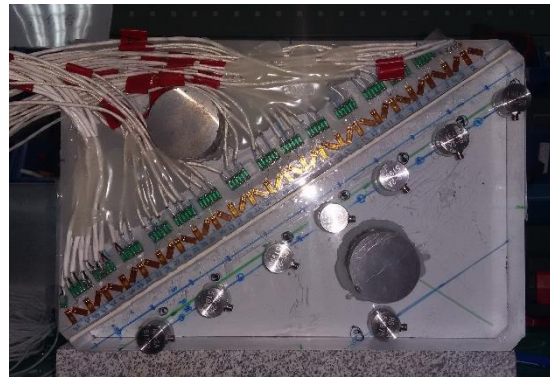
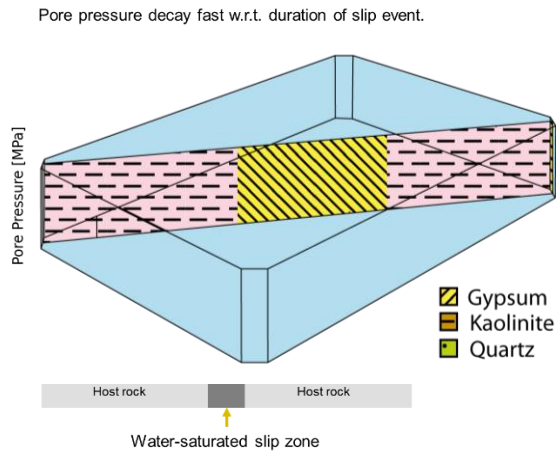


Figure A.23 Scale model experiments using 35-50 cm length scale samples to explore the effects of gouge compositional variations on unstable slip behaviour.

Experimental studies on the deformation behaviour of the Slochteren Sandstone, under simulated depletion and other triaxial test conditions, show significant inelastic deformation alongside conventional elastic behaviour. Inelastic strain increases with reservoir rock porosity and is characterised by a yield envelope that expands during triaxial compression and compaction (Fig A.24). This is expected to influence the partitioning of stored versus dissipated energy within the reservoir during on-going depletion, as well as the stress field in the neighbourhood of faults and the distribution of stress and energy dissipation associated with irregularities or asperities in fault geometry - thus affecting fault rupture. Work is in progress to incorporate such behaviour in the rupture modelling scheme.

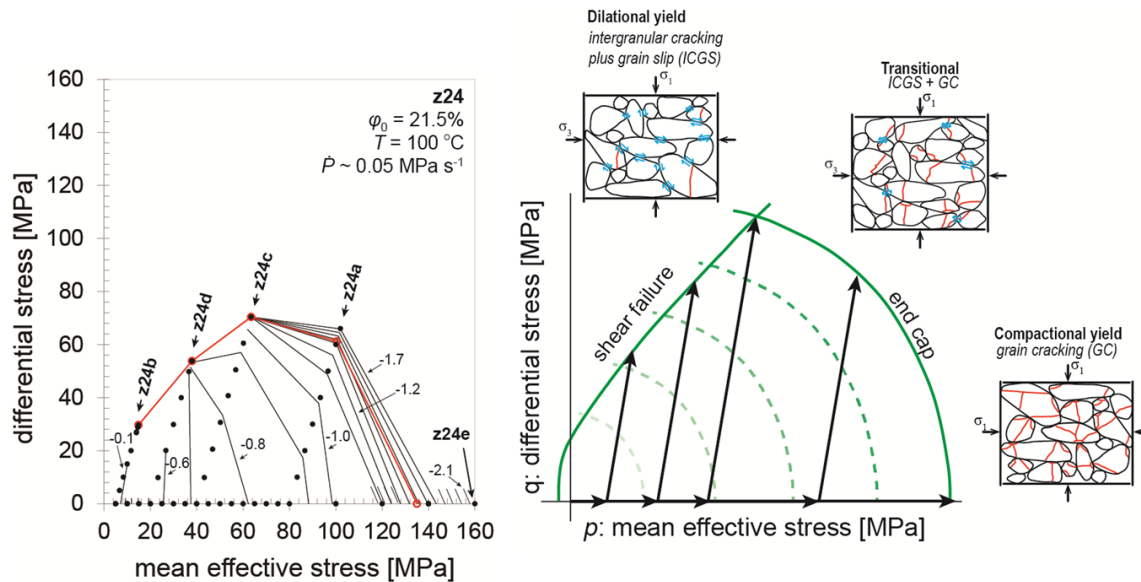


Figure A.24 Inelastic deformation behaviour recorded in triaxial compression tests on Slochteren Sandstone (initial porosity 21.5 %) showing expanding yield envelope with interpretation in right panel. The envelope expands from left to right with decreasing porosity and increasing strain.

Further steps

Significant progress has been made in geomechanical modelling of the rupture process, laboratory experiments measuring fault friction controlling rupture nucleation and geophysical interpretation of the seismic data obtained using the extended geophone and accelerometer network operated by KNMI and geophone arrays placed in deep wells over the reservoir section.

More and more, the results from these three study areas are informing each other. The experiments are progressing towards a constitutive model for fault and surrounding rock behaviour not only during rupture nucleation but during seismic slip, which can be incorporated in geomechanical models. The results from the geomechanical modelling can be compared with the geophysical field data. More integration and synthesis is required to obtain a fundamental understanding of the process inducing earthquakes in the Groningen field. However, promising results have been obtained and a foundation for progress established.

References

1. Buijze, L., Orlic, B., Wassing, B.B.T. (2015), Modelling fault rupture in a depleting gas field. Report TNO project report 2015 R10844, November 2015.
2. Chen, J., Yang, X., Duan, Q., Shimamoto, T., and Spiers, C.J. (2013), Importance of thermochemical pressurization in the dynamic weakening of the Longmenshan Fault during the 2008 Wenchuan earthquake: Inferences from experiments and modeling. *Journal of Geophysical Research: Solid Earth* 118, 4145-4169.
3. Glab, M. and Van Eijs, R. (2001), Localisation of Sensitive Reservoir Settings for Induced Seismicity using FEM, Report TNO-NITG 00-320-A
4. Marone, C.J. (1998), Laboratory-Derived Friction Laws and Their Application To Seismic Faulting. *Annual Review of Earth and Planetary Sciences*, 26(1), pp.643-696.
5. Mulders, F.M.M. (2003), Modeling of stress development and fault slip in and around producing gas reservoirs, Ph.D. thesis, Delft University of Technology
6. Orlic, B. and Wassing, B.B.T. (2012), Modeling stress development and fault slip in producing hydrocarbon reservoirs overlain by rock salt caprocks, ARMA 12-145, 46th US Rock Mechanics / Geomechanics Symposium, Chicago, IL, USA, 24-27 June 2012.

7. Rice, J. R. (2006), Heating and weakening of faults during earthquake slip, *J. Geophys. Res.*, 111, B05311, doi:10.1029/2005JB004006.
8. Roest, J.P.A., Kuilman, W. (1994), Geomechanical analysis of small earthquakes at the Eleveld gas reservoir. SPE 28097, SPE/ISRM Rock Mechanics in Petroleum Eng. Conference, Delft, The Netherlands, 29-31 August 1994.
9. Segall, P. (1989), Earthquakes triggered by fluid extraction. *Geology*, Vol. 17, pp.
10. Roest, J.P.A., Kuilman, W. (1994). Geomechanical analysis of small earthquakes at the Eleveld gas reservoir. SPE 28097, SPE/ISRM Rock Mechanics in Petroleum Eng. Conference, Delft, The Netherlands, 29-31 August 1994.
11. Uenishi, K., and J. R. Rice, (2003) Universal nucleation length for slip-weakening rupture instability under nonuniform fault loading, *J. Geophys. Res.*, 108(B1), 2042, doi:10.1029/2001JB00168.
12. Van den Bogert, P.A.J. (2015), Impact of various modelling options on the onset of fault slip and fault slip response using 2-dimensional Finite-Element Modelling. Report SR.15.11455, Shell Global Solutions International B.V.
13. Van den Bogert, P.A.J. (2017), Understanding fault stability and seismic rupture in depleting reservoirs with offset. Report SR.17.XXXXX, Shell Global Solutions International B.V. (IN PRESS)
14. Visser, C. (edt.), Groningen Field Review 2012, Static Modelling and Hydrocarbon Volume Determination, Document number: EP201203204663
15. World Stress Map Project, http://dc-app3-14.gfzpotdam.de/pub/introduction/introduction_frame.html
16. Zheng, Y. and Guises, R. (2014), Dynamic Geomechanical Modelling to Assess and Minimize the Risk of Fault Slip during reservoir depletion of the Groningen Field – 1D Geomechanical Model, Baker RDS NAM0001 Final Report.

Appendix B – List of Abbreviations

This list of abbreviations covers not only the abbreviations used in this document, but aims to include all abbreviations used in this dossier.

ALARA	As Low As Reasonably Achievable
ALARP	As Low As Reasonably Practicable
ARUP	Engineering Company named after founder: Ove Arup
Bcm	N.Bcm refers to a volume of a billion normal cubic meters. Normal means the volume is measured at a standard temperature (0 degree C) and pressure (1 bar)
BOA	Begeleidingscommissie Onderzoek Aardbevingen
CBS	Centraal Bureau Statistiek
CEA	China Earthquake Administration
CMI	Compaction Monitoring Instrument
CPT	Cone Penetration Test
CRR	Cyclic Resistance Ration (Liquefaction)
CSR	Cyclic Stress Ratio (Liquefaction)
CT	Coiled Tubing
CVW	Centrum Veilig Wonen
DAS	Distributed Acoustic Sensing
DLS	Damage Limit State
DS	Damage State
DSS	Distributed Strain Sensing
DTS	Distributed Temperature Sensing
EBN	Energy Beheer Nederland
EMS	European Macroseismic Scale
EU	European Union
EUCENTRE	European Centre for Training and Research in Earthquake Engineering
EZ	Ministerie van Economische Zaken
FEMA	Federal Emergency Management Agency (USA)
GPS	Global Positioning System
GR	Gamma-ray
GR	Group Risk
Gron	Groningen
FDSN	Federation of Digital Seismograph Networks
Frl	Friesland

GBB	Groninger Bodembeweging
GEM	Global Earthquake Model (Global Science Forum of the OECD)
GMPE	Ground Motion Prediction Equation
GMM	Ground Motion Model
GNSS	Global Navigation Satellite System
GPS	Global Positioning System
GR	Group Risk
GTS	Gas Transport Services B.V.
GWC	Gas water contact
F/N	Frequency / Number
HAZUS	US earthquake loss assessment models developed by FEMA
HRA	Hazard and Risk Assessment
HRBE	High Risk Building Element
IDR	Inter-storey Drift Ratio
ILPR	Inside Local Personal Risk
I&M	Ministerie van Infrastructuur en Milieu
IM	Intensity Measure
InSAR	Interferometric Synthetic Aperture Radar
KEM	Kennisplatform Effecten Mijnbouw
KNGMG	Koninklijk Nederlands Geologisch Mijnbouwkundig Genootschap
KNMI	Koninklijk Nederlands Meteorologisch Institute
KU Leuven	Katholieke Universiteit Leuven (Catholic University Leuven)
LIDAR	Laser Imaging Detection And Ranging
LOFAR	Low Frequency Array
LPI	Liquefaction Potential Index
LPI _{ISH}	Liquefaction Potential Index - Ishihara
LPR	Local Personal Risk
LNEC	Laboratorio Nacional de Engenharia Civil (Lisbon)
M	Earthquake Magnitude
M _L	Local Earthquake Magnitude
M/M _w	Moment magnitude
MDOF	Multiple Degree of Freedom System
MVR	Maatschappelijk Veiligheidsrisico
MASW	Multichannel Analysis of Surface Waves
MEA	Minister of Economic Affairs

MIT	Massachusetts Institute of Technology
MJP	Meerjaren Programma van de NCG
MSF	Magnitude Scaling Factor (Liquefaction)
NAM	Nederlandse Aardolie Maatschappij B.V.
NC	Near Collapse
NCG	Nationaal Coordinator Groningen
NEN	NEDerlandse Norm
NGO	Non-Governmental Organisation
NIED	National Research Institute for Earth Science and Disaster Resilience in Japan
NORSAR	Norwegian Seismic Array (Norwegian independent, not-for-profit, research foundation within the field of geo-science)
NPR	Nationale Praktijk Richtlijn
NTNU	Norges teknisk-naturvitenskapelige universitet (Norwegian University of Science and Technology in Trondheim)
NWO	Nederlandse Organisatie voor Wetenschappelijk Onderzoek (Netherlands Organisation for Scientific Research)
OGP	Onafhankelijk Geologen Platform
OIA	Objectgebonden Individueel Aardbevingsrisico (Object related individual earthquake risk)
OIR	Object-bound individual risk (same as OIA)
OLPR	Outside Local personal Risk
OVV	Onderzoeksraad voor Veiligheid (Safety Board)
PFA	Peak Floor Acceleration
PGA	Peak Ground Acceleration
PGV	Peak Ground Velocity
PNL	Pulsed Neutron log
PSHA	Probabilistic Seismic Hazard Assessment
PSHRA	Probabilistic Seismic Hazard and Risk Assessment
PS-InSAR	Persistent Scatterer Interferometric Synthetic Aperture Radar
QRM	Quantitative Reservoir Management
RFT	Repeat Formation Tester
RGR	Reference Group Risk
RIDR	Residual Inter-storey Drift Ratio
RIVM	Rijksinstitute voor Volksgezondheid en Milieu
RTCM	Rate-Type Compaction Model
RTCiM	Rate-Type Compaction isotach Model

RVS	Rapid Visual Screening
RUG	Rijksuniversiteit Groningen
SAC	Scientific Advisory Committee (Winningsplan 2016)
SBR	Stichting Bouw Research
SDOF	Single Degree of Freedom (System)
SED	Schweizerischer Erdbebendienst (Swiss Seismological Survey)
SINTEF	Stiftelsen for industriell og teknisk forskning (Foundation for Scientific and Industrial Research)
SMS	Stichting Mijnbouwschade
SodM	Staatstoezicht op de Mijnen (also SSM State Supervision of Mines)
SPTG	Static Pressure and Temperature Measurement
SSHAC	Senior Seismic Hazard Analysis Committee
TBO	Technische Begeleidingscommissie Ondergrond (Winningsplan 2013)
Tcbb	Technische commissie bodembeweging
TDT	Thermal Decay Time tool. A logging tool used in cased wells to measure water saturation in the reservoir.
TK	Tweede Kamer (Dutch equivalent of House of Commons)
TNO	Nederlandse Organisatie voor Toegepast Natuurwetenschappelijk Onderzoek, Netherlands Organisation for Applied Scientific Research
TNO-AGE	Nederlandse Organisatie voor Toegepast Natuurwetenschappelijk Onderzoek – Advies Groep Economische Zaken
TU Delft	Technische Universiteit Delft
ULS	Ultimate Limit State
UU	Universiteit Utrecht
URM	Un-reinforced Masonry
USGS	United States Geological Survey
USNRC	United States Nuclear Regulatory Commission

Appendix C – Complete Bibliography of Technical and Scientific Reports and Papers

a) Technical and Scientific Reports “Onderzoekrapporten”

December 2003

10. Winningsplan Groningen 2003, Nederlandse Aardolie Maatschappij BV, 19th December 2003.

May 2007

11. Update of the Winningsplan Groningen 2007, Nederlandse Aardolie Maatschappij BV, 31st May 2007.

December 2012

12. Letter Actualisation Winningsplan Groningen, Nederlandse Aardolie Maatschappij BV, 21st December 2012
13. Study and Data Acquisition Plan Induced Seismicity in Groningen, Nederlandse Aardolie Maatschappij BV, Jan van Elk & Dirk Doornhof, January 2013, submitted in November 2012.

December 2013

14. Winningsplan Groningen 2013, Nederlandse Aardolie Maatschappij BV, 29th November 2013.
15. Technical Addendum to the Winningsplan Groningen 2013; Subsidence, Induced Earthquakes and Seismic Hazard Analysis in the Groningen Field, Nederlandse Aardolie Maatschappij BV (Jan van Elk and Dirk Doornhof, eds), November 2013.
16. Supplementary Information to the Technical Addendum of the Winningsplan 2013, Nederlandse Aardolie Maatschappij BV (Jan van Elk and Dirk Doornhof, eds), December 2013.

September 2014

17. Voortgangsrapportage Diepe Geofoons, Nederlandse Aardolie Maatschappij BV, September 2014.

November 2014

18. Assessment for the Hazard Eemskanaal area of the Groningen field, Nederlandse Aardolie Maatschappij BV, November 2014.
19. Addendum to: Assessment for the Hazard Eemskanaal area of the Groningen field, Nederlandse Aardolie Maatschappij BV, November 2014.
20. Report on software verification against experimental benchmark data, Mosayk (F. Bianchi, R. Pinho), 16th November 2014.

December 2014

21. Study and Data Acquisition Plan Induced Seismicity in Groningen for the update of the Winningsplan 2016, Nederlandse Aardolie Maatschappij BV, Jan van Elk & Dirk Doornhof, December 2014, submitted in March 2015.
22. In-situ testing of URM houses (building unit: Loppersum, Zijlvest 25), Eucentre (F. Graziotti, A. Rossi, I. Senaldi, S. Peloso), 5th December 2014.

April 2015

23. Bierman, S, R. Paleja and M. Jones, Statistical methodology to test for evidence of seasonal variation in rates of earthquakes in the Groningen field, April 2015.

May 2015

24. Hazard and Risk Assessment for induced Seismicity Groningen, Part I Hazard Assessment, Nederlandse Aardolie Maatschappij BV (Jan van Elk and Dirk Doornhof, eds), 1st May 2015.
25. Hazard and Risk Assessment for induced Seismicity Groningen, Part II Risk Assessment, Nederlandse Aardolie Maatschappij BV (Jan van Elk and Dirk Doornhof, eds), 1st May 2015.
26. Meet- en Regel Protocol - mei 2015, Nederlandse Aardolie Maatschappij BV, 1st May 2015.
27. Risk Methodology; Back to the region, February 2015, Nederlandse Aardolie Maatschappij BV, (forwarded to the national committee on earth quake related risks in April 2015) (EP 201504200668).

June 2015

28. A re-estimate of the earthquake hypo-centre locations in the Groningen Gas Field, Matt Pickering, March 2015.
29. De ondergrond van Groningen: een Geologische Geschiedenis, Erik Meijles, April 2015.
30. Development of Version 1 GMPEs for Response Spectral Accelerations and for Strong-Motion Durations, Julian J Bommer, Peter J Stafford, Benjamin Edwards, Michail Ntinalexis, Bernard Dost and Dirk Kraaijpoel, March 2015.
31. Geological schematisation of the shallow subsurface of Groningen (For site response to earthquakes for the Groningen gas field) – Part I, Deltares, Pauline Kruiver, Ger de Lange, Ane Wiersma, Piet Meijers, Mandy Korff, Jan Peeters, Jan Stafleu, Ronald Harting, Roula Dambrink, Freek Busschers, Jan Gunnink
32. Geological schematisation of the shallow subsurface of Groningen (For site response to earthquakes for the Groningen gas field) – Part II, Deltares, Pauline Kruiver, Ger de Lange, Ane Wiersma, Piet Meijers, Mandy Korff, Jan Peeters, Jan Stafleu, Ronald Harting, Roula Dambrink, Freek Busschers, Jan Gunnink
33. Geological schematisation of the shallow subsurface of Groningen (For site response to earthquakes for the Groningen gas field) – Part III, Deltares, Pauline Kruiver, Ger de Lange, Ane Wiersma, Piet Meijers, Mandy Korff, Jan Peeters, Jan Stafleu, Ronald Harting, Roula Dambrink, Freek Busschers, Jan Gunnink
34. URM Modelling and Analysis Cross Validation – Arup, Eucentre, TU Delft, Reference 229746_032.0_REP127_Rev.0.03 April 2015.
35. In-situ compaction measurements using gamma ray markers, Pepijn Kole, June 2015
36. Meet- en Regel Protocol – juni 2015, Nederlandse Aardolie Maatschappij BV, June 2015.
37. Voortgangsrapportage Diepe Geofoons, Nederlandse Aardolie Maatschappij BV, June 2015.

July 2015

38. An activity rate model of induced seismicity within the Groningen Field, (Part 1), Stephen Bourne and Steve Oates, February 2015.
39. An activity rate model of induced seismicity within the Groningen Field, (Part 2), Stephen Bourne and Steve Oates, June 2015.

August 2015

40. Regularised direct inversion to compaction in the Groningen reservoir using measurements from optical levelling campaigns, S.M. Bierman, F. Kraaijeveld and S.J. Bourne, March 2015.
41. Impact of various modelling options on the onset of fault slip and fault slip response using 2-dimensional Finite-Element modelling, Peter van den Bogert, July 2015

42. Computing the Distribution of Pareto Sums using Laplace Transformation and Stehfest Inversion Break, C. K. Harris and S. J. Bourne, May 2015.

November 2015

43. Hazard and Risk Assessment for Induced Seismicity in Groningen Interim Update November 2015, Nederlandse Aardolie Maatschappij BV (Jan van Elk and Dirk Doornhof, eds), 1st November 2015.
44. Development of v2 fragility and consequence functions for the Groningen Field, H. Crowley, R. Pinho, B. Polidoro, P. Stafford, October 2015.
45. Development of Version 2 GMPEs for Response Spectral Accelerations and Significant Durations for Induced Earthquakes in the Groningen field, Julian J Bommer, Bernard Dost, Benjamin Edwards, Pauline P Kruiver, Piet Meijers, Michail Ntinalexis, Barbara Polidoro, Adrian Rodriguez-Marek & Peter J Stafford, October 2015
46. Eucentre Shake-table Test of Terraced House Modelling Predictions and Analysis Cross Validation, staff from ARUP, Eucentre (Pavia) and TU Delft, November 2015 [this document also includes; (1) Instruments full-scale test-house Eucentre Laboratory, (2) Protocol for Shaking Table Test on Full Scale Building (Eucentre) V_1, and (3) Selection of Acceleration Time-Series for Shake Table Testing of Groningen Masonry Building at the EUCENTRE, Pavia, all three by staff from Eucentre (Pavia)],
47. Induced seismicity in the Groningen field - statistical assessment of tremors along faults in a compacting reservoir, Rick Wentinck, July 2015.
48. Report on soil-structure interaction (SSI) impedance functions for SDOF systems, Mosayk (R. Nascimbene, R. Pinho, H. Crowley), 20th October 2015.
49. Report on structural modelling of non-URM buildings, Mosayk (H. Crowley, F. Bianchi, D. Cicola, R. Nascimbene, R. Pinho), 22nd October 2015.
50. Cyclic testing of precast panel connections for RC precast wall-slab-wall structures representative of the Groningen building stock. Eucentre (E. Brunesi, R. Nascimbene), 22nd October 2015.

December 2015

51. Summary report for the characterisation of original Groningen masonry, TU Delft (S. Safari, J. Rots), 18th December 2015.

January 2016

52. Neotectonic Stresses in the Permian Slochteren Formation of the Groningen Field, Rob van Eijs, November 2015.

February 2016

53. Groningen Pressure Maintenance (GPM) Study, Progress Report February 2016, Richard Hofmann and team, February 2016.
54. Groningen 2.0 Screening Study Alternatives to the base case approach of NAM to maintain pressure in the Groningen reservoir by nitrogen injection, with a focus on surface measures, Summary Report prepared by the Steering Committee, Chairman Prof. Dr W.C. Turkenburg Final Report February 2015.
55. Laboratory component testing: Modelling post-test predictions and analysis cross-validation, ARUP, TU Delft and Eucentre (several staff members from all three institutions), 16th February 2016.

March 2016

56. Terp composition in respect to earthquake risk in Groningen, Dr. ir. E.W. Meijles, Dr. G. Aalbersberg and Prof. Dr. H.A. Groenendijk, March 2016.

57. Unbiased Cyclic Resistance Ratio Relationships for Evaluating Liquefaction Potential in Groningen, Russell Green, Adrian Rodriguez-Marek, Peter Stafford, Julian Bommer, April 2016.
58. Risk Assessment of Falling Hazards in Earthquakes in the Groningen region, Tony Taig and Florence Pickup (TTAC Ltd.), March 2016.
59. Risk Assessment of Falling Hazards in Earthquakes in the Groningen region (Appendices), Tony Taig and Florence Pickup (TTAC Ltd.), March 2016.
60. Groningen 2015 Geomechanical Analysis, Suvrat P. Lele, Jorge L. Garzon, Sheng-Yuan Hsu, Nora L. DeDontney, Kevin H. Searles and Pablo F. Sanz (ExxonMobil Upstream Research Company, Spring, TX), March 2016.

April 2016

61. Winningsplan Groningen 2016, Nederlandse Aardolie Maatschappij BV, 1st April 2016.
62. Technical Addendum to the Winningsplan Groningen 2016 - Production, Subsidence, Induced Earthquakes and Seismic Hazard and Risk Assessment in the Groningen Field, PART I – Summary and Production, Nederlandse Aardolie Maatschappij BV (Jan van Elk and Dirk Doornhof, eds), 1st April 2016.
63. Technical Addendum to the Winningsplan Groningen 2016 - Production, Subsidence, Induced Earthquakes and Seismic Hazard and Risk Assessment in the Groningen Field, PART II - Subsidence, Nederlandse Aardolie Maatschappij BV (Jan van Elk and Dirk Doornhof, eds), 1st April 2016.
64. Technical Addendum to the Winningsplan Groningen 2016 - Production, Subsidence, Induced Earthquakes and Seismic Hazard and Risk Assessment in the Groningen Field, PART III - Hazard Assessment, Nederlandse Aardolie Maatschappij BV (Jan van Elk and Dirk Doornhof, eds), 1st April 2016.
65. Technical Addendum to the Winningsplan Groningen 2016 - Production, Subsidence, Induced Earthquakes and Seismic Hazard and Risk Assessment in the Groningen Field, PART IV - Risk Assessment, Nederlandse Aardolie Maatschappij BV (Jan van Elk and Dirk Doornhof, eds), 1st April 2016.
66. Technical Addendum to the Winningsplan Groningen 2016 - Production, Subsidence, Induced Earthquakes and Seismic Hazard and Risk Assessment in the Groningen Field, PART V - Damage and Appendices, Nederlandse Aardolie Maatschappij BV (Jan van Elk and Dirk Doornhof, eds), 1st April 2016.
67. Technisch addendum bij Winningsplan Groningen 2016 - Productie, bodemdaling, geïnduceerde bevingen en seismische dreiging en risicobeoordeling van het winningsveld in Groningen, DEEL I – Samenvatting en Productie, Nederlandse Aardolie Maatschappij BV (Jan van Elk and Dirk Doornhof, eds), 1st April 2016.
68. Technisch addendum bij Winningsplan Groningen 2016 - Productie, bodemdaling, geïnduceerde bevingen en seismische dreiging en risicobeoordeling van het winningsveld in Groningen, DEEL II - Bodemdaling, Nederlandse Aardolie Maatschappij BV (Jan van Elk and Dirk Doornhof, eds), 1st April 2016.
69. Technisch addendum bij Winningsplan Groningen 2016 - Productie, bodemdaling, geïnduceerde bevingen en seismische dreiging en risicobeoordeling van het winningsveld in Groningen, DEEL III - Dreigingsanalyse, Nederlandse Aardolie Maatschappij BV (Jan van Elk and Dirk Doornhof, eds), 1st April 2016.
70. Technisch addendum bij Winningsplan Groningen 2016 - Productie, bodemdaling, geïnduceerde bevingen en seismische dreiging en risicobeoordeling van het winningsveld in Groningen, DEEL IV – Risico Analyse, Nederlandse Aardolie Maatschappij BV (Jan van Elk and Dirk Doornhof, eds), 1st April 2016.
71. Technisch addendum bij Winningsplan Groningen 2016 - Productie, bodemdaling, geïnduceerde bevingen en seismische dreiging en risicobeoordeling van het winningsveld in Groningen, DEEL V - Schade en Bijlagen, Nederlandse Aardolie Maatschappij BV (Jan van Elk and Dirk Doornhof, eds), 1st April 2016.
72. Supplement to the Technical Addendum for Winningsplan Groningen 2016, Subsidence Development of Seismicity Maatschappelijk Veiligheidsrisico Epistemic Uncertainties, Nederlandse Aardolie Maatschappij BV (Jan van Elk and Dirk Doornhof, eds), 1st May 2016.
73. Study and Data Acquisition Plan Induced Seismicity in Groningen Update Post-Winningsplan 2016 -Part 1, Nederlandse Aardolie Maatschappij BV (Jan van Elk and Dirk Doornhof, eds), 1st April 2016.

74. Study and Data Acquisition Plan Induced Seismicity in Groningen Update Post-Winningsplan 2016 -Part 2, Nederlandse Aardolie Maatschappij BV (Jan van Elk and Dirk Doornhof, eds), 1st April 2016.
75. Oplegnotitie Winningsplan Groningen-gasveld 2016, Nederlandse Aardolie Maatschappij BV, 1st April 2016.
76. Meet- en Regelprotocol 2016 Nederlandse Aardolie Maatschappij BV, 1st April 2016.
77. Gravity monitoring of the Groningen gas field 2015, Quad Geometrics, Ola Eiken, April, 2016.

May 2016

78. Unbiased Cyclic Resistance Ratio Relationships for Evaluating Liquefaction Potential in Groningen, Russell Green, Adrian Rodriguez-Marek, Peter Stafford, Julian Bommer, April 2016.
79. Geometric characteristic study of current building selection for numerical modelling, Arup (A. Christodoulou), 13th April 2016.
80. Tests for the characterisation of replicated masonry and wall ties, TU Delft (R. Esposito, F. Messali, J. Rots), 18th April 2016.
81. In-plane tests of replicated masonry walls, TU Delft (G. Ravenshorst, F. Messali), 18th April 2016.
82. Induced seismicity in the Groningen field - second statistical assessment of tremors along faults in a compacting reservoir, Rick M. Wentinck, May 2016.

June 2016

83. Measuring changes in earthquake occurrence rates in Groningen – Update October 2016, Shell Statistics Group, Rakesh Paleja and Stijn Bierman, October 2016.
84. Meet en Regel Rapportage , NAM, June 2016.
85. Modifications of the Geological model for Site response at the Groningen field, Deltares, Pauline Kruiver, Ger de Lange, Ane Wiersma, Piet Meijers, Mandy Korff, Jan Peeters, Jan Stafleu, Ronald Harting, Roula Dambrink, Freek Busschers, Jan Gunnink
86. Experimental campaign on cavity walls systems representative of the Groningen building stock (incl. EUC-BUILD1), Eucentre (F. Graziotti, U. Tomassetti, A. Rossi, S. Kallioras, M. Mandirola, E. Cenja, A. Penna, G. Magenes), 16th June 2016.

July 2016

87. Report on Mmax Expert Workshop, Mmax panel chairman Kevin Coppersmith, June 2016
88. Geomechanical Round Table Workshop Report (Groningen Pressure Maintenance), Panel chairman Georg Dresen, June 2016
89. Groningen Field Review 2015 Subsurface Dynamic Modelling Report, Burkitov, Ulan, Van Oeveren, Henk, Valvatne, Per, May 2016.
90. Human induced Earthquakes, Gillian Foulger, Miles Wilson, Jon Gluyas and Richard Davies, Durham University and Newcastle University, July 2016.
91. Independent Review of Groningen Subsurface Modelling Update for Winningsplan 2016, SGS Horizon, July 2016.
92. Local and Moment Magnitudes in the Groningen Field, Bernard Dost, Ben Edwards and Julian J Bommer, March 2016.
93. Material Characterisation – Version 1.3, Eucentre, P&P, TU-Delft, TU-Eindhoven, October 2015.
94. Geophysical Measurements of shear wave velocity at KNMI accelerograph stations in the Groningen field area, Deltares, Marco de Kleine, Rik Noorlandt, Ger de Lange, Marios Karaoulis and Pauline Kruiver, July 2016.
95. Maximum magnitude from induced earthquakes in the Groningen field, Nora Dedontney et al., Exxonmobil Upstream Research Company, July 2016

96. Summary and discussion of software benchmarking for Groningen PSHRA code, Stephen Bourne and Steve Oates, April 2016.
97. A Database of Damaging Earthquakes of Moment Magnitude from 4.0 to 5.5, Cecilia Ines, Helen Crowley, Michail Ntinalexis and Julian Bommer, July 2016.
98. Validation booklet for LS-Dyna, Report n. 229746_031.0_REP1020, ARUP (several staff members), 1st July 2016.
99. Experimental campaign on a clay URM full-scale specimen representative of the Groningen building stock (EUC-BUILD2), Eucentre (F. Graziotti, U. Tomassetti, A. Rossi, B. Marchesi, S. Kallioras, M. Mandirola, A. Fragomeli, E. Mellia, S. Peloso, F. Cuppari, G. Guerrini, A. Penna, G. Magenes, G), 20th July 2016.

September 2016

100. EUC-BUILD2: Modelling predictions and analysis cross-validation of detached single-storey URM Building, ARUP, TU Delft, Eucentre and Arcadis (several staff members from all four institutions), 30th September 2016.

October 2016

101. Measuring changes in earthquake occurrence rates in Groningen – Update October 2016, Shell Statistics Group, Rakesh Paleja and Stijn Bierman, October 2016.
102. Structural behaviour of calcium-silicate brick masonry assemblage: quasi-static cyclic pushover and dynamic identification test, TU Delft (G. Ravenshorst, R. Esposito, R. Schipper, F. Messali, A. Tsouvalas, E.-M. Lourens, J. Rots), 21st October 2016.

November 2016

103. Liquefaction sensitivity of the shallow subsurface of Groningen, Deltares, November 2016
104. On the implementation of sedimentological data in Pososoty Modelling for the Groningen field, Clemens Visser, Richard Porter and Jose Solano Viota, November 2016
105. Empirical Ground-Motion Prediction Equations for Peak Ground Velocity from Small-Magnitude earthquakes in the Groningen field using multiple definitions for the Horizontal Component of Motion, Julian Bommer, Peter Stafford and Michail Ntinalexis, November 2016
106. Gaswinning Groningen Analyses van de ontwikkeling van seismiciteit en van de voorgestelde beheersmaatregelen, rapportage periode mei 2016 – september 2016, NAM, November 2016

December 2016

107. TNO rapport, Monitoring Network Building Vibrations - Analysis Earthquakes in 2014 and 2015, ir. H. Borsje, ir. J.P. Pruiksmas and ir. S.A.J. de Rlichemont TNO 2016 R11323/A, December 2016
108. TNO Monitoringsnetwerk gebouwentrillingen – Analyse aardbevingen 2014 tot 2015, ir. H. Borsje, ir. J.P. Pruiksmas and ir. S.A.J. de Rlichemont TNO 2016 R11323/A, December 2016
109. Study and Data Acquisition Plan Induced Seismicity in Groningen Update Post-Winningsplan 2016 - Progress and Schedule, Nederlandse Aardolie Maatschappij BV (Jan van Elk and Dirk Doornhof, eds), 1st December 2016.
110. Subsidence inversion on Groningen using leveling data only, Nederlandse Aardolie Maatschappij BV (Onno van der Wal, Rob van Eijs), December 2016.
111. EUC-BUILD-3 Prototype building description, 229746_031_NOT2007_Rev0.06_Issue, Arup (several staff members), 21st December 2016.
112. Using the Applied Element Method to model in-plane cyclic shear-compression testing of URM walls, Mosayk (D. Malomo, R. Pinho), 22nd December 2016.

January 2017

- 113. Exposure Database: V3 Post-analysis report, 229746_031.0_REP1011_Rev0.03_ISSUE, Arup (several staff members), 25th January 2017.
- 114. Petrographic study of well Zeerijp-3A (ZRP-3A) Final Report, Panterra Consultants, November 2016.
- 115. Petrographic Aspects of the Rotliegend of the Groningen field Inventory and quick-look analysis of petrographic data from the Groningen field, Nederlandse Aardolie Maatschappij BV (Clemens Visser), November 2016
- 116. Methodology Prognosis of Building Damage and Study and Data Acquisition Plan for Building Damage, Nederlandse Aardolie Maatschappij BV, Jan van Elk, Jeroen Uilenreef and Dirk Doornhof, February 2017

January 2017

- 117. Exposure Database: V3 Post-analysis report, 229746_031.0_REP1011_Rev0.03_ISSUE, Arup (several staff members), 25th January 2017.

February 2017

- 118. Harkstede 2A microseismic monitoring summary, Jelena Tomic, NAM, February 2017
- 119. EUC-BUILD-4 Prototype building description, 229746_031_NOT2008_Rev0.05_Issue, Arup (several staff members), 9th February 2017.

March 2017

- 120. Wat gebeurt er met het Flexibele Geofoon Netwerk?, Stand van zake 1 maart 2017, Nederlandse Aardolie Maatschappij BV, February 2017, Jan van Elk & Dirk Doornhof
- 121. Rapportage recente aardbevingen Wirdum en Garsthuizen 2016/2017, NAM, March 2017

April 2017

- 122. Monitoring Reservoir Pressure in the Groningen gasfield, Leendert Geurtsen, en Quint de Zeeuw, NAM, April 2017

May 2017

- 123. Cyclic testing of RC tunnel building (EUC-BUILD3), Eucentre (E. Brunesi, S. Peloso, R. Pinho, R. Nascimbene), 8th May 2017.

June 2017

- 124. Cyclic testing of RC precast building (EUC-BUILD4), Eucentre (E. Brunesi, S. Peloso, R. Pinho, R. Nascimbene), 22nd June 2017.
- 125. V4 Ground-motion Model (GMM) for Response Spectral Accelerations, Peak Ground Velocity and Significant Duration in the Groningen field, Julian Bommer, Bernard Dost, Benjamin Edwards, Pauline Kruiver, Pier Meijers, Michail Ntinalexis, Adrian Rodriguez-Marek, Elmer Ruigrok, Jesper Spetzler and Peter Stafford, Independent Consultants, Deltares and KNMI, June 2017 with Parameter files - V4 Ground-Motion Model (GMM) for Response Spectral Accelerations, Peak Ground Velocity, and Significant Durations in the Groningen Field, Supplement to V4 GMM, Julian Bommer and Peter Stafford, Independent Consultants, June 2017
- 126. Methodology - Optimisation of the Production Distribution over the Groningen field to reduce Seismicity, NAM, June 2017

- 127. Ground Motions from the ML 2.6 Slochteren Earthquake of 27th May 2017, Julian J Bommer, Michail Ntinalexis, Ewoud van Dedem, Jelena Tomic, Leendert Geurtsen and Jeroen Uilenreef, June 2017
- 128. Fault interpretation of the Groningen area supra-Zechstein Overburden, T. Logeman, NAM, June 2017.
- 129. Seismic interpretation and depth conversion of Top Carboniferous in the Groningen field, northeast Netherlands, B. van Assema, NAM, June 2017.
- 130. Trillingsschade aan gebouwen, Informatiedocument – versie 1.0, NAM, June 2017.
- 131. Production stand-by of the Loppersum clusters for Security of Supply (waakvlam), NAM, June 2017.
- 132. Meet- en Regelprotocol Groningen veld, NAM, June 2017
- 133. Measurement and Control protocol Groningen field, NAM, June 2017
- 134. Appendix bij het Meet- en Regelprotocol Groningen – Cases, NAM, June 2017
- 135. Appendix to the Measurement and Control protocol Groningen – Cases, NAM, June 2017
- 136. Technisch Addendum bij het Meet- en Regelprotocol Groningen, NAM, June 2017
- 137. Technical Addendum to the Meet-en Regel Protocol Groningen, NAM, June 2017

July 2017

- 138. Are Love- and Rayleigh seismic waves detectable in Groningen?, Jelena Tomic, NAM, June 2017
- 139. Production stand-by of the Loppersum clusters for Security of Supply (waakvlam), NAM, June 2017

August 2017

- 140. Trillingsschade aan gebouwen, Informatiedocument – versie 1.0, NAM, June 2017
- 141. Special Report on the earthquake density and activity rate following the earthquake in Appingedam ($M_L=1.8$) and Scharmer ($M_L=1.5$) in August 2017, NAM, Jan van Elk and Dirk Doornhof, September 2017

September 2017

- 142. Collapse shake-table testing of terraced house (LNEC-BUILD1), Eucentre and LNEC (U. Tomassetti, A. A. Correia, F. Graziotti, A.I. Marques, M. Mandirola, P.X. Candeias), 1st September 2017.
- 143. LNEC-BUILD1: Modelling predictions and analysis cross-validation, ARUP, TU Delft, Eucentre and Mosayk (several staff members from all four institutions), 8th September 2017.
- 144. Groningen 1978-2015 time-lapse gravity surveys results interpretation and scenario testing, M. Glegola, H. van Oeveren, L. Geurtsen, P. Valvatne, NAM, September 2017.

October 2017

- 145. Induces Seismicity in Groningen – Assessment of Hazard, Building Damage and Risk, NAM, Jan van Elk and Dork Doornhof, NAM, November 2017
- 146. DeepNL: Het Contract tussen NWO and NAM, NOW and NAM, October 2017.
- 147. Assessment of Dynamic Properties for Peat – Factual Report, Deltares, dr.ir. C. Zwanenburg and M. Konstantinou, Deltares, October 2017
- 148. Dynamic behaviour of Groningen peat - Analysis and parameter assessment, M. Konstantinou, dr.ir. C. Zwanenburg and dr.ir. P. Meijers, deltares, October 2017

November 2017

- 149. V5 Ground-Motion Model for the Groningen Field, J.J. Bommer, B. Edwards, P.P. Kruiver, A. Rodriguez-Marek, P.J. Stafford, B. Dost, M. Ntinalexis, E. Ruigrok, J. Spetzler, 30th October 2017.

150. Report on the v5 fragility and consequence models for the Groningen Field, H. Crowley and R. Pinho, 31st October 2017.
151. Rapportage Seismiciteit Groningen - 1 november 2017, NAM, November 2017.
152. Empirical Ground-Motion Prediction Equations for Peak Ground Velocity from Small-Magnitude Earthquakes in the Groningen Field Using Multiple Definitions of the Horizontal Component of Motion - Updated Model for Application to Smaller Earthquakes, Julian Bommer, Peter Stafford and Michail Ntinalexis, November 2017
153. Using the Applied Element Method to model the shake-table testing of two full-scale URM houses (EUC-BUILD1 and EUC-BUILD2), Mosayk (D. Malomo, R. Pinho), 31st October 2017.
154. Using the Applied Element Method to model the collapse shake-table testing of a URM cavity wall structure (LNEC-BUILD1), Mosayk (D. Malomo, R. Pinho), 31st October 2017.
155. Shake-table test up to collapse on a roof substructure of a Dutch terraced house (LNEC-BUILD2), Eucentre and LNEC (A.A. Correia, A.I. Marques, V. Bernardo, L. Grottoli, U. Tomassetti, F. Graziotti), 31st October 2017.
156. Using the Applied Element Method to model the collapse shake-table testing of a terraced house roof substructure (LNEC-BUILD2), Mosayk (D. Malomo, R. Pinho), 31st October 2017.
157. Shake-table testing of RC precast building (EUC-BUILD5), Eucentre (E. Brunesi, S. Peloso, R. Pinho, R. Nascimbene), 31st October 2017.
158. Nonlinear dynamic analysis of index buildings for v5 fragility and consequence models, Mosayk (R. Pinho, D. Malomo, E. Brunesi, H. Crowley), 31st October 2017.
159. Tests on URM clay and calcium-silicate masonry structures: identification of damage limit states, Eucentre (F. Graziotti, U. Tomassetti, A. Penna, G. Magenes), Working Version, 31st October 2017.
160. Out-of-plane two-way bending shaking table tests on single leaf and cavity walls, Eucentre (F. Graziotti, U. Tomassetti, S. Sharma, L. Grottoli, S. Dainotti, S. Scherini, A. Penna, G. Magenes), Working Version, 31st October 2017.
161. Using the Applied Element Method to model URM walls subjected to out-of-plane shake-table testing, Mosayk (D. Malomo, P. Comini, R. Pinho), 31st October 2017.
162. Typology Modelling: Analysis Results in Support of Fragility Functions – 2017 Batch Results, 229746_031.0_REP2005, Arup (several staff members), November 2017.
163. EDB V5 Data documentation, 229746_052.0_REP2014, Arup (several staff members), November 2017.
164. EDB V5 Post-Analysis Documentation, 229746_052.0_REP2018c, Arup (several staff members), November 2017.

b) Papers in Peer-reviewed Journals

1) Introduction

Much of the novel research done on induced seismicity in Groningen as part of the program led by NAM, is documented in detailed reports available at the NAM website and published in peer-reviewed journals. Publication in peer-reviewed journal provides additional assurance that the research is original and scientifically sound. These papers are published in reputable scientific journals with editorial boards consisting of highly respected experts recognised in their field.

A list of the most prestigious journals is the “master journals list”, which can be found using this link (<http://ip-science.thomsonreuters.com/mjl/>). The journal impact factor can be found in journal citation reports. For the 2016 citation report follow this link (<http://scientific.thomsonreuters.com/imgblast/JCRFullCovlist-2016.pdf>). This is a subscription based service.

An alternative ranked list of the most respected journals is the SCImago Journal & Country Ranking. This is a publicly available portal, available through the following link: <http://www.scimagojr.com/index.php>. It provides a size-independent indicator of scientific journal prestige, the SJR indicator.

Many of the papers on the Groningen earthquakes have been published in peer-reviewed journals on this list. The table below shows these journals and their ranking.

Title	ISSN	#	SJR	H index	Rank	Country
Geophysical Research Letters	ISSN 00948276	1	2.91	206	625	United States
Journal of Geotechnical and Geo-environmental Engineering - ASCE	ISSN 10900241	2	2.695	109	729	United States
Earthquake Engineering and Structural Dynamics	ISSN 10969845, 00988847	1	2.293	92	1003	United States
Journal of Geophysical Research	ISSN 21699380, 01480227	3	1.996	283	1272	United States
Seismological Research Letters	ISSN 08950695		1.971	55	1305	United States
Bulletin of the Seismological Society of America	ISSN 00371106	6	1.883	117	1438	United States
Earthquake Spectra	ISSN 87552930	1	1.878	69	1446	United States
Engineering Structures	ISSN 01410296	1	1.578	99	1976	United Kingdom
Bulletin of Earthquake Engineering	ISSN 1570761X	4	1.345	38	2605	Netherlands
Pure and Applied Geophysics	ISSN 00334553, 14209136	1	0.804	67	5405	Switzerland
Journal of Seismology	ISSN 1573157X, 13834649	2	0.633	43	7033	Netherlands

Table x.1 Prestigious peer-reviewed journal with their SJR (SCImago Journal Rank) indicator (It expresses the average number of weighted citations received in the selected year (2016) by the documents published in the selected journal in the three previous years) and H Index (The h index expresses the journal's number of articles (h) that have received at least h citations. It quantifies both journal scientific productivity and scientific impact). The number of papers published based on studies performed as part of the NAM-led research program of based on data acquired by this program is indicated (#).

2) List of papers in peer-reviewed journals

1. Bommer, J. J., H. Crowley, and R. Pinho, A risk-mitigation approach to the management of induced seismicity, *Journal of Seismology*, Vol: 19, Pages: 623-646, ISSN: 1383-4649, February 2015.
2. de Jager, J. and C. Visser, *Geology of the Groningen Field – an overview*, *Netherlands Journal of Geology*, 2017 (In-print).
3. Visser, C. and J. Solano Viota, The Groningen reservoir model, Part I: Static reservoir model, *Netherlands Journal of Geology*, 2017 (In print).
4. van Oeveren, H.E.J., P. Valvatne, L.E. Geurtsen and J. van Elk, The Groningen reservoir model, part II: Dynamic reservoir model, *Netherlands Journal of Geology*, 2017 (In print).
5. Van Eijs, R., O. van der Wal and Dirk Doornhof, Subsidence and compaction resulting from gas production in the Groningen field, The Netherlands, *Netherlands Journal of Geology*, 2017 (In print).
6. Bourne, S. J., S. J. Oates, J. van Elk, D. Doornhof, A seismological model for earthquakes induced by fluid extraction from a subsurface reservoir, *Journal of Geophysical Research: Solid Earth*, December 2014.
7. Bourne, S. J., S. J. Oates, J. J. Bommer, B. Dost, J. van Elk, and D. Doornhof, Monte Carlo method for probabilistic hazard assessment of induced seismicity due to conventional natural gas production, *Bulletin of the Seismological Society of America*, Vol: 105, Pages: 1721-1738, ISSN: 0037-1106, June 2015
8. Bourne, S.J., S.J. Oates, Extreme threshold failures within a heterogeneous elastic thin-sheet account for the spatio-temporal development of seismicity induced by fluid extraction from a subsurface reservoir, *Journal of Geophysical Research: Solid Earth*, 2017, (In print).
9. Bourne, S. J., S. J. Oates, Development of statistical geomechanical models for forecasting seismicity induced by gas production from the Groningen field, *Netherlands Journal of Geoscience*, 2017 (In print).
10. Harris, C. K. and S. J. Bourne, Computing the Distribution of Pareto Sums Using Laplace Transformation and Stehfest Inversion, *Pure and Appl. Geophys.* 174 (2017), 2039 – 2075, DOI: 10.1007/s00024-017-1517-y
11. Zöller G. and M. Holschneider, The Maximum Possible and the Maximum Expected Earthquake Magnitude for Production-Induced Earthquakes at the Gas Field in Groningen, The Netherlands, *Bulletin of the Seismological Society of America* December 2016 vol. 106 no. 6 2917-2921
12. Dempsey, D. and J. Suckale, (2017) Physics-based forecasting of induced seismicity at Groningen gas field, the Netherlands, *Geophysical Research Letters*, Accepted manuscript online: 25 July 2017
13. Bommer, J.J. and J. van Elk, Comment on “The Maximum Possible and the Maximum Expected Earthquake Magnitude for Production-Induced Earthquakes at the Gas Field in Groningen, The Netherlands” by Gert Zöller and Matthias Holschneider, *Bulletin of the Seismological Society of America*, March 2017, 107(3), 1564-1567.
14. Buijze, L., P. van den Bogert, B.B.T. Wassing, B. Orlic, J. ten Veen, Faulting mechanisms and rupture modelling of seismic events induced by gas depletion from a Rotliegend reservoir, *Netherlands Journal of Geology*, 2017, (In print).
15. Hunfeld, L. B., Niemeijer, A. R., and Spiers, C. J., (2017), Frictional properties of simulated fault gouges from the seismogenic Groningen gas field under in-situ P-T-chemical conditions, *Journal of Geophysical Research*, 2017
16. Bommer, J.J., Bernard Dost, Benjamin Edwards, Pauline P Kruiver, Michail Ntinalexis, Adrian Rodriguez-Marek, Peter J Stafford and Jan van Elk, Developing a model for the prediction of ground motions due to earthquakes in the Groningen gas field, *Netherlands Journal of Geosciences*, 2017 (In print).
17. Bommer J.J., B. Dost, B. Edwards, P.J. Stafford, J. van Elk, D. Doornhof, M. Ntinalexis, Developing an application-specific ground-motion model for induced seismicity, *Bulletin of the Seismological Society of America*, Vol: 106, Pages: 158-173, ISSN: 0037-1106, 2016.
18. Bommer, J.J., P.J. Stafford, B. Edwards, B. Dost, E. van Dedem, A. Rodriguez-Marek, P.P. Kruiver, J. van Elk, D. Doornhof, and M. Ntinalexis (2017) Framework for a ground-motion model for induced seismic hazard and risk analysis in the Groningen gas field, The Netherlands, *Earthquake Spectra*, March 2017, 33(2), 481-498
19. Kruiver P.P., E. van Dedem, R. Romijn, G. de Lange, M. Korff, J. Stafleu, J.L. Gunnink, A. Rodriguez-Marek, J.J. Bommer, J. van Elk, D. Doornhof, An integrated shear-wave velocity model for the Groningen gas field, The Netherlands, *Bulletin of Earthquake Engineering*, ISSN: 1573-1456, 2017, DOI 10.1007/s10518-017-0105-y.
20. Rodriguez-Marek, A., P. P. Kruiver, P. Meijers, J. J. Bommer, B. Dost, J. van Elk and D. Doornhof, A Regional Site-Response Model for the Groningen Gas Field, *Bulletin of the Seismological Society of America*, 2017. DOI: 10.1785/0120160123.
21. Kruiver, P.P., Wiersma, A., Kloosterman, F.H., de Lange, G., Korff, M., Stafleu, J., Busscher, F., Harting, R., Gunnink, J.L., Green, R.A., van Elk, J., and Doornhof, D. (2017). Characterisation of the Groningen Subsurface for Seismic Hazard and Risk Modelling, *Netherlands Journal of Geosciences*. (in press)
22. Noorlandt, R.P., P. Kruiver, M.P.E. de Kleine, M. Karaoulis, G. De Lange, A. Di Matteo, J. Von Ketelhodt, E. Ruigrok, B. Edwards, A. Rodriguez-Marek, J.J. Bommer, J van Elk and D. Doornhof, Characterisation of Ground-Motion Recording Stations in the Groningen Gas Field, *Journal of Seismology*, April 2017.

23. Lasley, S.J., R. A. Green, A. Rodriguez-Marek, Number of equivalent stress cycles for liquefaction evaluations in active tectonic and stable continental regimes, *Journal of Geotechnical and Geo-environmental Engineering* 143 (4), 04016116
24. Lasley, S.J., R. A. Green, A. Rodriguez-Marek, New Stress Reduction Coefficient Relationship for Liquefaction Triggering Analyses, *Journal of Geotechnical and Geo-environmental Engineering* 142 (11), 06016013
25. Graziotti, F., U. Tomassetti, A. Penna, G. Magenes (2016), Out-of-plane shaking table tests on URM single leaf and cavity walls, *Engineering Structures*, 125, pp. 455-470, doi:10.1016/j.engstruct.2016.07.011, July 2016.
26. Graziotti, F., U. Tomassetti, S. Kallioras, A. Penna, G. Magenes F. (2017), Shaking table test on a full scale URM cavity wall building, *Bull Earthquake Eng*, DOI 10.1007/s10518-017-0185-8, June 2017
27. Brunesi, E., Nascimbene, R. (2017), Experimental and numerical investigation of the seismic response of precast wall connections, *Bull Earthquake Eng.*, DOI 10.1007/s10518-017-0166-y, June 2017.
28. van Elk J., Doornhof D., Bommer J.J., Bourne S.J., Oates S.J., Pinho R., Crowley H. (2017), Hazard and risk assessments for induced seismicity in Groningen, *Netherlands Journal of Geosciences*, in press.
29. Crowley H., Pinho R., Polidoro B., van Elk J. (2017), Developing fragility and consequence models for buildings in the Groningen Field, *Netherlands Journal of Geosciences*, (In print).
30. Crowley H., Pinho R., Polidoro B., van Elk J. (2017) Framework for Developing Fragility and Consequence Models for Local Personal Risk, *Earthquake Spectra*, in press.
31. van Elk J., Bourne S.J., Oates S.J., Bommer J.J., Pinho R., Crowley H. (2018) A probabilistic seismic risk model to inform decision-making in response to induced earthquakes in the Groningen Gas Field, *Earthquake Spectra*, submitted for publication.
32. Malomo, D., R. Pinho, Penna A. (2018) Modelling of calcium-silicate brick masonry subjected to in-plane cyclic loading, *Earthquake Engineering and Structural Dynamics*, submitted for publication.
33. Kallioras S., Guerrini G., Tomassetti U., Marchesi B., Penna A., Graziotti F., Magenes G. (2018) Experimental seismic performance of a full-scale unreinforced clay masonry building with flexible timber diaphragms, *Engineering Structures*, submitted for publication.

3) List of Conference papers

The research studies have also been presented at various conferences resulting in Conference Papers and Poster Sessions. Below are the most important conference papers listed. As many of the studies initially presented at conferences were later also captured in peer-reviewed papers, this list is therefore limited to the most important papers and not complete.

1. Burnett, W., C. Gans, G. Gist, M. Terrell, J. Reilly, J. Tomic, J. Anderson, S. Tan, N. DeDontney and D. Pais, Applications of 3D elastic wavefield simulation to induced seismicity, Society of Exploration Geophysicists, International Exposition and Annual Meeting, 16-21 October, Dallas, Texas, 2016
2. Crowley, H., Polidoro, B., Pinho, R., van Elk, J., (2017) Fragility and Consequence Models for Probabilistic Seismic Risk Assessment in the Groningen Gas Field, 16th European Conference on Earthquake Engineering (16ECEE), Thessaloniki, Greece, June 18-21, 2018.
3. Graziotti F., Guerrini G., Kallioras S., Marchesi B., Rossi A., Tomassetti U., Penna A., Magenes G. (2017), Shaking table tests on a full-scale unreinforced clay masonry building with flexible diaphragms, 13th Canadian Masonry Symposium, 4-7 June, Halifax, Canada.
4. Graziotti F., Rossi A., Mandirola M., Penna A., Magenes G. (2016), Experimental characterization of calcium-silicate brick masonry for seismic assessment, 16th International Brick and Block Masonry Conference, Padova, Italy.
5. Graziotti, F., U. Tomassetti, L. Grottoli, S. Dainotti, A. Penna, G. Magenes F. (2017), Shaking table test of URM walls subjected to two-way bending out-of-plane seismic excitation, 17th Italian National Conference on Earthquake Engineering (XVII Anidisi), 17-21 September, Pistoia, Italy.
6. Korff, M., A. Wiersma, P. Meijers, F. Kloosterman, G. de Lange, J. van Elk, D. Doornhof, Liquefaction Mapping for Induced Seismicity in the Groningen Gas Field, 6th International Conference on Earthquake Geotechnical Engineering, 1-4 November 2015, Christchurch, New Zealand
7. Korff, M., A. Wiersma, P. Meijers, F. Kloosterman, G. de Lange, J. van Elk, D. Doornhof, Liquefaction Mapping for Induced Seismicity in the Groningen Gas Field, 3rd International Conference on Performance-based Design in Earthquake Geotechnical Engineering (PBD-III), Vancouver, Canada
8. Lele, Suvrat P., Hsu, Sheng-Yuan, Garzon, Jorge L., DeDontney, Nora, Searles, Kevin H., Gist, Grant A., Sanz, Pablo F., Biediger, Erika A. O., Dale, Bruce A., Geomechanical Modelling to Evaluate Production-Induced Seismicity at Groningen Field, 183554-MS SPE Conference Paper – 2016
9. Sanz, Pablo F., Lele, Suvrat P., Searles, Kevin H., Hsu, Sheng-Yuan, Garzon, Jorge L., Burdette, Jason A., Kline, William E., Dale, Bruce A., Hector, Paul D., Geomechanical Analysis to Evaluate Production-Induced Fault Reactivation at Groningen Gas Field 174942-MS SPE Conference Paper – 2015
10. Tomassetti, U., Graziotti, F., Penna, A., Magenes, G., 2016, Out-of-Plane Shaking Table Test on Unreinforced Cavity Walls, Proceedings of the 16th International Brick and Block Masonry Conference, 26-30/6/2016, Padua, Italia
11. Tomassetti, U., Grottoli, L., Graziotti, F., Penna, A., Graziotti, F., Magenes, G., (2017), Two-way Bending Out-of-Plane Shaking Table Tests of URM Walls Subjected to Seismic Excitation, IF CRASC '17, Milano, 14-16 September 2017
12. Tomassetti U., Graziotti F., Marques A., Penna A., Magenes G., Correia A.A. (2017) Collapse dynamic testing of a full-scale URM cavity-wall structure, 17th Italian National Conference on Earthquake Engineering (XVII Anidisi), 17-21 September, Pistoia, Italy.

Appendix D – Experts

Apart from scientist, engineers and researchers in NAM and the laboratories of Shell (Rijswijk) and Exxonmobil (Houston), NAM has also sought the advice of internationally recognised experts. Some of the experts collaborating in the research program on induced seismicity in Groningen, led by NAM, are listed below.

External Expert	Affiliation	Main Expertise Area
Damian Grant	ARUP	Building Fragility
Guido Magenes	Eucentre Pavia	Building Fragility
Rui Pinho	University Pavia	Building Fragility
Helen Crowley	Independent Consultant, Pavia	Building Fragility, Injury Model and Risk
Michelle Palmieri	ARUP	Building Fragility
Rinke Kluwer	ARUP	Building Fragility
Sinan Akkar	Bogazici, University Istanbul	Ground Motion Prediction
Ben Edwards	University Liverpool	Ground Motion Prediction
Michail Ntinalexis	Independent Consultant, London	Ground Motion Prediction
Barbara Polidoro	Independent Consultant, London	Building Fragility
Peter Stafford	Imperial College London	Ground Motion Prediction
Julian Bommer	Independent Consultant, London	Ground Motion Prediction and Site Response
Emily So	Cambridge Architectural Research Ltd	Injury model
Robin Spence	Cambridge Architectural Research Ltd	Injury model
Russell Green	Virginia Tech, USA	Liquefaction Model
Tony Taig	TTAC Limited	Injury Model and Risk
Loes Buijze	University Utrecht	Rock Physics / Core Experiments
Chris Spiers	University Utrecht	Rock Physics / Core Experiments
Bart Verberne	University Utrecht	Rock Physics / Core Experiments
Andre Niemeyer	University Utrecht	Rock Physics / Core Experiments
Matt Pickering	Student; Leeds University	Seismic Event Location
Marco de Kleine	Deltares	Site Response and Shallow Geological Model
Pauline Kruiver	Deltares	Site Response and Shallow Geological Model
Ger de Lange	Deltares	Site Response and Shallow Geological Model
Adrian Rodriguez -Marek	Virginia Tech, USA	Site Response Assessment
Mandy Korff	Deltares	Site Response, liquefaction and Shallow Geological Model

Piet Meijers	Deltares	Site Response, liquefaction and Shallow Geological Model
Jan Rots	TU Delft	Building Fragility

Table D.1 The most important expert collaborators.

The experts and academics on this list have worked for a considerable time on studies of this program.

To independently review the studies and assure their results the following experts and academics have been asked to familiarize themselves with the studies and provide their feedback in assurance workshops or reports:

External Expert	Affiliation	Main Expertise Area
Adriaan Janszen	Exxonmobil	Shallow Geological Model
Eric Meijles	University Groningen	Shallow Geological Model
Joep Storms	TU Delft	Shallow Geological Model
Tijn Berends	Student; University Groningen	Site Response and Shallow Geological Model

Table D.2 The assurance team for "Shallow Geological Model".

The assurance team for "Ground Motion Prediction" is shown in table C.3.

External Expert	Affiliation	Main Expertise Area
Norm Abrahamson	UC Berkeley	Ground Motion Prediction
Gail Atkinson	Western University, Ontario, Canada	Ground Motion Prediction
Hilmar Bungum	NORSAR, Norway	Ground Motion Prediction and panel for the maximum magnitude of earthquakes
Fabrice Cotton	GFZ Potsdam, Germany	Ground Motion Prediction
John Douglas	University of Strathclyde, UK	Ground Motion Prediction
Jonathan Stewart	UCLA, California, USA	Ground Motion Prediction
Ivan Wong	AECOM, Oakland, USA	Ground Motion Prediction Member and panel for the maximum magnitude of earthquakes
Bob Youngs	AMEC, Oakland, USA	Ground Motion Prediction Member and panel for the maximum magnitude of earthquakes

Table D.3 The assurance team for "Ground Motion Prediction". Hilmar Bungum, Ivan Wong and Bob Youngs sit also in the panel for the maximum magnitude of earthquakes.

The assurance team for "Building Fragility" is shown in table C.4.

External Expert	Affiliation	Main Expertise Area
Jack Baker	Stanford University, US	Fragility Functions and Risk Analysis
Paolo Franchin	University of Rome "La Sapienza"	Fragility Functions and Risk Analysis
Michael Griffith	University of Adelaide, Australia	Modelling and Testing of Masonry Structures
Curt Haselton	California State University, US	Numerical Modelling of Structures
Jason Ingham	University of Auckland	Seismic Response of Masonry Structures

Nico Luco	United States Geological Survey	Risk Analysis Building Fragility
Dimitrios Vamvatsikos	NTUA, Greece	Fragility Functions and Risk Analysis

Table D.4 The assurance team for "Building Fragility".

The assurance teams have been informed by the extensive technical documentation and in workshops. The recommendations of the assurance teams have been incorporated in the details technical reports (section further work) and in this document. Because of their highly mathematical nature, the seismological models supporting the hazard and risk assessment have been reviewed by Prof. Ian Main (of Edinburgh University).

The studies on building fragility have additionally been review by Ron O. Hamburger of the consultancy Gumpertz & Heger.

In a workshop conducted following the guidelines for a SSHAC level 3 process, a panel of experts has been asked to evaluate the distribution of Mmax values for the Groningen area, based on the current knowledge and uncertainty.

This panel consisted of:

External Expert	Affiliation	Role
Kevin Coppersmith	Geomatrix Consultants Inc.	Chairman SHACC Committee
Ivan Wong	AECOM, Oakland, USA	Ground Motion Prediction and Member SHACC Committee
Bob Youngs	AMEC, Oakland, USA	Ground Motion Prediction Member and SHACC Committee
Jon Ake	US Nuclear Regulatory Commission	Member SHACC Committee
Hilmar Bungun	Norsar Norway	Member SHACC Committee
Torsten Dahm	GFZ Potsdam	Member SHACC Committee
Art McGarr	US Geological Survey	Member SHACC Committee
Ian Main	University Edinburgh	Seismogenic Model / Statistics and Member SHACC Committee

Table D.5 The panel for the determination of Mmax distribution.

Additionally the following independent external experts presented to the expert panel:

External Expert	Affiliation	Role
Serge Shapiro	Freie Universiteit Berlin	Independent Advisor
Emily Brodsky	University of California, Santa Cruz	Independent Advisor
Jenny Suckale	Stanford University, Department of Geophysics	Independent Advisor
Gilian Foulger	Durham University, Department of Geophysics	Independent Advisor
Gert Zöller	University of Potsdam Institute of Mathematics and Focus Area for Dynamics of Complex Systems	Independent Advisor

Table D.6 The experts presenting to the panel for the determination of Mmax distribution.

Another workshop was held to discuss the state-of-the-art regarding incorporation of finite fault rupture simulations into the development of ground-motion prediction equations; external expert participants are listed in Table D.7.

External Expert	Affiliation	Role
Norm Abrahamson	University of California at Berkeley	Fault simulations in California GMPEs
Christine Goulet	Southern California Earthquake Center (SCEC)	Validation and benchmarking of fault rupture-based simulation codes
Luis Angel Dalguer	SwissNuclear	Capabilities of finite rupture simulations
Bob Youngs	AMEC Foster Wheeler	Fault simulations in NGA-East GMPEs

Table D.7 External experts participating in workshop on finite fault simulations in GMPE development

Appendix E – Universities and Knowledge Institutes

The main partners in the research program into induced seismicity in Groningen are listed below:

Partner	Expertise
Deltares	Shallow geology of Groningen, soil properties and measurements of site response/liquefaction.
University Utrecht (UU)	Measurements of rock compaction and rupture on core samples, understanding of physical processes determining compaction.
University Groningen (RUG)	Shallow geology of Groningen, archaeology.
ARUP	Modelling of building response to earthquakes, management of the program to measure strength of building materials.
Technical University Delft (TUD)	Measure strength of building materials and building elements.
Eucentre, Pavia, Italy	Measure strength of building materials, building elements and shake-table testing of full scale houses.
Mosayk	Modelling of building response to earthquakes.
Studio Calvi	All civil Engineering aspects of earthquake resistance to earthquakes including mitigation and strengthening measures like base isolation.
LNEC	Shake-table testing of full scale houses to collapse.
Magnitude (A Baker Hughes & CGG Company)	Seismic Monitoring (determination of location results deep geophones)
TNO	Potential for earthquakes resulting from injection. Building sensor project.
Avalon	Supplier of geophone equipment permanent seismic observations wells.
Baker-Hughes	Supplier of geophone equipment temporary observation wells.
Antea	Management of the extension of the geophone network.
Rossingh Drilling	Drilling of the shallow wells for the extension of the geophone network.
China Earthquake Administration	Experiments for friction on moving fault surfaces and upscaling of small scale experiments. Research led by University of Utrecht.
National Research Institute for Earth Science and Disaster Resilience, NIED (Japan)	Large Scale Earthquake Simulator facility at NIED, Tsukuba, Japan. Experimental facility for large experiments into friction during rupture.

Table E.1 Main partners in the research program into induced seismicity in Groningen

Appendix F – Raw Data Sharing with Universities and Knowledge Institutes

The raw unprocessed subsidence and seismic data collected by NAM is made available on request to academic and non-academic researchers for analysis and study. These are often very large data sets which are too big to be downloaded from a website.



Figure F.1 At 12th May 2014, Local NGO “Schokkend Groningen” receives at the NAM offices the two hard disks with 10 Terabyte data from the two deep geophone wells for independent study. (Photo: John Lanting).

Exchange of a hard disk is often the most practical approach to share this data. To date the following large data sets have been shared:

Data volume shared	Party data has been shared with	Time	Comments
Seismological data from temporary deep geophone wells	Mr. John Lanting Schokkend Groningen, The Netherlands	May 2014	
Seismological data from temporary deep geophone wells and VpVs velocity model	Gassnova Project, NORSAR, Norway	July 2014	Focus research: Locating hypo-centres of earthquakes.
VpVs velocity model and Geodetic Information.	Dr. Mike Fehler, Prof. Tom Herring and Prof. Brad Hager MIT (Massachusetts Institute of Technology), USA	August 2014	Focus research: (1) Analysis of historic seismic data and (2) Geomechanical and Geodetic investigation of seismic versus aseismic deformation.
VpVs velocity model and raw data deep geophones	Prof Gregory C. Beroza Stanford University, USA		Focus research: Ambient noise interferometry to infer shear wave velocities
VpVs velocity model and raw data deep geophones	Dr. H. Paulssen, University Utrecht	December 2015	Focus research: Noise interferometry to infer changes in medium properties and microseismicity
Subsidence measurements by InSar and seismological data from deep borehole arrays and KNMI shallow borehole network	Prof. Bob White Cambridge University, UK	December 2015	Focus research: Locating hypo-centres of earthquakes.
Seismological data from temporary deep geophone wells (update with recent data)	Gassnova Project, NORSAR, Norway	January 2016	Focus research: Locating hypo-centres of earthquakes.
Clarification of data request in progress	University of Bristol	March 2016	
Seismological data from deep borehole arrays and KNMI shallow borehole network	Prof. Pablo Ampuero, Utrecht University	November 2016	Focus Research: search for similar event waveforms (i.e. empirical Green's functions) to investigate source properties
Seismological data from deep borehole arrays and KNMI shallow borehole network	Prof. Serge Shapiro, Free University Berlin	November 2016	Focus Research: investigate source parameters using the empirical Green's functions
Seismological data from deep borehole arrays and KNMI shallow borehole network	Prof. Doug Dreger, University of California Berkeley	January 2017	Focus Research: investigate source parameters using the empirical Green's functions
	Secure Project		

Table F.5 Larger volume data sets have been exchanged with NGO's, Academic institutes and knowledge institutes.

The raw has been provided with "no-strings-attached". Progress reporting on these studies is strictly voluntary and NAM has no influence on the studies performed using the data sets.

